PB87-152500

Fundamental Studies of Calcium-Based Sorbents for SO2 Control from Coal-Fired Boilers

Energy and Environmental Research Corp.
Irvine, CA

Prepared for

Environmental Protection Agency
Research Triangle Park, NC

Jan 87

U.S. Department of Commerce
National Technical Information Service
NTIS

EPA/600/7-87/002
January 1987
PB87-152500

FUNDAMENTAL STUDIES OF CALCIUM-BASED SORBENTS FOR SO_2 CONTROL FROM COAL-FIRED BOILERS

by

J. A. Cole
J. C. Kramlich
G. S. Samuelsen
W. R. Seeker
G. D. Silcox

Energy and Environmental Research Corporation
18 Mason
Irvine, California 92718

EPA Contract No. 68-02-3633

EPA Project Officer: D. Bruce Henschel

Air and Energy Engineering Research Laboratory
Office of Environmental Engineering and Technology
Research Triangle Park, NC 27711

AIR AND ENERGY ENGINEERING RESEARCH LABORATORY
OFFICE OF RESEARCH AND DEVELOPMENT
U.S. ENVIRONMENTAL PROTECTION AGENCY
RESEARCH TRIANGLE PARK, NC 27711

REPRODUCED BY
U.S. DEPARTMENT OF COMMERCE
NATIONAL TECHNICAL
INFORMATION SERVICE
SPRINGFIELD, VA 22161

TECHNICAL REPORT DATA

(Please read Instructions on the reverse before completing)

1. REPORT NO.
EPA/600/7-87/002

2.

3. RECIPIENT'S ACCESSION NO.
PB87 152500/AS

4. TITLE AND SUBTITLE
Fundamental Studies of Calcium-based Sorbents for SO_2 Control from Coal-fired Boilers

5. REPORT DATE
January 1987

6. PERFORMING ORGANIZATION CODE

7. AUTHOR(S)
J. A. Cole, J. C. Kramlich, G. S. Samuelsen, W. R. Seeker, and G. D. Silcox

8. PERFORMING ORGANIZATION REPORT NO.

9. PERFORMING ORGANIZATION NAME AND ADDRESS
Energy and Environmental Research Corporation
18 Mason
Irvine, California 92718-2798

10. PROGRAM ELEMENT NO.

11. CONTRACT/GRANT NO.
68-02-3633

12. SPONSORING AGENCY NAME AND ADDRESS
EPA, Office of Research and Development
Air and Energy Engineering Research Laboratory
Research Triangle Park, NC 27711

13. TYPE OF REPORT AND PERIOD COVERED
Final; 10/83 - 9/84

14. SPONSORING AGENCY CODE
EPA/600/13

15. SUPPLEMENTARY NOTES AEERL project officer is D. Bruce Henschel, Mail Drop 54, 919/541-4112. EPA-600/7-85-027 is a related earlier report.

16. ABSTRACT The report gives results of laboratory-scale controlled-temperature experiments, studying aspects of SO2 capture by calcium-based sorbents in a flame/gas environment. Experimental parameters were sorbent type, temperature, residence time, and effects of mineral additives (promoters) on sorbent reactivity. The data revealed that isothermal capture is greatest at 1000 C, above which sintering of the sorbent can occur which reduces sorbent utilization. High-surface-area precalcined sorbents achieved moderately higher ultimate utilizations than their parent carbonates, but their real advantage was more rapid sulfation at lower temperatures where raw stones were limited by calcination. At 900 and 1000 C, the time for calcination for carbonate sorbents was significant. Pressure hydrated (type S) dolomitic limes consistently achieved the highest utilizations. The results suggest that (at ideal sulfation conditions--1000 C, isothermal residence times greater than 1 sec, no deactivation of the sorbent by coal ash minerals) the best calcium utilizations achievable would be about 25-30% with the raw limestone tested (Vicron 45-3), about 30-35% with the raw dolomite tested, and about 40% with both precalcined dolomite (precalcined to a surface area of 60 sq m/g) and pressure-slaked dolomitic lime. Adding Cr2O3, alkali metal salts, and other promoters increased limestone use.

17. KEY WORDS AND DOCUMENT ANALYSIS

a. DESCRIPTORS		b. IDENTIFIERS/OPEN ENDED TERMS	c. COSATI Field/Group	
Pollution	Boilers	Pollution Control	13B	13A
Sorbents	Calcium Oxides	Stationary Sources	11G	
Calcium	Calcium Carbonates		07B	
Sulfur Dioxide	Dolomite (Rock)			08G
Coal			21D	
Combustion			21B	

18. DISTRIBUTION STATEMENT
Release to Public

19. SECURITY CLASS *(This Report)*
Unclassified

20. SECURITY CLASS *(This page)*
Unclassified

21. NO. OF PAGES
218

22. PRICE

EPA Form 2220-1 (9-73)

NOTICE

This document has been reviewed in accordance with U.S. Environmental Protection Agency policy and approved for publication. Mention of trade names or commercial products does not constitute endorsement or recommendation for use.

Foreword

Subsequent to the preparation of this report, but prior to its publication, a systematic error was discovered resulting from the solid sampling system described in Section 4.2.2, that was used with the Isothermal Reactor (ITR). The effect of this error was to cause misleadingly high measurements of calcium utilization whenever the ITR was operated with a hydrogen-air flame. Thus, most of the ITR data presented in Section 5 reflect erroneously high calcium utilizations; only the data obtained with methane-air flames are not affected by this error.

The apparent cause of this problem is additional sorption of SO_2 by the sorbents during their residence time in the solid sampling system when no CO_2 is present (as when hydrogen is the fuel). When CO_2 is present (as when methane is the fuel), the predominant reaction in the sampling system appears to be recarbonation; little additional sulfur capture appears to occur. Since the calcium utilization values reported here are based upon sulfur analysis on the sorbent samples, any additional sulfation occurring in the sampling probe would lead to a mistaken conclusion, that the sulfation during the residence time in the ITR itself is higher than it actually was.

The magnitude of this error is illustrated in Figure F-1. This figure presents utilization as a function of residence time in the ITR for Vicron at 1000°C, under the following conditions: with a hydrogen-air flame, with utilization determined both by sulfur analysis on the solids and by SO_2 analysis in the combustion gases; and with a methane-air flame, with utilization again determined by both methods. The utilizations determined from the SO_2 measurements should avoid any problems resulting from reactions in the solid sampling system. As can be seen from the figure, the utilizations with the hydrogen-air flame were substantially lower when based upon the SO_2 sampling results, than they were when based upon solid samples. By comparison, the utilizations with the methane-air flame were the same based upon either method, and were consistent with the hydrogen-air utilizations based upon SO_2 sampling. These results strongly suggest that the hydrogen-air utilizations based upon solids sampling are erroneously high.

To help confirm that it is the absence of CO_2 in the hydrogen-air case which was causing the high apparent utilizations (based upon solids sampling), tests were run with a hydrogen-air flame doped with increasing amounts of CO_2. The results are shown in Figure F-2. As shown, an apparent utilization of 20 percent with no CO_2 (based upon solids sampling), rapidly falls to about 10 percent when 1 to 2 percent CO_2 is present in the gases; the utilization then holds at 10 percent as CO_2 is increased further.

From these results, it appears likely that the high apparent utilizations in the hydrogen-air/solids sampling case is due to additional uptake of SO_2 by the CaO in the solids sampling probe. When even a small amount of CO_2 is present in the gases, the CaO-CO_2 recarbonation reaction predominates.

The authors have concluded that this error in the ITR measurements does not affect the major conclusions of this report (Section 2.0). For example, the presence of an effective conversion ceiling between 0.5 and 1.0 second, and an optimum temperature of 1000°C, would still appear to hold. Of course, the quantitative utilization ceilings presented are erroneously high. Since the major content of this report thus remains basically correct, and since the results provide a number of significant insights regarding the sorbent-SO_2 reaction, this report is being released despite this known error. However, readers are cautioned to recognize--when comparing these data with the data of others--that many of the utilization figures reported here are high, in some cases by as much as a factor of 2. In addition, other investigators conducting similar studies should be alert to the possible impact of solids sampling systems on their results.

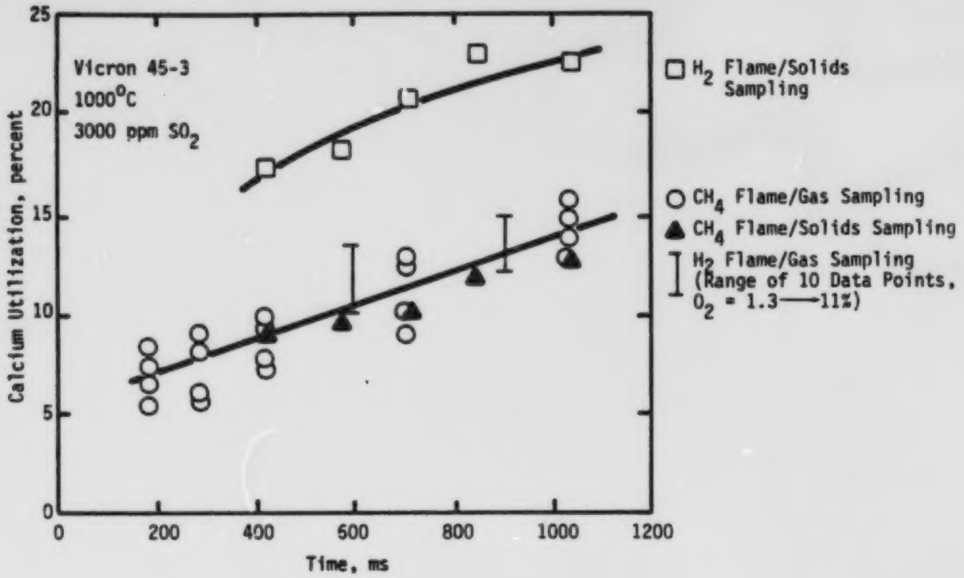

Figure F-1. Comparison of gas-phase and solids sampling results for both H_2/air and CH_4/air flames in the isothermal reactor (ITR).

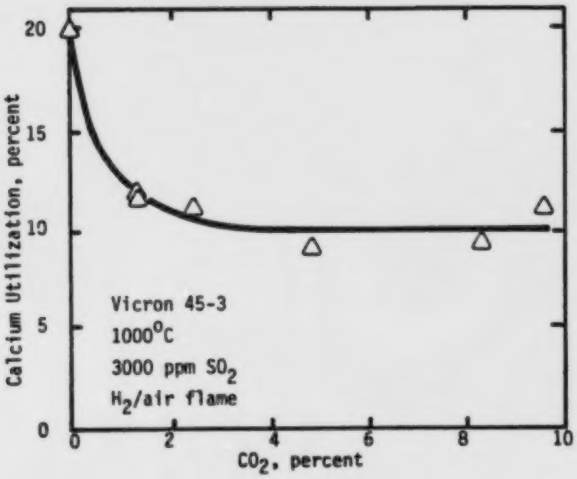

Figure F-2. Effect of CO_2 doping on measured calcium utilization by solids sampling from an H_2/air flame in the ITR.

Abstract

An isothermal drop-tube furnace and a non-isothermal flame reactor were used to study aspects of SO_2 capture by calcium-based sorbents in a flame-gas environment, over the range of temperatures where the sulfation reaction should proceed effectively. Parameters were sorbent type, temperature, residence time, SO_2 concentration and the presence of mineral additives (promoters or deactivators). To enable inclusion of high-surface-area precalcined limestones and dolomites in this effort (40-70 m^2/g), techniques were developed to generate such materials in sufficient quantities for SO_2 reactivity tests.

Most of the sorbents tested appeared to reach a ceiling on calcium conversion within 0.5 to 1.0 second during isothermal testing, probably due to pore plugging and product layer buildup resulting from sintering and sulfation. The highest ceilings were observed at 1000^oC for all sorbents; at higher temperatures, sintering (loss of surface area) reduced the ultimate utilizations. These results suggest that under ideal conditions--residence times greater than 1 second at 1000^oC--the best SO_2 removals achievable at a calcium-to-sulfur molar ratio of 2 would be about: 50-60 percent with the raw limestone tested or with this limestone precalcined to 40 m^2/g; 60-70 percent with the raw dolomite; and 80 percent with the precalcined dolomite (60 m^2/g) or with the pressure-slaked dolomite hydrate. In most cases, precalcined sorbents achieved only slightly higher utilization ceilings than did their parent carbonates; their main advantage was faster initial sulfation since there was no delay caused by the time required for calcination (up to 0.5 s or longer for raw sorbents). Pressure hydrated dolomites and calcites showed the highest utilizations, compared to other forms of dolomites and calcites (respectively), and, like the precalcined materials, showed no calcination delay at low temperatures.

Porisimetry studies on the precalcined sorbents before and after sulfation revealed that nearly all of the surface area of the unsulfated materials resided in small micropores (about 100-200 A^o) which contributed only about one-quarter of the pore volume. In the precalcined limestone, this micropore volume was almost totally lost upon sulfation, whereas for the dolomite, much of the micropore volume remained open, possibly providing one reason why dolomites are typically more reactive.

Deactivation of limestone by kaolin (a coal ash mineral) is relatively minor at the lower temperatures studied here (1000-1200°C). Thus, sorbent deactivation by coal ash should be much less of a concern when the sorbent is injected at upper furnace conditions, compared to injection in or near the burner zone.

The addition of minerals, notably Cr_2O_3 or alkali metal salts, increased the utilization of limestone. Five weight percent Cr_2O_3 premixed with limestone--exposed to 1600-1700°C prior to dropping into the sulfation window (which starts at about 1250°C)--increased the utilization of the sorbent by a factor of 3.5, relative to unpromoted limestone passing through the same profile. At 1100°C isothermal, the utilization ceiling of limestone is increased by a factor of about 1.2 by sodium carbonate or bicarbonate; at 1360°C, the enhancement factor is about 2.5. However, at the higher temperature, the benefits of the improved sodium activity are offset by increased sintering of the sorbent, so that the absolute value of the utilization ceiling is about the same at both temperatures. For the eight alkali metal salts tested, enhancement of the limestone increased linearly with the mole ratio of alkali-to-calcium in the premixture.

This report is submitted in partial fulfillment of EPA Contract No. 68-02-3633, and describes work conducted by Energy and Environmental Research Corporation under the sponsorship of the U.S. Environmental Protection Agency. This report covers the period from 1 October 1983 to 30 September 1984.

TABLE OF CONTENTS

Section Page

Foreword ii
Abstract v
List of Figures x
List of Tables xiii
List of Abbreviations, Symbols and Terms xiv
Acknowledgements xvi

1.0 INTRODUCTION 1-1

1.1 Background 1-1
1.2 Statement of the Problem 1-3

2.0 CONCLUSIONS 2-1

3.0 RECOMMENDATIONS 3-1

4.0 EXPERIMENTAL 4-1

4.1 Reactors 4-1
4.1.1 Thermal Decomposition Reactor 4-1
4.1.2 Isothermal Reactor Design and Operation . . . 4-3
4.2 Other New Apparatus 4-7
4.2.1 Fluidized Bed Off-Take Tube Assembly 4-7
4.2.2 ITR Solids Sampling Probe 4-7
4.2.3 Fine Wire Thermocouple Probes 4-10
4.2.4 Limestone Precalcination Apparatus 4-10
4.3 Analytical Procedures 4-13
4.4 Sorbents and Additives 4-15

Preceding page blank

TABLE OF CONTENTS (Continued)

Section Page

5.0 RESULTS AND DISCUSSION 5-1

5.1 Precalcined Sorbents 5-1
  5.1.1 Parametric Evaluation of Precalcination . . 5-3
  5.1.2 Storage Stability of Precalcines 5-8
5.2 Flame Processed Sorbent Reactivity 5-10
5.3 Isothermal Reactivity Tests 5-14
  5.3.1 Calcium Utilization Profiles 5-16
  5.3.2 Reactivity Vs. Injection Temperature 5-23
  5.3.3 Effects of Coincident Calcination on Reactivity 5-25
  5.3.4 High-Calcium Pressure-Slaked Hydroxides . . 5-28
  5.3.5 SO_2 Concentration Effects 5-33
5.4 Porisimetry Data 5-36
5.5 Sulfation Reaction Promoters 5-41
  5.5.1 Cr_2O_3 Tests 5-43
  5.5.2 Additional Additives 5-48
  5.5.3 Discussion 5-55
5.6 Sorbent Deactivation by Coal Ash Minerals 5-55
5.7 Mathematical Model Application 5-59
  5.7.1 Grain Model Description 5-59
  5.7.2 Prediction of Sorbent Performance 5-62
  5.7.3 Estimation of Sintering Effects 5-70
5.8 Summary 5-79

6.0 REFERENCES 6-1

TABLE OF CONTENTS (Continued)

Section | Page

APPENDICES

A. Raw Data A-1
B. Isothermal Reactor Flame Conditions and Temperature Profiles B-1
C. Approaches to Precalcine Generation C-1
D. Sorbent Injection Method in Isothermal Reactor D-1
E. Sampling Technique Evaluation E-1
F. Quartz Probe Sampling in the ITR F-1
G. Quality Control Evaluation Report G-1

LIST OF FIGURES

Figure Page

1-1 Juxtaposition of reactor operating conditions relative to a wall-fired utility boiler 1-5

4-1 Detail of the isothermal reactor with burner and probe installed 4-4

4-2 Centerline gas temperature profiles for the isothermal reactor system 4-5

4-3 Modified offtake tube assembly for transport of ultrafine particulate using a fluidized bed feeder 4-8

4-4 Stainless steel sampling probe with rapid quench sampling orifice 4-9

4-5 A supported wire thermocouple probe for gas temperature measurements in the isothermal reactor 4-11

4-6 Apparatus for generation of precalcined sorbents 4-12

5-1 Specific surface area vs. extent of calcination - Vicron 45-3 calcined in the transpirated thin bed 5-4

5-2 Effect of sweep gas flow rate on surface area developed at complete calcination by Vicron 45-3 in the precalcination apparatus at 700°C 5-7

5-3 Loss of surface area by precalcined sorbents during storage 5-9

5-4 Effect of peak calcination temperature in the TDR on subsequent SO_2 uptake in the dispersed-phase reactivity probe (1100°C, 6% SO_2, 0.6 s) 5-12

5-5 Reactivity of eight sorbents calcined in the thermal decomposition reactor at 1200 and 1500°C 5-13

5-6 Calcium utilization profiles for five sorbents at 900°C . . 5-17

5-7 Calcium utilization profiles for five sorbents at 1000°C . . 5-18

5-8 Calcium utilization profiles for five sorbents at 1100°C . . 5-19

5-9 Calcium utilization profiles for five sorbents at 1200°C . . 5-20

LIST OF FIGURES

Figure		Page
5-10	Relative levels of calcium utilization at 1.0 s by five sorbents as a function of reaction/calcination temperature	5-24
5-11	Calcium utilization profiles for D3002 dolomite at 900, 1000, 1100 and 1200°C, 3600 ppm SO_2	5-26
5-12	Composite plots of both calcination and calcium utilization data for A. -Vicron 45-3 and B. -D3002 dolomite in the ITR	5-27
5-13	Calcium utilization profiles for high-calcium pressure-slaked hydroxides at 1100°C, 3600 ppm SO_2	5-29
5-14	Calcium utilization profiles for high-calcium pressure-slaked hydroxides at 1200°C, 3600 ppm SO_2	5-30
5-15	Surface area profiles for high calcium pressure-slaked hydroxides in the ITR in the absence of SO_2	5-32
5-16	Effect of temperature on the surface area attained in 0.6 s by high-calcium pressure-slaked hydroxides in the ITR	5-34
5-17	SO_2 concentration effect on SO_2 capture by three sorbents in the ITR	5-35
5-18	Characterization of pore types based on interpretation of mercury intrusion porisemtry data	5-37
5-19	Pore size distributions for raw and sulfated V40 precalcined	5-39
5-20	Pore size distributions for raw and sulfated D60 precalcine	5-40
5-21	Calcium utilization of Vicron 45-3 with and without Cr_2O_3 as a function of initial flame temperature	5-44
5-22	Ratio of calcium utilization with and without Cr_2O_3 by Vicron 45-3	5-44
5-23	The residual chromium effect on calcium utilization by unpromoted Vicron 45-3 in the ITR	5-47
5-24	Calcium utilization by Vicron 45-3 fed premixed with promotors into isothermal conditions in the ITR	5-49

LIST OF FIGURES

Figure Page

5-25 Calcium utilization by Vicron 45-3 fed premixed with promotors in the ITR 5-51

5-26 Illustration that enhancement factor observed with different alkali metal salts correlates with the molar concentrations obtained with the different salts . . . 5-54

5-27 Effects of kaolin addition on calcium utilization by V40, D60, and Vicron 45-3 at three temperatures 5-57

5-28 Impact of kaolin on calcium utilization of sorbents in the ITR, 1360^{o}C CH_4-air flame, 1100^{o}C furnace, 3600 ppm SO_2 added 5-58

5-29 A porous, multigrain particle 5-60

5-30 Temperature profiles for the Shawnee and Weiher boilers estimated by the EER furnace thermal model 5-63

5-31 Sorbent performance predictions for thermal profiles representative of the Shawnee and Weiher boilers, for two different injection locations, Ca/S = 2.0. 5-67

5-32 Sorbent and sorbent/additive performance predictions for the Shawnee and Weiher boilers 5-69

5-33 Comparison of the grain model with ITR reactivity data for D60 and V40 at 1000^{o}C 5-72

5-34 Comparison of the grain model with ITR reactivity data for D60 and V40 at 1100^{o}C 5-73

5-35 Comparison of the grain model with ITR reactivity data for D60 and V40 at 1200^{o}C 5-74

5-36 Estimated rate of surface area decay due to thermal sintering only for (a) V40 and (b) D60 5-76

5-37 Estimated surface area history in tests with raw Vicron and D3002 dolomite 5-78

LIST OF TABLES

Table Page

4-1 In-House Analytical Procedures 4-14

4-2 Analytical Procedures Performed by Outside Laboratories . . 4-14

4-3 Physical and Chemical Properties of Limestone Sorbents . . . 4-16

4-4 Particle Size Distributions of Raw Sorbents 4-17

4-5 Sorbent Additives and Minerals 4-19

5-1 Properties of Sorbents after Injection into the Dispersed-Phase SO_2 Reactivity Probe Without the TDR 5-15

5-2 Summary of Mercury Intrusion Porisimetry Data of Raw and Sulfated D60 and V40 Precalcines 5-42

5-3 Composition of the Alkali Salt Mixtures with Vicron 45-3 . . 5-53

5-4 Estimated Surface Area and Predicted Boiler Capture as A Function of Sorbent Injection Temperature 5-56

LIST OF ABBREVIATIONS, SYMBOLS AND TERMS

Abbreviations

diam	diameter
i.d.	inside diameter
mol	mole of substance
o.d.	outside diameter
ppm	parts per million, volume basis
t.c.	thermocouple

Symbols

Å	Angstrom unit, 10^{-8} cm
C	carbon
CaO	calcium oxide, lime
ε	porosity, (void volume) ÷ (total volume)
g	gram
H	hydrogen
K	thermodynamic temperature, degrees Kelvin
kJ	kilojoule
kPa	kilopascal, $10^3\ N \cdot m^{-2}$
kW	kilowatt
L	liter
M_i	mass of substance i, g
N_2	nitrogen
Pt	platinum
Q	volumetric flowrate per mass of sample, $cm^3 \cdot g^{-1} \cdot s^{-1}$
Rh	rhodium
R_p	particle radius
R	distance from center of particle
r	unreacted core radius (shrinking core model)
r_g	grain radius (shrinking core model)
r_g'	expanded grain radius (shrinking core model)

LIST OF ABBREVIATIONS, SYMBOLS AND TERMS (continued)

Symbols

S	sulfur
s	seconds
ss	stainless steel
σ	standard deviation: $\pm 1\sigma \rightarrow$ 68 percent confidence interval $\pm 2\sigma \rightarrow$ 95 percent confidence interval
X_i	mole fraction of species i

Terms

Ca/S	molar ratio of calcium-to-sulfur (moles of calcium in feed sorbent divided by moles of sulfur in fuel feed)
di/dt	change of i with time
Type S	a hydrated lime produced by a pressurized process

ACKNOWLEDGEMENTS

The authors gratefully acknowledge T. C. Grogan and R. K. La Fond for performing the analytical tasks and R. D. Blethen for performing and assisting the development of many of the experimental procedures. Thanks also for the many valuable discussions and advice provided by the EPA Staff, D. B. Henschel, D. C. Drehmel and J. H. Abbott. We are grateful for EPA support under Contract No. 68-02-3633.

1.0 INTRODUCTION

This report describes the second phase of laboratory-scale research investigating the fundamental aspects of SO_2 removal from the flue gases of coal-fired utility boilers by the dry injection of calcium-based sorbents, such as limestones, dolomites, and the calcined or hydrated products from these minerals. The first phase of this research has been described in Reference 22. In the experimental section of the current report are discussed the experimental apparatus, analytical procedures, and the materials employed. Particular emphasis is placed on the design and operation of new equipment developed during this program. The subsequent sections on the results provide information on the parameters which control the ability of calcium-based sorbents to uptake SO_2. This ability, which is called reactivity, has been examined for a wide variety of natural and processed calcium-containing sorbents. A substantial level of effort was devoted to ancillary experiments which were required for the development of the apparatus and experimental procedures described herein. As these ancillary experiments did not directly address the program objectives, their results are presented in the Appendices.

1.1 Background

The concept of dry-limestone injection offers potentially an economically attractive means for intermediate levels of SO_2 emissions control in pulverized-coal-fired (p.c.) utility boilers. The process is especially attractive as a retrofit for older boilers because of the potentially limited space requirements and low capital costs relative to other SO_2 control technologies (1). In addition, the raw material is readily available and relatively inexpensive, with the bulk of the cost incurred in processing and transportation (2). Early demonstration tests in the late 1960's and early 1970's, however, met with little success (3) in that acceptable levels of SO_2 removal could not be achieved, even with a large stoichiometric excess of limestone.

Since that time, a large body of work has been produced in an attempt to better understand the limestone-SO_2 process and to extend the limits of its applicability in full-scale p.c. utility boilers. Some of the efforts have examined the overall process of SO_2 capture within the confines of the conditions present in full-scale systems (4, 5). Both calcination (6) and sulfation kinetics (7, 8) have been studied in fundamental experiments and have also been addressed theoretically (9-11). Also, the calcination of various limestones has been examined with regard to the properties--surface area, porosity, pore size, etc.--which are most likely to affect the reaction with SO_2 (12-16). Lastly, the interactions of limestones with other minerals (17, 18) which are found in coals, and the effects of these interactions on SO_2 capture--both positive (19, 20) and negative (14, 21)--have been investigated, mainly in recent years.

Several areas of research were addressed in this program. These were:

- Determination of the so-called "reactivity" of a wide variety of calcium-based sorbents. Reactivity generally refers to the rate at which a sorbent will capture sulfur under the dispersed-phase, high-temperature conditions which would exist in utility furnaces. The reactivities of a variety of sorbents, including hydrates and high-surface-area precalcines were determined in a single experimental system.

- Examination of the reactions of calcination and sulfation in the dispersed phase at the high temperatures and short residence times which are representative of those encountered in p.c. utility boilers.

- Study of the effects of mineral matter interactions on the ability of calcium-based sorbents to remove SO_2.

- Observation of physical changes of the sorbents which could be linked to reactivity.

The work described herein examined the SO_2 capture process in an isothermal drop-tube furnace and in a non-isothermal flame reactor under experimental conditions which were representative of the environment of a p.c. utility boiler, but which were well characterized, uniform and reproducible. Sufficient parametric control was available to allow examination of the effects of residence time, temperature, sorbent type and gas composition in the reactor, as well as other variables of interest. These objectives were met with the two reactors described in this report.

1.2 Statement of the Problem

The problem addressed by this project can be stated succinctly: define the conditions which will optimize SO_2 removal by dry calcium-based sorbent injection. For the purposes of the experimental work these conditions encompass temperature, residence time, gas composition, sorbent type and preparation, and the presence or absence of minerals other than calcium. The approach for addressing the problem can be outlined as follows:

- Reactor Preparation - Design and construction of an isothermal drop-tube reactor for calcination and sulfation studies.
- In-situ Calcination/Sulfation - Examine the factors governing reactivity and reactivity development when a "raw" (uncalcined) sorbent is injected directly into a furnace environment and is thus calcined in-situ. Include gas composition as well as sorbent type, temperature and residence time.
- Externally Calcined Sorbents - Develop a means for producing, and testing, high-surface-area sorbents calcined under controlled conditions prior to injection into the isothermal reactor.
- Sintering Kinetics - Examine and characterize the loss of surface area due to thermal sintering and due to sulfation of calcined sorbents.
- Mineral Matter Interaction - Examine the effects of mineral additives on the reactivity of limestones toward SO_2.

This program examined the physical and chemical changes of a wide variety of sorbents under different chemical environments and over a range of time-temperature histories. Two drop-tube reactors were employed for this purpose which covered the range of thermal environments found in a utility boiler (Figure 1-1).

A high temperature flame thermal decomposition reactor (TDR) was used to examine physical changes taking place in very short times at temperatures exceeding 1500°C. This reactor provided a heating rate for the injected sorbent particles on the order of 5×10^4 K/s, followed by a steep temperature decline. Samples were extracted from this high temperature environment at varying residence times in order to determine the effects on sorbent physical characteristics and reactivity in an environment similar to near-flame injection in a utility boiler.

An isothermal reactor (ITR) was also employed, providing lower temperatures and slower heating rates ($\sim 10^4$ K/s), with isotherm residence times up to 2 s. This controlled-environment reactor was used to study transient phenomena characteristic of sorbent injection into the upper furnace and early convective passages of a utility boiler. Sorbent reactivity toward SO_2 was studied as a function of temperature, isothermal residence time, and chemical environment.

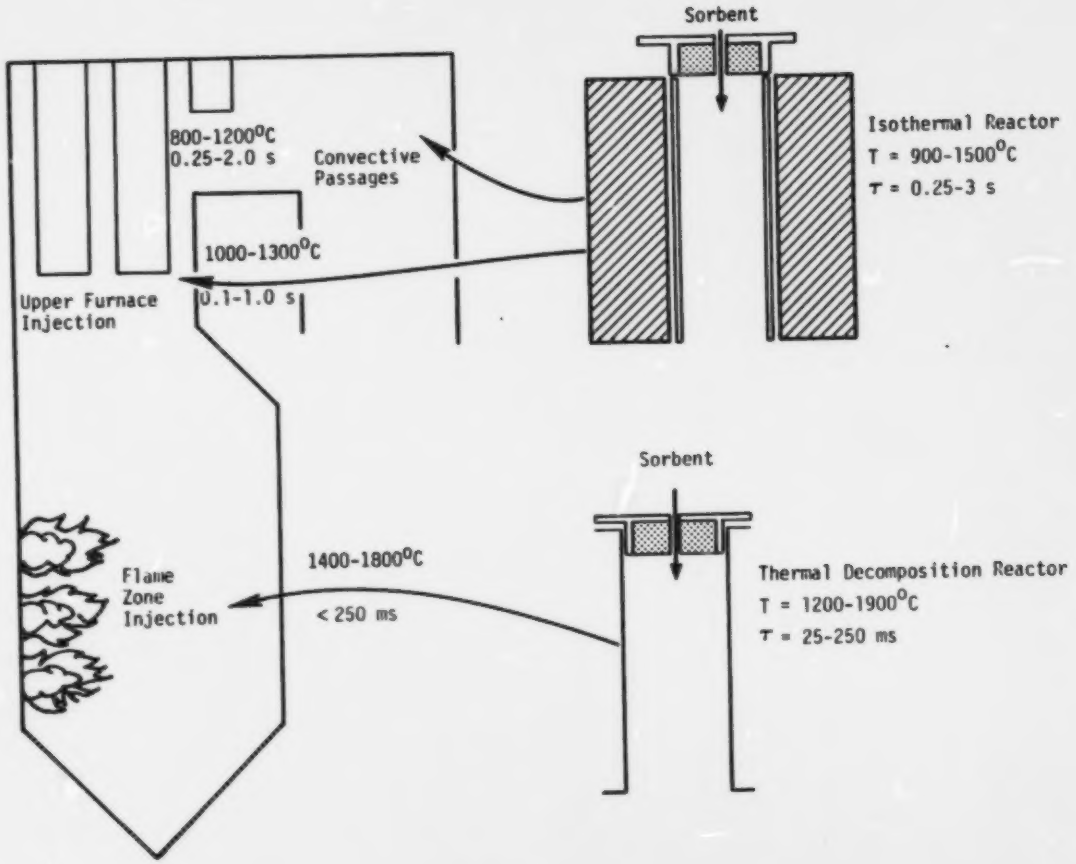
Sorbent
Isothermal Reactor
T = 900-1500°C
τ = 0.25-3 s
800-1200°C
0.25-2.0 s
Convective Passages
1000-1300°C
0.1-1.0 s
Upper Furnace Injection
Sorbent
Thermal Decomposition Reactor
T = 1200-1900°C
τ = 25-250 ms
1400-1800°C
< 250 ms
Flame Zone Injection

Figure 1-1. Juxtaposition of reactor operating conditions relative to a wall-fired utility boiler.

2.0 CONCLUSIONS

Based upon the results of this study, the following conclusions have been drawn:

- Most of the sorbents tested appear to reach an effective ceiling on calcium conversion within 0.5 to 1.0 second during isothermal drop-tube furnace testing at temperatures throughout the "sulfation temperature window." This apparent ceiling--at far less than 100 percent conversion--reflects a significant slowing of the sulfation rate, presumably due to increases in pore diffusion resistance and product layer diffusion resistance resulting from thermal sintering and the sulfation process. The ceiling could be raised by using particle sizes finer than those employed in this study.

- The optimum temperature for isothermal sulfation (and calcination, where required) is 1000°C for all sorbents, in terms of the conversion ceiling, so long as there is adequate residence time at that temperature (over 0.5 s) for calcination of the raw sorbents. At temperatures above 1000°C, sintering reduces conversion. (Residence times and temperature profiles in full-scale boilers would likely dictate injection at a higher temperature in practical applications.)

- Based upon the utilization ceiling, at ideal reaction conditions--1000°C, residence times greater than 1 second, no deactivation of the sorbent by coal ash--the best SO_2 removals achievable at a calcium-to-sulfur molar ratio of 2 would be about: 50 to 60 percent with the raw limestone tested, or with this limestone precalcined to 40 m^2/g; 60 to 70 percent with the raw dolomite tested; and 80 percent with the precalcined dolomite (60 m^2/g) or with the pressure-slaked dolomitic hydrate.

- The relative reactivity of the various sorbents remains essentially the same as that listed above, over the temperature range of

900-1200°C (although the absolute value of the utilization ceilings are different at the different temperatures).

- At temperatures below 1100°C, the time required for calcination of raw sorbents (up to 0.5 s or longer) becomes significant with respect to the time for sulfation.

- It is technically possible to generate precalcined limestones and dolomites having high surface areas (at least 40 to 70 m^2/g), by calcination under controlled conditions of temperature, time and sweep gas flow. These high-area precalcines initially react with SO_2 faster than their parent carbonates, especially at lower temperatures, because the time required for calcination in the furnace is eliminated. However, their ultimate utilization ceiling is not significantly higher than that of the raw sorbents. Thus, their major use in commercial boilers would likely be in cases where available residence times were short, such that delays due to calcination of raw sorbents could not be tolerated.

- Sintering reduces the reactivity of precalcined limes at temperatures as low as 1000°C. At 1100°C and above, one-half of the initial calcine area might be lost due to sintering within 0.25 s.

- Pressure-slaked dolomitic sorbents have higher capacity for sulfation than do raw or precalcined dolomite; likewise, pressure-slaked calcitic limestones have higher capacity than raw or precalcined calcites. This reactivity might be due to their small mean size (about 1 micron). Like the precalcines, these pressure hydrates show no delays in sulfation due to calcination (dehydration) at low temperatures.

- Nearly all of the active surface area in a high-area precalcined limestone and dolomite resided in small micropores, which constituted only perhaps one-quarter of the total pore volume. In the precalcined limestone, this micropore volume was almost totally lost upon sulfation, whereas for the dolomite, much of the micropore volume remained open after sulfation. This result might suggest why the limestone typically has lower reactivity than the dolomite.

- Kaolin--a coal ash mineral which has been shown in previous studies to deactivate sorbents when exposed to sorbents at flame temperatures--has little effect on the limestone or precalcined sorbents tested here when exposed at lower temperatures (1000-1200°C) representative of upper furnace injection. Thus, deactivation of sorbents by coal-ash--a significant concern earlier when sorbent injection into the burner zone was being considered--would appear to be much less of a concern if the sorbent is injected into the upper furnace.

- Mineral additives, or promoters (including Cr_2O_3 and alkali metal salts), can increase the sulfation reactivity of limestone. At 1100°C, the utilization ceiling of limestone is increased by a factor of about 1.2 by sodium carbonate or bicarbonate, compared to unpromoted limestone; at 1360°C, the enhancement factor is about 2.5. However, at the higher temperature, the benefits of the improved promoter activity are offset by the increased sintering of the sorbent--and perhaps by the reduced residence time in the sulfation window for the 1360°C case in these experiments--so that the absolute value of the utilization ceiling is about the same at both temperatures.

3.0 RECOMMENDATIONS

Based on the results and conclusions of this effort several areas are recommended for further investigation.

- Pressure Hydrated Sorbents. Investigate the reasons for the exceptional reactivity of pressure hydrated materials. Determine whether adjustments to the methods for generating pressure hydrates can further improve their reactivity.

- Particle Size. Examine the effects of particle size on sorbent reactivity toward SO_2, especially in the sub-micron range. Determine whether the reactivity of pressure hydrated materials is solely a particle size effect.

- Pore Structure/Porosity. Study the relationship between pore size and reactivity, and pore size and sorbent utilization. Determine how pore size distribution is affected by injection/calcination temperature--both for raw sorbents and for precalcines.

- Calcination and Sulfation Kinetics. Further examine the kinetics of in-situ SO_2 capture, and of surface area development and sintering. Especially concentrate on the simultaneous calcination and sulfation occurring at short residence times (less than 0.5 s); are transient high surface areas created during calcination? Quantify the effects of pore diffusion resistance and product layer diffusion resistance, and the variations in these resistances as sintering and sulfation proceed. Determine whether the reactivity of CaO can be determined solely on the basis of the sorbent's particle size, surface area and pore size distribution, and whether this reactivity is otherwise independent of the parent calcitic material from which the CaO was obtained.

4.0 EXPERIMENTAL

Much of the experimental equipment and procedures have been described in detail in the task Final Report for Phase I of this program (22) and in earlier references (23). These equipment and procedures are summarized in the following sections. Design and operation of more recent equipment, including sampling and injection systems, the limestone precalcination apparatus and the isothermal reactor (ITR) are discussed in more detail. Operating conditions are discussed along with the design of the ITR. Finally, a discussion of analytical procedures and materials is provided.

4.1 Reactors

The major apparatus used during the initial phase of this project were the thermal decomposition reactor (TDR) and associated sampling and thermocouple probes. This non-isothermal reactor provided fast heating rates, high temperatures and short residence times. These are reflective of the conditions which prevail for sorbent injection into the flame zone of a utility boiler. The TDR has been described in detail in an earlier report (22), but its main features are summarized below. Following that is a detailed description of the isothermal reactor (ITR). The ITR provides slower heating rates than the TDR but is capable of providing isothermal residence times up to 3.0 s in the temperature range of 900-1200°C. This permits temporal resolution of sorbent properties and reactivity in an environment reflective of the upper furnace and convective passages of a utility boiler. Characteristics and operating conditions for the ITR also are provided.

4.1.1 Thermal Decomposition Reactor

The TDR consists of a porous-bronze-plug flat-flame burner downfired into a 10 cm x 10 cm stainless steel chimney with optical, thermocouple and solids-sampling access. Solid materials, primarily limestones, were injected into the reactor through a 0.64 cm i.d. copper tube mounted axially through the burner. Solids were entrained in a fuel-air premixture prior to injection in order to ensure rapid heating to peak reactor temperature. Heat loss through the reactor walls then resulted in a steep temperature dropoff. Injection of the solids was accomplished with a Smith-type fluidized bed feeder and off-take tube assembly (24, 25).

Two different chimneys were used for the TDR. One of these was 1.2-m long with optically ground windows on opposite sides for visual access and optical diagnostics. The windows were removable and could be replaced with accessory plates which were adapted for either thermocouple probes or a water-cooled isokinetic solids sampling probe. On a third side were large Vicor windows for convenient visual access. The second chimney was 0.6-m long with Vicor windows for visual access and thermocouple access ports. The shorter chimney was a modification to allow for quartz-probe sampling through the bottom, using the dispersed-phase SO_2 reactivity probe.

Temperature measurements in the TDR were made using a 0.2-mm diameter butt-welded type-S thermocouple. Temperatures were read out on a digital thermometer and corrected for radiation losses. Flame conditions and temperature profiles are provided elsewhere (22).

Two modes of solids sampling were employed with the TDR. In the first mode, samples for calcination and specific surface area measurements were collected with a water-cooled isokinetic probe. Samples were quenched rapidly (10^5 K/s) by the probe to about 100°C and collected on a microporous filter maintained at 100-130°C. In the second sampling mode, reactivity toward SO_2 was determined using a dispersed-phase SO_2 reactivity probe. This quartz probe was inserted through the bottom of the short chimney and normally positioned 9 cm from the TDR burner (providing approximately 150 ms particle residence time in the TDR). Samples of dispersed sorbent--now calcined in the TDR, but not yet sulfated--entered the probe and were quenched slowly (10^4 K/s) to 650°C. At this point, the sample stream entered a reaction zone which was heated to 1100°C. In the reaction zone six-percent SO_2 was added and the sample stream allowed to react for 0.6 s. The sample then was quenched and collected on a glass fiber filter at 130°C for subsequent sulfation and calcination analysis. The dispersed-phase SO_2

reactivity probe was used principally with the TDR but also in limited tests with the isothermal reactor.

4.1.2 Isothermal Reactor Design and Operation

The isothermal reactor (ITR) is an electrically heated, gas-downfired laminar drop-tube furnace. It has a heated length of 90 cm and accommodates a 10-cm diameter reaction tube. Heating is provided by silicon carbide globars located in three independently regulated heating zones 22.5-, 45- and 22.5- cm long. Maximum power consumption is approximately 21 kW during heat up and high load operation. The ITR has a maximum wall temperature of 1500°C and dissipates about 5.8 kW while idling at this temperature.

A schematic of the reactor is shown in Figure 4-1 as it would appear with a probe installed. This particular configuration was chosen, in part, based upon calculations made with the EER Furnace Model. These calculations predicted that a nearly isothermal zone approximately 1-m long would be achieved by downfiring the reactor using a flame temperature equal to the set-point temperature of the reactor (i.e., the reactor temperature that would be maintained by the electrical heating elements alone). Other conditions considered were: slow heating by feeding cold simulated flue gases without any flame, maintaining temperature using only the electrical elements; and a rapid temperature decline obtained by downfiring with a flame temperature higher than the set-point temperature of the furnace controller. Calculated temperature profiles are shown in Figure 4-2 for several cases. In each instance, the profile is for temperature along the axis of the reactor. The delayed heating of the sample stream is indicated. Profile 1, specifically, was calculated for a non-adiabatic 5 kW stoichiometric methane-air flat flame stabilized on a 100°C water-cooled burner.

The reaction tube was a 99.8 percent alumina tube 96-cm long x 10-cm o.d. x 9.5-cm i.d. fitted with low-density alumina-silica refractory tubes at either end. The end tubes served two purposes. First of all, they protected the alumina tube from high thermal gradients at the ends, which might crack the tube. Secondly, they significantly reduced the conduction heat losses

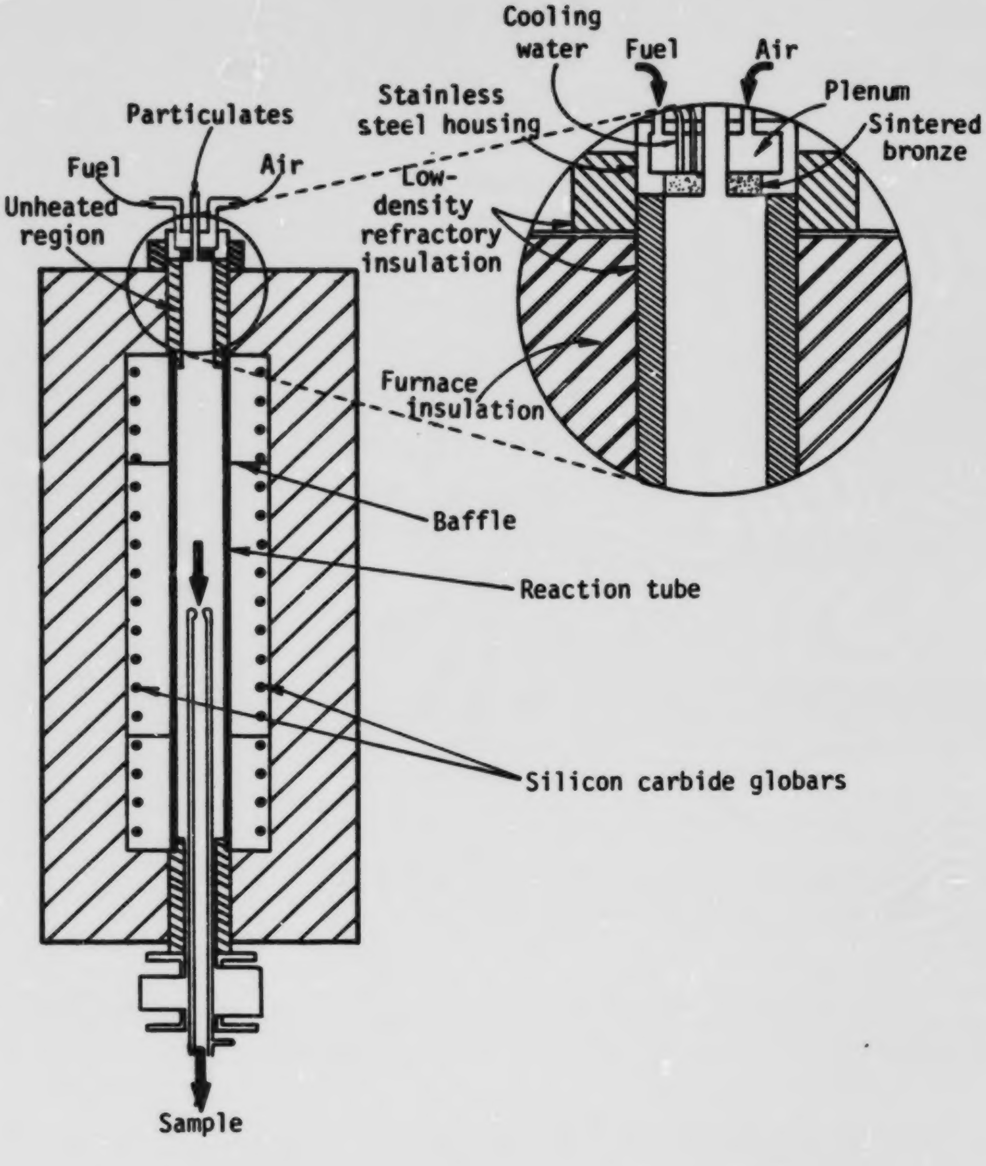
Cooling water
Fuel
Air
Stainless steel housing
Plenum
Sintered bronze
Particulates
Fuel
Air
Unheated region
Low-density refractory insulation
Furnace insulation
Baffle
Reaction tube
Silicon carbide globars
Sample

Figure 4-1. Detail of the isothermal reactor with burner and probe installed.

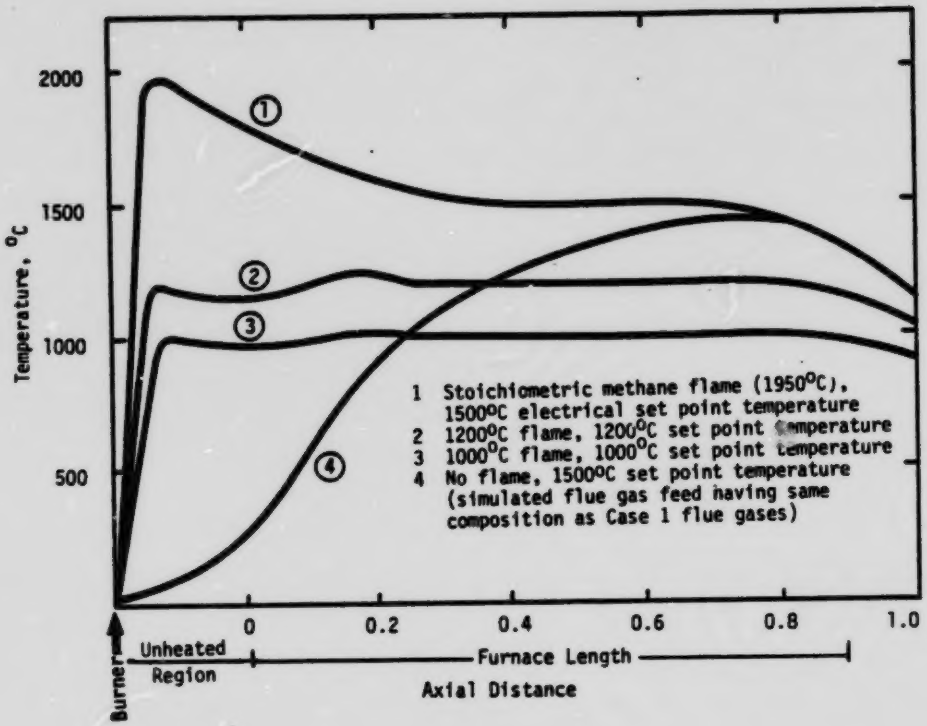

Figure 4-2. Centerline gas temperature profiles for the isothermal reactor system. Profiles are based on calculations using the EER furnace model.

from the furnace, preserving the flat temperature profile and protecting external furnace parts from heat damage. Other materials were also considered for the reaction tube. One of these was silicon carbide. The properties of thermal conductivity, emissivity, thermal expansion coefficient and chemical inertness, all at high temperature, are favorable for the intended application. Unfortunately, difficulties in manufacturing prevented its use. Also considered was 253 MA, an exotic stainless steel which contains silicon combined with the rare earth element, cerium. This alloy does not have the high temperature capabilities of the ceramic materials; however, it is highly resistant to chemical attack up to 1100°C and has excellent thermal shock resistance at lower temperatures where alumina is quite fragile.

The ITR is downfired by a porous-bronze-plug water-cooled flat-flame burner of identical design to the one employed in the TDR experiments. Most of the experimental work involved hydrogen flames although methane flames were employed exclusively in those cases where temperatures greater than 1350°C were involved. Limestone was injected into the ITR differently than in the TDR. Rather than laminar injection along the axis of the reactor, the limestones were injected from an axial 1.4-mm i.d. tube which initially produced a turbulent jet, rapidly dispersing the materials over a wide cross section of the reactor. (The local turbulence of the jet is due to the difference in velocity between the jet and the surrounding gases. Entrainment and momentum exchange which are responsible for dispersion of the sorbent, also quickly change the turbulence of the jet.) The residence times and heating rates of the particle streams were calculated based on confined jet mixing theory (26) and convective and radiative heat transfer calculations. Heating rates were on the order of 10^4 K/s. Total (end of reactor) residence times of 0.4 - 1.9 s were employed in this testing; residence times approaching 3.0 s are attainable in the ITR. Solids residence time in the ITR was adjusted by extending the water-cooled sampling probe up and down within the furnace.

Uptake of SO_2 by the sorbents occurred in-situ, and hence took place simultaneously with particle heatup and calcination. SO_2 was introduced by mixing it with the flame gas premixture prior to the burner. Both experimental (Appendix D) and analytical approaches (27) were employed to ensure that mass transfer of SO_2 into the sorbent stream would not impede SO_2 uptake by the sorbents.

Shakedown measurements confirming the temperature profiles in the ITR--with both hydrogen and methane flames--are presented in Appendix B.

4.2 Other New Apparatus

4.2.1 Fluidized Bed Off-Take Tube Assembly

The previous design of the off-take tube assembly for the fluidized-bed (FB) sorbent feeder did not function well with ultrafine particles. Prior solutions to clogging and pulsating flow included purge assemblies, FB operation at elevated pressure (40 kPa) and intense vibration of the entire FB assembly. While these approaches worked well with 10- μm materials, powders in the 1- μm diameter size range, and those which tended to clump or floculate, simply would not feed. A successful solution was the off-take tube assembly shown in Figure 4-3. This off-take tube provided an aspirating action at low transport air flow rates (7-10 cm^3/s) which enabled a smooth, dense (solid-to-gas ratio ~1:1 by mass) transport phase with a FB pressure of about 1.25 kPa.

4.2.2 ITR Solids Sampling Probe

Solids sampling within the ITR was accomplished with the water-cooled probe shown schematically in Figure 4-4. An important feature of this probe is the separation of the cooling jacket into two independent zones. Both cooling jackets are of a three-wall design. This permits water to enter through the outer jacket, thereby protecting the probe from the radiant flux of the reactor walls. The upper jacket provides the initial sample quench, rapidly cooling the samples to ~600°C in order to prevent further reaction. The lower jacket operates with a lower water flow rate. The water in the lower jacket is heated by the radiant flux to the outer wall of the probe.

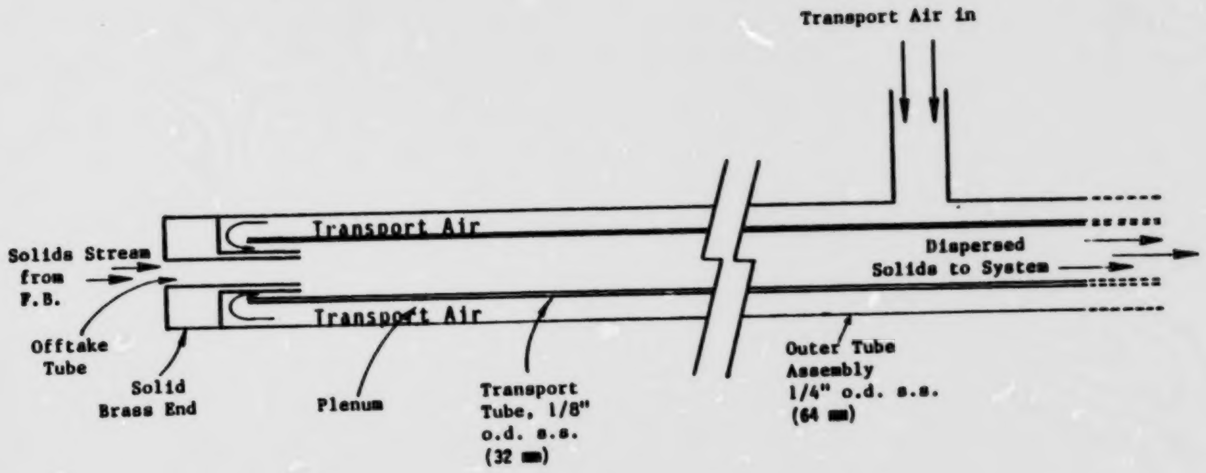
Transport Air in
Transport Air
Transport Air
Solids Stream from F.B.
Offtake Tube
Solid Brass End
Plenum
Transport Tube, 1/8" o.d. s.s. (32 mm)
Outer Tube Assembly 1/4" o.d. s.s. (64 mm)
Dispersed Solids to System

Figure 4-3. Modified offtake tube assembly for transport of ultrafine particulate using a fluidized bed feeder.

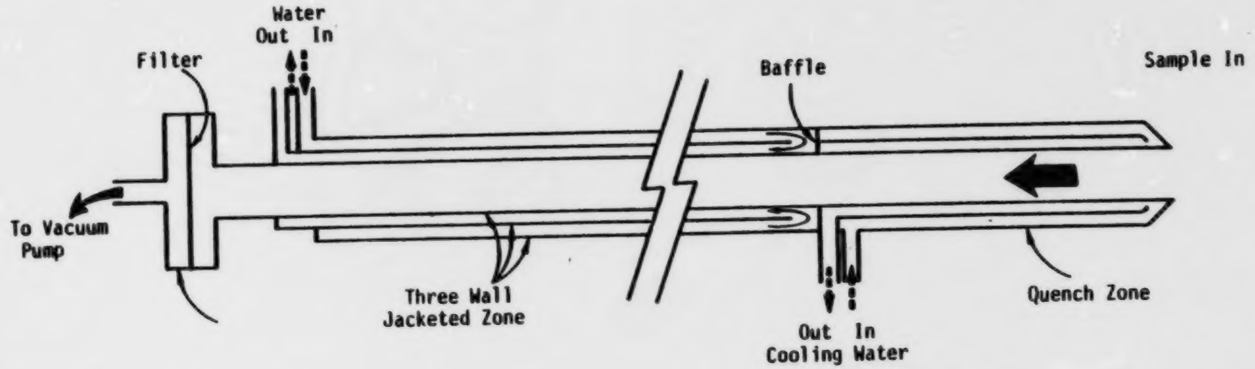
Water
Out In
Filter
To Vacuum
Pump
Three Wall
Jacketed Zone
Baffle
Out In
Cooling Water
Sample In
Quench Zone

Figure 4-4. Stainless steel sampling probe with rapid quench sampling orifice. Filter temperature is controlled by varying the water flrow through the lower jacketed zone.

While flowing down the inner wall, it maintains the sample temperature high enough to prevent moisture condensation at the probe walls or in the filter. Using this probe during isokinetic sampling, temperatures at the entrance to the filter can be adjusted from ambient to nearly 300°C. During normal operation, the temperature measured at the filter entrance is 150°C.

The probe, which was 1.2 m long, could be extended vertically within the ITR in order to sample solids after different residence times in the furnace. Samples could be collected within 40 cm of the sorbent injection location in the ITR, thus permitting sampling of the dispersed sorbent after short residence times (about 250 ms).

4.2.3 Fine Wire Thermocouple Probes

Gas temperatures within the ITR were measured using a fine-wire type-S thermocouple probe. The probe, shown in Figure 4-5, consists of a 0.025-mm diameter butt-welded type-S thermocouple supported by heavy platinum and 90 percent platinum/10 percent rhodium wires. Use of a butt-welded 0.025 mm diameter thermocouple wire minimizes radiation induced errors in the measured temperature. The support wires are cemented into a high-purity two-hole alumina rod with connecting wires leading to the cold end. The probe is 1.2 m long, enabling measurements to be taken from the exit of the reaction to within 40 cm of the burner.

4.2.4 Limestone Precalcination Apparatus

In order to generate high-surface-area precalcined materials for testing in both the TDR and ITR, the apparatus shown in Figure 4-6 was developed. Other approaches that were tested for precalcine generation are discussed in Appendix C. The apparatus in Figure 4-6 is a 20-cm diameter stainless-steel can placed inside a large electrically-heated box furnace. The can is fitted with a heavy lid which has a single hole for thermocouple access and to allow purge gas and CO_2 to escape. Limestone is supported in a thin bed on a 400 mesh stainless steel screen. Beneath the screen is a spiral made from 6.4 mm stainless steel tubing. The spiral has small holes drilled on the underside

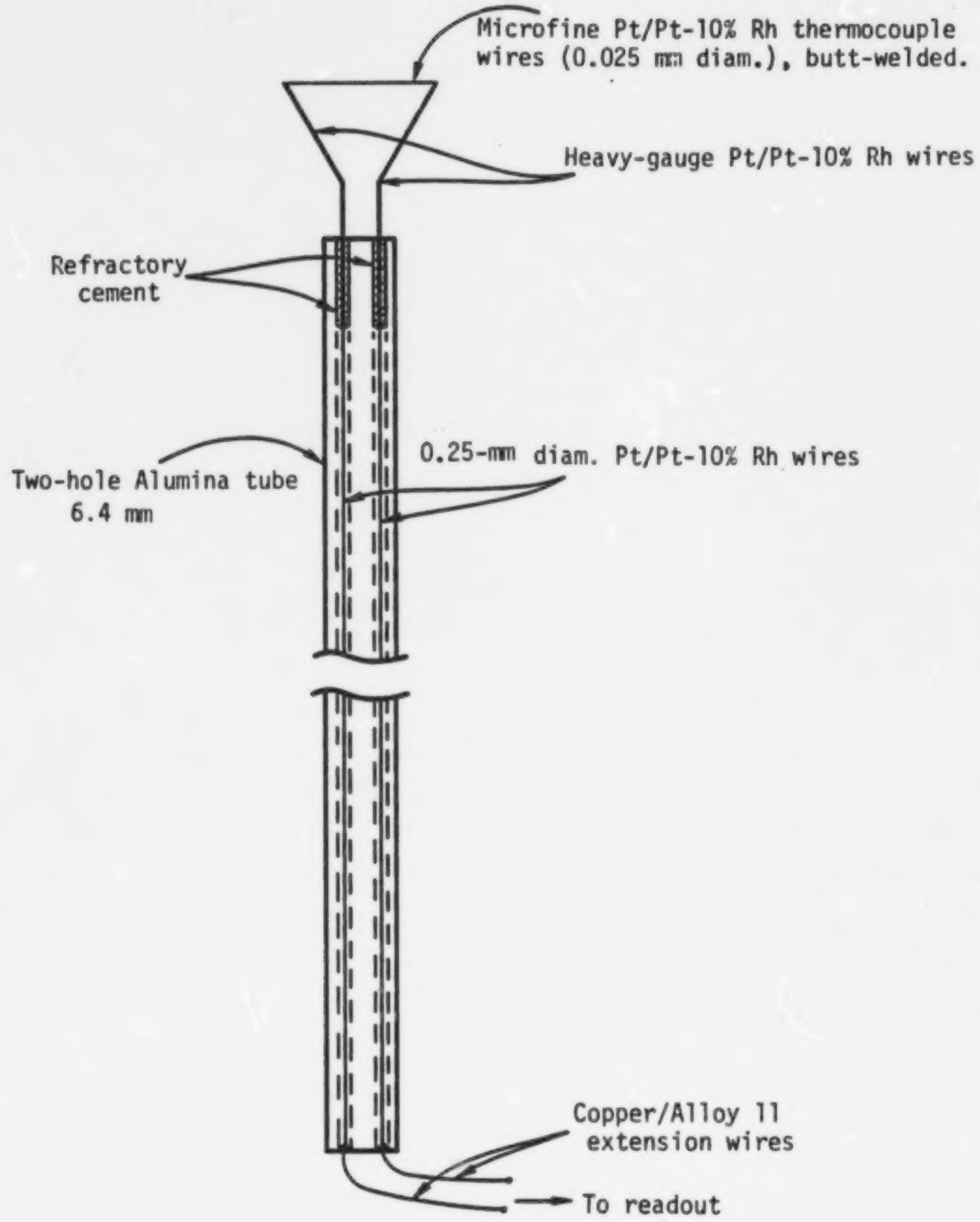
Microfine Pt/Pt-10% Rh thermocouple wires (0.025 mm diam.), butt-welded.
Heavy-gauge Pt/Pt-10% Rh wires
Refractory cement
0.25-mm diam. Pt/Pt-10% Rh wires
Two-hole Alumina tube 6.4 mm
Copper/Alloy 11 extension wires
To readout

Figure 4-5. A supported wire thermocouple probe for gas temperature measurements in the isothermal reactor.

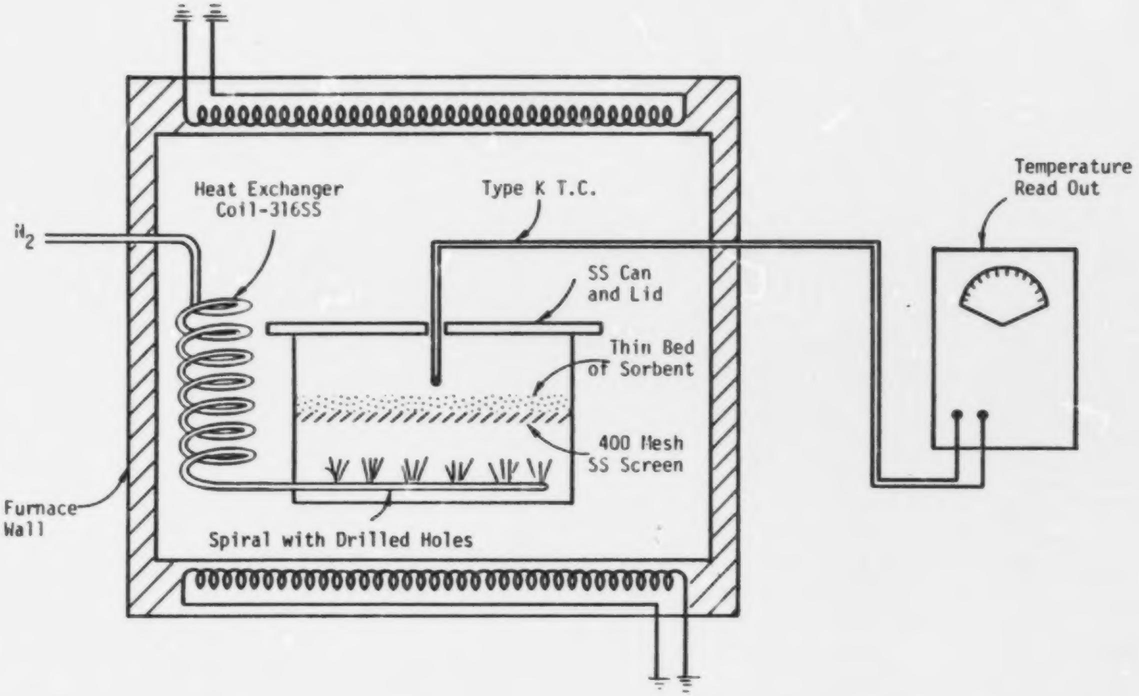

N_2
Heat Exchanger Coil-316SS
Type K T.C.
Temperature Read Out
SS Can and Lid
Thin Bed of Sorbent
400 Mesh SS Screen
Furnace Wall
Spiral with Drilled Holes

Figure 4-6. Apparatus for generation of precalcined sorbents.

and acts as a flow distributor for the purge gas which enters through the side of the can at the base. The purge gas, N_2, is preheated by passing through a long coil of stainless steel tubing located inside the box furnace. It was found that, even when operating with fine limestone having a mass mean size of 11 microns, the particles did not elutriate out of the bed; hence, no screen above the limestone bed was necessary.

Operation of the precalcination apparatus consisted of passing nitrogen through the bed of powdered limestone at high temperature. The mass of limestone and flow of nitrogen were balanced to provide the shortest practical calcination time at the lowest possible temperature. Typical operating conditions were 700°C, 60 g limestone, 0.55 L/s N_2. CO_2 resulting from calcination is swept away from the limestone by the nitrogen, thereby lowering the local CO_2 concentration and accelerating the calcination rate.

4.3 Analytical Procedures

Procedures employed for solid sample analysis have been described in a previous report (22) and will be discussed here only briefly. All of the routine analyses were performed in-house and are listed in Table 4-1. Additional analyses which were performed by outside laboratories are shown in Table 4-2.

The principle objective of samples' analyses was to determine the calcium utilization of sulfated limestones. A secondary parameter, generally determined to ensure data quality, was the extent of calcination. These were determined from the laboratory data using Equation (4-1), (4-2) and (4-3).

$$\text{Calcium Utilization} = 175 \times \frac{\%S}{\%CaO} \qquad (4\text{-}1)$$

$$\text{Calcination (Carbonate)} = 100 \times \left[1 - \frac{4.67 \times \%C}{\%CaO}\right] \qquad (4\text{-}2)$$

TABLE 4-1. IN-HOUSE ANALYTICAL PROCEDURES

PROCEDURES	DETERMINATION
Brunauer, Emmett, Teller N_2 adsorption isotherm	Specific Surface Area
Perkin-Elmer 240B Elemental analyser	Carbon, hydrogen determination Extent of calcination hydration
Leco SC32 instrumental Sulfur analyser	Total Sulfur
ASTM D2795 Chelometric Titration	Total Calcium

TABLE 4-2. ANALYTICAL PROCEDURES PERFORMED BY OUTSIDE LABORATORIES

PROCEDURES	DETERMINATION
Sedigran (X-ray sedimentation)	Particle size distribution, mean size
Mercury intrusion porisimetry	Pore size distribution, true porosity, porosity distribution

$$\text{Calcination (Hydroxide)} = 100 \times \left[1 - \frac{28 \times \%H}{\%CaO}\right] \qquad (4\text{-}3)$$

All three parameters are reported on a calcium basis only. For dolomitic materials, it was assumed that the magnesium component calcined rapidly and completely before substantial calcination of the calcium component was realized. Also, sulfation of magnesium oxide in dolomite has not been observed at these times and temperatures (8).

Specific surface area measurements by BET analysis were used in characterizing the physical properties of all of the raw sorbents, as well as in the study of precalcined, high-surface-area materials. Specific surface area measurements were also required as input parameters for a mathematical grain model (Section 5.6) for the limestone-SO_2 reaction. Previous results (22) have shown that the reactivity of a sorbent appears to be directly related to its surface area.

Table 4-2 lists analyses which were performed less frequently, or only for limited tests and so the procedures were not developed in-house. X-ray sedimentation was used to physically characterize raw limestone sorbents in terms of mean size and size distribution. This was also used in the grain model analyses. Mercury porisimetry was used to determine the pore size distributions of precalcined sorbents before and after sulfation and to relate that to sorbent reactivity (Section 5.4).

4.4 Sorbents and Additives

Table 4-3 lists the physical and chemical properties of the calcium-based sorbents employed in this program. Complete analyses were not available for all of the materials listed. Chemical analyses were performed by an outside laboratory. Specific surface areas for the precalcines and for the type-S dolomitic hydroxides varied from batch to batch and so representative values are indicated for each. Particle size distributions were available for two of the sorbents, Vicron 45-3 and D3002 dolomite. These are listed in Table 4-4.

TABLE 4-3. PHYSICAL AND CHEMICAL PROPERTIES OF LIMESTONE SORBENTS.

Material	Composition	Mean Size, μm	Surface Area*, m^2/g	Chemical Analysis, wt % Ca	Mg	Al	Si	Fe
Vicron 45-3	$CaCO_3$	11	0.6	39.2	0.49	0.07	0.07	0.04
Dolomite (Pfizer)	$CaCO_3 \cdot MgCO_3$	34	0.9	21.0	12.1	0.09	0.37	0.10
D3002 Dolomite	$CaCO_3 \cdot MgCO_3$	10	0.5	24.8	11.3	0.04	0.33	0.09
D60 Precalcine**	$CaO \cdot MgO$	---	60.7	---	---	---	---	---
V40 Precalcine***	CaO	---	41.4	---	---	---	---	---
Type S (Genstar)	$Ca(OH)_2 \cdot Mg(OH)_2$	1.4	18.2	28.6	16.0	0.26	---	0.07
Type S (Warner)	$Ca(OH)_2 \cdot Mg(OH)_2$	1.0	18.2	28.0	15.9	0.21	1.78	0.42
U.S. Gypsum A	$Ca(OH)_2$	---	10.3	---	---	---	---	---
U.S. Gypsum B	$Ca(OH)_2$	---	10.9	---	---	---	---	---
M and M Limestone	$CaCO_3$	6	1.1	---	---	---	---	---
German Hydroxide	$Ca(OH)_2$	---	14	---	---	---	---	---
RWE Hydroxide	$Ca(OH)_2$	---	26	---	---	---	---	---
Fisher Hydroxide	$Ca(OH)_2$	12.5	13	54.0	0.3	---	---	0.02

*With the exception of the D60 and V40 precalcines, the surface areas presented here are for the materials prior to calcination.

**D60 is the D3002 dolomite precalcined to approximately 60 m^2/g, using the apparatus in Figure 4-6.

***V40 is Vicron 45-3 precalcined to approximately 40 m^2/g.

TABLE 4-4. PARTICLE SIZE DISTRIBUTIONS OF RAW SORBENTS

Equivalent Spherical Diameter, μm	Mass Percent Finer	
	Vicron 45-3	D3002 Dolomite
80	100	100
50	100	99
30	95	97
20	80	80
10	46	42.5
8	37	35
5	24	21
3	14.0	13.5
2	8.5	10
1	3.0	5.5
0.8	2.5	4.5
0.5	1.0	3.1
0.3	--	1.0

Sorbent additives used to study mineral matter interactions and possible enhancement of calcium utilization are listed in Table 4-5. When available, the materials used were ACS reagent grade. Many of the materials were not available in powder form. In these cases, the additives were pulverized by hand using a mortar and pestle. In general, the additives were added to sorbents to make 5-percent-by-weight mixtures. The mixtures were first stirred with a spatula to distribute the additives and then sifted several times with a kitchen sifter to ensure complete and uniform dispersion.

TABLE 4-5. SORBENT ADDITIVES AND MINERALS

Mineral/Additive	Form
Kaolin, $Al_2Si_2O_5(OH)_4$	Powder, 1 μm, 9.4 m^2/g
Cr_2O_3	Powder
Na_2CO_3	Fine granules
$NaHCO_3$	Fine granules
K_2CO_3	Fine granules
$KHCO_3$	Fine granules
Li_2CO_3	Fine granules
Na_2SO_4	Anhydrous Powder
K_2SO_4	Anhydrous Powder
MoO_3	Powder
MoS_2	Powder (plateletts)
V_2O_5	Lump
TiO_2	Powder
Pt-black	Finely divided - 10 m^2/g, 0.07 μm diam
P_2O_5	Lump
NaCl	Granules

5.0 RESULTS AND DISCUSSION

Results are presented in this section from the experimental efforts which directly addressed the objectives of this program. A considerable body of data was also generated through ancillary experiments. These were required for the definition of experimental conditions and the development of new procedures or experimental techniques. The supplementary results are presented in the appendices.

The development of, and results from, the technique for batch generation of high-surface-area precalcined sorbents are discussed in this section. Also, data collected from both the flame thermal decomposition reactor (TDR) and the isothermal reactor (ITR) are presented. These data explore the effects of residence time and temperature on the reactivity of a wide variety of sorbents. Also, they are used in conjunction with a mathematical model for SO_2 sorption (referred to as the grain model) to predict boiler capture, and to make quantitative estimates of the effects and extent of sintering during sulfation. Mercury porisimetry data are presented of high-surface area precalcines, before and after sulfation at low temperatures, providing insight into the nature of sorbent reactivity and possibly into differences in reactivity between dolomitic and calcitic sorbents. The use of additives, or sorbent reactivity promoters, is studied, along with discussion of their potential for improvements in the limestone-SO_2 process. Finally, the grain model for sorbent reactivity, mentioned above, is described. The usefulness of the model for interpreting reactor data is shown, as well as means for applying the data and model together to make utilization predictions.

5.1 Generation of Precalcined Sorbents

Calcium-based sorbents must calcine to yield calcium oxide before significant reaction with SO_2 can occur. The calcination of a limestone or dolomite generally increases the surface area of the sorbent, due to the increased porosity that is created when the CO_2 is driven off. Sorbent reactivity has been shown in past work (22) to be directly related to the surface area (although other variables, such as pore size distribution, might also play a role). When raw (uncalcined) carbonates are injected into a furnace environment and calcine in situ in a fraction of a second at high temperatures (e.g., 1250°C), the surface areas measured on extracted solid samples are generally relatively low (typically 5 to 15 m^2/g for a limestone), likely due to thermal sintering which occurs simultaneously with calcination at those temperatures. On the other hand, when sorbents are calcined at lower temperatures (e.g., 700°C), much higher areas can be generated because thermal sintering is less severe. At such low temperatures, an extended particle residence time can be required for calcination (e.g., half an hour or longer), and a high sweep gas flow past the particles is necessary to remove the evolving CO_2 (since the local presence of CO_2 during calcination appears to reduce the surface area). As part of this project, tests were designed to measure the reactivity at upper furnace temperatures of high-surface-area sorbents which had been precalcined at the controlled, low temperature conditions prior to furnace injection at high temperature. A key concern was whether the high-area precalcines could capture significant amounts of SO_2 before the surface area was lost to thermal sintering at upper furnace conditions.

Therefore, an important task in this program was the generation of precalcined sorbents for subsequent SO_2 reactivity testing. This effort was carried out in parallel and in cooperation with similar in-house efforts by researchers of the LIMB Development Branch of the EPA's Air and Energy Engineering Research Laboratory (6, 28). Some of this EPA in-house research has been directed toward examining the kinetics and physical phenomena associated with calcination and the production of high-surface area sorbents. Their results have been useful in understanding and overcoming the difficulties of batch production of materials in quantities sufficient for testing in the isothermal reactor (ITR).

Both calcitic and dolomitic precalcined limes were produced, using Vicron 45-3 limestone and D3002 dolomite as the raw materials. Parametric studies were initiated to determine the most practical operating conditions for batch production of high-surface-area materials. Also part of the precalcination program was the study of the storage stability of high-surface-area materials under nitrogen, dry air, and CO_2.

5.1.1 Parametric Evaluation of Precalcination

In order to establish the optimal conditions for generation of high-surface-area precalcined materials, a brief parametric study was carried out using Vicron 45-3. A small batch (35 g) of the limestone was spread evenly across the support screen of the precalcination apparatus shown previously in Figure 4-6. Despite the small size of the limestone particles (50 percent < 11 μm) a negligible amount actually passed through the 400 mesh screen. The experiment was conducted by increasing the time allowed for calcination of successive batches until the mass recovery was approximately the 19.6 g expected at 100 percent calcination. Results of these experiments are shown in Figure 5-1. Calcination times and other experimental details are provided in Appendix A, Table A-1.

Several features are worth noting concerning the data in Figure 5-1. The slopes of the surface area versus calcination curves begin to increase after 70 percent calcination and continue to increase as 100 percent calcination is approached. Since the extent of calcination increases monotonically with time, this increase in slope suggests that calcination under these conditions is mass-transfer limited--as will be explained below.

Due to limitations of thermodynamic equilibrium, the local CO_2 concentration around a $CaCO_3$ particle cannot exceed about 3 percent (3.1 kPa) at 700°C and about 9.5 percent (9.6 kPa) at 750°C (29) if the calcination reaction is to proceed. As a result, assuming that chemical kinetics are not controlling, calcination can occur only as fast as the nitrogen sweep gas can remove CO_2. Under these circumstances the maximum rate of calcination can be expressed as

$$\frac{dCaCO_3}{dt} = \frac{X_{CO_2} \times Q_{N_2} \times M_{CaCO_3}}{24450\ \text{cm}^3/\text{mol}} \qquad (5\text{-}1)$$

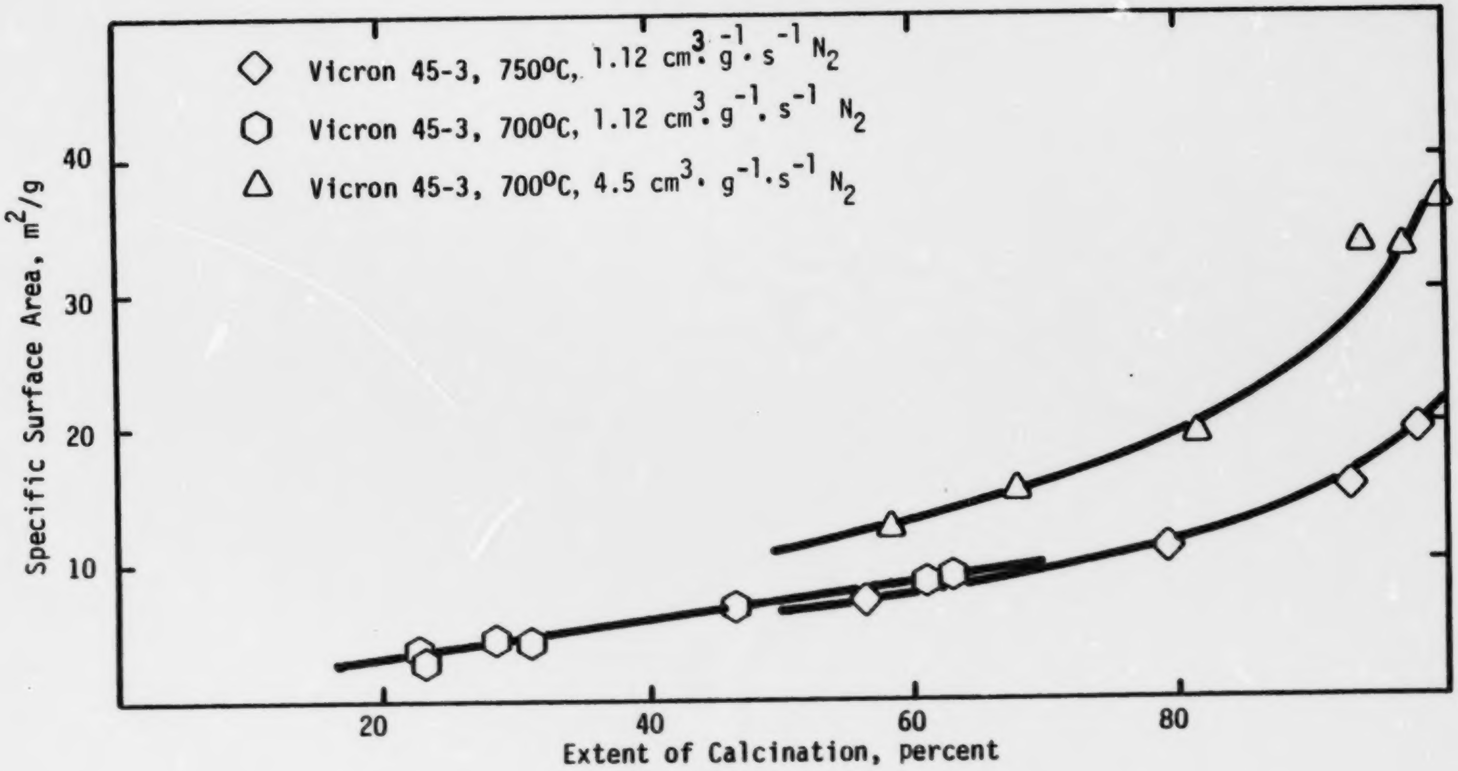

Figure 5-1. Specific surface area vs. extent of calcination - Vicron 45-3 calcined in the transpirated thin bed. Variables are temperature and nitrogen flow rate.

where:

$\frac{dCaCO_3}{dt}$ = molar rate of calcination, $mol \cdot s^{-1}$

X_{CO_2} = equilibrium mole fraction CO_2 at 1 atm over $CaCO_3$

Q_{N_2} = sweep gas flow rate per initial mass of $CaCO_3$, $cm^3 \cdot g^{-1} \cdot s^{-1}$

M_{CaCO_3} = mass of $CaCO_3$, g

If Equation (5-1) is divided by M_{CaCO_3}, it is seen that the rate of calcination increases although the mass of calcium carbonate is decreasing. Referring back to Figure 5-1, it was shown that the incremental specific surface area also increases as calcination proceeds. Coupling these observations suggests that faster calcination results in higher specific surface area. This is also demonstrated by the difference in the two curves for 700°C, where a four-fold increase in nitrogen flow rate (and, by implication, a corresponding increase in calcination rate) results in roughly a 5 m^2/g increase in surface area at a given value for the extent of calcination. Comparison of Equation (5-1) with the calcination times in Appendix A will show that, in fact, the actual rate of calcination is somewhat slower than predicted. This illustrates that CO_2 removal by the N_2 is not 100 percent efficient.

Figure 5-1 also shows that increasing the temperature from 700 to 750°C did not increase the surface area despite the fact that, according to Equation (5-1), the calcination rate could have increased by a factor of three due to the increased equilibrium mole fraction of CO_2. This illustrates another factor which comes into play during calcination, namely sintering. The rate at which a calcine sinters increases with temperature (30). The data in Figure 5-1 suggest that any effects increased calcination rate on surface area at 750°C were more than offset by an increase in the rate of sintering.

At 700°C, increasing the sweep gas flow rate by a factor of 4 resulted in a 50 percent increase in surface area at 60 percent calcination. The non-proportional behavior suggests a limit to the surface area attainable by this technique. Figure 5-2 shows the effect of sweep gas flow rate on surface area attained at nearly complete calcination. The data shown on Figure 5-2 are for samples removed from the furnace at the shortest time found to produce near-complete calcination under each condition, in order to reduce the effects of sintering due to prolonged exposure to 700°C. Because of this, there is a general increase in calcination time with decreasing sweep gas flow rate. The higher flow rates were achieved by decreasing the sample mass as well as increasing the volumetric flow of nitrogen. It would appear that the limit for area generation in Vicron 45-3 using this particular apparatus is about 50 m^2/g.

It is now clear that there is a limit to the surface area attainable by this technique. Comparison of the time for complete calcination at 39 $cm^3 \cdot g^{-1} \cdot s^{-1}$ (40 min, Appendix A, Table A-1) with that predicted by Equation (5-1) (210 s) shows that convective mass transfer is no longer controlling the calcination rate. Neither is it kinetically controlled; based on interpretation (22) of differential reactor data (31), a calcination time of about 1 minute would be predicted based upon calcination kinetics.

Physical observation of the sorbent bed after calcination provides an explanation for this discrepancy. When calcination is complete, the sorbent layer is found to be broken up into "islands" about two- to- four-cm across. Furthermore, the calcine in these islands is fused together into extremely friable plateletts. The channels between the islands provide space for channelling of the sweep gas. The net result is that the N_2 is not lowering the local CO_2 concentration around individual particles, but, rather maintains a lower CO_2 level in the free stream gas. In practice, therefore, the calcination rate by this approach appears to be limited by diffusion of CO_2 from the sorbent bed into the free stream of sweep gas.

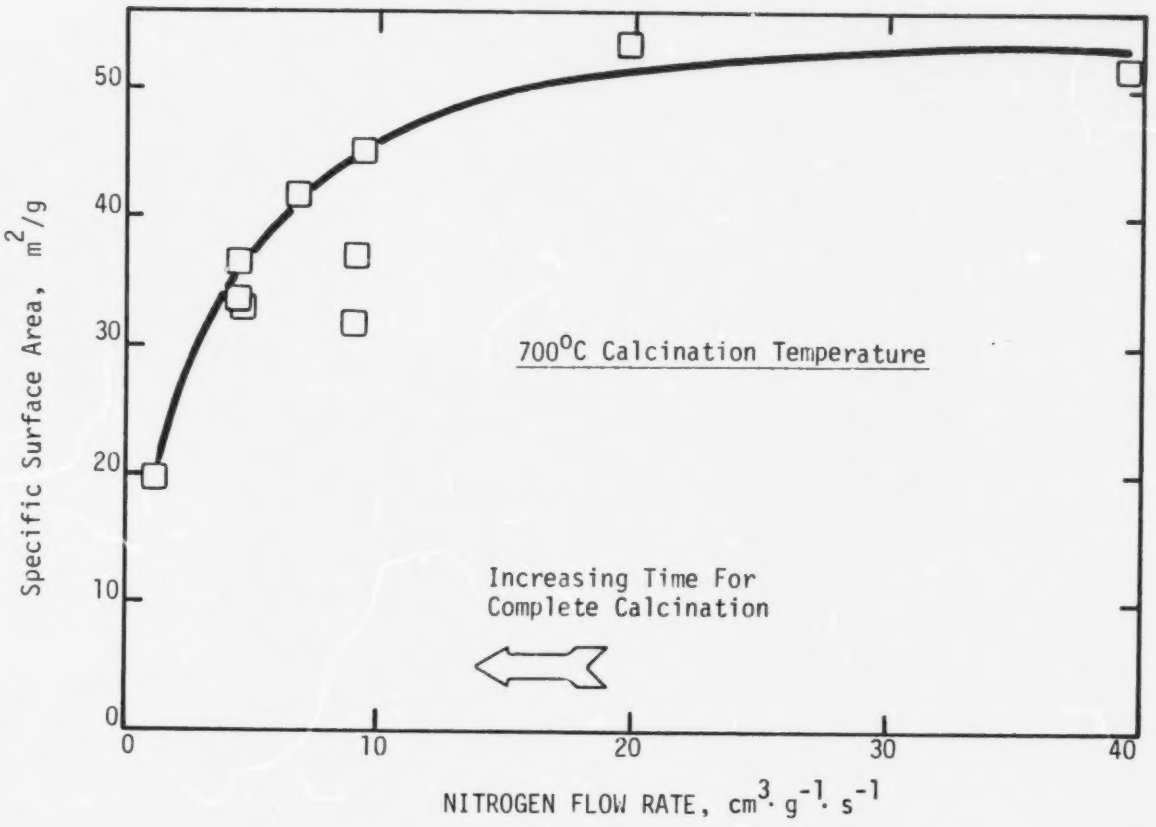

Figure 5-2. Effect of sweep gas flow rate on surface area developed at complete calcination by Vicron 45-3 in the precalcination apparatus at 700°C.

5.1.2 Storage Stability of Precalcines

In any commercial application of precalcined sorbents, an external precalcination system would be located either adjacent to, or possibly remote from, the boiler into which the precalcine was to be injected. The precalcine would thus have to be transported a number of feet, or a number of miles, and possibly stored for some period of time before injection. A key concern is how well the precalcine would retain its high surface area, and whether any special storage requirements (e.g., under nitrogen) would exist.

Thus, an integral part of the precalcine study was examination of the storage stability of precalcines at ambient temperature. Precalcined Vicron 45-3 and D3002 dolomite with various initial specific surface areas were placed in septum vials. The vials were then evacuated of all gases and backfilled with either N_2, dry air, or CO_2. Periodically, some of these materials were removed and analyzed for specific surface area and H_2O and CO_2 uptake. Figure 5-3 shows the results of these tests. In several cases the points shown represent two or more overlying data.

Only two samples experienced a severe drop in surface area, and in each of these instances it was found that the samples had taken up water. The first instance was a precalcined Vicron 45-3 with an initial surface area of 30 m^2/g. The sample had an initial water content of 10.5 percent and was stored in atmospheric rather than dry air. After nine days, the surface area had dropped 10 percent to 27 m^2/g. After 56 days, however, the surface area had decreased to 9 m^2/g and the water increased to 17 percent. In the second instance, a precalcined dolomite with an initial surface area of 22 m^2/g--which had been stored for 97 days in nitrogen with no loss in surface area--was then transferred to a container backfilled with CO_2 and stored for another 30 days. Upon analysis it was found that the surface area had dropped to 12 m^2/g, concurrent with an increase in water content from 1.2 to 4.5 percent, suggesting that water vapor had inadvertently been introduced when the material had been transferred to the CO_2 container. There was, however, no noticeable change in the CO_2 content of the sample.

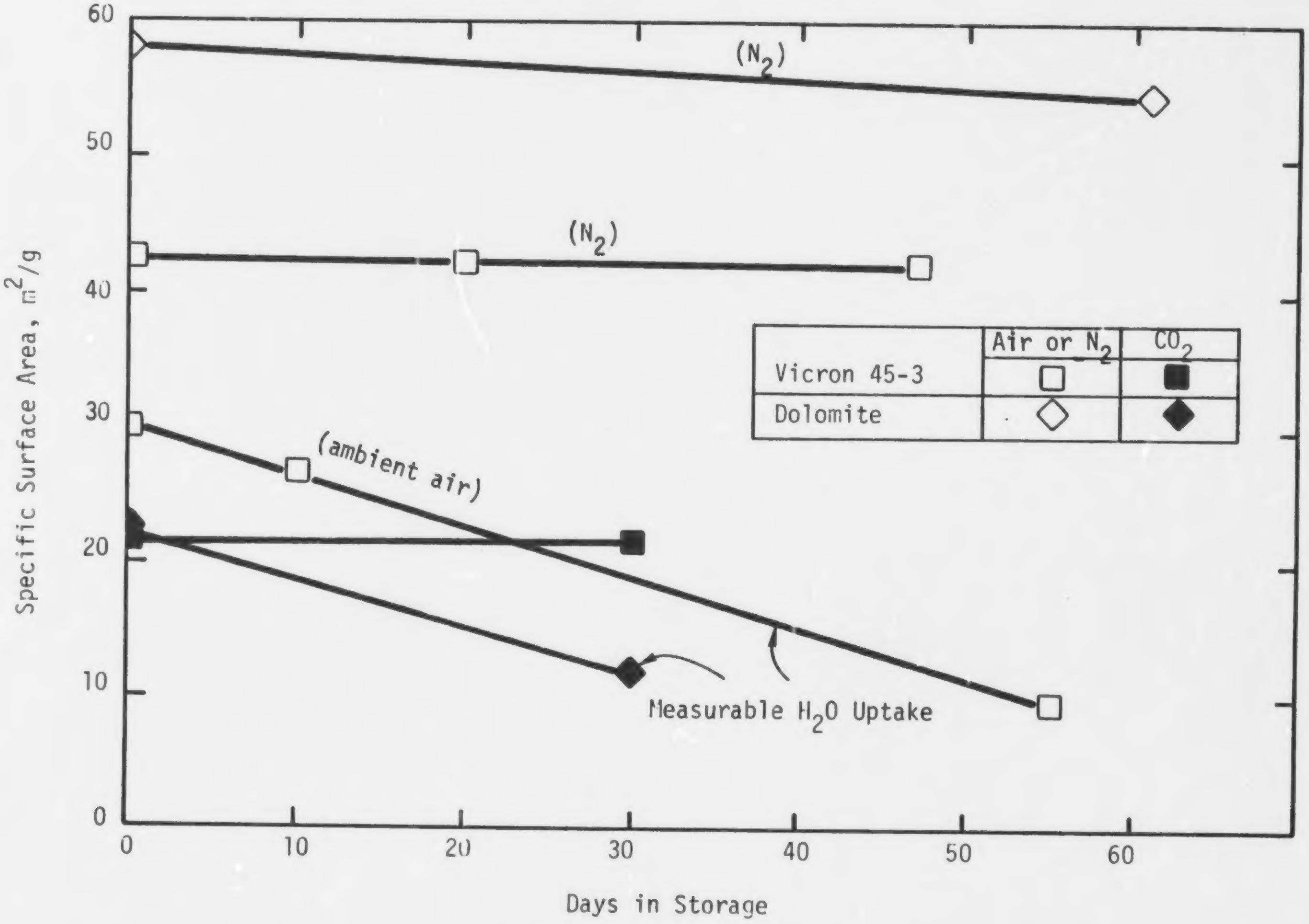

Figure 5-3. Loss of surface area by precalcined sorbents during storage.

No difference was found between materials stored in any of the three gases, so long as water vapor was not present. In most cases, a moderate but not significant loss of surface area was observed with time. This showed that in the absence of hydration, the specific surface area of precalcines is stable over reasonably long times.

The impact that this result would have on bulk storage of precalcines is not clear. These tests only showed the circumstances under which a precalcine is desurfaced with time; and, to some extent, the rate at which this occurs. It is conceivable that during the storage of ton quantities of material the portion which is desurfaced amounts only to a "skin" covering the bulk where it is exposed to air.

5.2 Flame Processed Sorbent Reactivity

The reactivities of four sorbents calcined at flame and upper furnace conditions in the thermal decomposition reactor (TDR) were measured with the SO_2 reactivity probe. Results for the Pfizer Dolomite were first presented in an earlier report (22) but are included for comparison. These tests were performed in order to compare the effect of calcination temperature on reactivity for a variety of sorbents. The sorbents were calcined at peak temperatures ranging from 1100 to 1630°C by injection into the TDR, operating with a methane-air flame; under TDR conditions, particle heating rates are rapid (ca. 5×10^4 K/s), so that calcination is also rapid. After a residence time of no more than 250 ms in the TDR, the calcined materials were then extracted from the unit, still in the dispersed phase, and exposed to SO_2 in the reactivity probe under controlled, reproducible conditions (1100°C, 0.6 s, 6 percent SO_2). The sulfation of all materials under constant conditions, independent of calcination conditions, simplified the interpretation of the sulfation data and allowed direct comparison of the results obtained for different TDR peak calcination temperatures. It is emphasized that the reactivity probe is an experimental convenience; the calcium utilizations measured with this probe might be higher than would be achieved in a real boiler, since the sorbent in the probe experiences a very high level of SO_2 at a near-optimum temperature for a relatively long residence time.

The data for the four sorbents are shown in Figure 5-4, along with a shaded band indicating the range of data obtained for Vicron 45-3 during the previous effort. The M&M limestone, although it had a smaller mean size (6 µm), showed approximately the same reactivity as raw 11 µm Vicron 45-3. The German hydroxide was more reactive than raw Vicron. The precalcined Vicron 45-3, with a surface area of 34 m^2/g, displayed considerable advantage over all but the Pfizer dolomite. At the high-temperature side of the graph all of the data appear to be converging. All of the data show the same trend of increasing reactivity with decreasing calcination temperature, as would be expected based on surface area data (22); thermal sintering, and hence deactivation, becomes less severe for all sorbents at lower temperatures. In addition, between 1200 and 1100°C a dramatic increase in reactivity occurs.

Some experimental details for these TDR tests are presented in Appendix A, Table A-2.

Figure 5-5 displays the reactivity ranking for eight sorbents injected into the TDR at peak temperatures of a) 1200°C and b) 1500°C. These data supplement the curves in Figure 5-4 and show again that as the calcination temperature is increased, all of the sorbents' reactivities are severely diminished. At 1500°C, in fact, a change in reactivity ranking occurs with the D3002 dolomite, although the difference between that and the 34 m^2/g precalcine is so small that it may not be significant.

Figures 5-4 and 5-5 also indicate that at low injection temperatures, the dolomitic materials are distinctly superior to all of the calcitic materials on a calcium utilization basis. This behavior is consistent with previous observations in bench-scale studies (5). However, the small difference between the 34 m^2/g precalcine and the D3002 dolomite--indeed, the superiority of the precalcine over the other high-calcium materials--suggests that careful preparation of quicklimes might produce a practical high-calcium

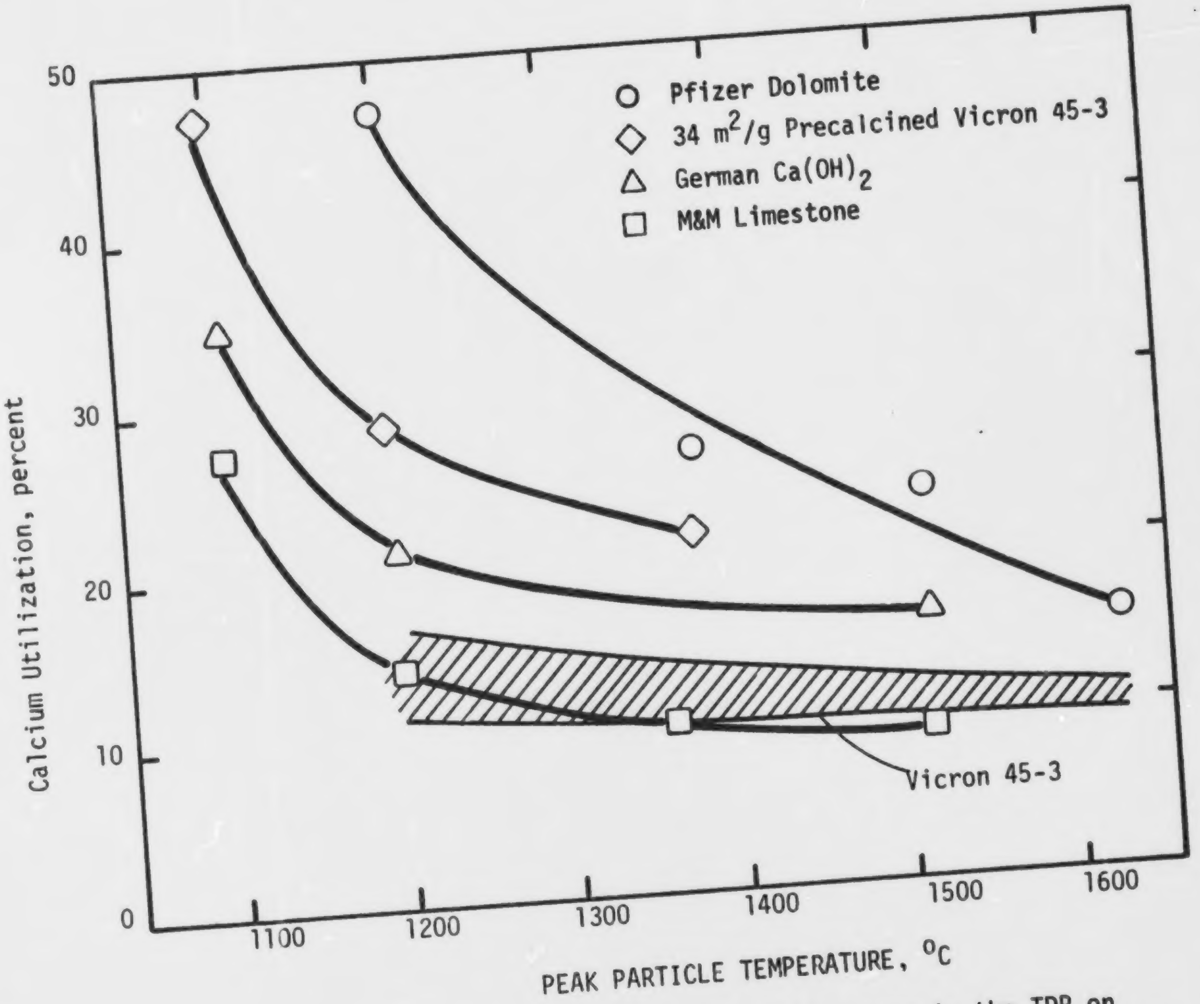

Figure 5-4. Effect of peak calcination temperature in the TDR on subsequent SO_2 uptake in the dispersed-phase reactivity probe (1100°C, 6% SO_2, 0.6 s).

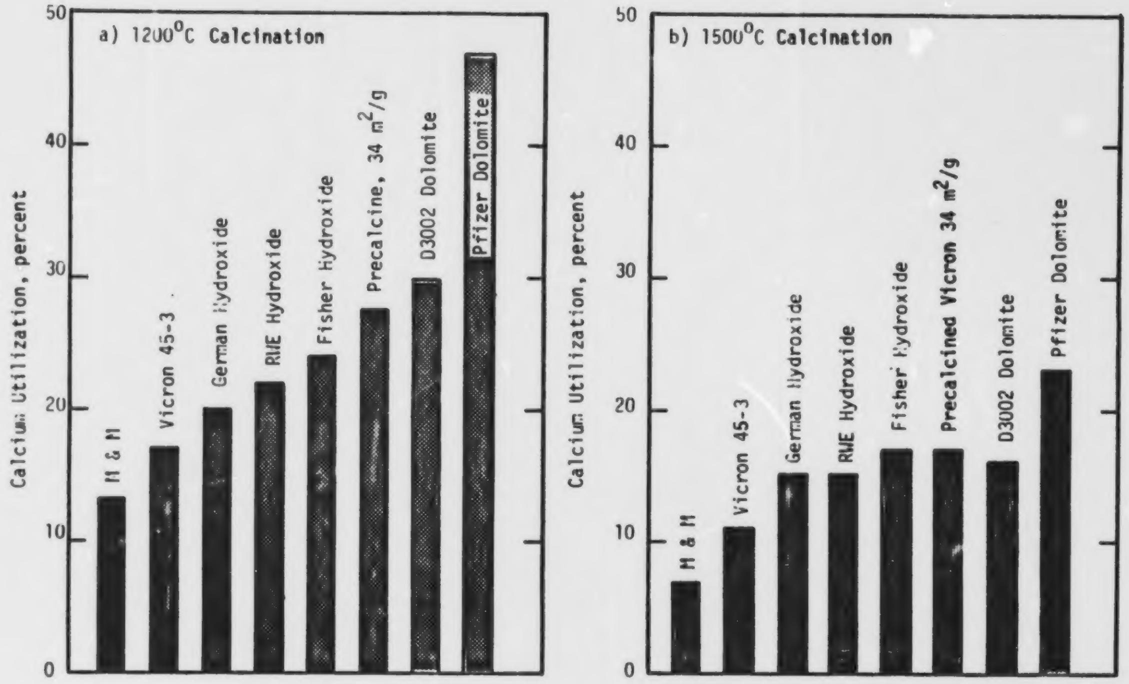

Figure 5-5. Reactivity ranking of eight sorbents calcined in the thermal decomposition reactor at 1200 and 1500°C. Subsequent reactivity probe conditions were 1100°C, 0.6 s, 6% SO_2.

sorbent (although, as discussed in Section 5.3, precalcines did not show this same degree of superiority in the ITR tests).

The SO_2 reactivity probe was used without the TDR in an attempt to examine coincident calcination and sulfation. An auxiliary furnace was added to the probe to heat the sorbent stream to 650°C at the entrance to the 1100°C reaction zone so that the entrance conditions would be unchanged relative to when the probe was used with the TDR. Sorbents were injected both with an without SO_2, and their specific surface areas and extents of calcination were measured. Calcium utilization was determined for the samples injected with SO_2. The data are presented in Table 5-1.

In the absence of SO_2, only dolomite showed an exceptional increase in surface area after calcination. All of the sorbents displayed relatively low extents of calcination. Since the extents of calcination were higher in the presence of SO_2, this indicates that recarbonation (or rehydration, as the case may be) occurred during sampling; in the presence of SO_2, the sulfation reaction consumed the most reactive sites, reducing the amount of recarbonation/rehydration that was possible. The precalcined material used in this test was incompletely calcined to start with, and its extent of calcination did not appear to increase after injection without SO_2. In summary, the results of this reactivity probe test series are ambiguous, because of recarbonation/rehydration during sampling, and possibly because of incomplete calcination of some of the raw sorbents at 1100°C/0.6 s.

5.3 Isothermal Reactivity Tests

The isothermal reactor (ITR) was used for the majority of the reactivity tests performed in this study. It is complementary to the TDR because it allows exploration of calcination/sulfation phenomena at a lower range of temperatures (900-1200°C) and at a full range of residence times (from 0.25 s up to 2.0 s), not achievable in the TDR. Furthermore, sulfation in the ITR occurs under isothermal conditions, and hence can be studied as a function of residence time at constant temperature. As a result, fundamental data are

TABLE 5-1. PROPERTIES OF SORBENTS AFTER INJECTION INTO THE DISPERSED-PHASE SO_2 REACTIVITY PROBE WITHOUT THE TDR. THE SORBENTS WERE NOT FLAME TREATED BUT WERE HEATED TO 650°C BY AN AUXILIARY FURNACE LOCATED JUST PRIOR TO THE REACTION ZONE OF THE PROBE. 1100°C, 0.6 sec, 6% SO_2.

SURFACE AREA AND EXTENT OF CALCINATION AFTER INJECTION INTO THE SO_2 REACTIVITY PROBE

	Initial SA,	Without SO_2,		With 6% SO_2,		Calcium Utilization
Sorbent	m^2/g	m^2/g	Percent Calcination	m^2/g	Percent Calcination	Percent
Precalcine	19.3	11	67.9	9.2	99	19.7
Dolomite (Pfizer)	0.9	25.4	47.8	4.2	74.5	28.5
German hydroxide	13.6	19.2	66.9	2.2	92.4	34.1
RWE hydroxide	26.2	14.9	50.7	5.6	86.4	20.3
Fisher hydroxide	12.7	15.3	42.7	3.1	80.6	22.0

provided to aid in mathematical model development and in the further understanding of the sulfation process.

5.3.1 Calcium Utilization Profiles

Calcium utilization was measured as a function of residence time in the ITR for five sorbents at temperatures of 900, 1000, 1100 and 1200°C. The five sorbents include: raw Vicron limestone and raw D3002 dolomite; precalcined Vicron (labeled V40) and D3002 (labeled D60), precalcined to 40 and 60 m^2/g, respectively; and Warner Type S pressure hydrated dolomite. The data are presented in Figures 5-6 through 5-9. In each case, the ITR was operated with a hydrogen-air flame, doped with SO_2 such that the initial SO_2 concentration in the burned gases was 3600 ppm. The sorbent feedrate was adjusted to ensure a calcium-to-sulfur ratio (Ca/S) less than 1.0 so that in no case would the SO_2 concentration be significantly depressed (i.e., so that the reaction would not be limited by an inadequate amount of SO_2).

At 900°C (Figure 5-6) the utilizations of the D60 precalcine and the Type S hydrate are distinctly the greatest at all residence times, the V40 precalcine being the next most reactive. The raw Vicron and dolomite are the least reactive, especially at low residence times; the roughly half-second delay in the onset of sulfation for the raw sorbents is undoubtedly due to the time required for particle heatup and calcination at this relatively low temperature. The precalcines, being already calcined, do not experience this delay, and have almost reached their ultimate sulfation level before the raw stones have even started sulfating. The Type S sorbent also appears to suffer no delay due to calcination (dehydration); the dehydration of the hydrate requires a lower temperature, and is less endothermic, than the calcination of the raw carbonates, so that even at 900°C, dehydration appears to offer no impediment to sulfation. The similarity in the reactivities of the 60 m^2/g D60 and the Type S at all times might be an indication of the surface area attained upon dehydration by the Type S material. The D60 would not be expected to sinter (lose surface area) so rapidly at this temperature.

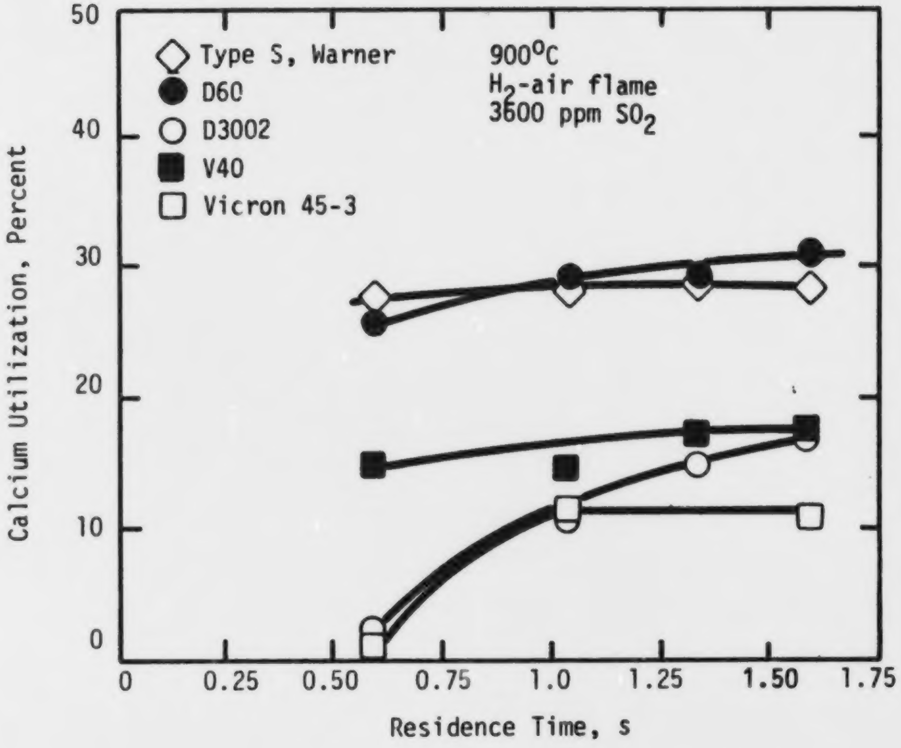

Figure 5-6. Calcium utilization profiles for five sorbents at 900°C.

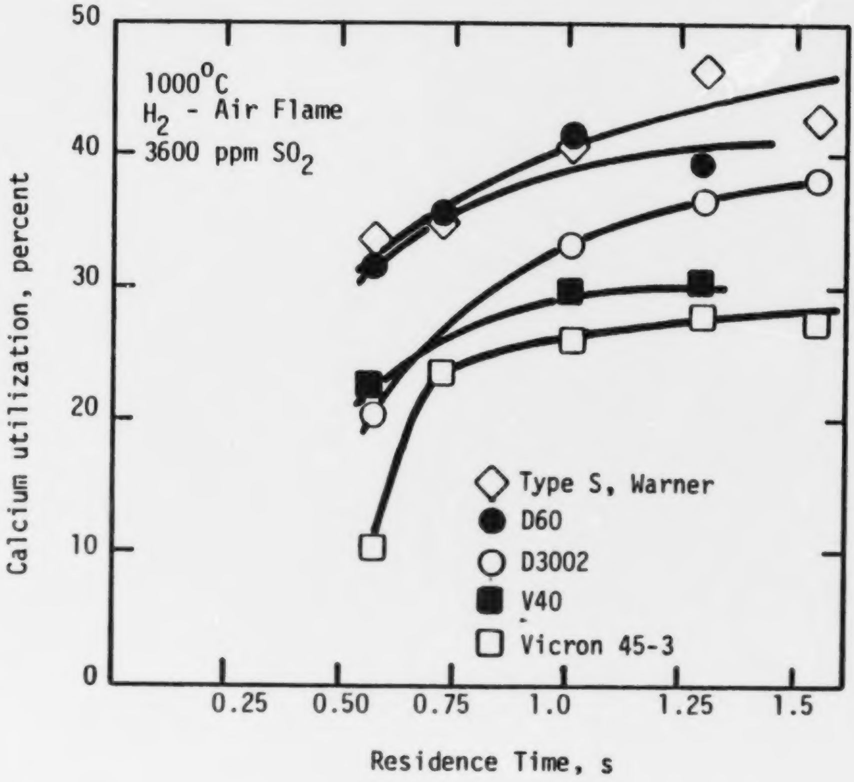

Figure 5-7. Calcium utilization profiles for five sorbents at 1000°C.

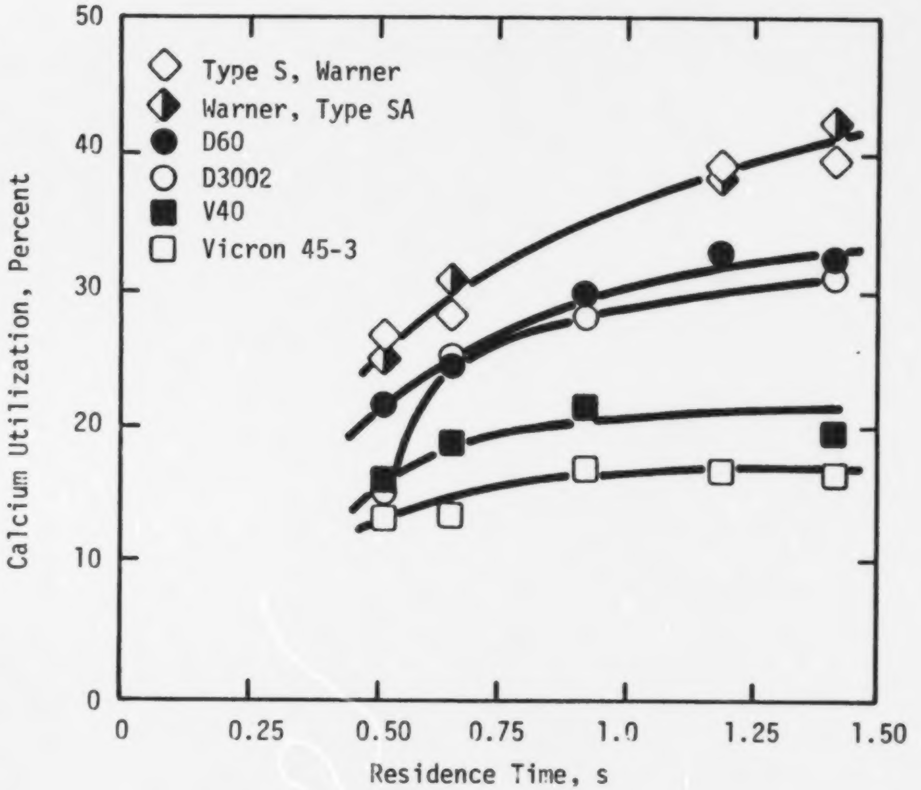

Figure 5-8. Calcium utilization profiles to five sorbents at 1100°C. Type SA is a type S hydroxide with an air-entraining agent added.

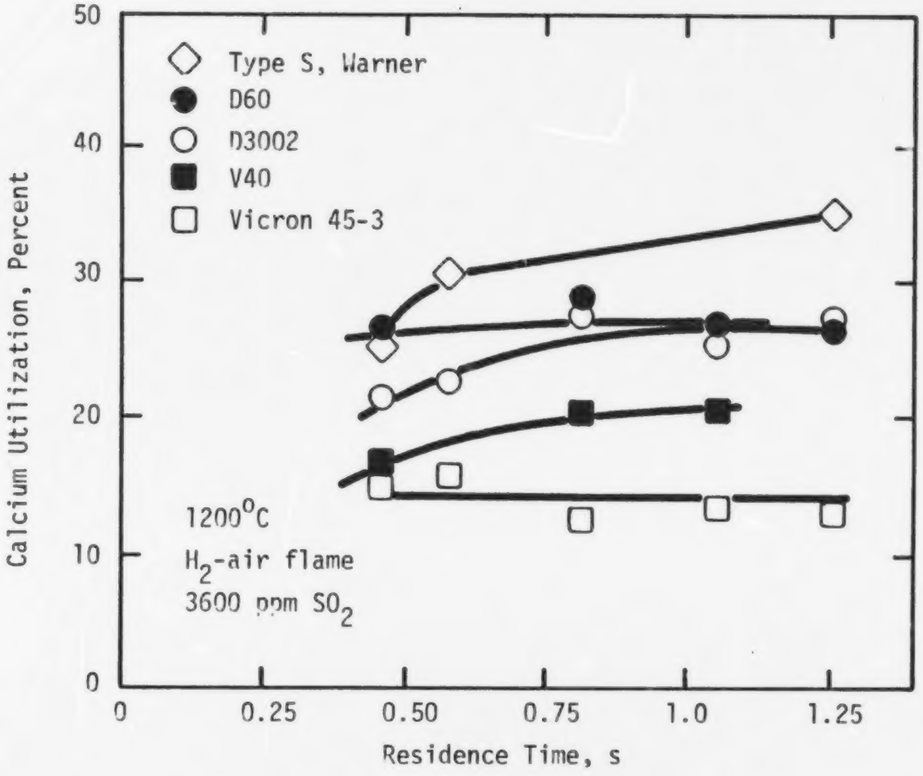

Figure 5-9. Calcium utilization profiles for five sorbents at 1200°C.

All five sorbents appear to be approaching an effective "ceiling" on utilization at long residence times (although the utilization of D3002 still seems to be climbing somewhat after 1.5 s). This ceiling--at far less than 100 percent utilization--reflects a significant slowing of the sulfation rate, presumably due to increases in pore diffusion resistance (as internal sorbent pores become blocked due to sulfation and thermal sintering) and to increases in product layer diffusion resistance (as the sulfate layer becomes thicker). The D60 and the Type S achieve the highest utilization before leveling off (about 30 percent); the V40 and the raw dolomite reach a lower utilization (less than 20 percent); the raw Vicron had the lowest ceiling of all (about 10 percent). The raw Vicron was only one-half calcined at 900°C (see Table A-3 in Appendix A); this is undoubtedly one explanation for the low utilization achieved by the limestone. Insofar as pore diffusion and product layer diffusion resistances are responsible for the apparent utilization ceiling, the utilizations can be increased by going to even finer particle sizes than those tested here.

The effective ceiling on utilization is probably not a true ceiling, in the sense of total cessation of calcium conversion. Rather, the phenomenon is a significant decrease in the sulfation rate due to increased diffusional resistances. Continued exposure of the sorbent to SO_2 for many additional seconds would undoubtedly result in some additional calcium conversion. However--since the residence time at sulfation temperatures in a boiler will generally be less than 1 s--this decrease in the sulfation rate represents a ceiling for all practical purposes, as far as the sorbent injection process is concerned.

At 1000°C (Figure 5-7), all five sorbents display a dramatic increase in reactivity compared to 900°C. However, the relative order of reactivity has changed to Vicron 45-3 <V40 <D3002 <D60 < Type S, reflecting a large increase in the relative reactivity of D3002. Both of the raw sorbents still exhibit some delay in SO_2 uptake due to calcination, but the delay is not as severe as that experienced at 900°C. The Vicron, which was only half calcined at 900°C, is essentially fully calcined at 1000°C.

The apparent ceilings on calcium utilization are much higher for each sorbent at 1000°C relative to 900°C, with the Type S achieving utilization of over 40 percent after 1 second. After 1.5 s, the utilization of the raw dolomite is approaching that of the D60 precalcine; after 0.75 s, the V40 utilization levels off at a value perhaps only 2 to 3 percentage points above the raw Vicron. Thus, at this temperature, it would appear that the primary value of a precalcine would be for the case where only short residence times are available, and delays due to calcination cannot be accepted.

The ultimate utilizations that are observed for a given sorbent are determined by the tradeoffs between surface are/porosity development (during calcination or dehydration), surface area decay (due to sulfation and sintering), and sulfation reaction kinetics. The key issue is how much sulfation has a chance to occur before large increases in pore diffusion and product layer diffusion resistances (due to sulfation and sintering) effectively stop the reaction. At 1000°C, surface area/porosity will tend to develop faster than at 900°C (for the precalcines, and the readily-dehydrated Type S, this effect is not significant); the surface area that is created will tend to decay faster; and the sulfation kinetics will be faster. As seen in the comparison of Figures 5-6 and 5-7, the net effect of these three phenomena, when the temperature is raised from 900 to 1000°C, is to significantly increase the ultimate utilization of the sorbents.

At 1100 and 1200°C (Figures 5-8 and 5-9) the orders of reactivity are unchanged from that at 1000°C. In addition, the ultimate calcium utilization of every sorbent declined with each increase in temperature. With increasing temperature, the advantage of precalcination for Vicron 45-3 becomes more apparent as the discrepancy between the calcium utilizations of V40 and Vicron 45-3 increases. With the dolomite, however, the difference between D3002 and D60 decreases with increasing temperature. The overall decline in capture for the precalcines is a clear indication of sintering since the intrinsic kinetic rate of SO_2 capture by limestones is known to increase dramatically with temperature in this temperature range.

At higher temperatures the Type S hydroxide is more reactive than any of the other materials. This enhanced reactivity may be due to the smaller particle size, which results from the pressure calcination process. At 1100°C (Figure 5-8) a Type S material was also tested which contained an air-entraining agent, an organic compound which affects the masonry properties of the hydrated lime. Although some improvement in the smoothness of the sorbent feed was noted, the data show that the agent had no impact on calcium utilization.

Some detailed data from these ITR tests are presented in Appendix A, Table A-3.

5.3.2 Reactivity Vs. Injection Temperature

Figure 5-10 summarizes the ultimate utilization at long times for the five sorbents as a function of temperature. The data shown in Figure 5-10 were taken from the smoothed curves in Figures 5-5 through 5-9 at the residence time of 1.0 s. There is little uncertainty associated with the ranking in Figure 5-10 because the slopes of calcium utilization profiles were all very shallow at 1.0 s. What has not been taken into account is the delay of the onset of sulfation for Vicron 45-3 and D3002 due to slow calcination at 900 and 1000°C. Accounting for the delay would alter the shapes of the temperature/utilization profiles somewhat; however, it would not be reflective of the ultimate result of low-temperature injection into a p.c. utility boiler where calcination time is bound to be a factor.

The most significant aspect of Figure 5-10 is the appearance of a maximum in the utilization achieved as a function of temperature. The location of the true maximum appears to be very near 1000°C but may be somewhat different for each sorbent. Although a maximum would have been predicted purely as a result of the tradeoff between surface area development/decay and sulfation reaction kinetics, there had been no indication that it would occur at the same temperature for five different sorbents.

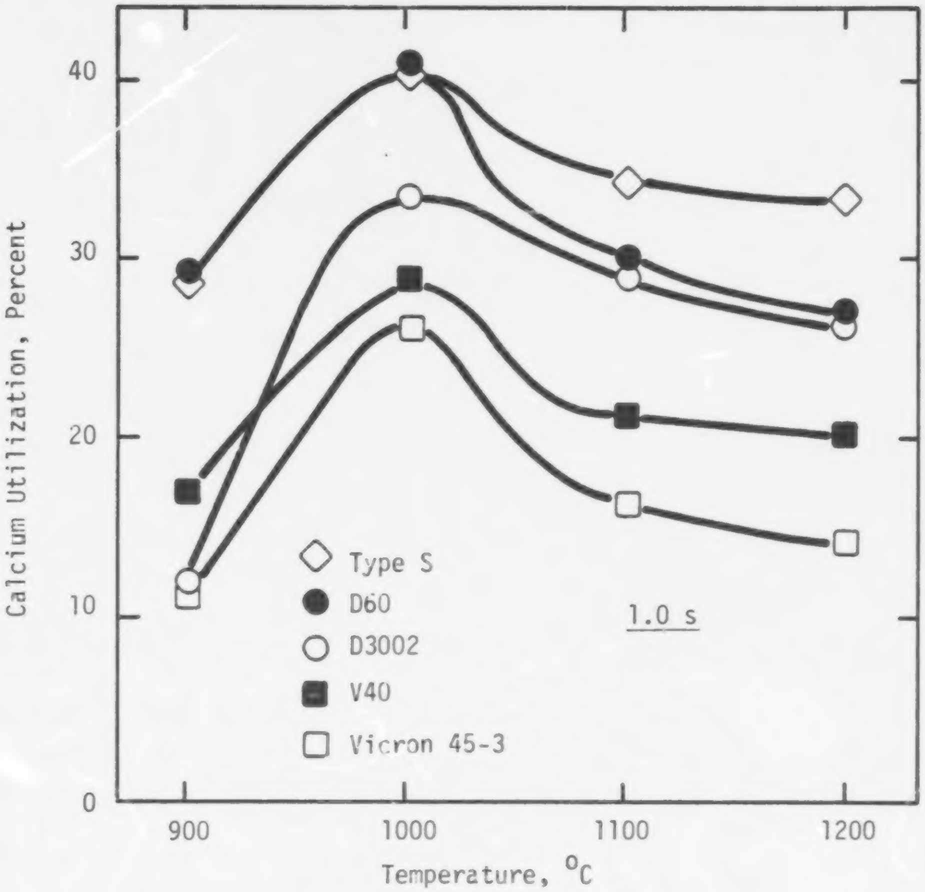

Figure 5-10. Relative levels of calcium utilization at 1.0 s by five sorbents as a function of reaction/calcination temperature.

Figure 5-11 summarizes the effect of temperature on the calcium utilization profiles for the raw dolomite. One interesting feature of these data is that the slopes of the utilization profiles decrease monotonically with increasing temperature at the longer times. At 1200°C, the sorbent has achieved nearly its maximum utilization at 1.25 s (the slope is close to zero). The sorbent injected at 1000°C, however, is still about twice as reactive at 1.54 s (has about twice the slope) compared to the 1200°C case at that residence time. The sorbent injection at 900°C is taking up SO_2 after 1.5 s at nearly the same rate as at 0.6 s. These points all suggest that high sorbent utilization might be achievable at low temperatures if the temperatures are sustained for long times.

5.3.3 Effects of Coincident Calcination on Reactivity

The TDR studies had concluded that calcination would not impede sulfur capture for injection temperatures of 1200°C and higher. However, data collected at 900 and 1000°C in the ITR suggested that particle heating and calcination could be slow for low-temperature injection and could, in fact, delay the onset of sulfation. Figure 5-12 is a composite plot, using data from the ITR tests described in Section 5.3.1, showing both calcium utilization and calcination profiles for Vicron 45-3 and D3002 dolomite at 1000°C (solid samples were analyzed for both calcination and calcium utilization). The calcination data for the dolomite are shown both on a total basis (including magnesium) and on an estimated calcium basis (assuming that all of the magnesium is calcined before the calcium begins to calcine). The increase in calcium utilization for the dolomite exceeds the apparent rate of calcination of the calcium. Rather than suggest sulfation of the magnesium, this probably demonstrates the error in assuming that magnesium is completely calcined before calcination of the calcium fraction begins. The parallel behavior of the calcination and calcium utilization profiles at short times reinforces the proposition that SO_2 uptake is delayed by slow calcination.

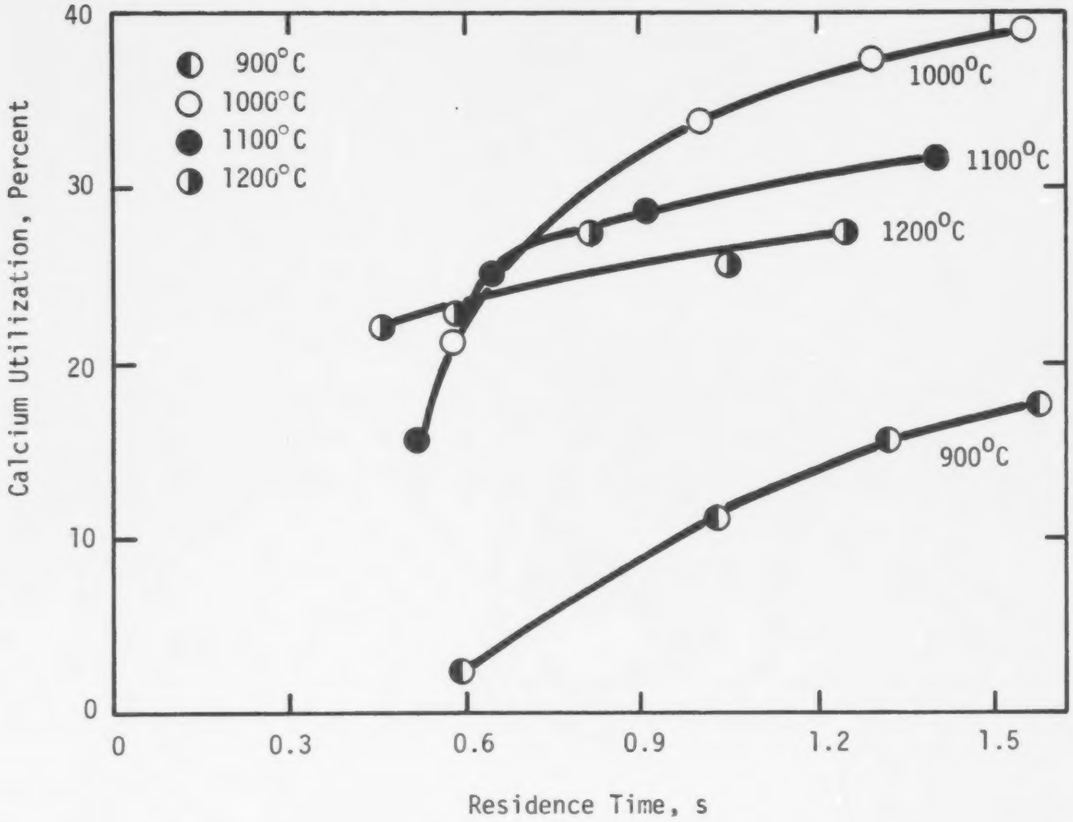

Figure 5-11. Calcium utilization profiles for D3002 dolomite at 900, 1000, 1100 and 1200°C, 3600 ppm SO_2.

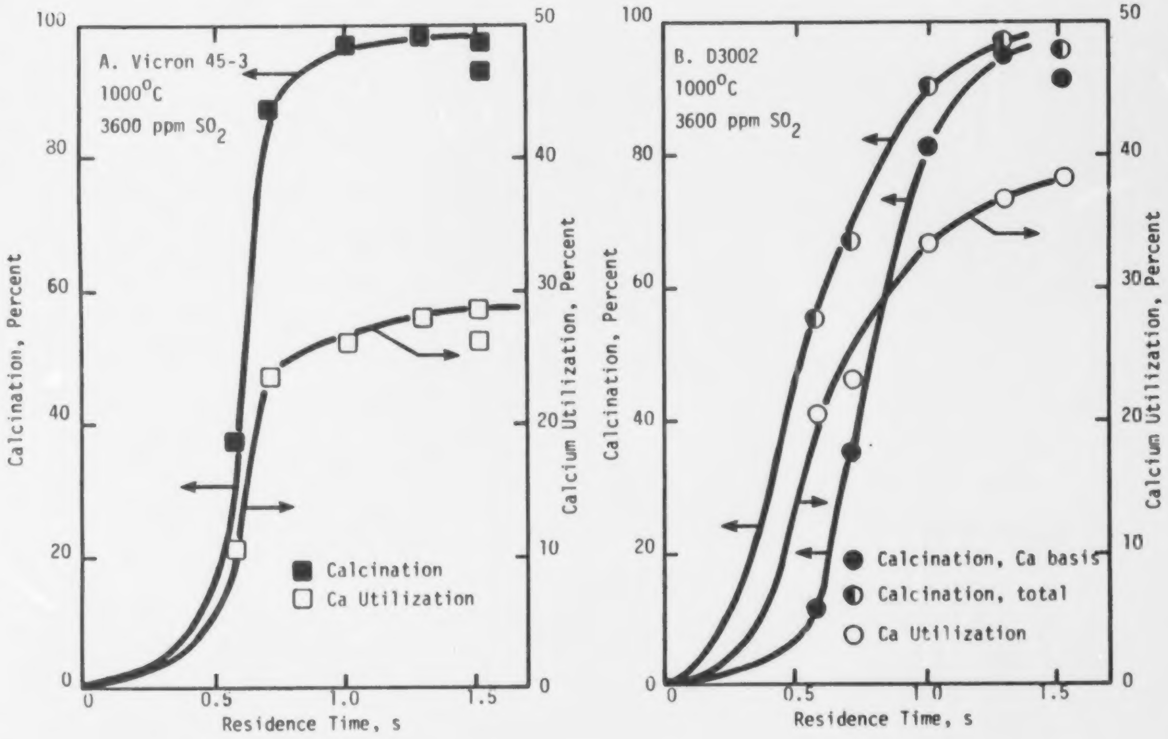

Figure 5-12. Composite plots of both calcination and calcium utilization data for A.-Vicron 45-3 and B.-D3002 dolomite in the ITR. The dolomite calcination data are presented on a total basis (including the magnesium) and on a calcium-only basis.

An unexpected aspect of the calcination profiles is that the Vicron 45-3 calcines faster than the D3002 dolomite. More important, however, is the rate of SO_2 uptake during calcination. At 0.55 s Vicron 45-3 is only 38 percent calcined, yet it has attained over 10 percent calcium utilization. In the next 0.15 s the calcium utilization increases by a factor of nearly 2.5, roughly as fast as calcination does. Such a rapid rate of sulfation could be due to a transient high surface area which has not been detected by solids sampling. A more plausible explanation, however, is that immediately after calcination the CaO is poorly crystallized. Having the CaO in a higher potential energy state would reduce the activation energy, and hence increase the intrinsic rate, of the sulfation reaction. The difference between these two hypotheses is subtle, however; the former refers to a bulk physical property and the latter to a molecular chemical property. Whether either of these hypotheses is correct, the data also show that as soon as calcination is essentially complete the rate of SO_2 uptake abruptly declines. At 1100 and 1200°C this comparison cannot be made as easily because the samples showed high levels of calcination even at the shortest residence times measured.

5.3.4 High-Calcium Pressure-Slaked Hydroxides

Two high-calcium (calcitic) pressure-slaked hydroxides (referred to as U.S. Gypsum A and B) were made available and tested under DOE contract No. DE-AC18-84FC10616. The data are presented here with permission from the DOE. Beyond the surface areas in Table 4-3, little is known about these materials other than that the original limestones were from two different Western Lime quarries, but they were processed under the same calcination conditions (by Western Lime) and the same pressure hydration conditions (by U.S. Gypsum). Both sorbents were used in DOE's recent pressure hydrate injection testing at the Hoot Lake station of Otter Tail Power Company. The designations "A" and "B" are used to distinguish between the two sorbents.

Figures 5-13 and 5-14 show calcium utilization profiles for both materials at 1100 and 1200°C. Also included in the figures are data for the dolomitic Warner Type S sorbent collected at the same conditions. The

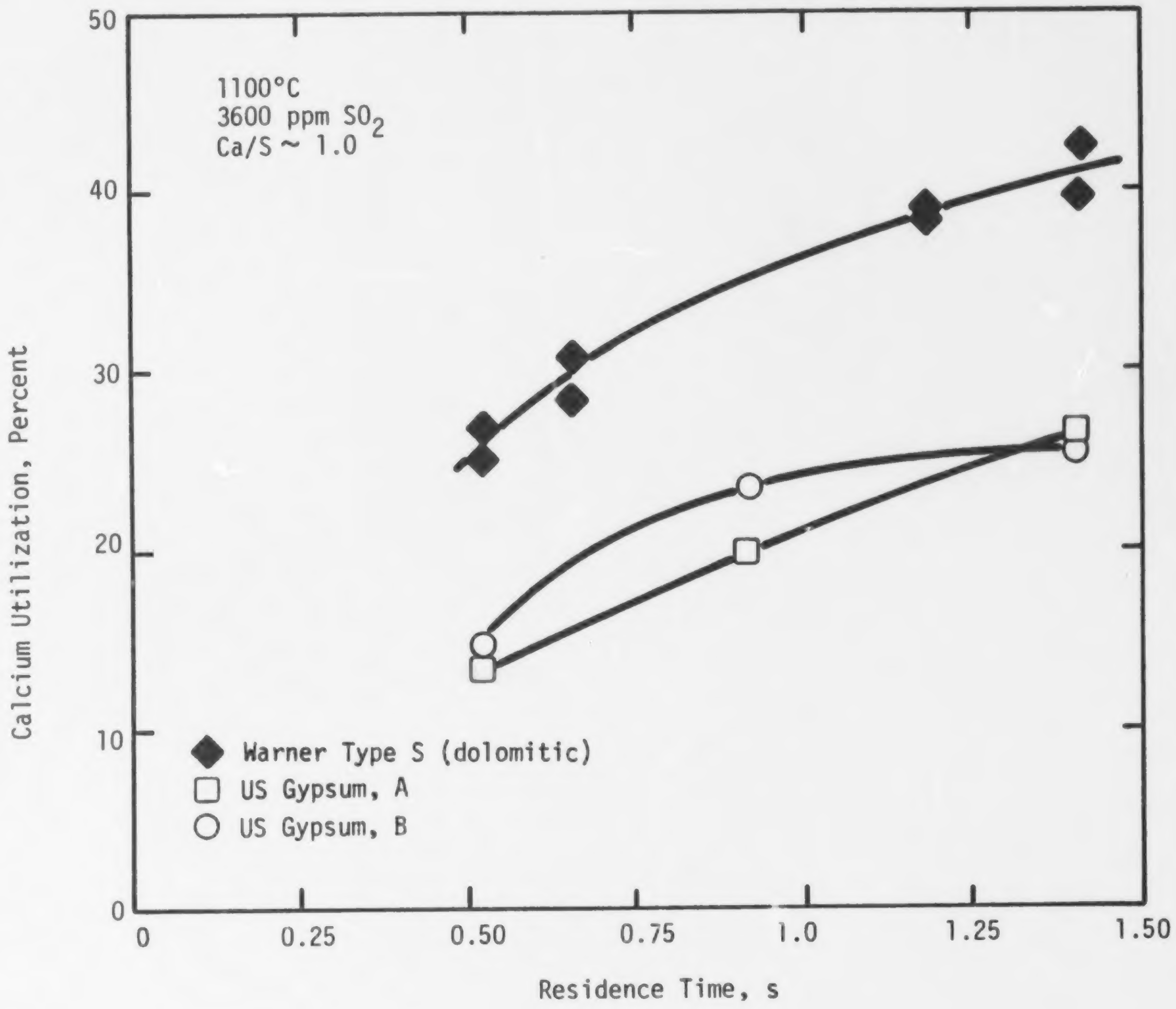

Figure 5-13. Calcium utilization profiles for high-calcium pressure-slaked hydroxides at 1100°C, 3600 ppm SO_2. Warner Type S data are shown for comparison.

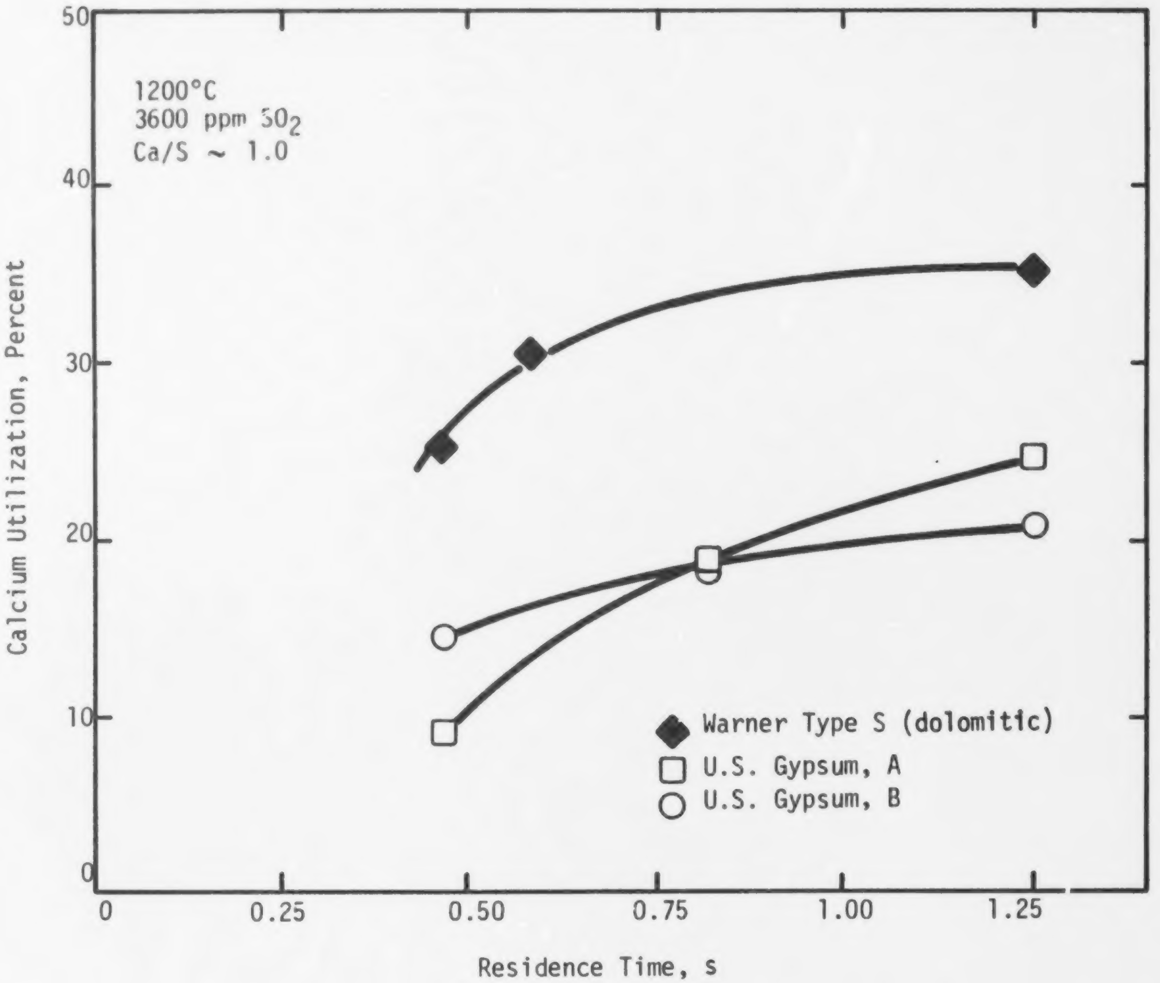

Figure 5-14. Calcium utilization profiles for high-calcium pressure-slaked hydroxides at 1200°C, 3600 ppm SO_2. Warner type S data are shown for comparison.

figures show that sorbents A and B have similar reactivities, despite being from different quarries. They are not as reactive as the dolomitic pressure-slaked hydroxide. However, comparing these figures with Figures 5-8 and 5-9, it appears that A and B are somewhat more reactive than the V40 precalcine. At both 1100 and 1200°C, they are somewhat less reactive than the raw D3002 dolomite. A ranking is suggested by the limited data in this section which seems to hold for both calcitic and dolomitic materials, namely:

Increasing Reactivity
Raw Stone → High SA Precalcine → Pressure Slaked
(40-60 m^2/g) (Type S)

with the dolomitic materials always having an advantage over calcitic, or high-calcium, materials. The advantage of pressure-hydrated materials may result from the reduced particle size which is a product of the pressure hydration process.

The decline in calcium utilization between 1100 and 1200°C is slight for the high-calcium pressure-slaked hydroxides. Similar behavior at 1100 and 1200°C was also observed for the Warner Type S and V40 sorbents.

A possible reason was investigated for the similarity in utilizations by the sorbents A and B at 1100 and 1200°C. Samples of both sorbents were collected from the ITR--operating with a hydrogen-air flame, this time containing no SO_2--and analyzed for specific surface area. Figure 5-15 shows surface area profiles for both A and B at 1100 and 1200°C. Again, within the accuracy of the surface area measurements, it is unclear whether any real difference exists between the two materials. There is a distinct decline in surface area as the temperature is increased. Surface areas measured at 1100°C are 25 to 80 percent higher than those measured at 1200°C. Assuming an activation energy of about 53.6 kJ/mole for the sulfation reaction, the intrinsic reaction rate should be about 40 percent higher at 1200°C than at 1100°C. These two effects, therefore, come very close to canceling each other and thus explain the similarity in the utilizations attained at the two temperatures.

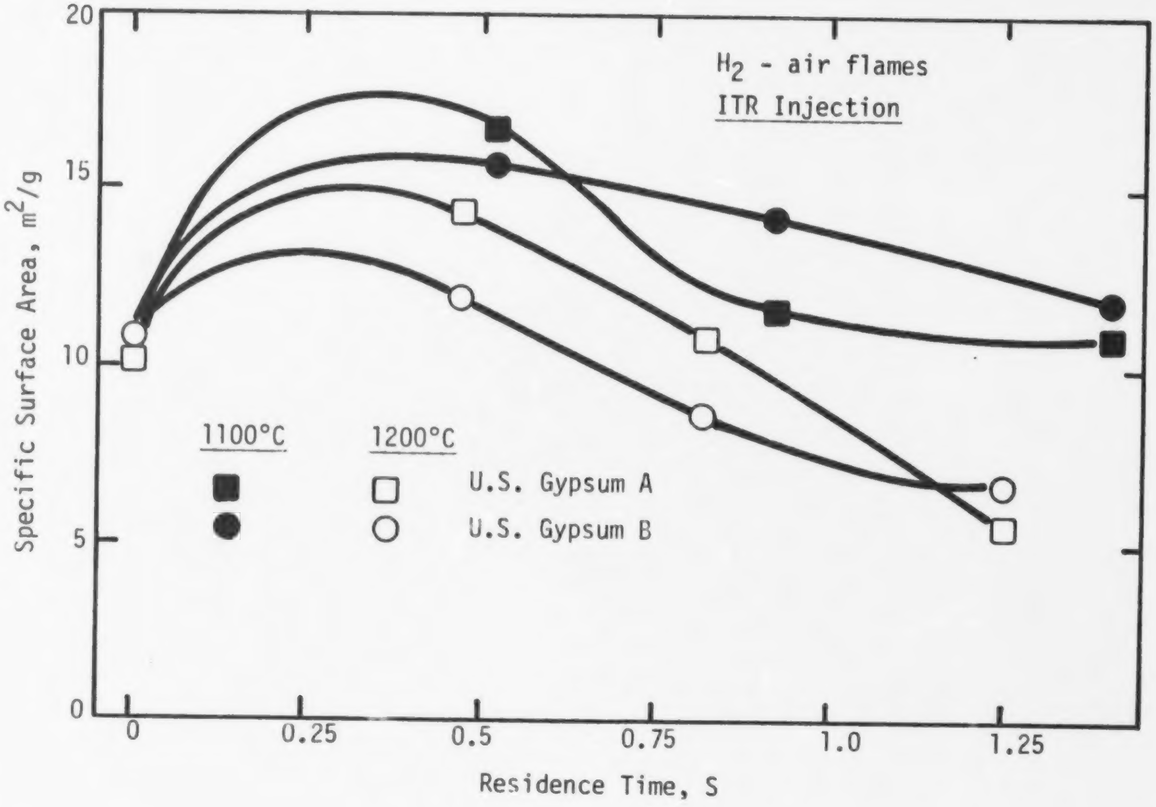

Figure 5-15. Surface area profiles for high calcium pressure slaked hydroxides in the ITR in the absence of SO_2. Data were collected at 1100 and 1200°C.

These data also suggest sintering rates for the sorbents. After an initial increase, the average surface areas at each temperature decline almost linearly with increasing time. The declining slopes of the surface area profiles following the peak also become more negative with temperature, with the 1200°C profile dropping nearly 70 percent more steeply than than the 1100°C profile. This behavior is qualitatively consistent with other sintering rate data obtained for other sorbents at lower temperatures (30).

Additional surface area samples were collected using a 1360°C condition in the ITR while downfiring with a methane-air flame which gave a total residence time of 0.6 s. Figure 5-16 compares the surface areas measured for sorbents A and B at 1100, 1200 and 1360°C at a residence time of 0.6 s. The data at 1100 and 1200°C were taken off the smoothed curves in Figure 5-15. Again, the differences between sorbents A and B are marginal. However, the effect of temperature on surface area is made apparent and is consistent with the prior results obtained with other sorbents in the TDR.

Some detailed data from these calcitic pressure hydrate tests are presented in Appendix A, Table A-4.

5.3.5 SO_2 Concentration Effects

There is some controversy concerning the intrinsic order of the reaction of SO_2 with calcium oxide. Recently the SO_2-lime reaction has been assumed by some investigators to be zero order in SO_2 concentration over a wide concentration range starting at about 500 ppm (33). However, in order to ensure that SO_2 depletion did not affect the results of this study, three sorbents were tested at three different SO_2 concentrations. Vicron 45-3, Warner Type S and D-60 precalcine were all injected into the ITR at 1100°C and sampled after 1.4 s residence time. SO_2 concentrations of 1800, 3600 (prior condition) and 7200 ppm were used. The feed rate of sorbent was about the same in all cases. If the reaction were truly zero order, a plot of calcium utilization versus SO_2 concentration should show no change in utilization with SO_2. The results of these tests are shown in Figure 5-17.

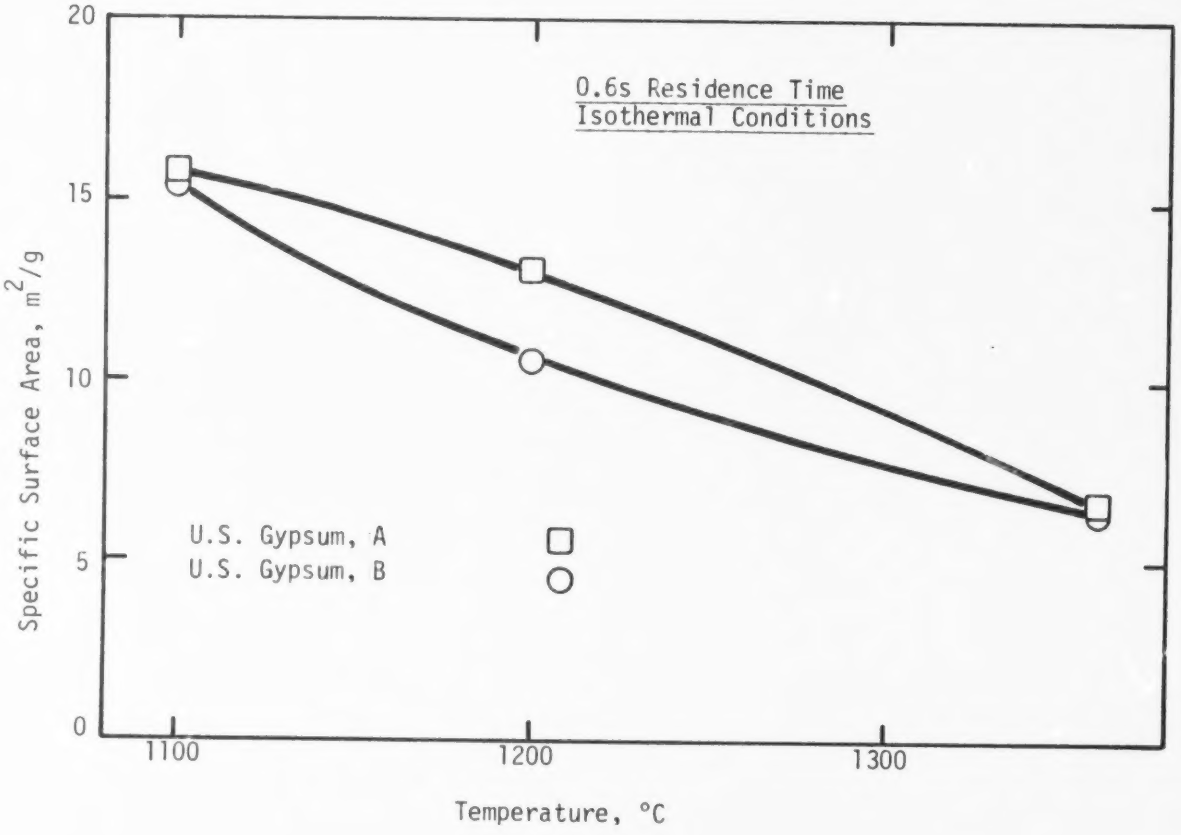

Figure 5-16. Effect of temperature on the surface area attained in 0.6 s by high-calcium pressure-slaked hydroxides in the ITR. The 1360°C flame was methane-air, the 1100 and 1200°C flames were hydrogen-air (no SO_2).

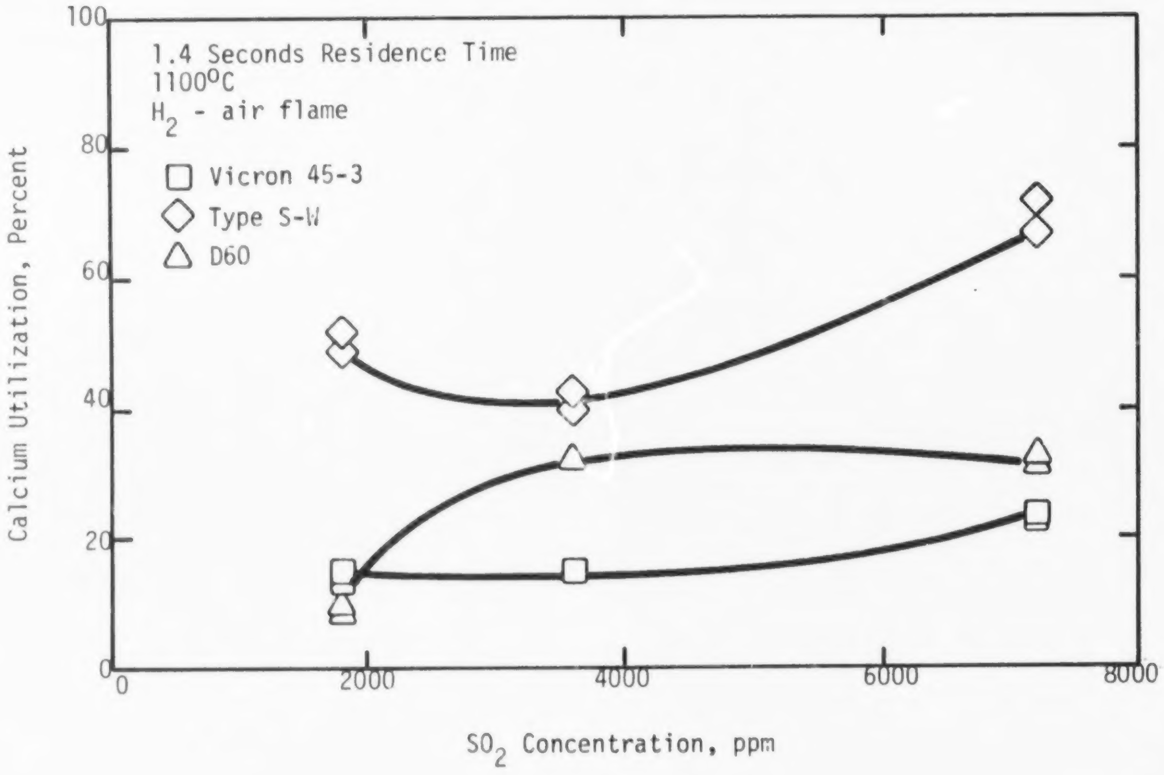

Figure 5-17. SO_2 concentration effect on SO_2 capture by three sorbents in the ITR. Data were collected at 1100°C with a hydrogen-air flame.

The behavior of the Type S material is very unusual. However, similar behavior has been observed previously for several calcium hydroxides (34). The hydroxide data from Reference 34 showed a decline in utilization as SO_2 concentration increased from 1000 to 4000 ppm. The subsequent increase in utilization shown in Figure 5-17 is outside of the range of the earlier study. Only the D60 precalcine displays a significant decline in utilization with decreasing SO_2 concentration. The decrease in utilization for D60 is greater than would be expected on the basis of a first-order sulfation reaction and cannot be accounted for by SO_2 depletion because the experiment was run with $Ca/S < 1.0$. The data for Vicron 45-3 suggest only that a moderate increase in utilization might occur with unusually high levels of SO_2. Overall, the curves drawn in Figure 5-17 indicate that in the vicinity of 3600 ppm SO_2 a small effect of concentration is observed which should not affect the earlier results.

5.4 Porisimetry Data

Pore size distributions obtained by mercury intrusion porisimetry were used to characterize precalcined sorbents before and after sulfation in order to illuminate some of the physical aspects which affect SO_2 uptake. The precalcines were D60 and V40 whose measured BET surface areas were 65.2 and 43.4 m^2/g, respectively, prior to sulfation. Sulfation was carried out at 300°C in order to prevent sintering, and to thus reveal the impact upon pore size distribution of sulfation alone. One-gram samples of precalcine were placed into the ITR probe filter holder and a hot mixture of 3600 ppm SO_2 in air was drawn through. The probe cooling water was adjusted to maintain a filter temperature of 270-300°C for 30 min. Only dry air and SO_2 were used in order to avoid competing reactions such as hydration and carbonation. Calcium utilizations of the in-filter sulfated samples were 25 percent for the D60 and 28.5 percent for the V40.

Figure 5-18 shows a caricature of a collection of particles which can be used to define the three porosity ranges detected by mercury intrusion. The first of the three, referred to as bulk porosity, is the void volume

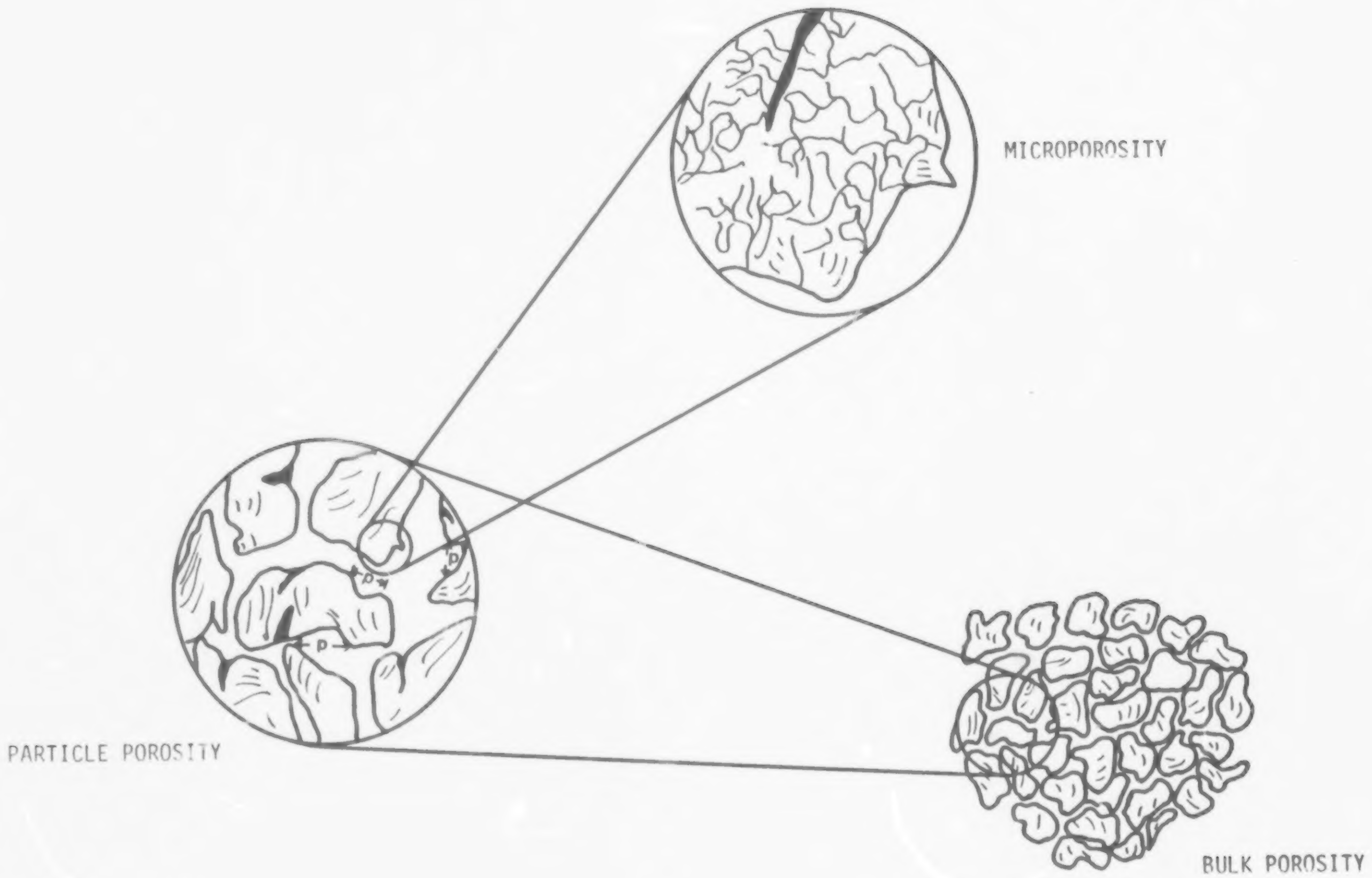
MICROPOROSITY
p
p
p
PARTICLE POROSITY
BULK POROSITY

Figure 5-18. Characterization of pore types based on interpretation of mercury intrusion porismetry data.

attributed to the interstitial space between the particles (i.e., not associated with the internal pore structure of the particles). For all four samples here, the bulk porosity effectively consisted of volume contained in "pores" (interstices) larger than 6.0 μm; i.e., on the order of the mean particle diameter. The second type of porosity, referred to as particle porosity, is defined by the volume occupied by pores which might be characterized as gross surface characteristics, including relatively large cracks and fissures, such as have been observed by electron microscopy (12). In these samples, the particle porosity included pores in the size range of 0.5 to 6.0 μm in diameter. Such macropores might include significant pore volume, but they are too large to represent significant surface area unless the total porosity is extremely large (~1.0). The third type of porosity, referred to as microporosity, might be defined as the pore structure between individual grains within a calcined particle. For all four samples analyzed here, the microporosity existed in pores smaller than 0.03 μm (300 Angstroms). Tiny internal pores in this size range account for nearly all of the surface area of the four samples.

Pore size distributions for the unsulfated and sulfated V40 are shown in Figure 5-19, and for the unsulfated and sulfated D60 in Figure 5-20. These figures show a distinctly bimodal pore size distribution, with a well-defined peak for the particle porosity (0.5 to 6.0 microns) and a second peak for the microporosity (0.003 to 0.03 μm, or 30 to 300 A^{0}). This bimodal pore size distribution is not typical of all calcines, but is probably a product of the precalcination technique. Data for pores larger than 6.0 μm (bulk porosity) are disregarded in the figures because they are subject to the effects of sample preparation (i.e., packing of the powder into the sample chamber), and have no bearing on the following discussion.

In Figure 5-19 the curves show that sulfation has produced a 24 percent reduction in the particle porosity of V40. In addition, the microporosity has been reduced by 40 percent. Since the surface area resides in the smaller pores, the reactivity of the precalcine should be severely impaired once those pores are blocked even though the overall porosity of the particle has not reached zero. Plugging of the pores should also result in a shift of

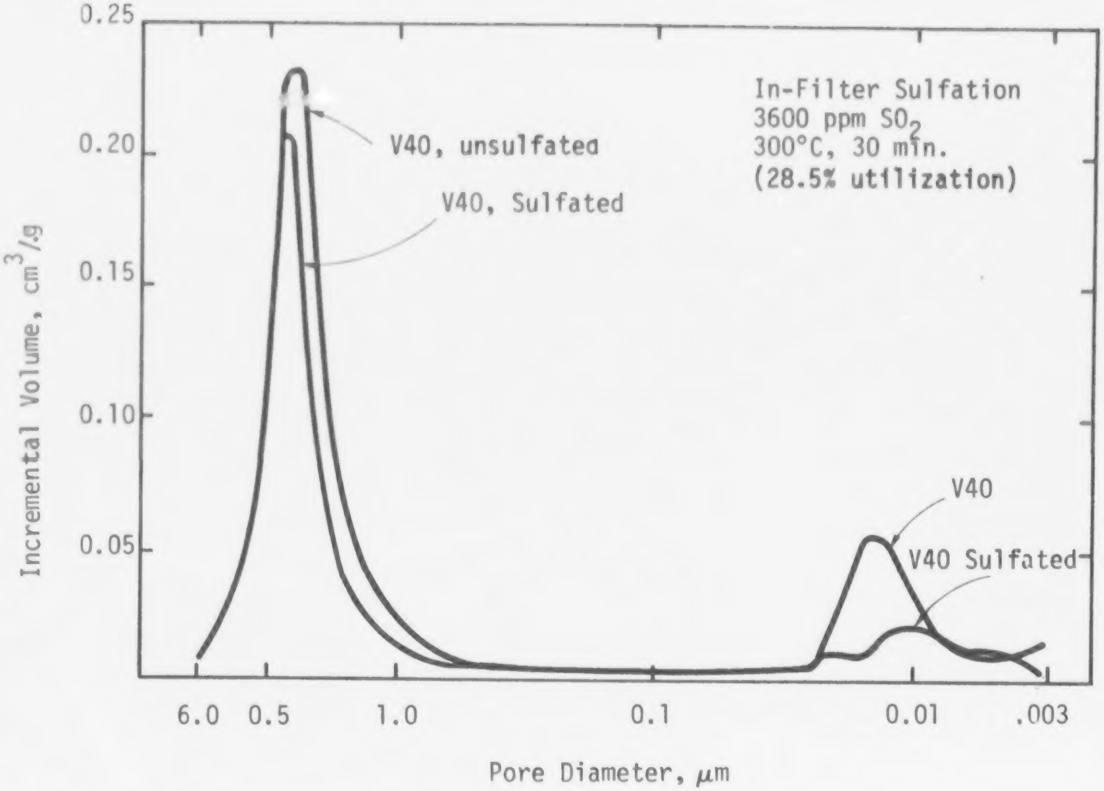

Figure 5-19. Pore size distributions for raw and sulfated V40 precalcine. Data were obtained by Mercury Intrusion Porisimetry.

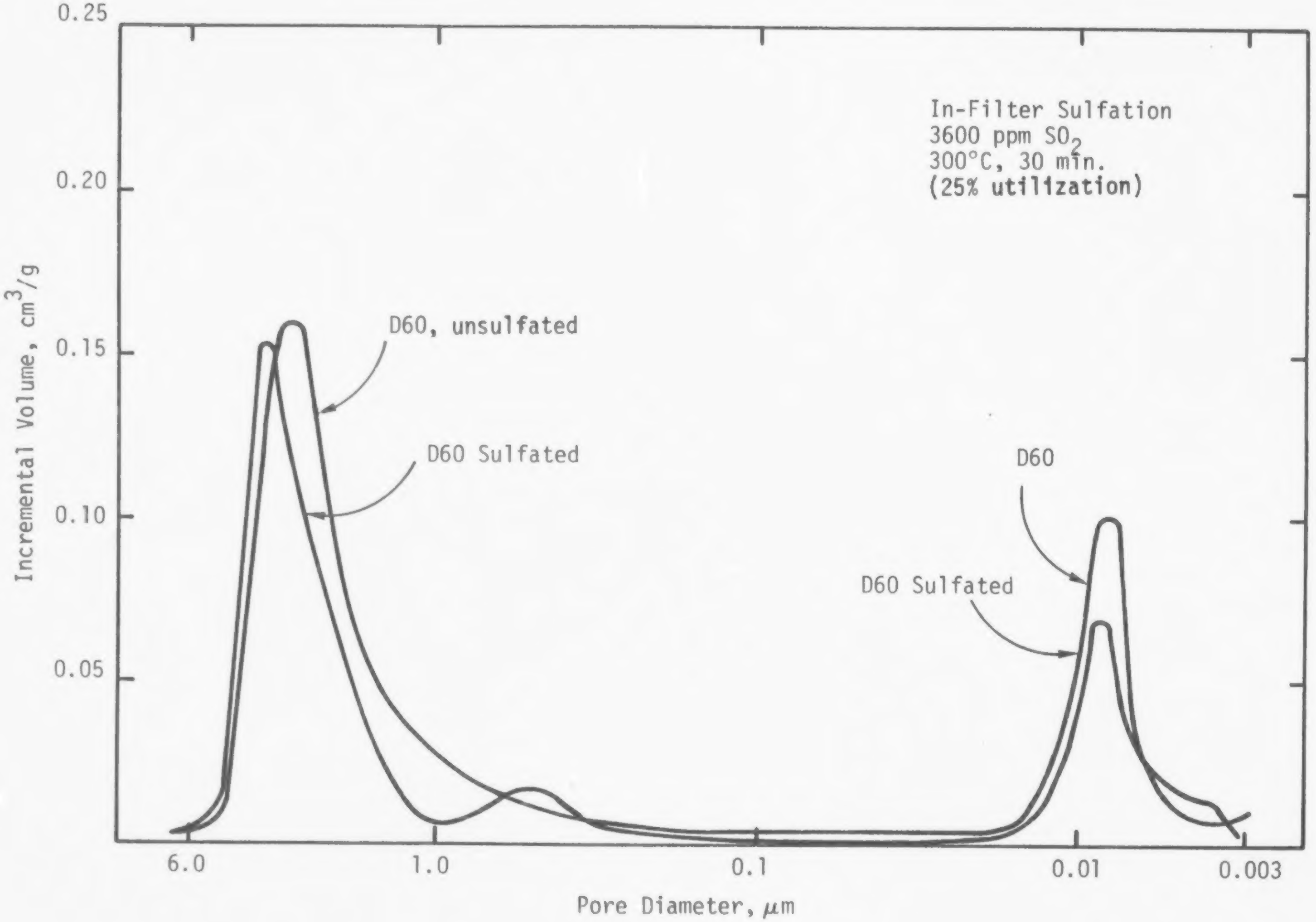

Figure 5-20. Pore size distributions for raw and sulfated D60 precalcine. Data were obtained by Mercury Intrusion Porisimety.

the pore size distribution, as the pore openings shrink. This too is apparent in Figure 5-19 for the microporosity where the peak in the pore size distribution has shifted from just over 130 Angstroms to under 100 Angstroms.

There are obvious differences in the porisimetry data for the D60 precalcine. The reduction in particle porosity due to sulfation is small (8.3 percent). However, so is the reduction in microporosity; only 14 percent. Further more, the peak in the microporosity distribution has not shifted as a result of sulfation; the unsulfated and the sulfated distributions show distinct maxima at 80 Angstroms.

The porisimetry data for all four samples are summarized in Table 5-2.

Differences in the pore structure behaviors of the V40 and D60 precalcines during low-temperature sulfation are an indication of the role played by the magnesium component of the D60. Without drawing any conclusions, it is instructive to consider how MgO might have served to maintain higher porosity and a more open pore structure in the D60 after sulfation.

MgO is relatively unreactive (compared to CaO) toward SO_2. Its presence within a pore would provide discrete locations where no SO_2 sorption would occur. Hence, half of the pore surface would not be susceptible to swelling, and pore closure would be substantially reduced. Extrapolation of this hypothesis to higher temperatures should be viewed cautiously. If this is an accurate representation of the effect of MgO upon low-temperature sulfation, it is probably also an active mechanism at high temperatures. At high temperatures (>900°C), however, MgO may play other, more important roles in preventing pore closure. For example, the discrete distribution of MgO within a CaO matrix may inhibit sintering and CaO crystal growth.

5.5 Sulfation Reaction Promoters

Fifteen different chemicals were tested to determine their potentials as promoters for the sulfation of limestone. Tests were carried out in the ITR

TABLE 5-2. SUMMARY OF MERCURY INTRUSION PORISIMETRY DATA OF RAW AND SULFATED D60 and V40 PRECALCINES

Parameter	D60	Sulfated D60	V40	Sulfated V40
Bulk Porosity	0.7441	0.6974	0.7844	0.7254
Particle Porosity	0.6281	0.5761	0.5408	0.4117
Change		8.28%		23.87%
Microporosity	0.1789	0.1545	0.1290	0.0773
Change		13.64%		40.08%
Pore Diameter at Peak	79.9 Å	79.9 Å	130 Å	102 Å
Range of Pore Diam	30-213 Å	38-213 Å	30-213 Å	38-213 Å

with 3600 ppm SO_2 under a variety of flame and reaction conditions. All of the materials, added 5 percent by weight to Vicron 45-3, were tested under isothermal conditions at 1000 and 1100°C and also by injection into a 1360°C flame with the ITR wall temperature at 1100°C. In addition, one of them, Cr_2O_3, was tested in the ITR using a series of flame temperatures up to 1950°C with the reactor wall temperature at 1100°C. The purpose of the elevated temperatures was to determine whether high temperatures might enhance any physical or chemical reactions between the sorbent and additive which might lead to higher sorbent reactivity toward SO_2. The temperature profiles that would be experienced by the Vicron-Cr_2O_3 mixtures under these flame and wall temperature conditions are described in Appendix B.

5.5.1 Cr_2O_3 Tests

The first additive tests were performed using Cr_2O_3 in order to explain results which were obtained in another project involving an experimental 380 kW (thermal) boiler-simulator furnace (BSF) (5). The BSF tests found relatively high levels of chromium present in certain limestone samples which were associated with high levels of SO_2 capture. Subsequently it was found that the furnace refractory contained Cr_2O_3 which was being picked up by the limestone. In addition, the results were improved when the sorbent (VIcron 45-3) was injected near the burner (i.e. at high temperature). A wide variety of additive studies have been subsequently undertaken to confirm these effects and optimize the interaction (30, 35).

Figure 5-21 shows results obtained in the ITR in the current study, comparing the calcium utilization of the Vicron-5 percent Cr_2O_3 premixture with the data obtained for Vicron 45-3 alone. Solids sampling was done with a quartz probe which had a slow quench rate; as a result, the utilization values shown for all samples (with and without Cr_2O_3) are inflated somewhat due to in-probe capture. Despite any effects of in-probe capture, it is nevertheless apparent from the figure that the Cr_2O_3 has increased the utilization of Vicron 45-3 at every temperature studied, with the possible exception of the lower temperatures. The maximum overall utilization was obtained using a 1360°C flame.

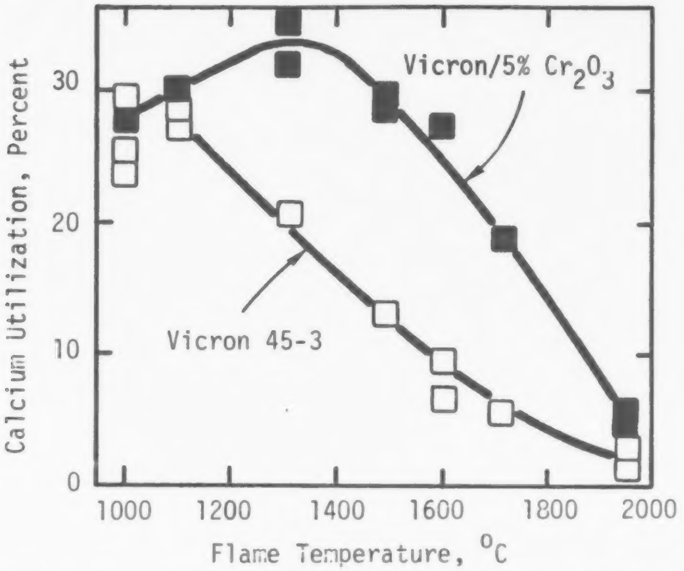

Figure 5-21. Calcium utilization of Vicron 45-3 with and without Cr_2O_3 as a function of initial flame temperature. ITR, 1100°C wall temperature, 3600 ppm SO_2, hydrogen-air or methane-air flames.

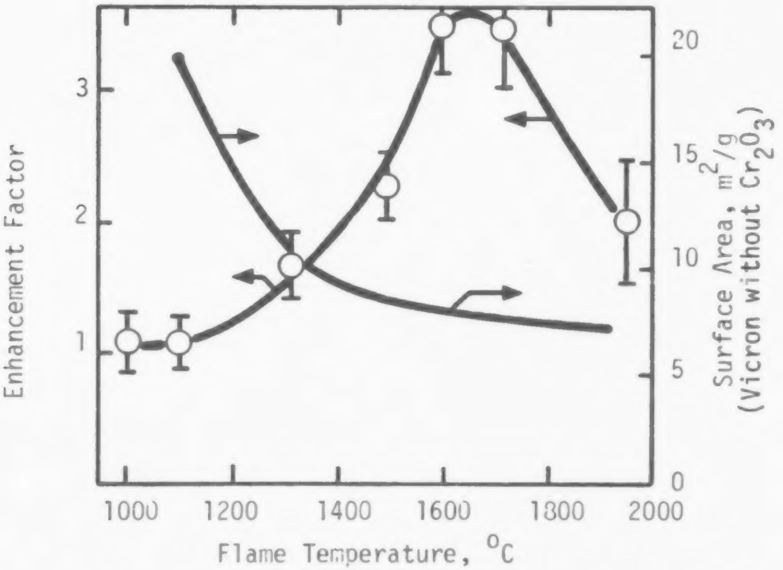

Figure 5-22. Ratio of calcium utilization with and without Cr_2O_3 by Vicron 45-3. Error bars signify 1σ level of confidence. Also shown is the surface area measured for Vicron 45-3 as a function of peak calcination temperature (ref. 22).

Figure 5-22 shows the enhancement factor due to Cr_2O_3 addition as a function of flame temperature. The enhancement factor is the ratio of utilization with and without Cr_2O_3. The error bars shown represent the 1 (67 percent) confidence level based on the population of data shown in Figure 5-21. A maximum in the enhancement factor appears to occur between 1600 and 1700°C. Also represented in the figure is the measured specific surface area of Vicron 45-3 alone (without Cr_2O_3) as a function of peak calcination temperature. That the reactivity and enhancement both are increasing in a region where the surface area of the sorbent is declining rapidly further suggests the magnitude of the effect produced by the Cr_2O_3.

Several hypotheses have been proposed to explain the effects of Cr_2O_3. These fall into two classification - promoter-based hypothesis and catalyst-based hypotheses. Promoters are defined here as materials which physically interact with the sorbent to assist a chemical process; catalysts are substances which expedite the chemical reaction, sometimes by adding new intermediates into the reaction mechanism, without making permanent physical changes in the sorbent or otherwise becoming integrated into the reaction products. Several of these hypotheses are listed below.

- Promoter Hypotheses

  - Physical interaction to produce a solid mixture which reduces the resistance to diffusion of SO_2 through the $CaSO_4$ product layer (e.g., creating defects in the $CaSO_4$ lattice).

  - Physical deposition of Cr_2O_3 resulting in a reduced sintering rate, thus maintaining a more open pore structure and hence facilitating SO_2 diffusion through the pores.

  - Formation of a Ca-Cr flux which promotes the solid-phase diffusion of CaO to surface sites for SO_2 sorption.

- Catalyst Hypotheses

  - Deposition of Cr_2O_3 on the sorbent to form a contact oxidation catalyst for the $SO_2 + 1/2\ O_2 \longrightarrow SO_3$ reaction.

  - Activation of Cr_2O_3 at high temperatures to form a heterogeneous gas-phase oxidation catalyst, oxidizing SO_2 to SO_3.

  - Formation of a $CaCrO_4$ intermediate for the sulfation reaction.

The possible role of Cr_2O_3 as an oxidation catalyst is considered because available data suggest that the reaction

$$CaO + SO_3 \longrightarrow CaSO_4 \tag{5-1}$$

is much faster than

$$CaO + 1/2\ O_2 + SO_2 \longrightarrow CaSO_4 \tag{5-2}$$

(36). In the absence of an oxidation catalyst, the equilibrium level of SO_3 is so low that equation 5-1 would not be a major contributor to sorbent sulfation.

During the Cr_2O_3 testing, the calcium utilization values obtained when Vicron 45-3 was tested without chrome increased, relative to earlier Vicron-only tests before Cr_2O_3 had ever been introduced into the ITR. Figure 5-23 shows the magnitude of this residual chromium effect. The solid symbols represent data from two ITR samples, obtained during the injection of unpromoted Vicron, which were collected immediately after a run where a Vicron-Cr_2O_3 premixture had been injected. In the Cr_2O_3 tests, several precautions had been taken to avoid contamination of subsequent samples, including: use of a separate sorbent feed system, cleaning the burner and injection tube, and using a clean quartz probe which had not been exposed to Cr_2O_3. In spite of these precautions a layer of chromium was sufficient to produce the 30-50 percent increase in calcium utilization shown in Figure

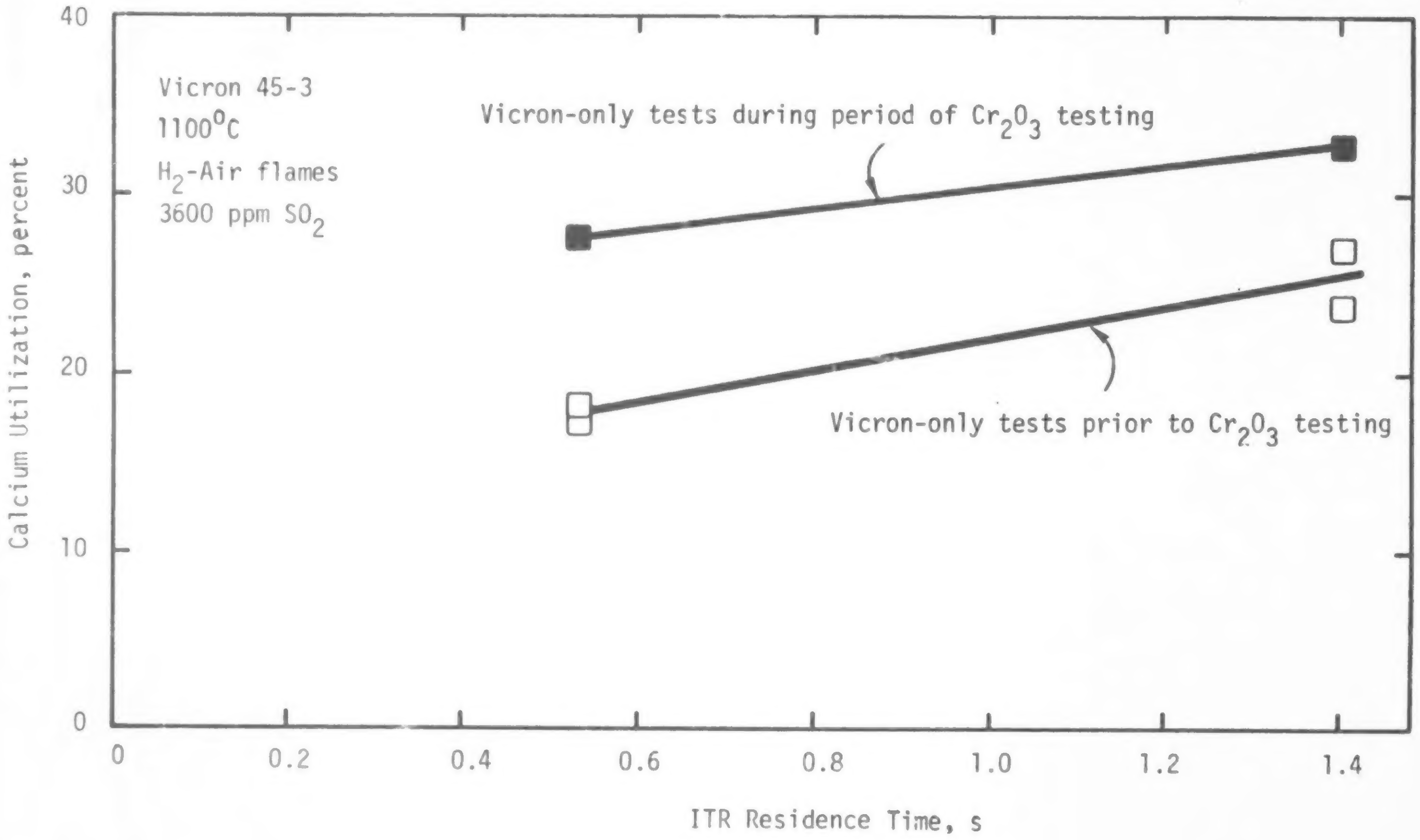

Figure 5-23. The residual chromium effect on calcium utilization by unpromoted Vicron 45-3 in the ITR. Samples were collected with the quartz sampling probe.

5-23. The magnitude of utilization is not as great as that produced by physical mixing of Cr_2O_3 with Vicron 45-3, but it demonstrates that premixing is not necessary for chromium to enhance the reactivity of Vicron 45-3 toward SO_2 in the ITR.

Detailed data for the Cr_2O_3 tests are presented in Table A-5, Appendix A.

5.5.2 Additional Additives

Fourteen additional additives were examined in a series of screening tests in order to determine their potentials as sorbent reactivity promoters. The materials, in 5 percent-by-weight premixtures with Vicron 45-3, were exposed in the ITR to 3600 ppm SO_2 under the 1100°C isothermal condition, as well as with a 1360°C flame fired into the ITR with a wall temperature of 1100°C. In order to detect any residual effects as were observed with Cr_2O_3 addition, samples of Vicron 45-3 were collected before, during and after the additives testing.

Figure 5-24 shows the results of the isothermal tests at 1100°C in bar graph form. The open section of each bar is the utilization achieved in 0.92 s, the shaded portion represents the additional utilization up to 1.4 s. The horizontal lines are the averages of the utilizations measured for Vicron 45-3 without additives at the two residence times. Down-pointing vertical arrows adjacent to the data for Na_2SO_4, K_2SO_4 and MoS_2 show the true calcium utilizations after correction for the sulfur present in the additives (i.e., the calcium utilization resulting only from reaction with feed SO_2, assuming that all sulfur in the additives remains with the additives). For the Li_2CO_3 mixture, the utilization measured at 1.4 s was lower than that at 0.92 s.

Every additive tested, except MoS_2, caused a net increase in utilization after 1.4 s compared to unpromoted Vicron. The magnitudes of the increases are not as great as were observed with Cr_2O_3. However, all of the results are above the 95 percent (2σ) confidence limit based on the four replicate samples of unpromoted Vicron 45-3 collected at 1.4 s. The utilizations for

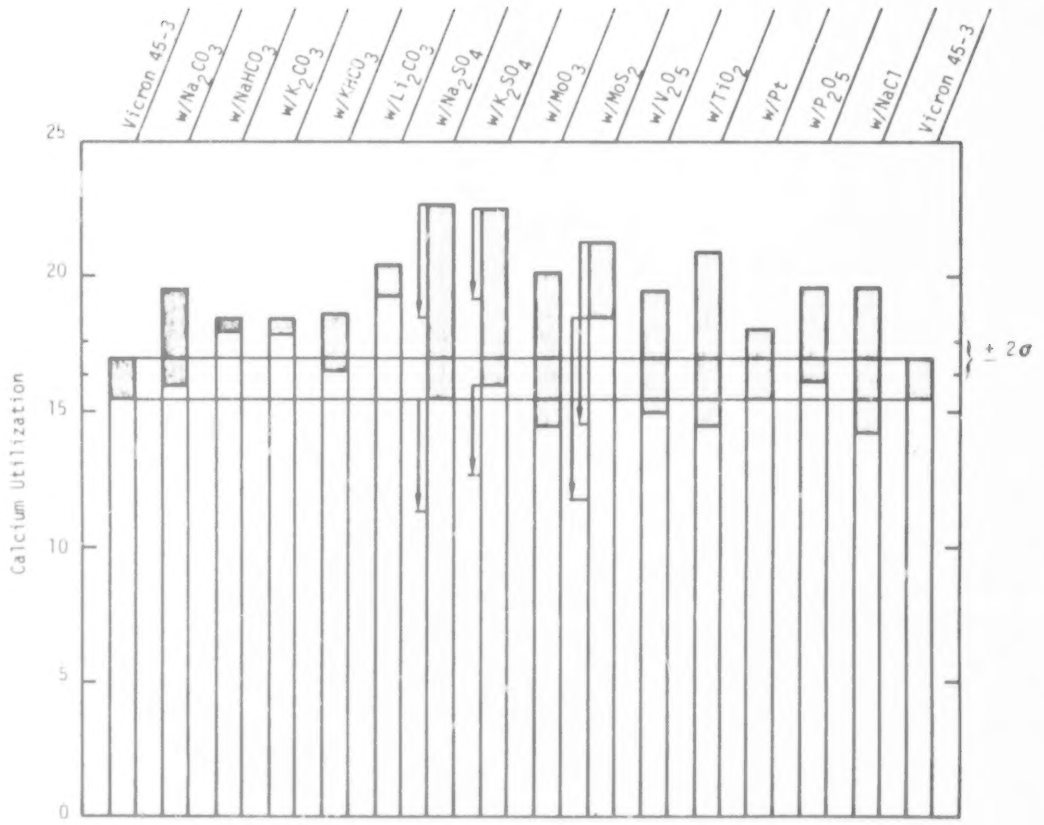

Figure 5-24. Calcium utilization by Vicron 45-3 fed premixed with promoters into isothermal conditions in the ITR. 1100°C, 3600 ppm SO_2. The open portion of the bars present utilization achieved in 0.92 s. The shaded portion shows the additional utilization at 1.4 s. For Li_2CO_3 the data at 0.92 s were higher than at 1.4 s. Arrows adjacent to Na_2SO_4, K_2SO_4, and MoS_2 designate the correction for the sulfur content of the additives.

Vicron 45-3 compare well with those shown in Figure 5-8, demonstrating that no residual promotion effect is present. Both platinum and V_2O_5 are known oxidation catalysts for SO_3 formation, as is Cr_2O_3. However, neither of these materials produced the magnitude of effect that was observed with Cr_2O_3.

The results of these tests are at odds with the data of Borgwardt (30) which shows a factor of 4.3 increase in reaction rate due to Na_2CO_3 addition at 1125°C. Those data, however, represent an increase in the reaction rate extrapolated to zero time, rather than calcium utilization at long times (~1 s). Other results of Borgwardt do show substantially increased utilization at 800°C, promoted by alkali salt addition. These low-temperature data, however, were obtained at extremely long times (up to 12 min.) and so may not be comparable to the results shown here. Other differences in experimental conditions which are not easy to account for are that Borgwardt's data were obtained in a differential flow reactor and that his sorbent was a low surface area (3 m^2/g) monodisperse particle size (1 μm) precalcined calcite.

The same set of promoters shown in Figure 5-24 was tested again in the ITR using a 1360°C flame with the walls still at 1100°C. Results of these tests are shown in Figure 5-25. The calcium utilization by unpromoted Vicron 45-3 was considerably lower at this condition compared to 1100°C isothermal. This was due in part to thermal deactivation, but also stems from the substantially shorter time that the sorbent had in the sulfation window for the 1360°C flame condition. The total residence time of the sorbent in the ITR was only 0.6 s for the 1360°C flame case (compared to 0.9-1.4 s for the 1100°C isothermal case); furthermore, for much of the 0.6 s, the temperature was above the 1250°C upper end of the sulfation window (see the thermal profile in Appendix B, Figure B-7). As apparent in Figure 5-25, the percentage improvement in utilization effected by many of the promoters at 1360°C (relative to unpromoted Vicron) was well above that for the same promoters at 1100°C (Figure 5-24). However, at the higher temperature, the benefits of improved promoter activity have been offset by increased sintering, and perhaps by the reduced time in the sulfation window in these experiments; as a result, the absolute value of the utilization at 1360°C

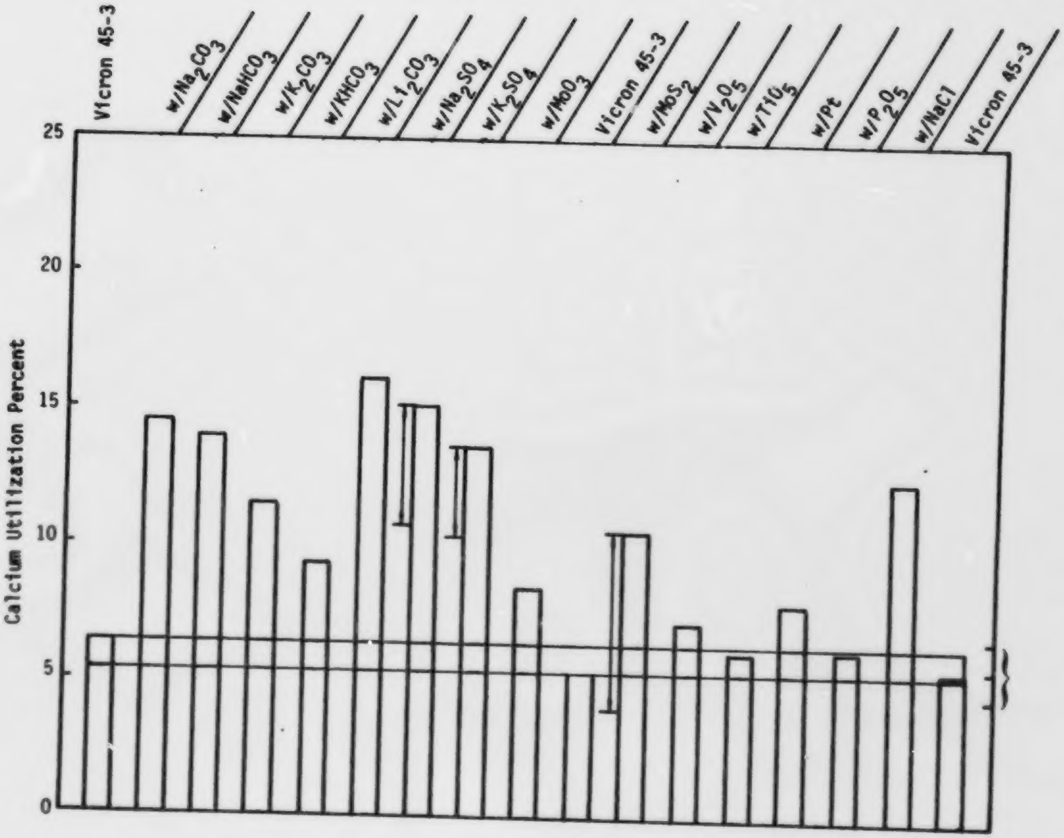

Figure 5-25. Calcium utilization by Vicron 45-3 fed premixed with promotors in the ITR. The horizontal band shows the range of results obtained for Vicron 45-3 alone. Downward arrows adjacent to the data for Na_2SO_4, K_2SO_4 and MoS_2 indicate the correction for the original sulfur content of the additive. Operating Conditions: 3600 ppm SO_2, 1360°C, CH_4-air flame, 1100°C wall temperature, 0.6 sec residence time.

never exceeds that at 1100°C for any one promoter. In fact, in no case does an additive at the 1360°C condition raise the utilization to a level significantly greater than that of unpromoted Vicron at 1100°C isothermal. Only two additives, TiO_2 and V_2O_5, had no effect on calcium utilization. After correction for its initial sulfur content, utilization by the MoS_2 sample actually lay below the 95 percent confidence interval for the five Vicron 45-3 samples collected. Platinum and V_2O_5 both had very little effect.

The additives which stand out as a group are the alkali metal salts, including the sulfates. The order of enhancement suggests that the results improve with decreasing atomic weight of the alkali. A more likely explanation is that the results improve with increasing molar concentration. Since all mixtures includes 5 weight percent additive, the lower molecular weight salts would have been present at a relatively higher molar percent concentration. Table 5-3 lists the measured enhancement factor for each of the sorbent alkali salt mixtures (relative to unpromoted Vicron) for the 1360°C flame condition, as well as the weight percent and mole percent of the additive in the mixture. The final column shows the atom percent of the alkali, relative to calcium, in the mixture. This is the mole percent corrected for the number of moles of alkali per mole of additive. These data are plotted against the enhancement factor in Figure 5-26. Linear regression of the enhancement factor on the atom percent alkali for all eight data gave the dashed line in Figure 5-26. Two of the data (shaded) appear to be outliers; these are for $NaHCO_3$ and Na_2CO_3. If these are eliminated from the liner regression then the correlation coefficient, shown in the figure, is improved considerably. In both cases, the intercepts of the lines (0.94 and 1.2) lie extremely close to the true intercept of 1.0. This analysis suggests that, among the alkali metal salts, apparent differences in promotion potential in Figure 5-25 might in fact be due simply to the fact that some salts were present at higher molar concentration than others. The analysis also suggests that $NaHCO_3$ and Na_2CO_3 might be better promoters than the average alkali salt, or the basis of required molar addition rate. These observations would need to be confirmed through tests in which the molar concentration of a single salt is varied over a controlled range.

TABLE 5-3. COMPOSITION OF THE ALKALI SALT MIXTURES WITH VICRON 45-3.

Alkali Metal Salt Additive	Enhancement Factor for 1360°C Flame Condition	Additive Wt. Percent	Additive Mole Percent	Alkali/Ca Atom Percent
Li_2CO_3	2.86	5.01	6.66	13.32
Na_2CO_3	2.58	5.01	4.74	9.49
$NaHCO_3$	2.49	5.01	5.90	5.90
NaCl	2.21	5.01	8.27	8.27
K_2CO_3	2.04	5.01	3.68	7.36
$KHCO_3$	1.64	5.00	4.99	4.99
Na_2SO_4	1.91[a]	5.01	3.58	7.17
K_2SO_4	1.82[a]	5.01	2.94	5.89

[a] corrected for the additive sulfur content

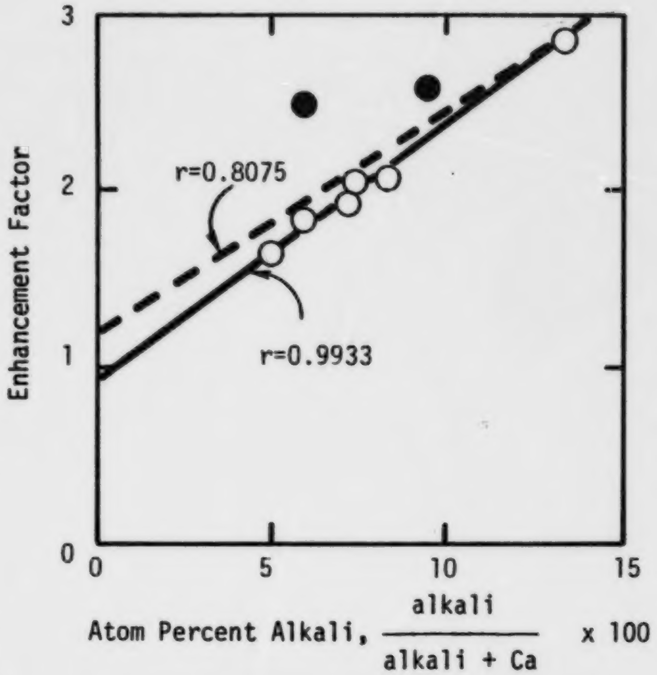

Figure 5-26. Illustration that enhancement factor observed with different alkali metal salts correlates with the molar concentrations obtained with the different salts (data from Table 5-3). ITR, 1360°C flame condition. Solid circles are data points for $NaHCO_3$. Dotted line represents regression fit for the complete data set. Solid line is regression of open circles only.

Detailed data for this additive heating are presented in Table A-6, Appendix A.

5.5.3 Discussion

While it is not possible from the preceding data to identify the mechanism(s) by which promoters function, one hypothesis which is consistent with the data is that some of the promoters include a vaporization/ condensation step in their mechanism.

Thermodynamic and vapor pressure data from several sources (29, 37, 38) indicate that at equilibrium, for both temperatures tested here, all of the alkali metal salts in Table 5-3 would be in the vapor phase. As a result, the alkali-to-calcium atomic ratios would be related to the vapor-phase partial pressures of the alkalis, and Figure 5-26 would thus be suggesting an increase in promoter performance with increased alkali partial pressure, a concept which is intuitively reasonable.

Calculations performed using the NASA equilibrium program (39) for flame conditions similar to those used in the Cr_2O_3 tests showed that a considerable amount of chromium species could exist in the vapor phase. For example, at 1600°C where the Cr_2O_3 enhancement was near its maximum, between 10 and 20 percent of the chromium in the system would have been in the vapor phase at equilibrium.

The other known oxidation catalysts, V_2O_5 and Pt, have negligible vapor pressures at the temperatures of these experiments, although V_2O_5 does have a relatively low melting point (690°C) (29, 40).

5.6 Sorbent Deactivation by Coal Ash Minerals

In earlier tests on the 380 kW (thermal) boiler simulator furnace (5), and on the thermal decomposition reactor (22), it was found that some of the minerals which are present in coal ash (e.g., kaolin) can significantly reduce the reactivity of some sorbents if the sorbent and ash mineral come into contact at high temperatures. For example, a mixture of 5 weight percent kaolin in Vicron limestone dramatically decreased the surface area and the utilization, relative to pure Vicron, at temperatures ranging from flame temperatures (1800°C) down to as low as 1200°C. Other sorbents, including Fisher calcium hydroxide and Pfizer dolomite, showed less deactivation by kaolin than did Vicron, especially at temperatures below 1400°C.

This result suggests that some sorbents might be seriously deactivated in coal-fired systems if injected near the flame. However, the possibility exists that such deactivation might not be so severe if the sorbent were injected at the lower temperatures of the upper furnace, near the upper end of the sulfation temperature window (about 1250°C).

Accordingly, the ITR was employed to determine whether kaolin deactivation would be observed at lower temperatures. Mixtures of 5 percent by weight kaolin in Vicron 45-3, V40 and D60 were injected into the ITR at 1000, 1100 and 1200°C. Results of these tests are shown in Figure 5-27 (see the shaded bars in the figure), and are compared with the performance of the pure sorbents without kaolin (open bars). At none of the temperatures does kaolin have a significant impact on calcium utilization by Vicron 45-3. Some effect is observed for D60 and V40 at 1100 and 1200°C, but the impact is small. Further tests were carried out by firing a 1360°C flame into the ITR with the ITR walls 1100°C. Those data are indicated in Figure 5-28. Under this condition again no effect is observed for Vicron 45-3. However, the utilization of Vicron 45-3 alone is so low that absence of effect may only be an artifact of the experimental condition. For the other sorbents injected at 1360°C a substantial effect on utilization is observed.

These results suggest that significant sorbent deactivation by ash minerals might be avoided if the sorbent is injected in the cooler regions of the upper furnace.

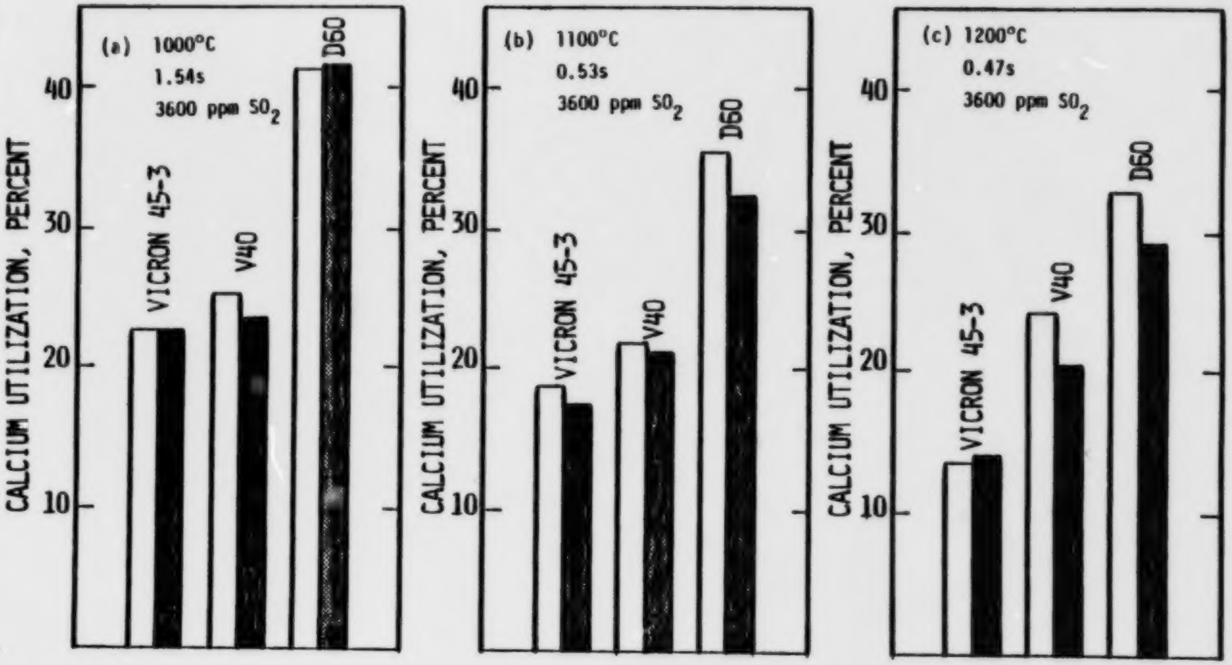

Figure 5-27. Effects of kaolin addition on calcium utilization by V40, D60, and Vicron 45-3 at three temperatures. Open bars represent data for the sorbent alone; shaded bars indicate sorbent-kaolin mixture data (ITR, hydrogen-air flame).

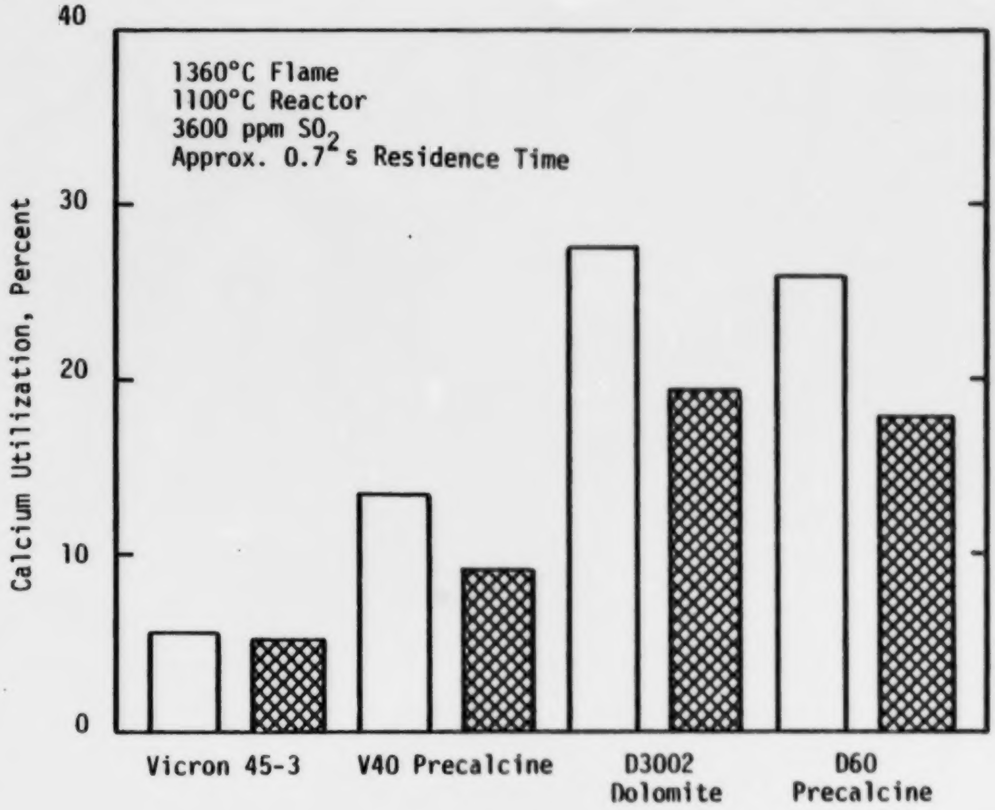

Figure 5-28. Impact of kaolin on calcium utilization of sorbents in the ITR, 1360°C CH_4-air flame, 1100°C furnace, 3600 ppm SO_2 added. Open bars represent data for the sorbent alone, shaded bars indicate sorbent kaolin mixtures.

As discussed Section 5.5, some minerals--including some elements which might be present in coal ash--tend to increase the reactivity of calcium-based sorbents. Accordingly, when a sorbent is injected into a coal-fired boiler, its ultimate reactivity will likely be determined by the tradeoff between any deactivating effects of ash minerals such as kaolin, and any activating effects of ash components such as chromium or sodium.

5.7 Mathematical Model Application

The mathematical model for limestone sulfation developed at the University of Utah under EPA support (33, 41), referred to as the grain model, is intended primarily as a tool for predicting relative levels of sulfur capture by sorbents in different furnaces. On of its applications in this study was to predict the capture in two boilers for a variety of limestones based on the utilization data from both the TDR and the ITR, and previous surface area vs. temperature data (22). The other important application of the model was the comparison of model predictions with utilization profiles from the ITR. In this manner it was possible to estimate how physical properties of the sorbents changed with time during in-situ sulfation.

5.7.1 Grain Model Description

The grain model is based on the assumption that porous lime particles can be represented as conglomerates of non-porous, spherical grains of pure CaO. This is represented in Figure 5-27. Gases reacting with the grains of CaO must first diffuse through pores to reach a grain, and then penetrate a solid $CaSO_4$ product layer surrounding each grain. The overall process of sulfation includes the following steps:

- Diffusion of SO_2 to the particle surface.
- Pore diffusion of SO_2 to the particle's interior.
- Solid diffusion of SO_2 through the product layer surrounding a grain.

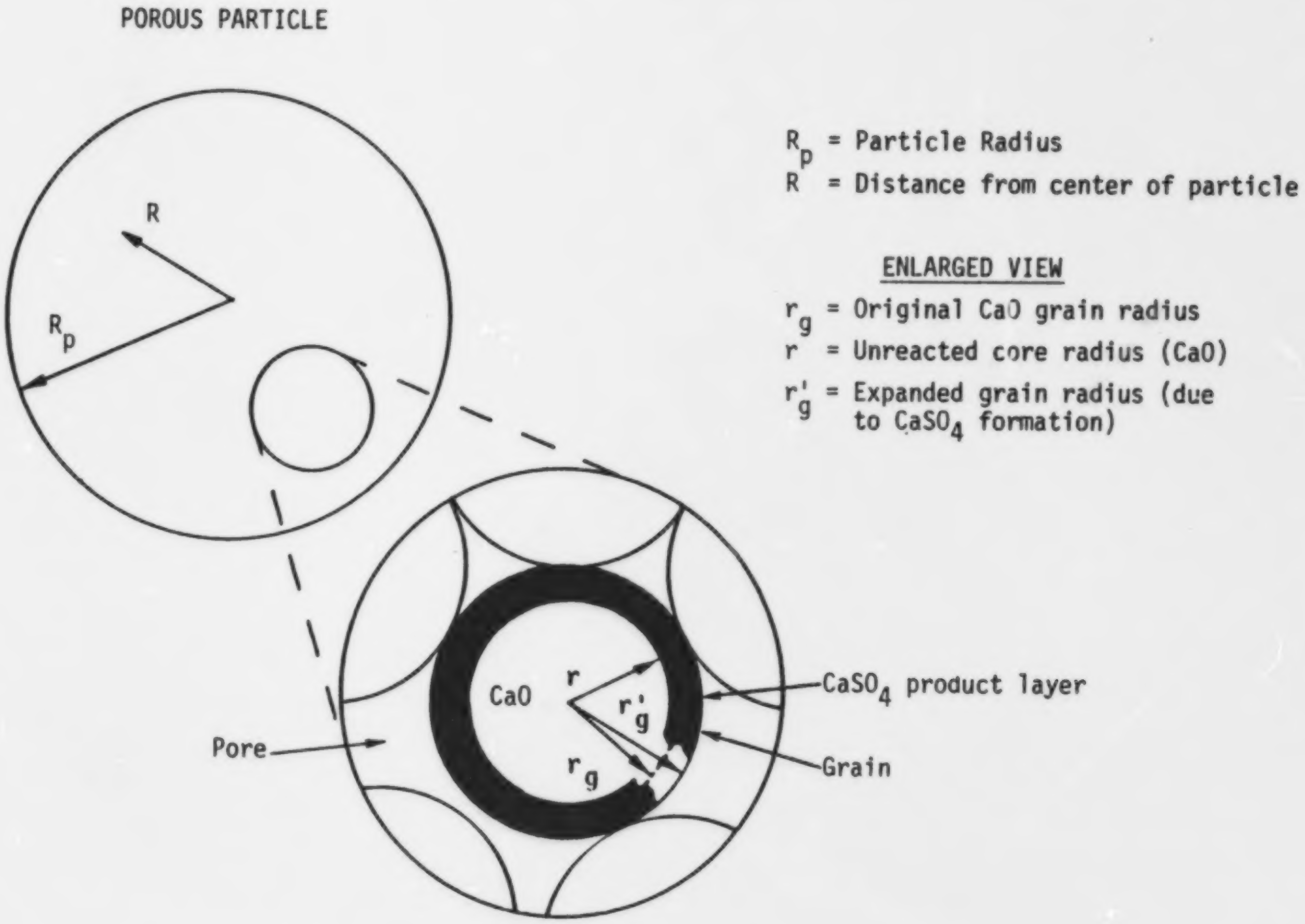
POROUS PARTICLE
R
R_p
CaO
r
r_g'
r_g
Pore
$CaSO_4$ product layer
Grain

R_p = Particle Radius
R = Distance from center of particle

ENLARGED VIEW

r_g = Original CaO grain radius
r = Unreacted core radius (CaO)
r_g' = Expanded grain radius (due to $CaSO_4$ formation)

Figure 5-29. A porous, multigrain particle.

- Reaction to form a solid product at the product-CaO interface.

The molar volume of the product $CaSO_4$ (46.0 cm^3/mol) is greater than the molar volume of CaO (16.9 cm^3/mol). Therefore the pore volume of a reacting particle must decrease as the reaction proceeds, since the grains will be expanding. In the case of calcitic limestones, complete pore blockage may occur since the product molar volume exceeds that of the starting material, $CaCO_3$ (37.0 cm^3/mol). With dolomitic limestones, however, the magnesium component is comparatively inert after calcination and so complete pore blockage is averted. The grain model accounts for pore blockage by decreasing the porosity of the particle as the reaction proceeds.

The following assumptions were made in the development of the grain model:

- The lime particles are completely calcined.
- The particles are spherical and isothermal.
- The rate of mass transfer to the particle surface is not rate-limiting.
- The reaction takes place in the presence of excess oxygen and is irreversible.
- The grains of CaO are small enough that variations in reactant concentrations over their surfaces are negligible.
- The reaction is zero order with respect to SO_2 concentration and proceeds by the unreacted shrinking core model.
- The grains which constitute a particle are either pure CaO or else consist entirely of unreactive compounds. That is, there are no grains which are part impurity and part CaO.

- CaO grains and MgO grains are of the same average size.

- Only CaO and MgO make significant contributions to a particle's surface area.

The model does not account for the loss of surface area due to thermal sintering, but it does account for pore plugging as the CaO molecules expand to become $CaSO_4$ molecules. It also accounts for increased product layer diffusion resistance as the sulfate shell around a grain grows.

Input parameters for the model are limited to:

- Particle radius

- Surface area

- Porosity

- Mole fraction calcium in the particle

- Reaction conditions, including Ca/S molar ratio and including the time-temperature history experienced by the particle.

The simplicity of the model reduces the possibility of misinterpretation of the results. This can occur when a large number of parameters are available which can be adjusted to match a model to a set of data.

5.7.2 Prediction of Sorbent Performance

Sorbent performance was predicted for two p.c. utility boilers with the post-furnace temperature profiles shown in Figure 5-30. The temperature profiles were generated using the EER mathematical model which describes furnace thermal characteristics. The grain model was first applied to the TDR data which were shown in Figure 5-5. The model was used to determine the

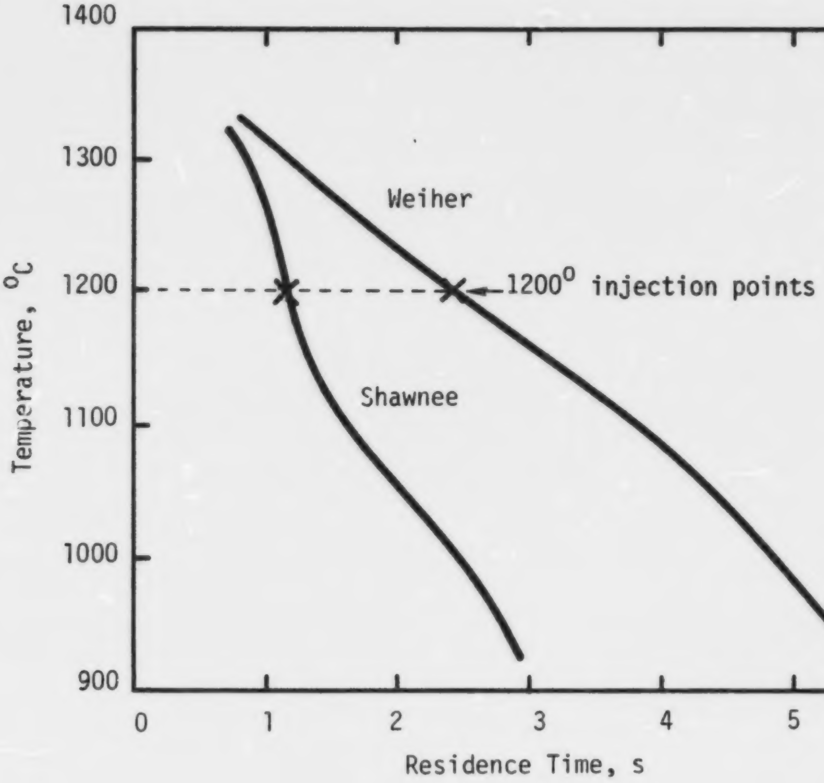

Figure 5-30. Temperature profiles for the Shawnee and Weiher boilers estimated by the EER furnace thermal model.

surface areas which would have been necessary for each of the eight sorbents in order to achieve the measured capture under the reactivity probe conditions (1100°C, 0.6 s). Those surface areas were assumed to be representative of injection at the two TDR temperatures addressed in Figure 5-5 (1200 and 1500°C). The model then was used to predict the capture which would be achieved with each of the sorbents in the Weiher and Shawnee p.e. utility boilers assuming that: a) each sorbent is injected into each boiler at that point where the bulk gas temperature is either 1200°C or 1500°C; b) the sorbent instantaneously calcines to yield the surface area that would be back-calculated from the Figure 5-5 data for the selected injection temperature; and c) the sorbent then experiences the time-temperature history indicated for the particular boiler in Figure 5-30, for that portion of the profile following the injection point.

Estimated surface areas and the boiler capture predictions are listed in Table 5-4. A Ca/S of 2.0 and SO_2 concentration of 1300 ppm were assumed in the calculations. One of the first observations from Table 5-4 is that the surface areas estimated for Vicron 45-3 are very close to those which were measured for this sorbent under identical flame conditions in prior work (22). Also, the surface area of the 34 m^2/g precalcine Vicron has apparently been reduced (due to sintering). This is consistent with the results presented in Section 5.3 for the V40 precalcine. Finally, the results for the two dolomites require some explanation. At 1200°C the estimated surface area of the Pfizer dolomite (38.6 m^2/g) is significantly higher than that for D3002 (23.5 m^2/g). However, the predicted capture for the Pfizer dolomite is only slightly better than D3002 in the Shawnee boiler, and lower in the Weiher boiler. The reason for this is that the model views higher surface area materials as achieving the increased areas by having an increased proportion of tiny micropores (since, as discussed in Section 5.4, the microporosity is the major contributor to surface area). As shown in Section 5.4, these micropores are more susceptible to plugging as the CaO grains expand to become $CaSO_4$. According to the model the net effect in this particular case would be that--although Pfizer would have a higher initial reactivity--much of its internal area would become unaccessible for SO_2 reaction because of plugging. At 1500°C, the estimated surface area for the

TABLE 5-4. ESTIMATED SURFACE AREA[a] AND PREDICTED BOILER CAPTURE[b] AS A FUNCTION OF SORBENT INJECTION TEMPERATURE

	Injection at 1200°C			Injection at 1500°C		
	Area	Percent Capture		Area	Percent Capture	
Sorbent	(m^2/g)	Shawnee	Weiher	(m^2/g)	Shawnee	Weiher
M and M	9.6	31.5	47.0	5.4	19.0	30.0
Vicron 45-3	12.0	38.0	55.0	8.5	29.0	44.0
German $Ca(OH)_2$	14.5	45.0	61.0	11.9	38.0	55.0
RWE $Ca(OH)_2$	16.2	48.0	64.5	11.9	38.0	55.0
Fisher $Ca(OH)_2$	17.9	50.0	67.0	13.5	42.5	59.0
Precalcine, 34 m^2/g	21.4	53.5	69.0	13.5	42.5	59.0
D3002 Dolomite	23.5	55.0	68.0	13.1	42.0	58.0
Pfizer Dolomite	38.6	55.5	61.0	19.3	52.0	69.0

[a] Surface areas are estimated as those required by the grain model to explain the capture levels measured in the TDR - reactivity probe experiments at the indicated temperature (Figure 5-5).

[b] Predicted boiler captures are for Ca/S = 2.0, 1300 ppm SO_2, assuming that the sorbent instantaneously achieves the estimated surface area, and that it experiences that portion of the time-temperature history shown in Figure 5-30 which follows the injection temperature.

Pfizer dolomite is only 19.3 m^2/g. Despite the decrease in area compared to 1200°C, the predicted capture is up to 69 percent in the Weiher boiler (compared to 61 percent at 1200°C), while it is reduced to 52 percent in the Shawnee (compared to 55 percent at 1200°C). The increase in capture in the Weiher profile is due not only to reduced pore plugging (since, at 19.3 m^2/g, the model would predict a longer mean pore size than at 38.6 m^2/g); but also, with injection at 1500°C, there would be increased residence time in the sulfation window, which starts at about 1250°C. The capture predictions listed in Table 5-4 are shown on the bar graph in Figure 5-31.

It is emphasized that the grain model does not explicitly address calcination/activation or thermal sintering, since the kinetics of surface area development and sintering are not sufficiently well understood to permit mathematical formulation into a model. The effects of sintering are implicitly included in the effective surface areas that were back-calculated from the TDR data. In the TDR tests, the sorbents were briefly exposed to the peak temperatures of 1200 and 1500°C in the absence of SO_2, these temperatures dropped steeply, and the sorbent was then exposed (in the reactivity probe, in the presence of SO_2) to 1100°C for 0.6 s. In the performance estimates shown in Table 5-4 and in Figure 5-31, it is being assumed--through the use of the back-calculated effective TDR surface areas--that the thermal sintering which would occur in the Shawnee and Weiher thermal profiles would be the same as that which took place in the TDR/reactivity probe profile. Without a better understanding of thermal sintering kinetics, it is not possible to rigorously conclude how good this assumption is. Not only are the boiler time-temperature histories different from the TDR's--which could influence sintering kinetics--but the presence of SO_2 at the higher temperatures in the boilers could influence sintering. (That is--in addition to causing CaO grains to expand simply due to the difference in molecular volume between CaO and $CaSO_4$--the sulfation reaction might contribute via other mechanisms to the sintering/grain growth process.) As discussed in Section 5.3.1, sintering can contribute to an effective ceiling on calcium conversion for a given sorbent; hence, differences in sintering rates between the TDR and commercial boiler profiles could

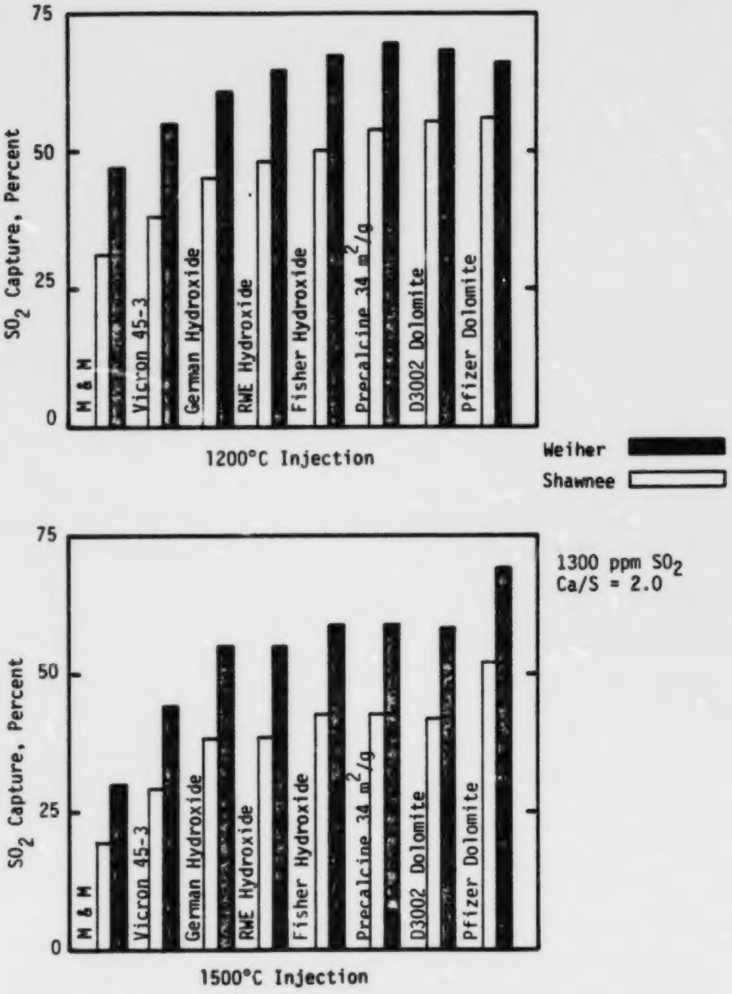

Figure 5-31. Sorbent performance predictions for thermal profiles representative of the Shawnee and Weiher boilers, for two different injection locations, Ca/S = 2.0. Sorbent reactivities estimated from TDR data.

significantly influence the utilizations calculated by the model for the commercial profiles.

In the same manner as that described for the eight TDR sorbents, the model was used also to predict the effects of Cr_2O_3 addition. In this case, the effective surface areas of Vicron/5 percent Cr_2O_3 mixtures at 1200°C and 1500°C were back-calculated from the ITR data shown in Figure 5-21. Predicted capture in the Shawnee and Weiher boilers are shown in Figure 5-32. The unpromoted Vicron data and the Pfizer dolomite data are retained from Figure 5-31. At 1200°C, the Cr_2O_3-promoted sorbent results in somewhat higher sulfur captures for both boiler thermal profiles, compared to unpromoted Vicron, although the calcium utilization levels (percent capture divided by two) are approximately the same in both cases. This result is consistent with Figure 5-22, which shows little enhancement by Cr_2O_3 at 1200°C in the ITR. At 1500°C the measured enhancement in the ITR (Figure 5-22) was 2.5 while that predicted for the Weiher boiler in Figure 5-32 is 1.7.

One reason why the enhancement factor might be lower in these predictions, relative to the ITR data, is that--with the Weiher thermal profile--the sorbent becomes more highly utilized (about 35 percent utilized according to the model), compared to the results in Figure 5-21 with the thermal profile of the ITR (about 28 percent utilized at 1500°C). At the higher utilizations predicted for Weiher, pore plugging by sulfate is greater, and the predicted capture rate by the Vicron-Cr_2O_3 mixture is correspondingly slowed.

The Pfizer dolomite predictions are included in Figure 5-30 to provide a perspective of the advantage of additives. At 1200°C the dolomite is superior to the Cr_2O_3 mixture. For 1500°C injection, Cr_2O_3 addition shows some advantage in both boilers.

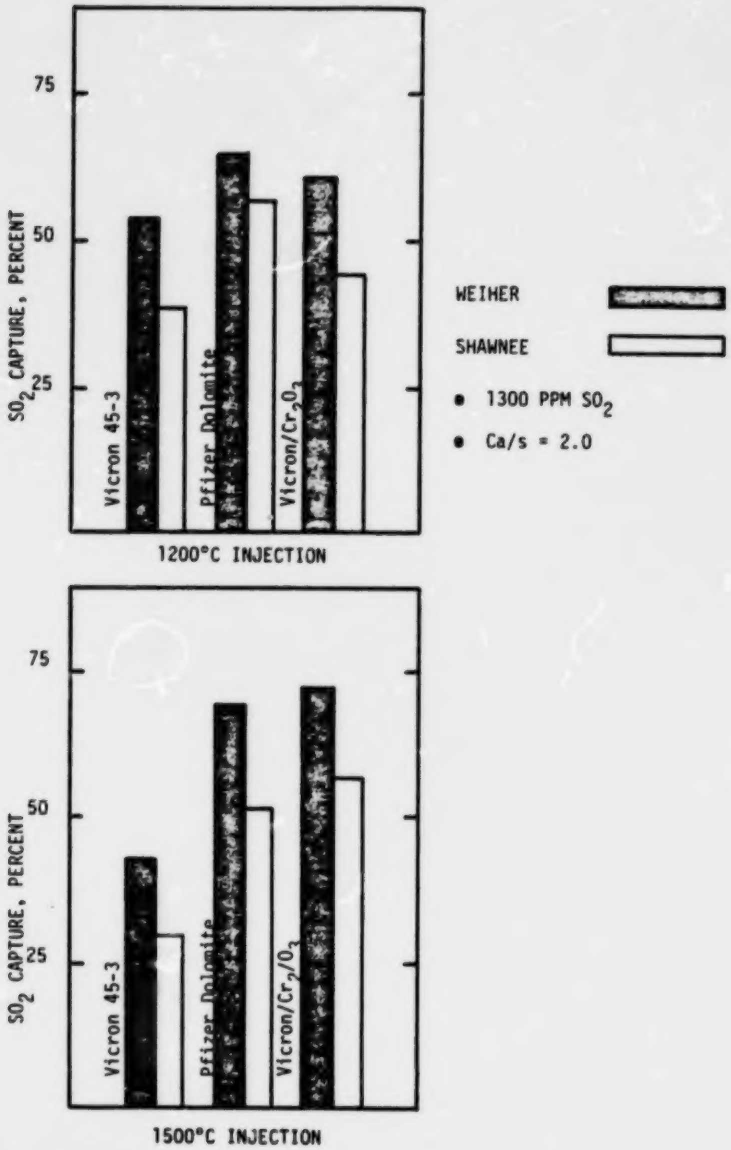

Figure 5-32. Sorbent and sorbent/additive performance predictions for the Shawnee and Weiher boilers. Results are based on in-situ sulfation studies in the isothermal reactor and reactivity probe data from the thermal decomposition reactor.

5.7.3 Estimation of Sintering Effects

The grain model was used to estimate sintering rates for the various sorbents, based upon the ITR sulfation data shown in Figure 5-6 through 5-9.

When sorbent is injected into combustion gases, the surface area which is initially formed during calcination starts to decay, for two reasons: a) thermal sintering; and b) the sulfation reaction, as CaO expands upon conversion to $CaSO_4$. The grain model accounts for the latter phenomenon; beginning with the initial surface area and (calculated) pore size distribution, the model calculates the grain expansion, and the resultant pore plugging and surface area reduction, as the reaction proceeds and the degree of calcium conversion increases. However, the model does not explicitly account for thermal sintering, since the understanding of sintering kinetics is not yet adequate to permit quantitative modeling of the sintering process.

According to the model, the rate of sulfation at any selected level of sorbent utilization is dependent upon the initial surface area (at zero utilization). That is, the actual reactivity (surface area) of the sorbent at a given degree of utilization is calculated, based upon the initial area, by considering the amount of grain expansion (and the resultant loss of initial area) that would presumably have occurred following that degree of calcium conversion. In typical use of the model, the initial surface area is provided as input (along with other parameters, such as temperature profile), and the model then calculates the disappearance of surface area with time. In the application of the model here, however, the reverse is done; the increase in utilization with time is obtained from the ITR data, and the model is then used to back-calculate what the initial area must have been. This back-calculation is performed for several segments of each ITR utilization-versus-time curve (i.e., between several different conversion levels). If thermal sintering did not occur--if sulfation, as accounted for in the model, were the only cause of surface area decay--then, for a given utilization-versus-time curve, the model should back-calculate the same value of initial area, no matter which segment of the curve was used as input to the model. On the other hand, if the segment of the curve between 0 percent and 20 percent utilization suggests one initial surface area, and the segment between 20 percent and 30 percent suggests a lower initial area, then the difference between the two values would be a measure of how much area was lost to thermal sintering during the time period that that increase in utilization was occurring. By performing this calculation for all segments of the curve, a plot of surface area loss (due to sintering) versus time can be generated.

Figure 5-33 illustrates this situation for the case of the two precalcines, V40 and D60, using the ITR data for 1000°C. The two solid curves labeled "Grain Model" show the utilization versus time that would be predicted by the model for a sorbent which was initially 60 m^2/g, and one initially 40 m^2/g, if sintering did not occur (only area loss due to sulfation). The solid lines labeled "ITR Data" (connecting the data points), show the utilization versus time that was actually observed (taken from Figure 5-7); due to sintering effects, these observed utilizations are somewhat less than the grain model would have predicted. The other dotted and dashed segments of lines illustrate how the "initial surface area" inputted to the model would have to be adjusted with time in order to make the model curves fit the actual data curves. For example, for the 60 m^2/g dolomite, the 60 m^2/g model curve fits the data quite well up to about 0.5 s (about 32 percent utilization), suggesting that little sintering took place during this time period. However, for that segment of the curve between 0.5 and 0.8 s, the model would back-calculate an initial area of only about 35 m^2/g, suggesting that something on the order of 25 m^2/g in area has been lost to sintering. Likewise, the segment between 0.8 and 1.0 s suggests an initial area of 25 m^2/g, implying the loss of another 10 m^2/g due to sintering. Similarly, the curve for 40 m^2/g Vicron would suggest that thermal sintering alone would reduce the area of this materials to less than 10 m^2/g within 1 to 1.5 seconds.

Similar curves for V40 and D60 are shown in Figures 5-34 and 5-35, for the cases for 1100°C and 1200°C, respectively. The ITR data for these curves were taken from Figures 5-8 and 5-9. Comparing Figures 5-33, -34 and -35,

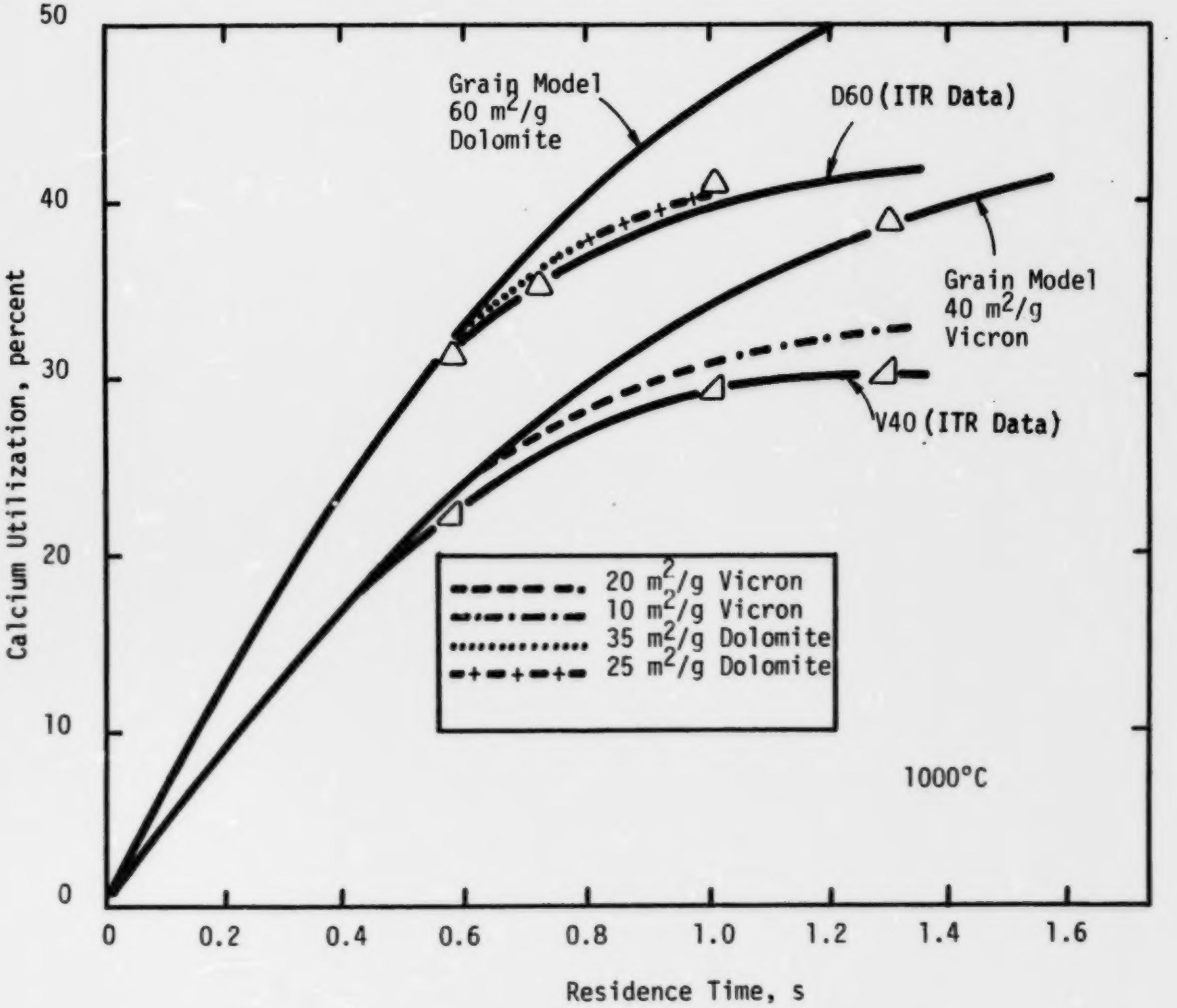

Figure 5-33. Comparison of the grain model with ITR reactivity data for D60 and V40 at 1000°C.

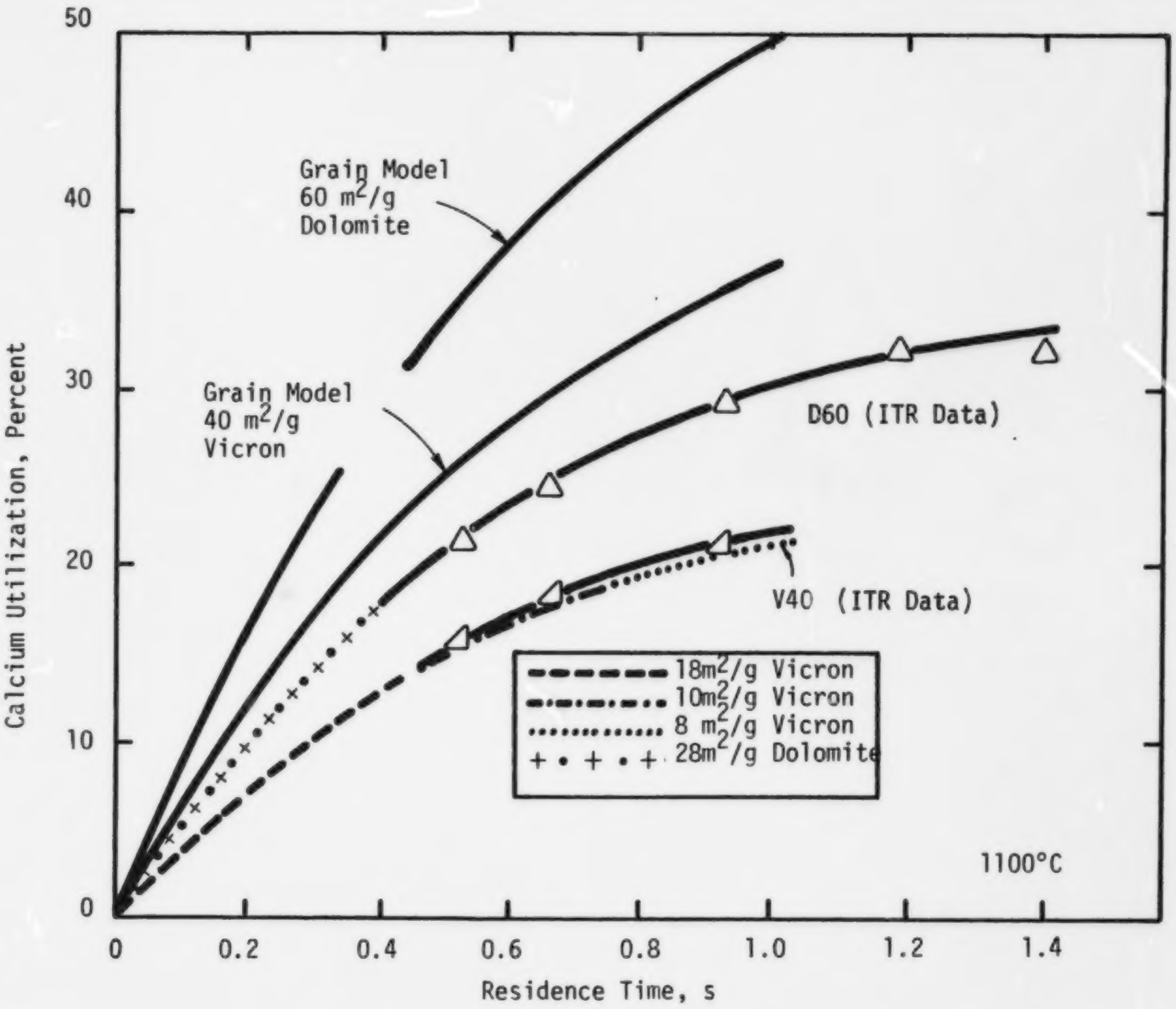

Figure 5-34. Comparison of the grain model with ITR reactivity data for D60 and V40 at 1100°C.

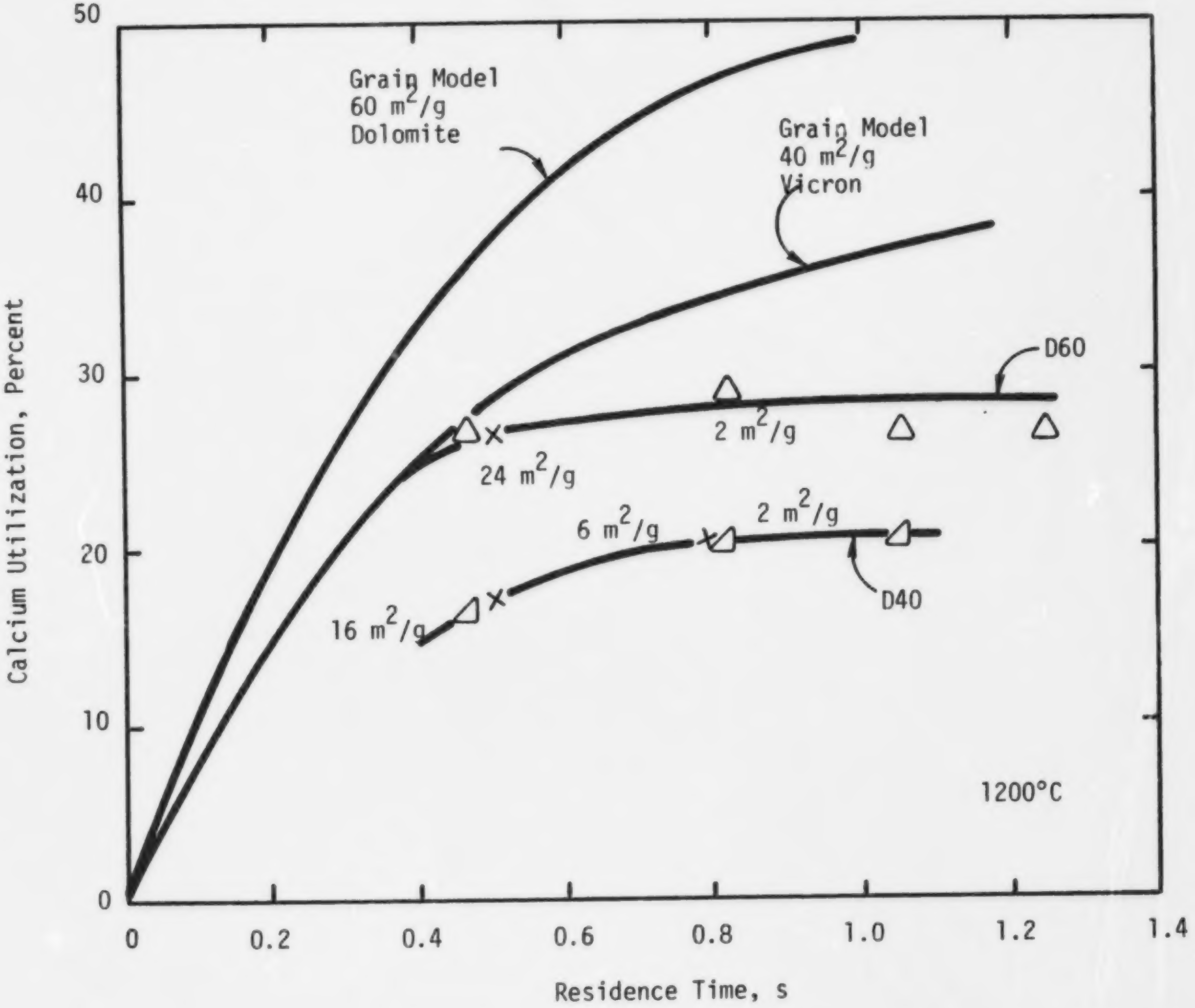

Figure 5-35. Comparison of the grain model with ITR reactivity data for D60 and V40 at 1200°C.

the model is suggesting that the rate of sintering becomes faster at higher temperatures, as expected. For example, the 40 m^2/g Vicron--which appeared to lose little area to sintering during the first 0.4 s at 1000°C--appeared to drop almost immediately to about 18 m^2/g at 1100°C, and to about 16 m^2/g (and ultimately 2 m^2/g) at 1200°C.

Sintering rates for V40 and D60 are illustrated more clearly in Figure 5-36, where the model calculations from the preceding three figures are replotted in the form of calculated initial surface area versus time. It is re-emphasized that the area decay shown here is the estimated result of sintering only; the area loss due to the sulfation reaction has been accounted for by the model, and would represent additional area decay beyond that shown in Figure 5-36. From the figure, it appears that the onset of sintering is delayed at 1000°C. This result might reflect a real delay in particle heating, or it might suggest that sintering does not become pronounced until a certain level of sulfation is achieved; sintering of CaO is known to be accelerated in the presence of $CaSO_4$ (14). At higher temperatures, the sintering rate is greatly increased; e.g., more than half of the initial area is lost in less than 250 ms above 1100°C.

It is of interest to apply this same mathematical modeling approach to the ITR results on raw Vicron and raw D3002 dolomite. In the case of the precalcined materials, the surface area-versus-time relationship is relatively more simple: the materials start with a known area, and this area decays with time after injection, due to sulfation and sintering, as illustrated in Figure 5-36. With raw sorbents, however, the calcination/surface area development process is superimposed, and the area-versus-time history becomes more complex. It would be expected that, initially area would rise from that of the raw stones (less than 1 m^2/g) up to some value, as calcination proceeded, and that the area would then fall as the sulfation and sintering effects began to predominate. The grain model does not account for calcination kinetics and surface area development, and, as stated previously, it does not account for sintering. Therefore, in applying the model to the ITR data with the raw sorbents, it is not possible to separate out the individual effects of area development and of sintering (as was

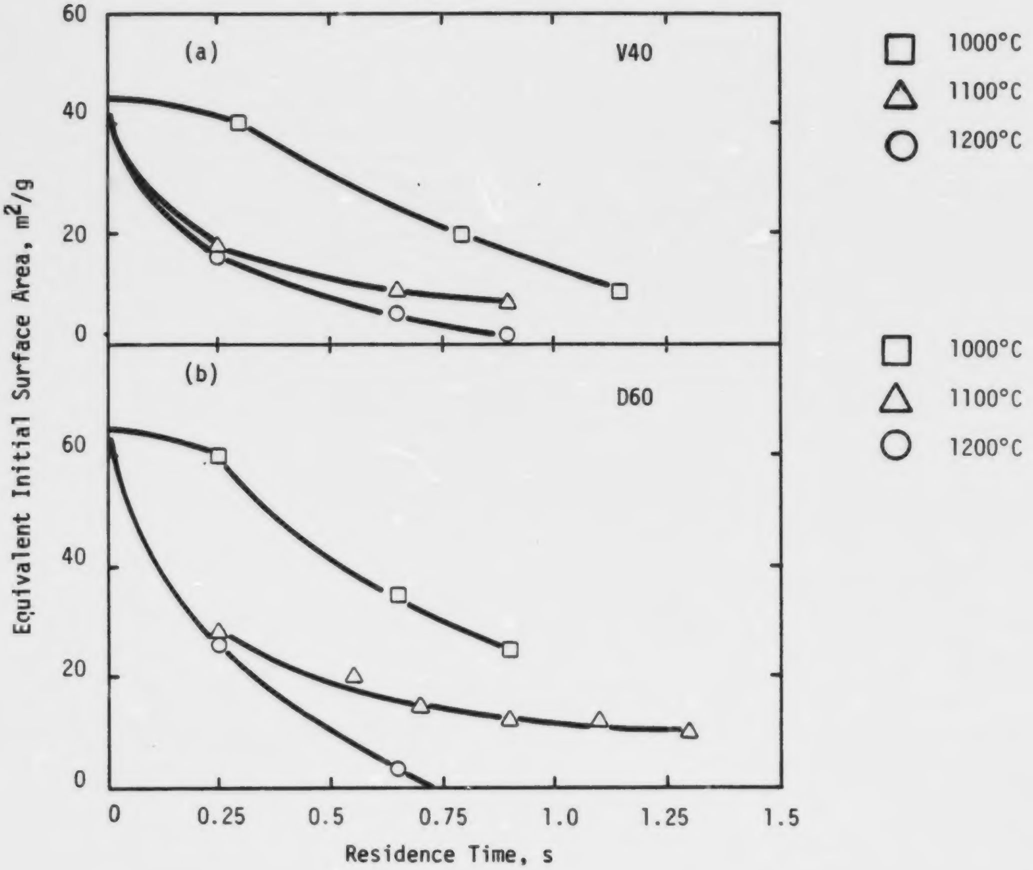

Figure 5-36. Estimated rate of surface area decay due to thermal sintering only, for (a) V40 and (b) D60. Estimates obtained by applying grain model to ITR Sulfation rate data.

possible for sintering with the precalcine data). Nevertheless, it is instructive to look at the net effects of the area development and decay phenomena in combination.

Figure 5-37 shows the back-calculated surface areas for raw Vicron and D3002 dolomite, obtained by applying the grain model to the ITR data at 1000°C and 1100°C. As seen from the figure, the model analysis would suggest that surface area does indeed pass through a peak (after perhaps 0.6 s at these temperatures), which exists only briefly (about 0.1 s) before decaying rapidly. However, the height of this transient peak (over 60 m^2/g in several cases, according to the model calculations) is surprisingly great, much higher than typically observed when sorbent samples are extracted and analyzed after short residence times in experimental units. One possible explanation for these apparent high transient areas is that they might be artifacts of the calculational approach used here, with scatter in the ITR conversion-versus-time data, or with modeling uncertainties, causing the model to predict high areas which were in fact never present. Another possible explanation is that the high transients were in fact real, and that such high transients have not been detected by B.E.T. analysis on extracted samples because much of this short-lifetime area decays in the sampling system.

Other than the height of the peaks, the remainder of the curves in Figure 5-37 appear intuitively reasonable. There is an initial period (during the first 0.5 to 0.75 s) when surface area rises from below 1 m^2/g to some peak, concurrent with particle heatup and calcination. (As indicated by the calcination data presented in Table A-3 for these ITR runs, the sorbents might be perhaps only 35 to 85 percent calcined at these temperatures at the residence times at which the surface area peaks occur.) Following the peaks, the area drops rapidly to values (2 to 10 m^2/g) representative of those which have been measured on extracted samples. For a given sorbent, an increase in temperature from 1000 to 1100°C shifts the peak toward earlier times (because calcination occurs more rapidly), and reduces the height of the peak (since area decay phenomena occur more rapidly and begin to predominate sooner). The effect of increased temperature is more pronounced for Vicron than for the dolomite; this result is consistent with earlier TDR data (22).

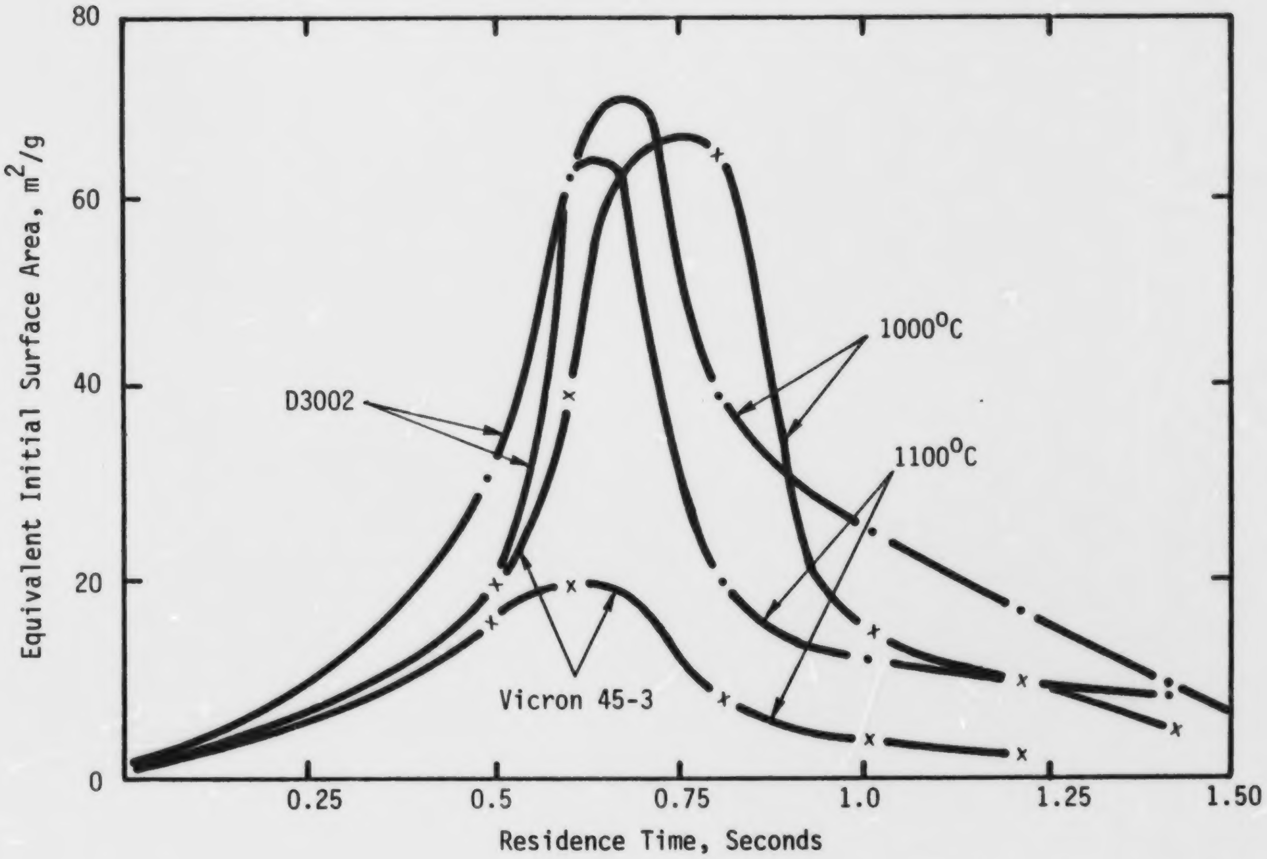

Figure 5-37. Estimated surface area history in tests with raw Vicron and D3002 dolomite. Estimates obtained by applying grain model to ITR sulfation rate data.

5.8 Summary

Several significant findings were made in this study and outlined in the preceding sections. A technique was developed to enable the batch production of high-surface area precalcined sorbents in quantities sufficient for extensive testing in a dispersed-phase reactor. A number of sorbents were tested in one of two dispersed-phase reactors with overlapping thermal environments. The first reactor provided high temperatures (>1200°C) and short residence times (<250 ms) reflective of the conditions prevailing in the flame zone of a utility boiler. The second reactor allowed sorbents to experience the lower temperatures (900-1200°C) and longer residence times (0.25-2.0 s) prevalent in the upper furnace and early convective passages of a utility boiler.

Results of reactivity tests involving a variety of sorbents in the two reactors revealed that SO_2 reactivity increases with decreasing calcination temperature above 1000°C. Furthermore, for simultaneous calcination and sulfation under isothermal conditions, the maximum utilization for five different sorbents occurred at 1000°C. At a given temperature, most sorbents appeared to reach a ceiling in conversion to sulfate, such that little, if any, additional conversion occurred with further increases in residence time (up to 1.5 s).

Mercury porisimetry was used to study precalcined sorbents before and after low-temperature sulfation. The results showed that nearly all of the surface area of both precalcines lay in pores around 100-130 A° in diameter. After sulfation to nearly equal calcium utilizations, the high-calcium sorbent showed 40 percent closure of these pores while for the dolomitic materials the loss in porosity was only 14 percent. This provided insight into the role of magnesium in the typically higher utilizations attained by dolomites.

The use of chemical additives to promote the capture of SO_2 by limestone was investigated. Fifteen additives were examined to determine their potential for increasing limestone utilization. High temperature

(1600-1700°C) injection was necessary to obtain the greatest relative increase in reactivity with Cr_2O_3 addition, albeit at the cost of decreased overall utilization. Next to Cr_2O_3 the most promising materials were alkali metal salts. The enhancement of reactivity by alkalis increased linearly with the molar concentration of the alkali added to the limestone.

Finally, a grain model was used to apply and interpret the results of several tests performed in both the TDR and the ITR. Results of 1200 and 1500°C injection into the TDR were used to predict capture by Vicron 45-3 and Pfizer dolomite in two boilers (Shawnee and Weiher). ITR test results with Cr_2O_3 addition were then used to predict the effects of Cr_2O_3 on capture in the same boilers as a function of injection location. The grain model was also applied to estimate rates of sintering for the precalcines V40 and D60 during sulfation in the ITR, and to estimate the surface area history for raw sorbents.

6.0 REFERENCES

1. Kelly, M. E. and S. A. Shareef. Second Survey of Dry SO_2 Control Systems. EPA-600/7-81-018, U.S. Environmental Protection Agency, February 1981, NTIS No. PB81-157919.

2. Boynton, R. S. Chemistry and Technology of Limestone, 2nd ed. J. Wiley and Sons, N.Y., 1980.

3. Attig, R. C. and P. Sedor. Additive Injection for Sulfur Dioxide Control: A Pilot Plant Study. APTD-1176, U.S. Environmental Protection Agency, March 1970, NTIS No. PB 226761.

4. Coutant, R. W., R. Simon, B. Campbell, and R. E. Barrett. Investigation of the Reactivity of Limestone and Dolomite for Capturing SO_2 from Flue Gas. APTD-0802, U.S. Environmental Protection Agency, October 1971, NTIS No. PB204385.

5. Case, P. L., L. Ho, W. D. Clark, E. Kan, D. W. Pershing, R. Payne, and M. P. Heap. Testing of Experimental Wall-Fired Furnaces to Reduce Emissions of Nitrogen and Sulfur Oxides, Volumes 1 and 2, EPA-600/7-85-026a and -026b, U.S. Environmental Protection Agency, June 1985, NTIS Nos. PB85-224632 and -224640.

6. Borgwardt, R. H. Calcination Kinetics and Surface Area of Dispersed Limestone Particles. AIChE J. 1985, 31 (1), 103-11.

7. Borgwardt, R. H. Kinetics of the Reaction of SO_2 with Calcined Limestone. Environ. Sci. and Technology. 1970, 4 (1), 59-63.

8. Borgwart, R. H. and R. D. Harvey. Properties of Carbonate Rocks Related to SO_2 Reactivity. Environ. Sci. and Technology. 1972, 6 (4), 350-60.

9. Bhatia, S. K. and D. D. Perlmutter. AIChE J. 1980, 26 (3), 379-86.

10. Bhatia, S. K. and D. D. Perlmutter. AIChE J. 1981, 27 (2), 226-34.

11. Bhatia, S. K. and D. D. Perlmutter. AIChE J. 1981, 27 (2), 247-54.

12. McClellan, G. H. Physical Characterization of Calcined and Sulfated Limestones. Presented at the Fourth Dry Limestone Process Symposium. Gilbertsville, KY, June 1970.

13. Harvey, R. D. Petrographic and Mineralological Characteristics of Carbonate Rocks Related to Sorption of Sulfur Oxides in Flue Gases. APTD-0920, U.S. Environmental Protection Agency, July 1971, NTIS No. PB206487.

14. Glasson, D. R., J. Appl. Chem 1967, 17, 91-6.

15. Glasson, D. R. and P. O'Neill in Characterization of Porous Solids. S. J. Gregg, Ed. Soc. of Chem. Ind., London: 1979.

16. Beruto, D., L. Barco, A. W. Searcy, and G. Spinolo. J. Am. Cer. Soc., 1980, 63 (7-8), 439-43.

17. Huggins, F. E., D. A. Kosmack, and G. F. Huffman. Fuel 1981, 60, 577-84.

18. Wibberley, L. J. and T. F. Wall. Fuel 1982, 61, 93-9.

19. Yang, R. T. and M. S. Shen. AIChE J. 1979, 25 (5), 811-9.

20. Frazier, G. C. and E. J. Badin. Chemically Improved Limestones for Fluidized Bed Coal Combustion. Paper presented at the meeting of the Central States Section of The Combustion Institute. Lexington, KY; March 1983.

21. Baker, D. C. and A. Attar. Environ. Sci. and Technol. 1981, 15 (3) 288-93.

22. Cole, J. A., W. D. Clark, M. P. Heap, J. C. Kramlich, G. S. Samuelsen, and W. A. Seeker. Fundamental Studies of Sorbent Calcination and Sulfation for SO_2 Control from Coal-Fired Boilers. EPA-600/7-85-027, U.S. Environmental Protection Agency, June 1985, NTIS No. PB85-221729.

23. Seeker, W. R., G. S. Samuelsen, M. P. Heap, and J. D. Trolinger. 18th Symp (Intl) on Combustion: The Combustion Institute, Pittsburg, PA, 1981: p. 1213-26.

24. Hamor, R. J. and I. W. Smith. Fluidizing Feeders for Fine Particles at Low Stable Flows. Fuel, 1971, 50 394-404.

25. Altenkirch, R. A., R. E. Peck and S. L. Chen. Fluidized Bed Feeding of Pulverized Coal. Powder Technology, 1978, 20 189-196.

26. Field, M. A., D. W. Gill, B. B. Morgan, and P. G. W. Hawksley. Combustion of Pulverized Coal. British Coal Utilization Research Association. Leatherhead, England, 1967.

27. Arpaci, V. S. Conduction Heat Transfer. Addison-Wesley; Reading, MA; 1966, p. 284.

28. Kirchgessner, D. A. "Laboratory-Scale Production and Characterization of High Surface Area Sorbents." In: Proceedings: First Joint Symposium on Dry SO_2 and Simultaneous SO_2/NO_x Control Technologies, Volume 1, EPA-600/9-85-020a, U.S. Environmental Protection Agency, July 1985, NTIS No. PB85-232353.

29. CRC Handbook of Chemistry and Physics. R. C. Weast, Ed. CRC Press, Cleveland, OH, 1976; pp. F90, D183-8, B174.

30. Borgwardt, R. H., K. R. Bruce, and J. Blake. "EPA Experimental Studies of the Mechanisms of Sulfur Capture by Limestone." In: Proceedings: First Joint Symposium on Dry SO_2 and Simultaneous SO_2/NO_x Control Technologies, Volume 1, EPA-600/9-85-020a, U.S. Environmental Protection Agency, July 1985, NTIS No. PB85-232353.

31. Borgwardt, R. H., G. R. Gillis, and N. F. Roache. IERL-RTP Research on Sulfur Capture in LIMB. In: Proceedings of the 1982 Joint Symposium on Stationary Combustion NO_x Control, Volume I, EPA-600/9-85-022a, U.S. Environmental Protection Agency, July 1985, NTIS No. PB85-235604.

32. Not used.

33. Silcox, G. D., D. M. Slaughter, and D. W. Pershing. Paper presented at the 20th Symp (Intl) on Combustion. Ann Arbor, MI: August 1984.

34. Slaughter, D. M. Ph.D. Dissertation. University of Utah. Salt Lake City, 1984.

35. Overmoe, B. J., S. L. Chen, L. Ho, W. R. Seeker, M. P. Heap, and D. M. Pershing, "Boiler Simulator Studies on Sorbent Utilization for SO_2 Control." In: Proceedings: First Joint Symposium on Dry SO_2 and Simultaneous SO_2/NO_x Control Technologies, Volume 1, EPA-600/9-85-020a, U.S. Environmental Protection Agency, July 1985, NTIS No. PB85-232353.

36. Fieldes, R. B., N. A. Burdett, and J. F. Davidson. Trans. I. Chem. E. 1979, 57, 276-80.

37. JANAF Thermochemical Tables. 2nd ed. Stull, D. R. and H. Prophet, Eds. NSRDS-NBS-37, 1971.

38. Chase, M. W. Jr., J. L. Curnutt, J. R. Downey Jr., R. A. McDonald, A. N. Syverud, and E. A. Valenzuela. J. Phys. Chem. Ref. Data. 1982, 1 (3), 695-940.

39. Gordon, S. and B. J. McBride. Computer Program for Calculation of Complex Chemical Equilibrium Compositions, Rocket Performance, Incident and Reflected Shocks and Chapman-Jouquet Detonations. NASA SP-273, 1976.

40. Chase, M. W., J. L. Curnutt, H. Prophet, R. A. McDonald, and A. N. Syverud. J. Phys. Chem. Ref. Data, 1975, 4 (1) 1-175.

41. Silcox, G. D. Mathematical Modelling of the SO_2-Lime Reaction System: Mathematical Modelling and Experimental Studies with Emphasis on Stoke Applications. Ph.D. Dissertation, University of Utah, Salt Lake City, 1984.

42. McCabe, W. L. and J. C. Smith. Unit Operations of Chemical Engineering. McGraw-Hill; NY: 1967, p. 352.

APPENDIX A

Raw Data

TABLE A-1. PRECALCINE GENERATION DATA*
(See Note on Page A-6)

Sample No	Material	Starting Mass, g	N_2 Flow, $cm^3 \cdot g^{-1} \cdot s^{-1}$	Temperature °C	Time Minutes	Calcination[a], Percent	Surface Area m^2/g
101779	Vicron 45-3	35	4.5	700	150	99	35.4
101625	Vicron 45-3	35	4.5	700	150	99	35.4
101760	Vicron 45-3	35	4.5	700	150	99	34.9
101639	Vicron 45-3	35	4.5	700	150	99	35.6
101832	Vicron 45-3	35	4.5	700	150	99	34.1
101710	Vicron 45-3	35	4.5	700	150	99	33.6
101587	Vicron 45-3	35	6.75	700	192	99	21.8
101585	Vicron 45-3	35	6.75	700	192	99	38.9
101586	Vicron 45-3	35	6.75	700	150	98	32.5
101588	Vicron 45-3	35	6.75	700	150	98	38.2
102084	Vicron 45-3	35	6.75	700	270	99	28.5
102083	Vicron 45-3	35	6.75	700	150	99	40.7
101589	Vicron 45-3	35	6.75	700	150	98	41.7
102073	Vicron 45-3	35	6.75	700	150	--	40.8
102071	Vicron 45-3	35	6.75	700	120	96	40.0
102059	Vicron 45-3	35	6.75 air	700	90	94	36.7
102058	Vicron 45-3	35	6.75 air	700	60	9,0	1.2
102057	Vicron 45-3	35	6.75 air	700	150	99	41.2
102056	Vicron 45-3	35	6.75 air	700	120	99	40.8
102055	Vicron 45-3	35	6.75 air	700	150	99	41.9
102028	Vicron 45-3	35	6.75 air	700	150	99	44.9
102029	Vicron 45-3	35	6.75 air	700	150	99	42.5
102030	Vicron 45-3	35	6.75 air	700	150	98	43.3
102031	Vicron 45-3	35	6.75 air	700	150	99	43.1
102032	Vicron 45-3	35	6.75 air	700	150	99	35.1
102032	Vicron 45-3	35	6.75 air	700	150	99	39.2
102038	Vicron 45-3	35	6.75 N_2	750	60	99	40.8
102037	Vicron 45-3	35	6.75 air	750	60	100	24.8
101558	Vicron 45-3	35	1.12	750	30	56	7.2
103520	Vicron 45-3	35	1.12	750	60	79	11.0
103521	Vicron 45-3	35	0.0	750	120	12	1.4
103556	Vicron 45-3	35	1.12	750	120	98	19.7
101969	Vicron 45-3	35	1.12	750	60	93	15.5
101970	Vicron 45-3	35	1.12	700	60	23	3.7
101978	Vicron 45-3	35	1.12	700	60	23	2.9
101977	Vicron 45-3	35	1.12	700	90	29	4.2
101976	Vicron 45-3	35	1.12	700	75	31	4.0

[a] Calcium Basis

TABLE A-1. CONTINUED

Sample No.	Material	Starting Mass, g	N2 Flow, $cm^3 \cdot g^{-1} \cdot s^{-1}$	Temperature $^{\circ}C$	Time Minutes	Calcination[a], Percent	Surface Area m^2/g
101965	Vicron 45-3	35	1.12	700	120	46	6.4
101966	Vicron 45-3	35	1.12	700	150	63	9.0
101967	Vicron 45-3	35	1.12	700	180	60	8.3
101968	Vicron 45-3	35	4.5	700	60	81	19.3
101971	Vicron 45-3	35	4.5	700	90	68	15.1
101972	Vicron 45-3	35	4.5	700	180	94	33.4
101973	Vicron 45-3	35	4.5	700	60	58	12.5
101964	Vicron 45-3	35	4.5	700	120	99	36.5
101962	Vicron 45-3	35	4.5	700	150	97	33.1
101699	Dolomite (Pfizer)	35	4.5	700	180	98	58.0
101636	Dolomite (Pfizer)	35	4.5	700	60	31	28.3
101846	Vicron 45-3	35	4.5	700	150	98	23.5
101829	Vicron 45-3	35	4.5	700	150	97	31.5
101681	Vicron 45-3	35	4.5	700	150	99	36.9
101734	Vicron 45-3	35	4.5	700	150	99	32.6
101791	Vicron 45-3	35	4.5	700	150	99	38.4
101611	Vicron 45-3	35	4.5	700	150	99	34.0
101845	Vicron 45-3	35	4.5	700	150	98	32.8
101827	Vicron 45-3	35	4.5	700	150	98	37.0
102034	Vicron 45-3	35	6.75	700	150	99	40.4
102035	Vicron 45-3	35	6.75	700	150	99	32.5
102064	Vicron 45-3	35	6.75	700	150	99	42.7
102036	Vicron 45-3	35	9.00 air	700	120	--	24.7
102039	Vicron 45-3	35	9.00 air	750	90	12	1.9
101724	Vicron 45-3	35	9.00 N_2	750	60	99	41.0
101765	Vicron 45-3	35	9.00 N_2	750	60	99	42.3
101767	Vicron 45-3	35	9.00 N_2	750	60	99	42.1
101722	Vicron 45-3	35	9.00 N_2	750	60	99	43.5
101775	D3002	35	9.00 N_2	700	60	97	65.7
101782	D3002	35	9.00 N_2	700	60	98	65.6
101796	D3002	35	9.00 N_2	700	45	95	63.5
101797	D3002	35	9.00 N_2	700	45	97	65.2
101810	D3002	35	9.00 N_2	700	45	90	59.1
101834	D3002	35	9.00 N_2	700	45	95	62.9
101838	D3002	35	9.00 N_2	700	45	97	65.8
101840	D3002	35	9.00 N_2	700	45	97	60.5
101850	D3002	35	9.00 N_2	700	45	84	56.4

[a] Calcium Basis

TABLE A-1. CONTINUED

Sample No.	Material	Starting Mass, g	N_2 Flow, $cm^3 \cdot g^{-1} \cdot s^{-1}$	Temperature ^oC	Time Minutes	Calcination[a], Percent	Surface Area m^2/g
100606	D3002	35	9.00 N_2	700	45	97	62.4
100607	D3002	35	9.00	700	45	98	64.3
100608	D3002	35	9.00	700	45	96	61.9
100610	D3002	35	9.00	700	45	97	65.5
100612	D3002	35	9.00	700	45	97	62.3
100613	D3002	35	9.00	700	45	97	66.9
100634	D3002	35	9.00	700	45	97	62.4
100635	D3002	35	9.00	700	45	98	64.1
100636	D3002	35	9.00	700	45	98	62.5
100637	D3002	35	9.00	700	45	97	67.1
100650	D3002	35	9.00	700	45	96	64.1
100651	D3002	35	9.00	700	45	96	67.2
100652	D3002	35	9.00	700	45	97	62.4
100653	D3002	35	9.00	700	45	93	65.5
100654	D3002	35	9.00	700	45	97	65.6
100655	D3002	35	9.00	700	45	88	57.8
100656	D3002	35	9.00	700	45	98	-
100653	D3002	35	9.00	700	45	99	-
100672	Vicron 45-3	16	19.7	700	80	99	53.7
100675	Vicron 45-3	8	39.4	700	40	99	51.2
100677	Vicron 45-3	5	63.0	700	20	86	38.5
100691	D3002	35	9.00	700	45	94	61.8
100695	D3002	35	9.00	700	45	98	66.5
100697	D3002	35	9.00	700	45	98	66.1
114104	D3002	35	9.00	700	45	96	66.4
114106	D3002	35	9.00	700	45	95	63.1
114108	D3002	35	9.0	700	45	96	63.3
114110	D3002	35	9.0	700	45	99	58.5
114125	Vicron 45-3	60	9.18	700	90	97	42.9
114126	Vicron 45-3	60	9.18	700	75	98	42.4
114127	Vicron 45-3	60	9.18	700	75	99	40.2
114128	Vicron 45-3	35	9.00	700	75	99	31.5
114131	Vicron 45-3	35	9.00	700	75	99	37.0
114132	D3002	35	9.00	700	45	94	60.3
114135	Vicron 45-3	60	9.18	700	75	98	40.2
114136	Vicron 45-3	60	9.18	700	60	97	40.7
114138	Vicron 45-3	60	9.18	700	60	96	38.9
114143	Vicron 45-3	60	9.18	700	60	94	41.9

[a] Calcium Basis

TABLE A-1. CONTINUED

Sample No.	Material	Starting Mass, g	N_2 Flow, $cm^3 \cdot g^{-1} \cdot s^{-1}$	Temperature, ^oC	Time Minutes	Calcination[a], Percent	Surface Area m^2/g
114145	Vicron 45-3	69	9.18	700	75	99	41.6
114149	Vicron 45-3	120	4.59	700	150	89	26.8
114158	Vicron 45-3	60	9.18	700	75	98	45.5
114160	Vicron 45-3	60	9.18	700	75	96	39.1
114161	Vicron 45-3	60	9.18	700	75	98	48.8
114168	Vicron 45-3	60	9.18	700	75	99	44.2
114171	Vicron 45-3	60	9.18	700	75	99	43.9
114173	Vicron 45-3	60	9.18	700	75	93	41.1
114177	Vicron 45-3	60	9.18	700	75	98	39.5
114180	Vicron 45-3	60	9.18	700	75	98	42.9
114184	Vicron 45-3	60	9.18	700	75	98	43.1
114187	Vicron 45-3	60	9.18	700	75	84	48.4
114189	D3002	60	9.18	700	75	98	69.7
114192	D3002	60	9.18	700	75	99	58.0
114199	D3002	60	9.18	700	75	97	67.2
114200	D3002	60	9.18	700	75	98	65.9
114201	D3002	60	9.18	700	75	98	68.3
114202	Vicron 45-3	60	9.18	700	75	98	42.1
114205	Vicron 45-3	60	9.18	700	75	97	40.2
114206	Vicron 45-3	60	9.18	700	75	96	40.8
114207	Vicron 45-3	60	9.18	700	75	96	42.3
114209	Vicron 45-3	60	9.18	700	75	94	40.1
114211	Vicron 45-3	60	9.18	700	75	87	45.9
114213	Vicron 45-3	60	9.18	700	75	98	38.7
114218	Vicron 45-3	60	9.18	700	75	99	43.9
114222	Vicron 45-3	60	9.18	700	75	99	43.7
114224	Vicron 45-3	60	9.18	700	75	98	44.7
114267	Vicron 45-3	60	9.18	700	75	99	29.9
114228	Vicron 45-3	60	9.18	700	75	99	47.0
114229	Vicron 45-3	69	9.18	700	75	98	43.5
114235	Vicron 45-3	60	9.18	700	75	99	41.9
114236	Vicron 45-3	69	9.18	700	75	98	39.7
114237	Vicron 45-3	60	9.18	700	75	98	46.5
114238	Vicron 45-3	60	9.18	700	75	99	46.3
114241	Vicron 45-3	60	9.18	700	75	99	42.8
114273	D3002	60	9.18	700	75	97	66.0
114274	D3002	60	9.18	700	75	99	43.3

[a] Calcium Basis

TABLE A-1. CONTINUED

Sample No.	Material	Starting Mass, g	N_2 Flow, $cm^{3}\cdot g^{-1}\cdot s^{-1}$	Temperature ^{o}C	Time Minutes	Calcination[a], Percent	Surface Area m^2/g
114285	D3002	60	9.18	700	75	98	53.0
114286	D3002	60	9.18	700	75	98	53.0
114287	D3002	60	9.18	700	75	99	25.0
111158	D3002	60	9.18	700	75	94	60.0
111159	D3002	60	9.18	700	75	94	69.6
111165	D3002	60	9.18	700	75	--	67.0
111172	D3002	60	9.18	700	75	97	66.6
111179	D3002	60	9.18	700	75	--	60.2
111180	D3002	60	9.18	700	75	97	70.5
111181	D3002	60	9.18	700	75	97	68.8
111182	D3002	60	9.18	700	75	97	74.1
111183	D3002	60	9.18	700	75	97	67.2
111184	D3002	60	9.18	700	75	95	65.6
111187	D3002	60	9.18	700	75	97	62.2
111188	D3002	60	9.18	700	75	--	-
111297	Genstar	60	9.18	500	45	--	-
111302	Genstar	60	9.18	500	45	--	-
111311	Genstar	60	9.18	500	45	--	-
111326	Genstar	60	9.18	500	45	--	-
111327	Genstar	60	9.18	500	30	--	-
111328	Genstar	60	9.18	500	20	--	-
111329	Genstar	60	9.18	500	20	--	-

[a] Calcium Basis

* NOTE: These precalcines generation data cover only operation of the precalcination apparatus shown in Figure 4-6. Results from work on other precalcination approaches--tested as part of the effort to develop an adequate precalciner for this laboratory study--are discussed in Appendix C.

TABLE A-2. THERMAL DECOMPOSITION REACTOR SULFATION DATA

Sample	Sorbent	Peak Flame Temperature, °C	Calcination[a], Percent	Calcium Utilization, Percent
101774	German $Ca(OH)_2$	1100	-	34.4
101715	German $Ca(OH)$	1200	-	20.7
101605	German $Ca(OH)_2$	1515	-	15.3
101735	34 m^2/g Precalcine	1200	-	26.1
101637	34 m^2/g Precalcine	1100	-	44.7
101814	34 m^2/g Precalcine	1360	-	20.0
102075	M&M Limestone	1360	76.8	9.6
102079	M&M Limestone	1515	82.4	8.6
102076	M&M Limestone	1200	74.7	13.2
102077	M&M Limestone	1100	84.3	26.9

[a] Calcium Basis

TABLE A-3. ISOTHERMAL REACTOR IN-FLAME SULFATION DATA

Sample No.	Sorbent	ITB Temp, °C	Flame Temp °C	SO_2, ppm	Residence Time, s	Calcination[a], Percent	Ca Utilization Percent
114388	Vicron 45-3	900	900	3600	1.58	48.9	10.9
114389	D3002	900	900	3600	1.58	-	31.8
114390	D60	900	900	3600	1.58	-	31.8
114391	V40	900	900	3600	1.58	-	17.6
114392	Type S, Warner	900	900	3600	1.58	-	28.2
114393	Type S, Warner	900	900	3600	1.33	-	29.2
114394	V40	900	900	3600	1.33	-	17.1
114395	D60	900	900	3600	1.33	-	29.6
114396	D3002	900	900	3600	1.33	48.1[b]	15.3
114398	Vicron 45-3	900	900	3600	1.03	10.4[b]	11.5
114399	D3002	900	900	3600	1.03	22.4[b]	11.2
114400	V40	900	900	3600	1.03	-	14.7
111101	D60	900	900	3600	1.03	-	29.4
111102	Type S, Warner	900	900	3600	1.03	-	28.2
111108	D3002	900	900	3600	0.59	13.6[b]	2.0
111109	Vicron 45-3	900	900	3600	0.59	0	0.9
111110	V40	900	900	3600	0.59	-	14.6
111111	D60	900	900	3600	0.59	-	25.9
111112	Type S, Warner	900	900	3600	0.59	-	28.0
114288	Vicron 45-3	1000	1000	3600	1.54	98.0	28.7
114289	Vicron 45-3	1000	1000	3600	1.54	93.4	26.2
114181	D60	1000	1000	3600	1.54	-	42.7
114300	D3002	1000	1000	3600	1.54	91.5	38.1
114302	Type S, Warner	1000	1000	3600	1.54	-	42.8
114303	Type S, Warner	1000	1000	3600	1.30	-	46.2
114304	D3002	1000	1000	3600	1.30	94.9	36.8
114305	Vicron 45-3	1000	1000	3600	1.30	98.4	28.0
114306	D60	1000	1000	3600	1.30	-	39.1
114307	V40	1000	1000	3600	1.30	-	30.2
114308	V40	1000	1000	3600	1.01	-	29.5
114309	D60	1000	1000	3600	1.01	-	41.3
114310	Vicron 45-3	1000	1000	3600	1.01	97.3	26.1
114311	D3002	1000	1000	3600	1.01	80.7	33.4
114312	Type S, Warner	1000	1000	3600	1.01	-	40.5
114313	Type S, Warner	1000	1000	3600	0.72	-	34.9
114315	Vicron 45-3	1000	1000	3600	0.72	87.7	23.7
114316	D60	1000	1000	3600	0.72	-	35.5
114318	V40	1000	1000	3600	0.58	-	22.3

[a] Calcium Basis
[b] Total Basis

TABLE A-3. CONTINUED

Sample No.	Sorbent	ITR Temp, °C	Flame Temp, °C	SO_2, ppm	Residence Time, s	Calcination,[a] Percent	Ca Utilization, Percent
114319	D60	1000	1000	3600	0.58	-	31.9
114320	Vicron 45-3	1000	1000	3600	0.58	37.9	10.2
114321	D3002	1000	1000	3600	0.58	11.5	20.5
114322	Type S, Warner	1000	1000	3600	0.58	-	33.7
114323	Type S, Warner	1100	1100	3600	1.40	-	39.9
114324	D3002	1100	1100	3600	1.40	98.1	31.2
114325	Vicron 45-3	1100	1100	3600	1.40	97.1	16.2
114326	V40	1100	1100	3600	1.40	-	19.3
114327	D60	1100	1100	3600	1.40	-	32.1
114328	D60	1100	1100	3600	1.18	-	32.8
114329	V40	1100	1100	3600	1.18	-	15.6
114330	Vicron 45-3	1100	1100	3600	1.18	97.5	16.9
114331	D3002	1100	1100	3600	1.18	94.5	27.6
114332	Type S, Warner	1100	1100	3600	1.18	-	39.3
114333	Type SA, Warner	1100	1100	3600	1.18	-	38.8
114334	Type SA, Warner	1100	1100	3600	1.40	-	42.2
114337	D3002	1100	1100	3600	0.92	96.2	28.4
114338	Vicron 45-3	1100	1100	3600	0.92	96.2	16.9
114339	V40	1100	1100	3600	0.92	-	21.2
114340	D60	1100	1100	3600	0.92	-	29.8
114341	D60	1100	1100	3600	0.65	-	24.7
114342	V40	1100	1100	3600	0.65	-	18.3
114343	Vicron 45-3	1100	1100	3600	0.65	83.1	13.4
114344	D3002	1100	1100	3600	0.65	86.6	24.6
114345	Type S, Warner	1100	1100	3600	0.65	-	28.1
114346	Type SA, Warner	1100	1100	3600	0.65	-	30.9
114347	Type SA, Warner	1100	1100	3600	0.52	-	25.1
114348	Type S, Warner	1100	1100	3600	0.52	-	26.9
114349	D60	1100	1100	3600	0.52	-	16.0
114350	V40	1100	1100	3600	0.52	-	16.0
114351	D3002	1100	1100	3600	0.52	45.4	15.6
114352	Vicron 45-3	1100	1100	3600	0.52	85.0	13.8
114353	Vicron 45-3	1200	1200	3600	1.25	98.7	12.9
114354	D3002	1200	1200	3600	1.25	98.5	27.2
114356	D60	1200	1200	3600	1.25	-	26.2
114357	Type S, Warner	1200	1200	3600	1.25	-	35.1
114359	D60	1200	1200	3600	1.05	-	26.2

[a] Calcium Basis

TABLE A-3. CONTINUED

Sample No.	Sorbent	ITR Temp, °C	Flame Temp, °C	SO_2, ppm	Residence Time, s	Calcination,[a] Percent	Ca Utilization, Percent
114360	V40	1200	1200	3600	1.05	-	20.2
114361	Vicron 45-3	1200	1200	3600	1.05	96.0	13.1
114362	D3002	1200	1200	3600	1.05	98.3	25.1
114363	D3002	1200	1200	3600	0.82	94.1	27.1
114364	Vicron 45-3	1200	1200	3600	0.82	96.5	12.3
114365	D60	1200	1200	3600	0.82	-	28.9
114366	V40	1200	1200	3600	0.82	-	20.1
114368	Type S, Warner	1200	1200	3600	0.58	-	30.4
114371	D3002	1200	1200	3600	0.58	94.4	22.4
114372	Vicron 45-3	1200	1200	3600	0.58	98.8	15.7
114373	Vicron 45-3	1200	1200	3600	0.47	98.7	14.9
114374	D3002	1200	1200	3600	0.47	87.6	21.8
114375	V40	1200	1200	3600	0.47	-	16.1
114376	D60	1200	1200	3600	0.47	-	26.6
114377	Type S, Warner	1200	1200	3600	0.47	-	25.5
111136	US Gypsum B	1100	1100	3600	1.40	-	25.5
111138	US Gypsum A	1100	1100	3600	1.40	-	26.3
111140	US Gypsum A	1100	1100	3600	0.92	-	19.9
111142	US Gypsum B	1100	1100	3600	0.92	-	23.5
111144	US Gypsum B	1100	1100	3600	0.52	-	14.8
111145	US Gypsum A	1100	1100	3600	0.52	-	13.3
111122	US Gypsum A	1200	1200	3600	1.25	-	24.8
111124	US Gypsum B	1200	1200	3600	1.25	-	21.0
111126	US Gypsum B	1200	1200	3600	0.82	-	18.3
111128	US Gypsum B	1200	1200	3600	0.82	-	18.6
111130	US Gypsum A	1200	1200	3600	0.47	-	9.0
111132	US Gypsum B	1200	1200	3600	0.47	-	14.5
111166	D60	1100	1100	1800	1.40	-	15.0
111167	D60	1100	1100	7200	1.40	-	31.3
111168	Vicron 45-3	1100	1100	7200	1.40	98.8	23.8
111169	Vicron 45-3	1100	1100	1800	1.40	98.2	17.0
111170	Type S, Warner	1100	1100	1800	1.40	-	48.9
111171	Type S, Warner	1100	1100	7200	1.40	-	66.4
111291	Vicron 45-3	1100	1100	7200	1.40	96.1	23.8
111292	Vicron 45-3	1100	1100	1800	1.40	94.8	13.9
111293	D60	1100	1100	1800	1.40	-	9.2
111294	D60	1100	1100	7200	1.40	-	32.0
111295	Type S, Warner	1100	1100	7200	1.40	-	71.1
11296	Type S, Warner	1100	1100	1800	1.40	-	51.8

[a] Calcium Basis

TABLE A-4. ISOTHERMAL REACTOR SPECIFIC SURFACE AREA DATA

Sample	Sorbent	ITR Temp, °C	Flame Temp, °C	Residence Time, s	Specific Surface Area, m^2/g
111135	US Gypsum B	1100	1100	1.4	11.9
111137	US Gypsum A	1100	1100	1.4	10.9
111139	US Gypsum A	1100	1100	0.92	11.5
111141	US Gypsum B	1100	1100	0.92	14.1
111143	US Gypsum B	1100	1100	0.52	15.7
111146	US Gypsum A	1100	1100	0.52	16.6
111121	US Gypsum A	1200	1200	1.25	5.6
111123	US Gypsum B	1200	1200	1.25	6.8
111125	US Gypsum B	1200	1200	0.82	8.7
111127	US Gypsum A	1200	1200	0.82	10.9
111129	US Gypsum A	1200	1200	0.47	14.1
111131	US Gypsum B	1200	1200	0.47	12.0
111113	US Gypsum A	1360	1360	0.60	6.5
111115	US Gypsum B	1360	1360	0.60	6.4

TABLE A-5. VICRON 45-3/Cr_2O_3 SULFATION ENHANCEMENT DATA OBTAINED USING THE QUARTZ SAMPLING PROBE

Sample No.	Sorbent	ITR Temp, °C	Flame Temp, °C	SO_2, ppm	Calcination, Percent	Ca Utilization, Percent
101654	Vicron/Cr_2O_3	1100	1100	3600	97.8	29.5
101670	Vicron/Cr_2O_3	1100	1100	3600	93.3	29.5
101687	Vicron/Cr_2O_3	1100	1950	3600	a	5.2
101688	Vicron/Cr_2O_3	1100	1950	3600	84.4	4.4
101695	Vicron/Cr_2O_3	1100	1730	3600	82.9	18.2
101698	Vicron/Cr_2O_3	1100	1600	3600	87.5	27.1
101709	Vicron/Cr_2O_3	1100	1480	3600	85.8	28.8
101711	Vicron/Cr_2O_3	1100	1480	3600	85.7	29.1
101718	Vicron/Cr_2O_3	1100	1315	3600	87.9	31.7
101720	Vicron/Cr_2O_3	1100	1315	3600	89.5	35.3
101723	Vicron 45-3	1100	1100	3600	98.4	26.6
101730	Vicron 45-3	1100	1315	3600	96.3	20.4
101731	Vicron 45-3	1100	1950	3600	94.0	1.7
101736	Vicron 45-3	1100	1480	3600	91.7	13.1
101737	Vicron 45-3	1100	1730	3600	88.4	5.3
101751	Vicron 45-3	1100	1600	3600	86.6	9.4
101752	Vicron 45-3	1100	1600	3600	83.9	6.1
101764	Vicron 45-3	1100	1950	3600	97.2	3.3
101768	Vicron 45-3	1100	1950	3600	97.0	3.5
101771	Vicron 45-3	1100	1480	3600	94.2	12.2
101773	Vicron 45-3	1000	1000	3600	87.0	23.3
101798	Vicron 45-3	1000	1000	3600	90.2	25.2
101815	Vicron 45-3	1000	1000	3600	97.5	29.5
101816	Vicron/Cr_2O_3	1000	1000	3600	93.9	27.2

[a] Not determined

TABLE A-6. RESULTS OF SCREENING TESTS FOR SULFATION PROMOTERS ADDED TO VICRON 45-3 AT 5 PERCENT BY WEIGHT

Sample No.	Additive	ITR Temp, °C	Flame Temp, °C	SO_2,ppm	Residence Time, s	Calcination, Percent	Ca Utilization,[a] Percent
111185	-	1100	1100	3600	1.40	97.0	17.4
111186	Na_2CO_3	1100	1100	3600	1.40	87.7	8.1
111192	$NaHCO_3$	1100	1100	3600	1.40	93.7	18.0
111193	K_2CO_3	1100	1100	3600	1.40	91.1	18.1
111194	$KHCO_3$	1100	1100	3600	1.40	95.0	18.8
111195	Li_2CO_3	1100	1100	3600	1.40	95.3	19.3
111196	Na_2SO_4	1100	1100	3600	1.40	92.8	17.6
111197	K_2SO_4	1100	1100	3600	1.40	96.6	22.3
111198	MoO_3	1100	1100	3600	1.40	77.3	12.2
111199	-	1100	1100	3600	1.40	78.4	9.4
111200	MoS_2	1100	1100	3600	1.40	95.0	21.3
111201	V_2O_5	1100	1100	3600	1.40	86.3	13.9
111202	TiO_2	1100	1100	3600	1.40	58.6	11.4
111203	Pt	1100	1100	3600	1.40	98.6	17.0
111204	P_2O_5	1100	1100	3600	1.40	74.5	11.2
111205	NaCl	1100	1100	3600	1.40	89.5	19.3
111206	-	1100	1100	3600	1.40	98.7	18.1
111207	-	1100	1100	3600	1.40	93.5	16.7
111208	Na_2CO_3	1100	1100	3600	1.40	96.7	19.6
111209	$NaHCO_3$	1100	1100	3600	1.40	94.8	19.5
111210	K_2CO_3	1100	1100	3600	1.40	94.3	19.0
111211	$KHCO_3$	1100	1100	3600	1.40	95.7	18.7
111212	Li_2CO_3	1100	1100	3600	1.40	90.6	19.4
111213	Na_2SO_4	1100	1100	3600	1.40	97.1	22.6
111214	-	1100	1100	3600	1.40	97.6	18.00
111215	K_2SO_4	1100	1100	3600	1.40	98.3	22.2

[a] not corrected for additive sulfur content

TABLE A-6. CONTINUED

Sample No.	Additive	ITR Temp, °C	Flame Temp, °C	SO_2,ppm	Residence Time, s	Calcination, Percent	Ca Utilization[a], Percent
111216	MoO_3	1100	1100	3600	1.40	98.5	20.1
111217	MoS_2	1100	1100	3600	1.40	98.7	21.3
111218	V_2O_5	1100	1100	3600	1.4	97.9	19.5
111219	TiO_2	1100	1100	3600	1.4	98.6	20.9
111220	Pt	1100	1100	3600	1.4	98.7	19.1
111221	P_2O_5	1100	1100	3600	1.4	96.7	19.7
111222	NaCl	1100	1100	3600	1.4	98.6	19.8
111223	-	1100	1100	3600	1.4	94.5	15.1
111224	-	1100	1100	3600	0.92	82.3	13.0
111225	Na_2CO_3	1100	1100	3600	0.92	90.3	15.9
111226	$NaHCO_3$	1100	1100	3600	0.92	91.1	18.2
111227	K_2CO_3	1100	1100	3600	0.92	87.0	17.9
111228	$KHCO_3$	1100	1100	3600	0.92	88.1	16.6
111229	Li_2CO_3	1100	1100	3600	0.92	87.0	20.5
111230	Na_2SO_4	1100	1100	3600	0.92	87.2	15.5
111231	K_2SO_4	1100	1100	3600	0.92	80.6	16.0
111232	-	1100	1100	3600	0.92	65.8	9.5
111233	MoO_3	1100	1100	3600	0.92	88.6	14.3
111234	MoS_2	1100	1100	3600	0.92	86.5	18.6
111235	V_2O_5	1100	1100	3600	0.92	90.5	15.0
111236	TiO_2	1100	1100	3600	0.92	89.9	14.5
111237	Pt	1100	1100	3600	0.92	82.7	15.4
111238	P_2O_5	1100	1100	3600	0.92	94.7	16.1
111239	NaCl	1100	1100	3600	0.92	77.4	14.3
111240	-	1100	1100	3600	0.92	94.3	15.6
111241	Na_2CO_3	1100	1100	3600	0.92	79.1	16.3

[a] Not corrected for additive sulfur content

TABLE A-6. CONTINUED

Sample No.	Additive	ITR Temp, °C	Flame Temp, °C	SO_2,ppm	Residence Time, s	Calcination, Percent	Ca Utilization,[a] Percent
111242	$NaHCO_3$	1100	1100	3600	0.92	89.3	18.1
111243	K_2CO_3	1100	1100	3600	0.92	87.1	14.9
111244	$KHCO_3$	1100	1100	3600	0.92	90.4	16.1
111245	Li_2CO_3	1100	1100	3600	0.92	97.1	12.9
111246	Na_2SO_4	1100	1100	3600	0.92	84.8	17.2
111247	K_2SO_4	1100	1100	3600	0.92	89.6	18.6
111248	-	1100	1100	3600	0.92	63.0	9.3
111249	MoO_3	1100	1100	3600	0.92	74.7	11.6
111250	MoS_2	1100	1100	3600	0.92	93.9	20.5
111251	V_2O_5	1100	1100	3600	0.92	82.0	12.4
111252	TiO_2	1100	1100	3600	0.92	83.9	14.7
111253	Pt	1100	1100	3600	0.92	85.1	15.0
111254	P_2O_5	1100	1100	3600	0.92	95.9	20.4
111255	NaCl	1100	1100	3600	0.92	89.7	20.8
111256	-	1100	1100	3600	0.92	87.8	17.9
111257	-	1100	1360	3600	0.60	69.7	6.4
111258	Na_2CO_3	1100	1360	3600	0.60	91.1	15.3
111259	$NaHCO_3$	1100	1360	3600	0.60	67.00	6.9
111260	K_2CO_3	1100	1360	3600	0.60	87.5	11.6
111261	$KHCO_3$	1100	1360	3600	0.60	85.9	9.8
111262	Li_2CO_3	1100	1360	3600	0.60	84.2	16.3
111263	Na_2SO_4	1100	1360	3600	0.60	81.0	15.4
111264	K_2SO_4	1100	1360	3600	0.60	86.5	13.8
111265	-	1100	1360	3600	0.60	72.8	5.5
111266	MoO_3	1100	1360	3600	0.60	73.6	8.7
111267	MoS_2	1100	1360	3600	0.60	98.4	7.5

[a] Not corrected for additive sulfur content

TABLE A-6. CONTINUED

Sample No.	Additive	ITR Temp, °C	Flame Temp, °C	SO_2,ppm	Residence	Calcination, Percent	Ca Utilization,[a] Percent
111269	TiO_2	1100	1360	3600	0.60	75.8	7.1
111270	Pt	1100	1360	3600	0.60	85.9	8.0
111271	P_2O_5	1100	1360	3600	0.6	73.7	5.8
111272	NaCl	1100	1360	3600	0.6	86.5	11.5
111273	-	1100	1360	3600	0.6	71.8	5.1
111274	Na_2CO_3	1100	1360	3600	0.6	91.4	13.9
111275	$NaHCO_3$	1100	1360	3600	0.6	86.5	14.0
111276	K_2CO_3	1100	1360	3600	0.6	83.5	11.4
111277	$KHCO_3$	1100	1360	3600	0.6	77.8	8.9
111278	Li_2CO_3	1100	1300	3600	0.6	b	16.0
111279	Na_2SO_4	1100	1360	3600	0.6	82.2	14.7
111280	K_2SO_4	1100	1360	3600	0.6	82.2	13.6
111281	-	1100	1360	3600	0.6	72.7	5.0
111282	MoO_3	1100	1360	3600	0.6	73.1	8.2
111283	MoS_2	1100	1360	3600	0.6	77.4	10.3
111284	V_2O_5	1100	1360	3600	0.6	66.2	6.9
111285	TiO_2	1100	1360	3600	0.6	68.9	5.1
111286	Pt	1100	1360	3600	0.6	86.1	7.9
111287	P_2O_5	1100	1360	3600	0.6	b	6.6
111288	NaCl	1100	1360	3600	0.60	87.9	13.5
111290	-	1100	1360	3600	0.6	72.4	5.7

[a] Not corrected for additive sulfur content

[b] Not determined

APPENDIX B

Isothermal Reactor Flame Conditions and Temperature Profiles

TABLE B-1. ISOTHERMAL REACTOR FLAME CONDITIONS

Temperature	Flow Rates, L/S			SO_2 Flow at	Sorbent Residence
^oC	Air	H_2	CH_4	3600 ppm, cm^3/s	Time @ 107 cm, s
900	0.846	0.092	-	3.2	
1000	0.846	0.152	-	3.3	1.54
1100	0.846	0.188	-	3.4	
1100	2.42	0.418	-	9.5	0.53
1200	0.846	0.276	-	3.5	
1200	2.42	0.492	-	9.6	0.47
1315	1.98	0.529	-	8.1	
1360	2.18	-	0.119	8.3	0.49
1480	1.21	-	0.083	4.7	
1600	2.42	-	0.195	9.4	
1730	2.42	-	0.215	9.5	
1950	2.42	-	0.252	9.6	

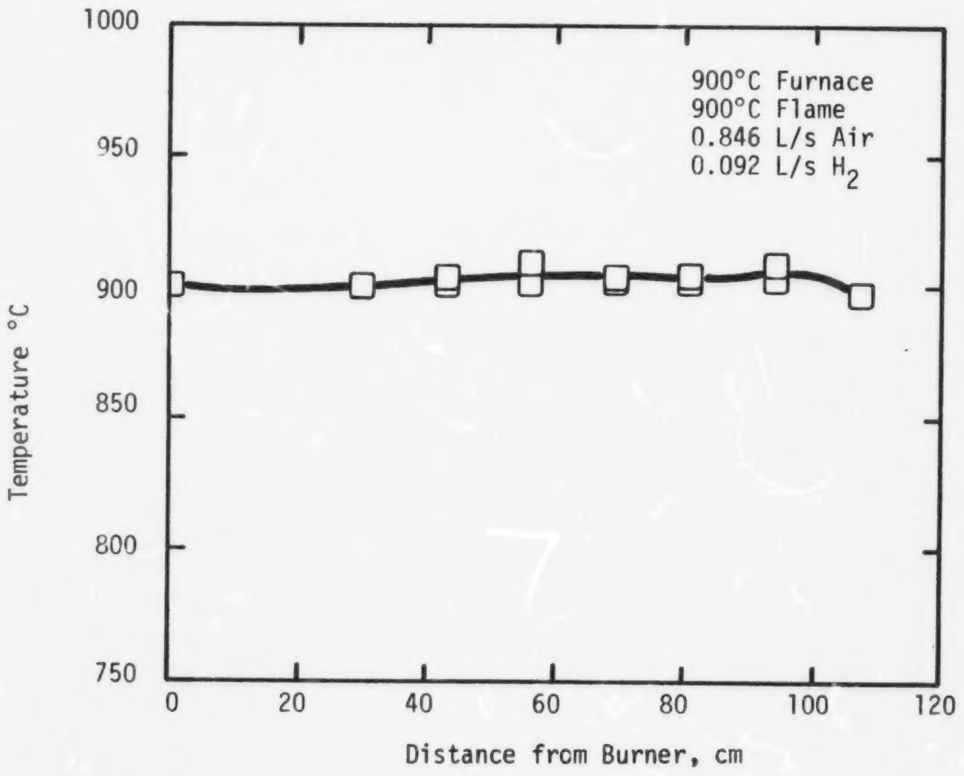

Figure B-1. Isothermal Reactor Temperature Profile. 900°C H_2-Air Flame.

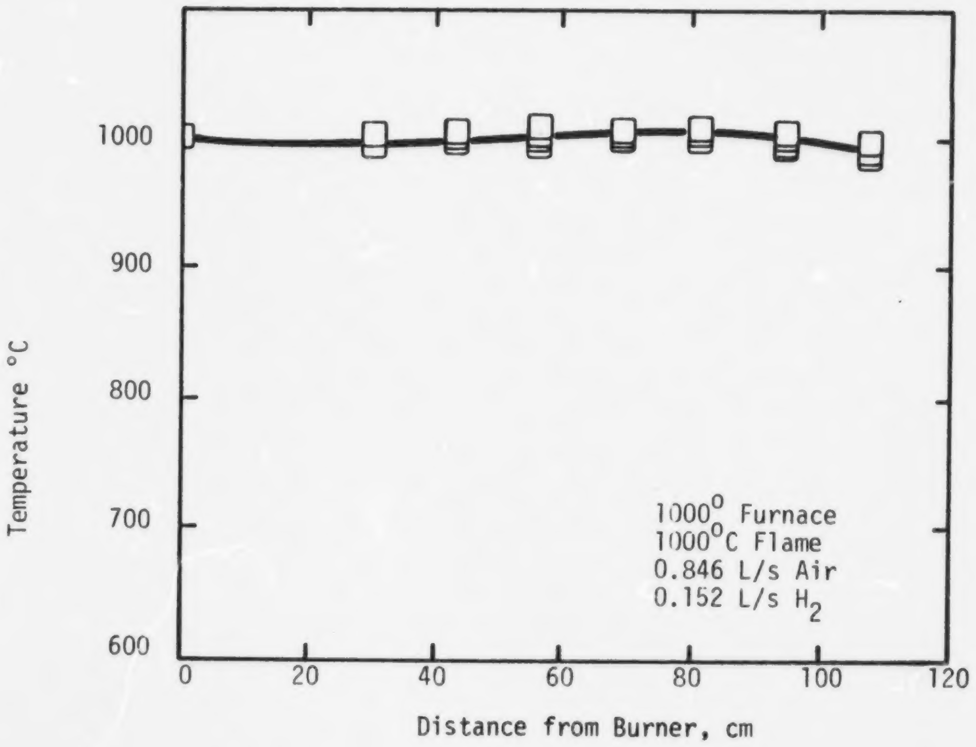

Figure B-2. Isothermal Reactor Temperature Profile. 1000°C H_2-Air Flame.

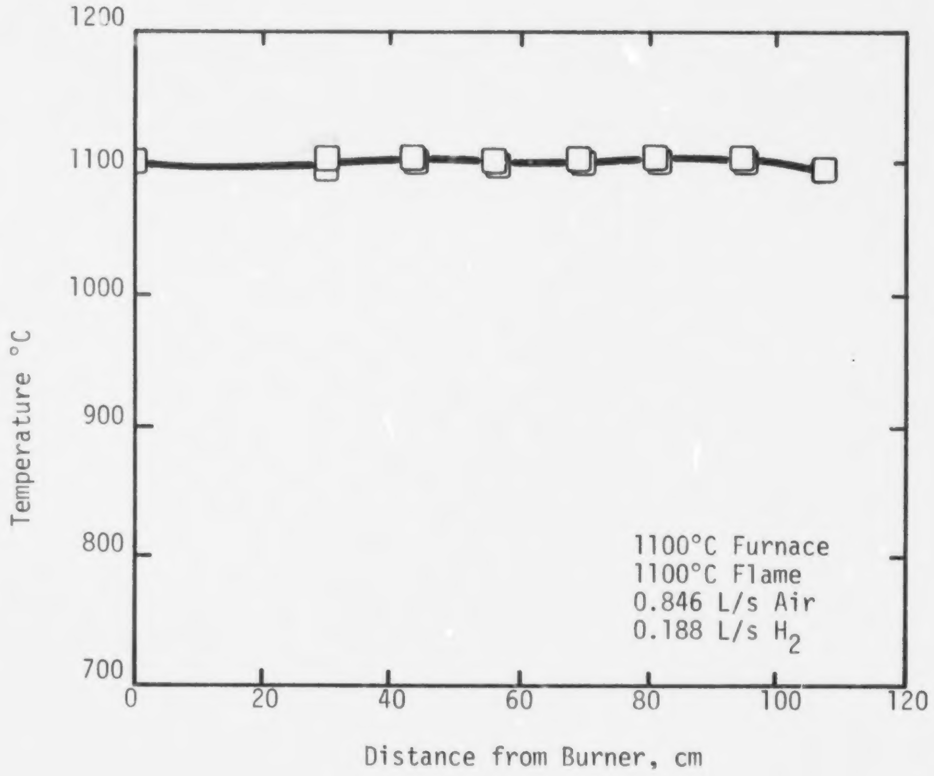

Figure B-3. Isothermal Reactor Temperature Profile. 1100°C H_2-Air Flame.

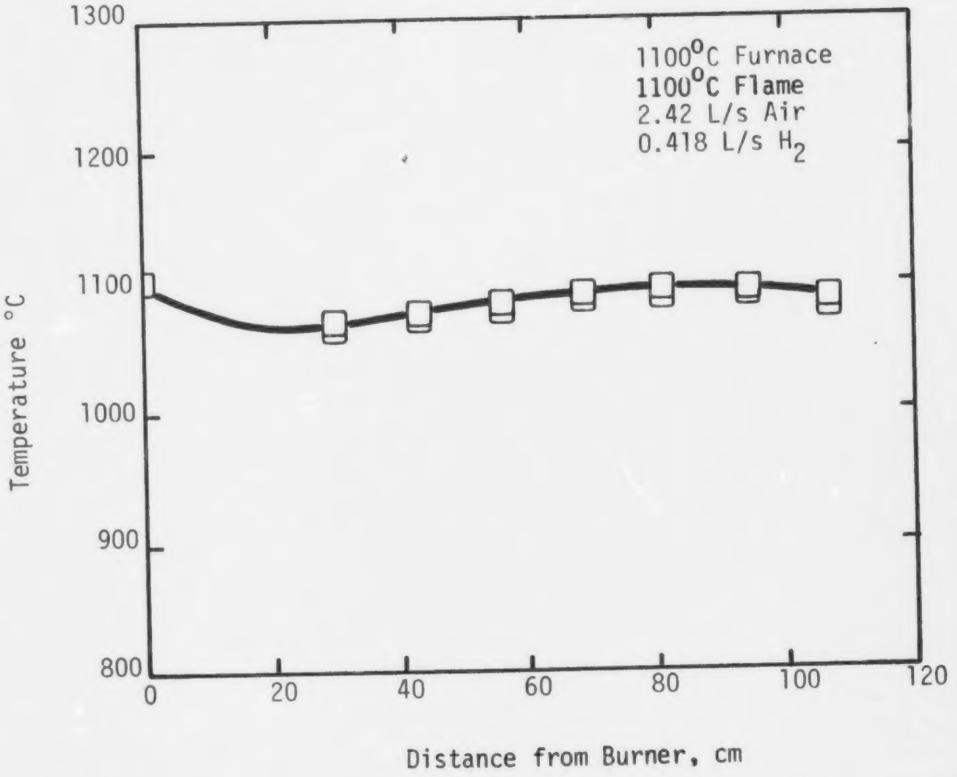

Figure B-4. Isothermal Reactor Temperature Profile, 1100°C H_2-Air Flame, 1100°C Furnace.

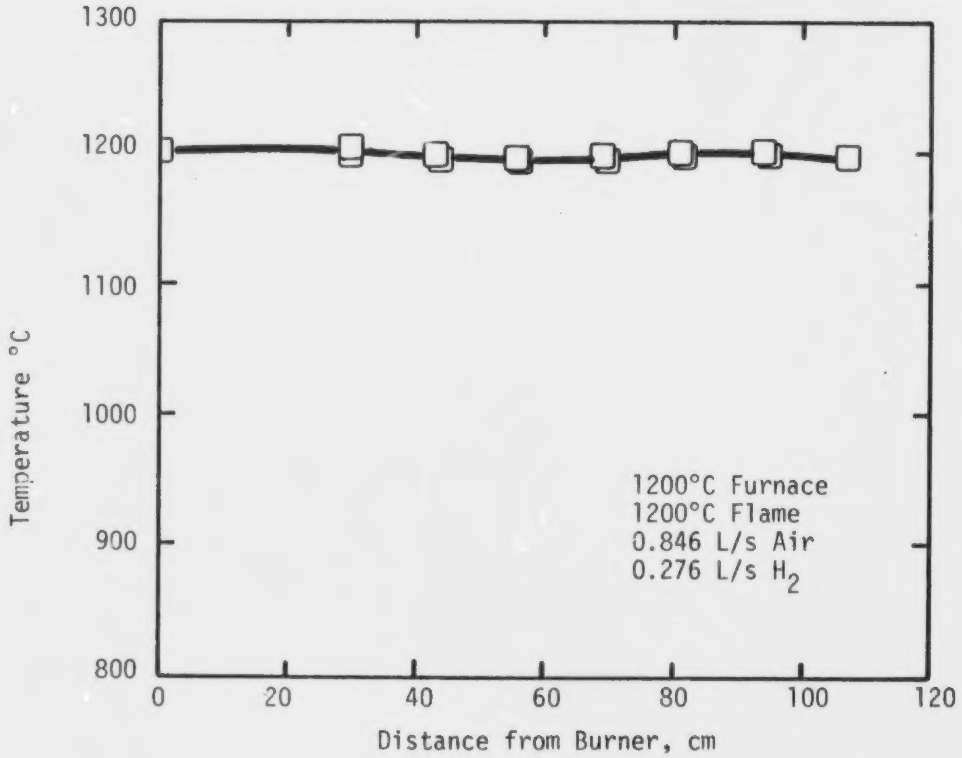

Figure B-5. Isothermal Reactor Temperature Profile. 1200°C H_2-Air Flame

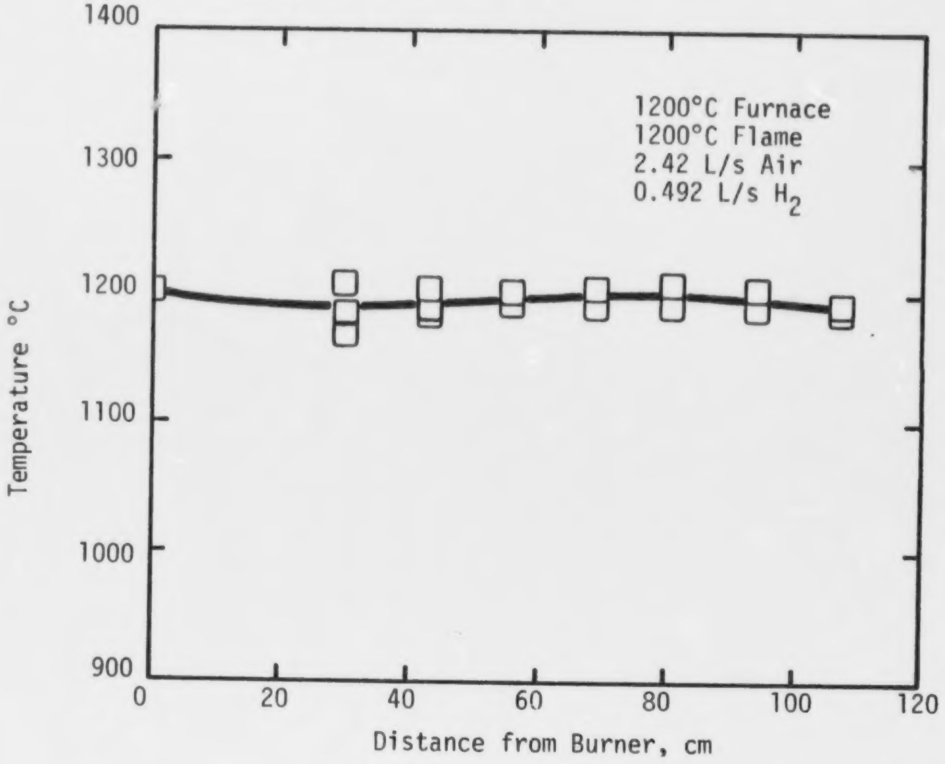

Figure B-6. Isothermal Reactor Temperature Profile 1200°C H_2-Air Flame.

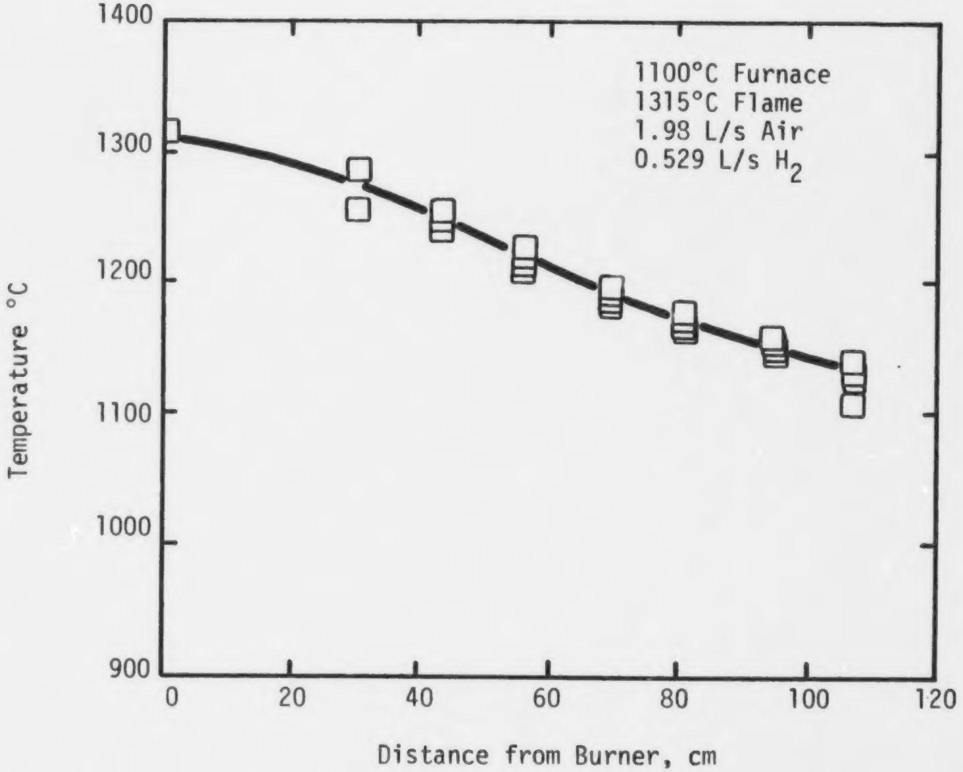

Figure B-7. Isothermal Reactor Temperature Profile. 1100°C Furnace Temperature, 1315°C H_2-Air Flame.

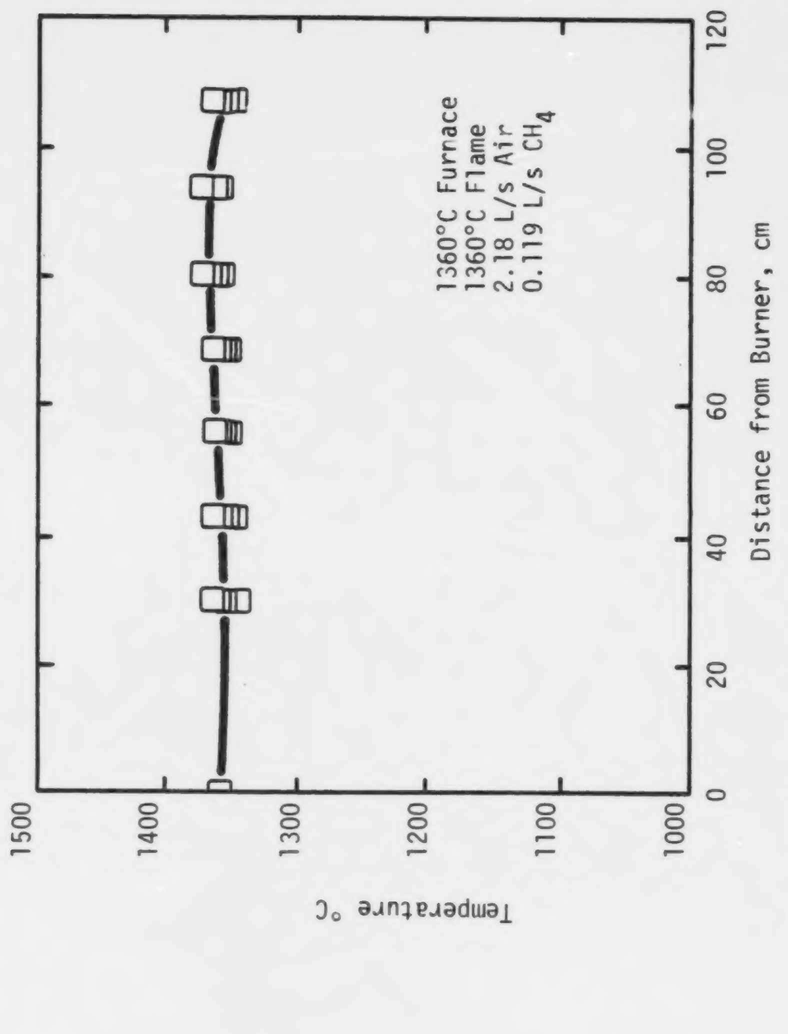

Figure B-8. Isothermal Reactor Temperature Profile. 1360°C CH_4-Air Flame.

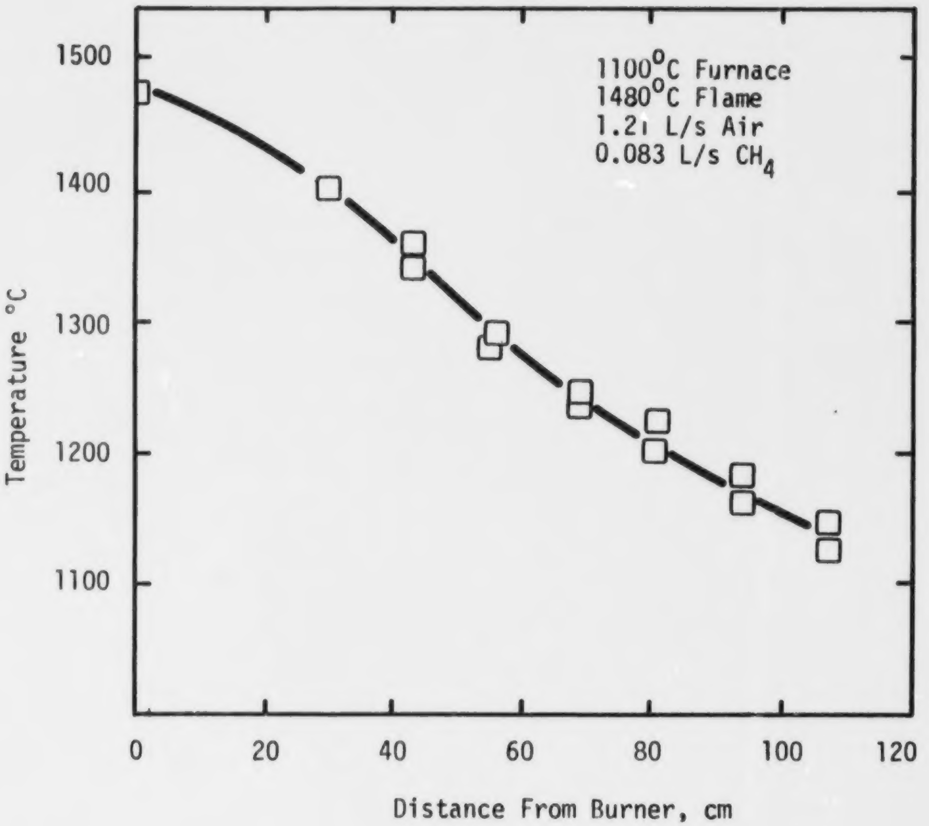

Figure B-9. Isothermal Reactor Temperature Profile. 1100°C Furnace Temperature, 1480°C CH_4-Air Flame.

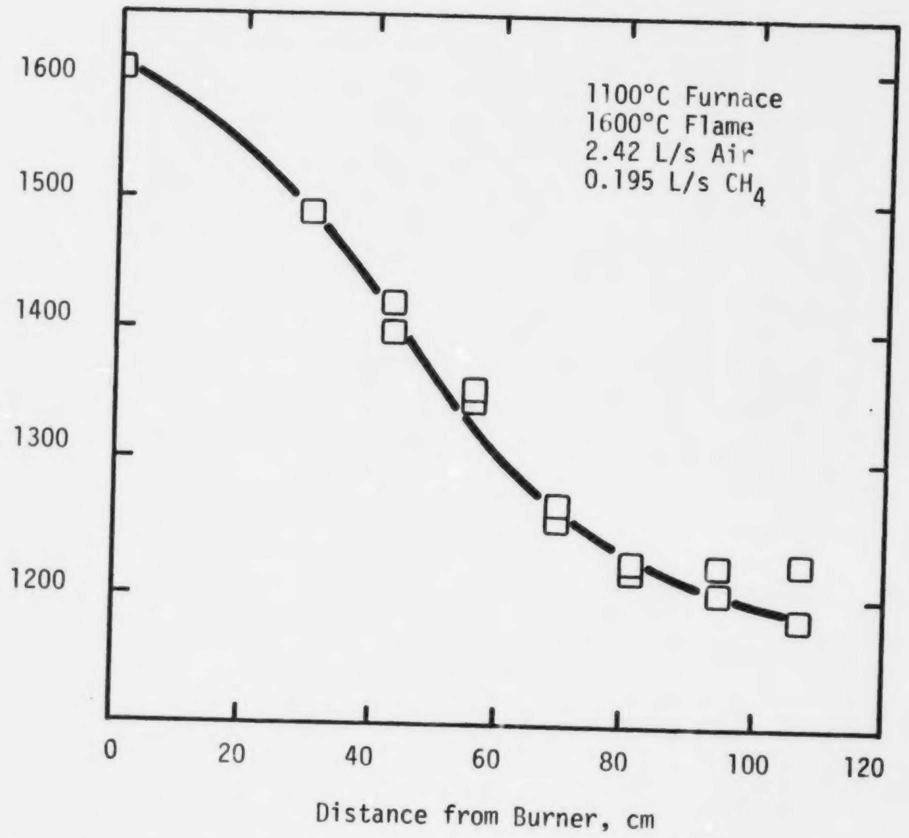

Figure B-10. Isothermal Reactor Temperature Profile. 1100°C Furnace Temperature, 1600°C CH_4-Air Flame.

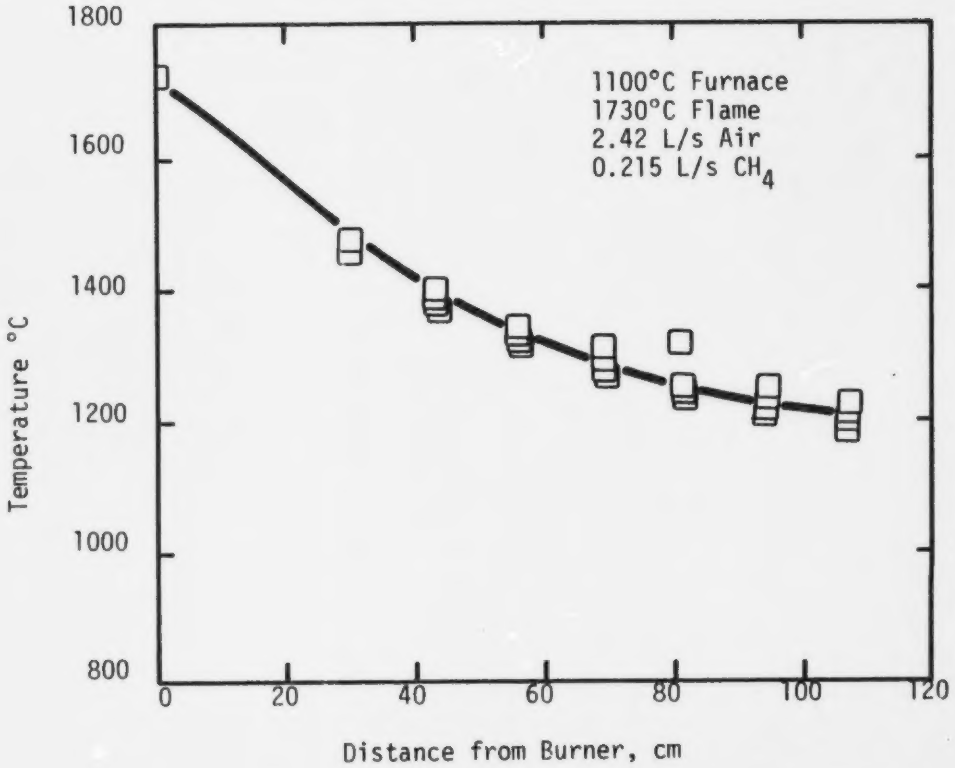

Figure B-11. Isothermal Reactor Temperature Profile. 1100°C Furnace Temperature, 1730°C CH_4-Air Flame.

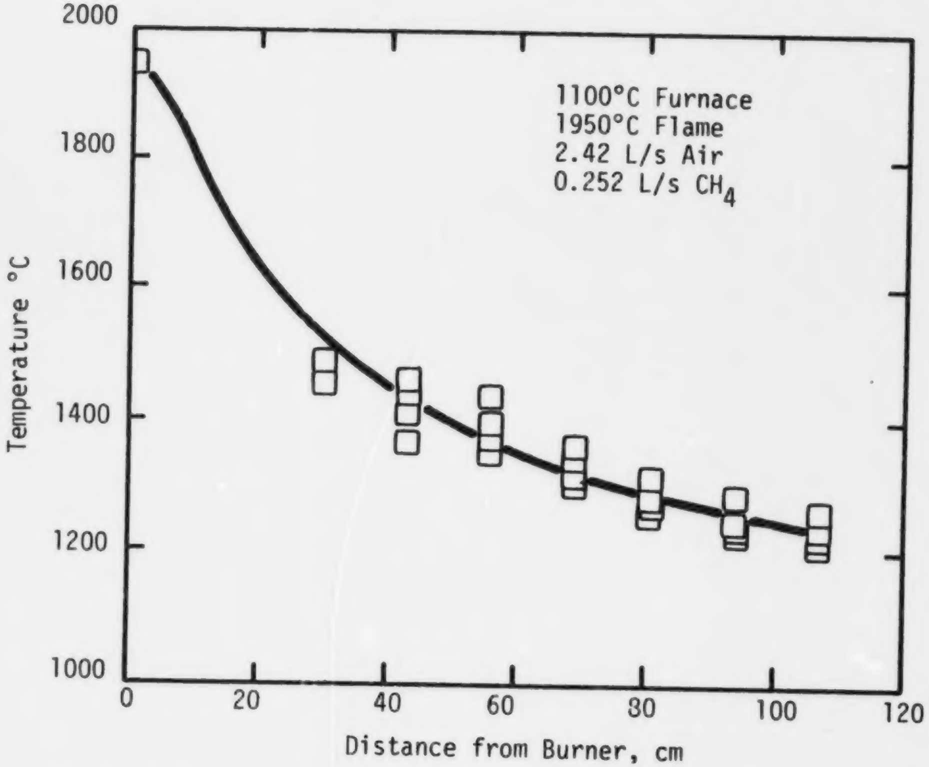

Figure B-12. Isothermal Reactor Temperature Profile. 1100°C Furnace Temperature, 1950°C CH_4-Air Flame.

APPENDIX C

Approaches to Precalcine Generation

APPENDIX C. APPROACHES TO PRECALCINE GENERATION

Four approaches were employed during the development of the precalcine generation apparatus described in Section 4.2.4 of this report. A brief description of these, as well as examples of the results obtained, are included in this appendix.

Schematics of the four developmental approaches to precalcine generation are shown in Figure C-1. These are divided into two groups, batch approaches and continuous process approaches. The continuous approaches are characterized by shorter residence times, higher temperatures, and generally higher local CO_2 levels than the batch approaches.

Two continuous approaches were employed. In the first, dispersed-phase calcination, the sorbent was injected into a 2.2 cm i.d. x 30 cm long stainless steel tube, heated by an electric tube furnace set at $1100^{o}C$. A typical residence time would be 2.5-3.0 s assuming that the sorbent stream reaches $1000^{o}C$ at about halfway down the tube. At the exit of the tube cold N_2 was added to cool the gases and to dilute the CO_2 which would otherwise tend to recarbonate the lime. The second continuous approach is labeled transport-phase calcination. A 7.6-m long x 3.2-mm o.d. stainless steel tube was heated either by placing it in the thermal decomposition reactor near the burner or by coiling it inside of an electric tube furnace set at $1100^{o}C$. The residence time in this case, again assuming that the sorbent stream reaches $1000^{o}C$ halfway down the coil, is about 0.4 s.

In the continuous process methods for calcination, the sorbent was constantly exposed to the CO_2 produced during calcination. Injection was accomplished with a fluidized-bed feeder providing a sorbent-to-transport gas mass ratio of about 1.0. At complete calcination the CO_2 fraction in the gas surrounding the calcine was about 0.3 at the exit of the heated zone, assuming complete calcination. As a result, some recarbonation inevitably occurred during sample collection. Results of pre-calcination by continuous approaches are shown in Figure C-2 as specific surface area versus percent calcination. The only immediately plausible distinction between the three

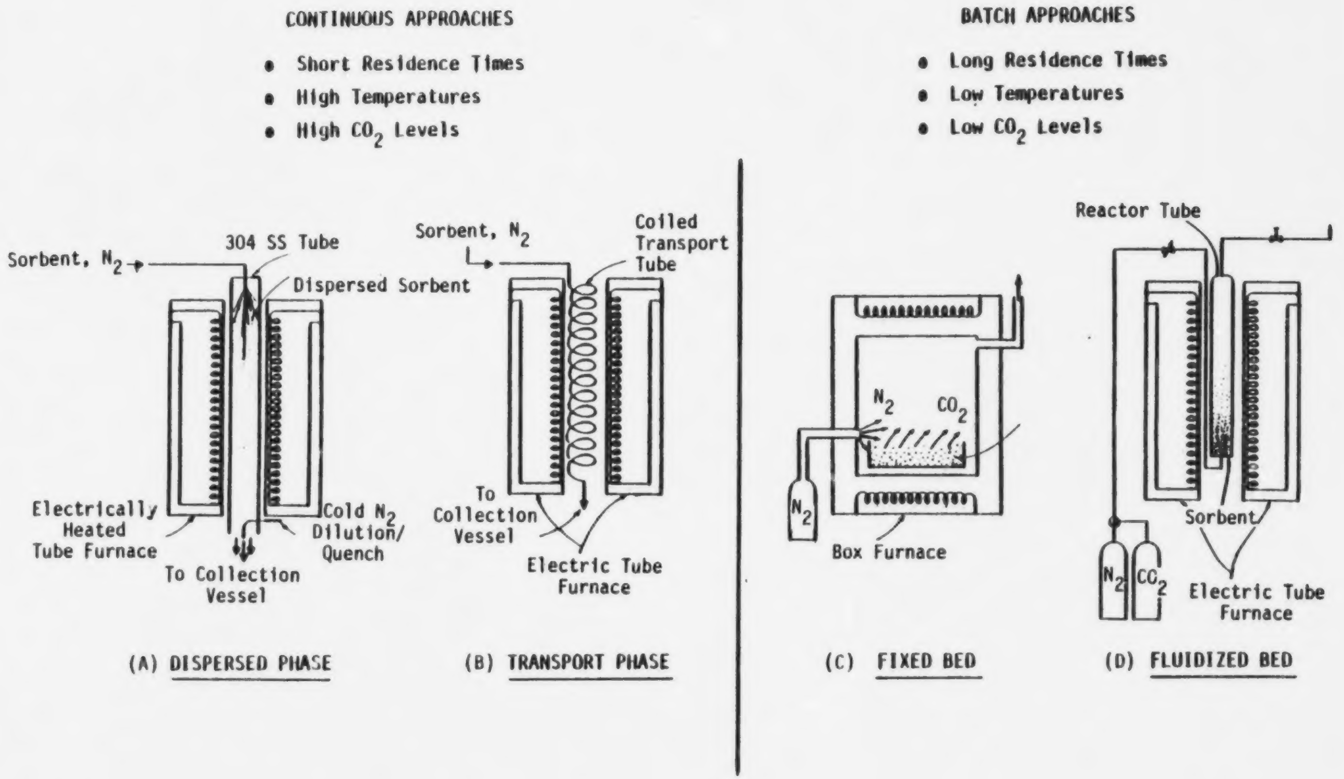
CONTINUOUS APPROACHES
• Short Residence Times
• High Temperatures
• High CO_2 Levels
BATCH APPROACHES
• Long Residence Times
• Low Temperatures
• Low CO_2 Levels
Sorbent, N_2
304 SS Tube
Dispersed Sorbent
Electrically Heated Tube Furnace
Cold N_2 Dilution/ Quench
To Collection Vessel
(A) DISPERSED PHASE
Sorbent, N_2
Coiled Transport Tube
To Collection Vessel
Electric Tube Furnace
(B) TRANSPORT PHASE
N_2
CO_2
N_2
Box Furnace
(C) FIXED BED
Reactor Tube
Sorbent
N_2
CO_2
Electric Tube Furnace
(D) FLUIDIZED BED

Figure C-1. Schematic configuration for external generation of high surface area precalcined sorbents.

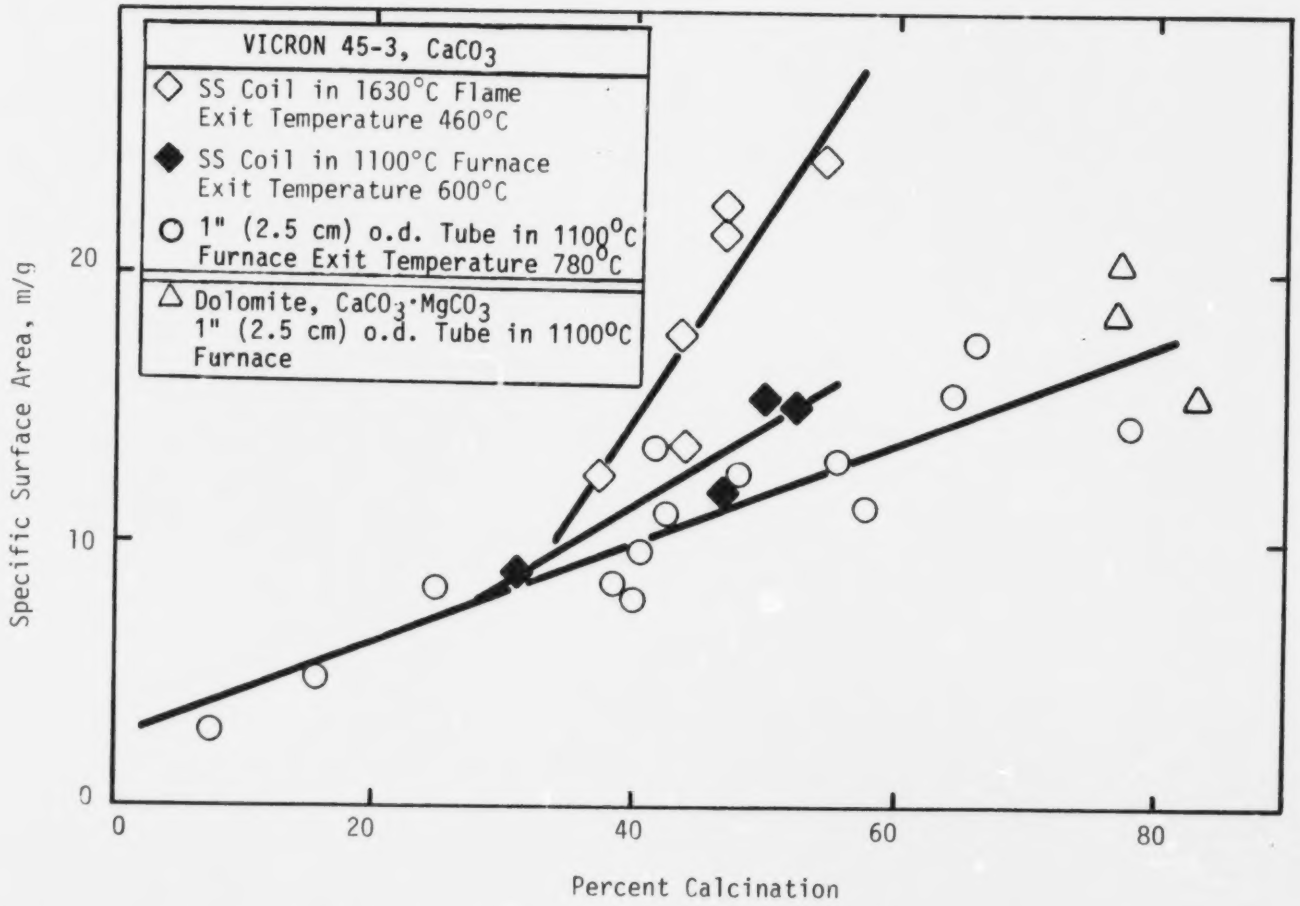

Figure C-2. Results of Continuous Approaches in the Development of the Precalcine Generation Apparatus.

data groups shown is that the data which shows the steeper trends of surface area versus calcination correspond with the techniques suspected of providing faster heating rates for the sorbent stream.

The ultimate difficulty encountered with the continuous calcination approaches, besides low extents of calcination, was corrosion. At the temperatures involved the lime reacted with the stainless steel producing a brittle, porous crystalline structure which had little strength.

Two batch approaches to precalcine generation also were tested prior to adopting the procedure described in Section 4.1. The first approach involved spreading limestone evenly across the bottom of a small pan which was then placed into a box furnace at a temperature of 700-800°C for varying lengths of time. The low temperatures precluded the problem of corrosion experienced with the continuous process approaches. It was determined that purging the furnace chamber with N_2 reduced the required calcination time and also increased the sample surface area. In addition, higher surface areas were obtained with smaller sample sizes. Table C-1 provides some data from the fixed bed calcination experiments. It was also determined that the evenness with which the limestone was spread, as well as the thickness of the bed affected both calcination rate and surface area. The first experiments were performed using a small porcelain crucible lid to contain the sorbent. Subsequently, a 20 cm diameter bronze sieve collection tray was employed. This enabled much larger samples to be employed. Some of the fixed-bed batch calcination results are shown graphically in Figure C-3. No effect of calcination temperature on surface area is evident and there appears to be a limiting surface area of about 20 m^2/g.

Results of the batch calcination tests suggested that increasing transport of CO_2 away from the limestone would increase the calcination rate. Besides decreasing the calcination time this could also increase the specific surface area of the sample obtained. A small fluidized-bed calciner was built to test these hypothesis. The unit consisted of a 2.5-cm o.d. stainless steel tube with a sintered stainless steel disk placed inside, near the center of the length, to act as a flow distributor and sample holder. A

TABLE C-1. RESULTS FROM BATCH FIXED-BED SORBENT PRE-CALCINATION EXPERIMENTS

Sample No.	Temperature °C	Sample Mass, g	N_2 Range?	Time Hrs.	Calcination Percent	Surface Area, m^2/g	Pan Size cm
101469	750	8.0	No	1.0	40.9	4.48	6.4
101470	750	10.0	No	1.0	68.1	8.09	6.4
101471	750	10.0	Yes	1.0	34.8	5.50	6.4
101472	750	10.0	Yes	1.0	98.4	20.84	6.4
101473	750	8.0	Yes	1.0	98.3	21.22	6.4
101475	750	8.0	Yes	1.0	98.3	22.82	6.4
101494	500	8.0	Yes	3.0	3.3	0.66	6.4
101504	750	89.7	Yes	1.0	61.1	8.45	20.0
101508	750	35.0	Yes	2.0	98.7	19.25	20.0
101511	650	35.0	Yes	1.0	22.4	3.21	20.0
101536	600	35.0	Yes	1.0	5.9	1.06	20.0
101543	750	35.0	Yes	1.0	97.3	19.34	20.0
101545	700	35.0	Yes	1.0	51.88	7.43	20.0
101547	700	35.0	Yes	1.5	87.97	15.96	20.0
101548	700	35.0	Yes	2.0	95.24	17.74	20.0
101552	700	35.0	Yes	2.5	97.56	19.50	20.0
101556	700	35.0	Yes	3.0	96.96	18.35	20.0

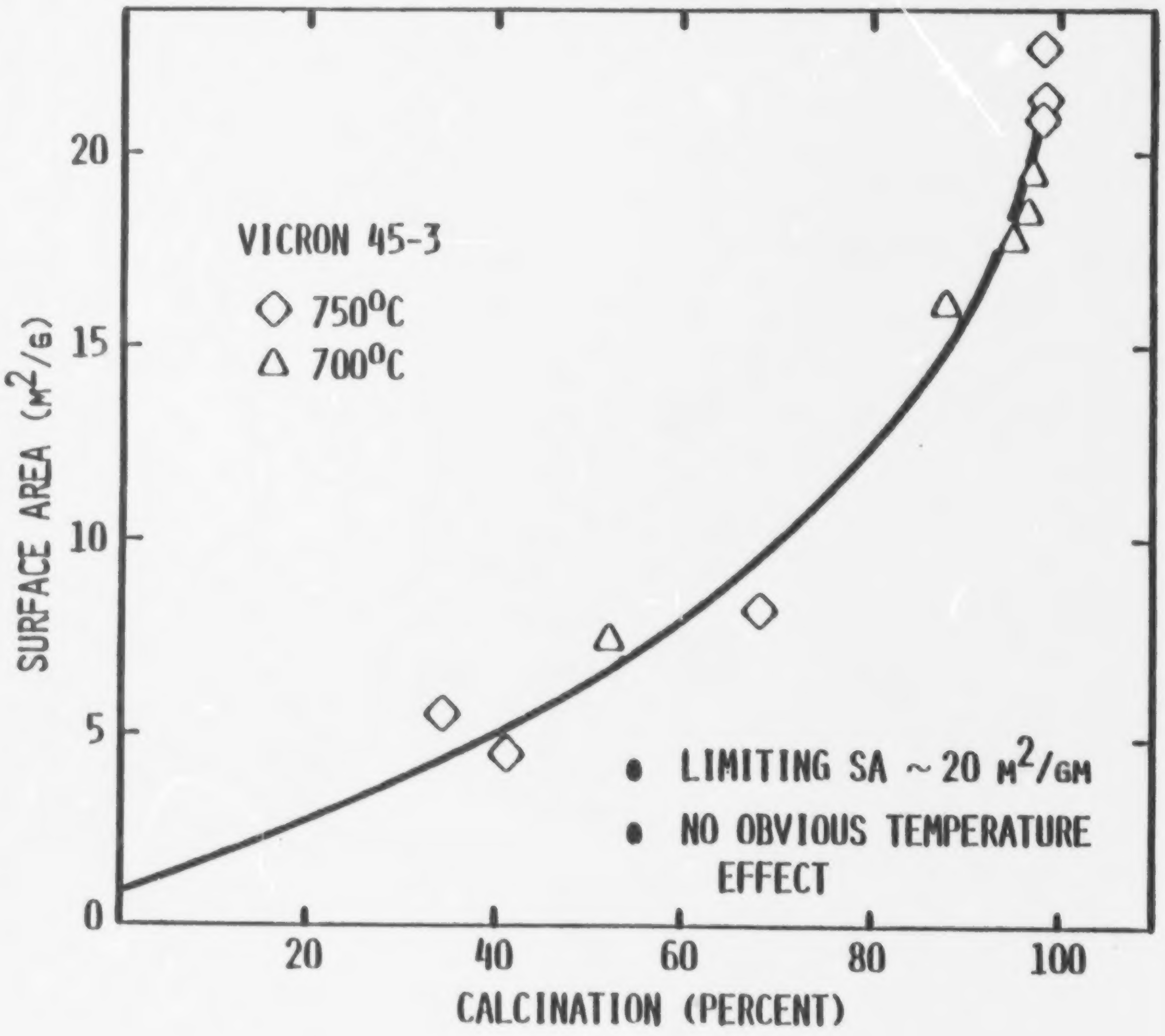

Figure C-3. Results of Batch Fixed-Bed Approach in the Development of the Pre-calcine Generation Apparatus, similar unit, with no provision for gas flow was also used to test the possibility of calcination of the sample in vacuo. Table C-2 provides the results of experiments in these apparatuses. The single experiment run in vacuo produced a reasonably high surface area, however, the necessary sample mass was extremely small (~0.25 g) so that it was not considered as a means for batch calcination. Using the fluidized bed calciner, however, a surface area near 30 m^2/g was achieved with only 94 percent calcination.

TABLE C-2. RESULTS FOR FLUIDIZED BED AND VACUUM CALCINATION TESTS

Sample No.	Temperature °C	Sample Mass, g	Calcination Environment	N_2 Flow cm^3/min	Time Hrs.	Surface Area, m^2/g	Calcination Percent
101867	500	-	Vacuum	-	1.0	22.86	73.40
101405	740	1.0	$N2$	120	1.0	29.95	93.72
101414	680	1.0	N_2	54	1.0	7.82	a
101415	500	1.0	N_2	46	1.0	3.93	a
101416	850	1.0	N_2	100	1.0	13.89	a
101425	750	1.0	N_2	100	1.0	1.01	a
101431	850	1.0	N_2	100	1.0	14.67	a
101445	750	1.0	N_2	120	1.0	14.64	85.16
101451	650	1.0	N_2	100	1.0	1.03	a
101510	750	1.0	N_2	17	1.0	16.26	97.50

a= Not Measured

APPENDIX D

Sorbent Injection Method in Isothermal Reactor

APPENDIX D. SORBENT INJECTION METHOD IN ISOTHERMAL REACTOR

The question of sorbent injection in the ITR is important because of the potential effect that it could have on both calcination and sulfation of limestones, especially at low temperatures. The mode of injection employed previously with the sintered bronze burner was to inject the sorbent stream (sorbent entrained in air) at a velocity near the cold-gas velocity of the burner. This was accomplished as shown in Figure D-1 (a) by injecting the sorbent into the 0.64-cm i.d. tube mounted through the burner. The turbulence of injection stabilized inside of the 0.64-cm i.d. tube and the sorbent stream experienced minimal expansion upon passing through the flame and into the reactor. This mode of injection greatly facilitated sample recovery.

Figure D-1 (b) shows how turbulent injection was accomplished. In this instance, the sorbent transport tube (1.4 mm i.d. stainless steel) was terminated just beyond the burner face. Because of the smaller diameter of the injection tube, the injection velocity was 20 times as fast at the burner face. As a result, turbulent mixing and jet entrainment caused greater dispersal of the sorbent.

Qualitative differences in the sorbent response to injection under these two conditions can be described as follows: With laminar injection, the main modes of heat transfer are conduction and radiation. Using turbulent injection, both small- and large-scale convection (mixing) are introduced, effecting a faster sorbent stream heat-up rate. With laminar injection, the concentration of CO_2 within the sorbent stream due to calcination can reach 100 percent and diffusion calculations suggest that as long as 0.2 s might be required for the concentration along the axis to decay to 10 percent, assuming that there is no CO_2 in the surrounding gases. Using turbulent injection, the CO_2 is dispersed due to bulk mixing. Finally, with laminar injection, SO_2 must diffuse into the sorbent stream, while under turbulent injection it is entrained, along with the flame gases.

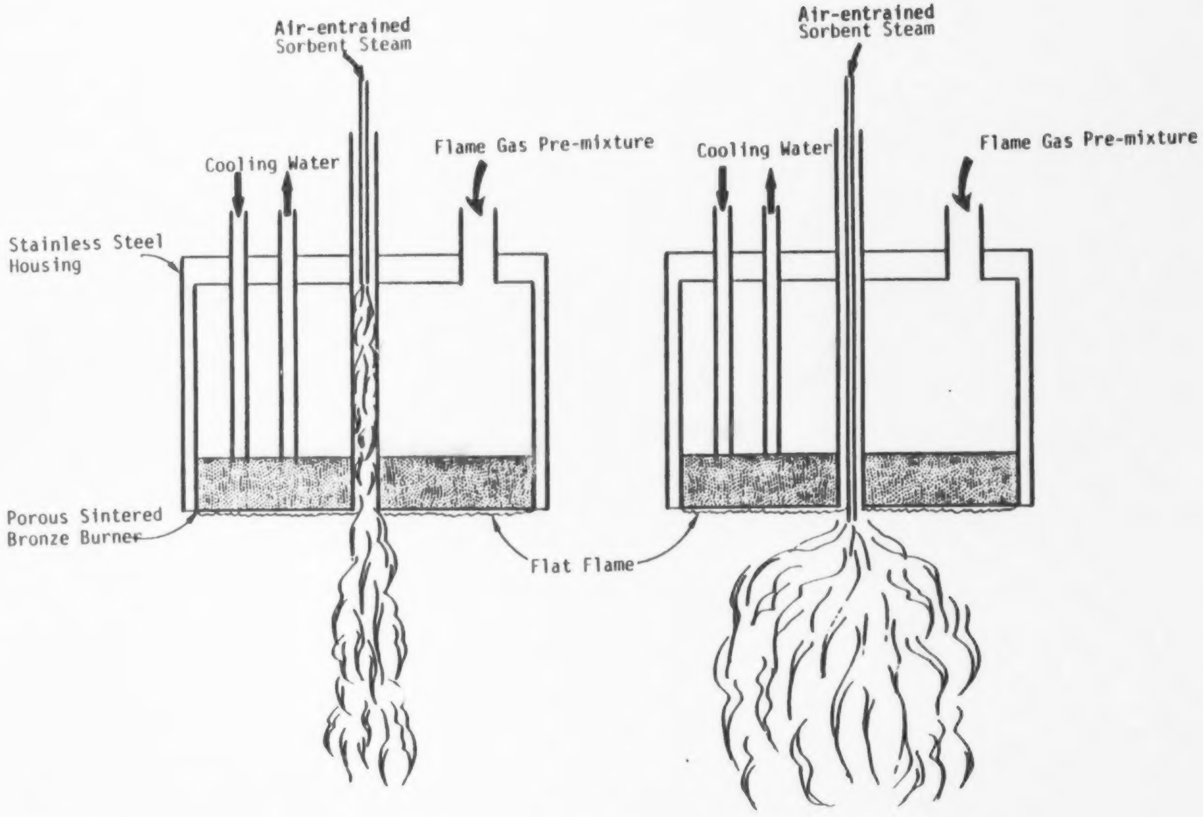
Air-entrained Sorbent Steam
Cooling Water
Flame Gas Pre-mixture
Stainless Steel Housing
Porous Sintered Bronze Burner
Flat Flame
Air-entrained Sorbent Steam
Cooling Water
Flame Gas Pre-mixture

(a) Laminar Injection

(b) Dispersed Injection

Figure D-1. Effect of ITR Sorbent Injector Technique

The problem of CO_2 diffusion out of and SO_2 diffusion into the sorbent stream was addressed mathematically by treating the stream as a cylinder with negligible axial gradients and by assuming a step change in concentration at the outer boundary of the cylinder as an initial condition. Mathematical treatment of this problem is similar to that discussed in reference (27). The governing equation used was:

$$\frac{\partial C}{\partial t} = D \frac{1}{r} \frac{\partial}{\partial r} \left(r \frac{\partial C}{\partial r} \right) \qquad \text{D-1}$$

Separation of variables was applied so that:

$$C^{*} = C - C_{o} = \chi(r)\,\theta(t) \qquad \text{D-2}$$

$$\frac{1}{\theta} \frac{\partial \theta}{\partial t} = \frac{1}{\chi r} \frac{\partial}{\partial r} \left(r \frac{\partial \chi}{\partial r} \right) = -\lambda^{2} \qquad \text{D-3}$$

with boundary conditions

$$\frac{\partial \chi(o)}{\partial r} = 0 \qquad \text{D-4}$$

$$\chi(r_{o}) = 0 \qquad \text{D-5}$$

and the initial condition

$$\theta(o) \sim -C_{o} \qquad \text{D-6}$$

where:

C = SO_2 concentration in sorbent stream
C_o = SO_2 concentration in flame gases
D = diffusivity of SO_2 in flame gases
r = radial distance from axis of stream

r_o = radius of sorbent stream
t = time

The solution to the equation is the series:

$$C^*(r,t) = -\sum \frac{2\ C_o}{\lambda_n r_o J_1(\lambda_n r_o)} \exp\ (-2\lambda_n t)\ J_o\ \lambda_n r \qquad \text{D-7}$$

where λ_n are eigen functions of the equation and J_1 and J_o represent Bessel functions.

The concentration of SO_2 along the axis of the sorbent stream was estimated by the the first term of the series shown in Equation D-7. Assuming a bulk SO_2 concentration of 3600 ppm and no loss of SO_2 by chemical reaction, nearly 0.1 s would be required at 1500 K for the SO_2 concentration at the axis of the laminar jet to exceed 1000 ppm. In addition, nearly 1.0 s is required for the concentration in the jet to reach that of the bulk gas. In the presence of effusing CO_2 due to calcination, the flux of SO_2 into the sorbent stream is expected to be further reduced.

The true effect of injection mode was established experimentally in the ITR. In these tests, the ITR was operated with a 1100°C hydrogen-air flame, doped to yield 3000 ppm SO_2 in the combustion gases; each of the injection methods shown in Figure D-1 were tested using Vicron 45-3. In addition, to indicate the effect of bulk gas CO_2 concentration, the bulk CO_2 level was adjusted by replacing some of the burner feed air with a CO_2/O_2 mixture. Following a 1.4 sec residence time in the ITR, the dispersed solids were extracted from the furnace and analyzed to determine degree of sulfation and of calcination. These results are shown in Figure D-2. (It is noted that these samples were collected using a quartz sampling probe, prior to the implementation of the stainless-steel water-cooled probe shown in Figure 4-4. This quartz probe resulted in a slower quench rate and a longer sampling time, so that a greater degree of sulfation would have occurred in the probe, relative to the stainless probe.)

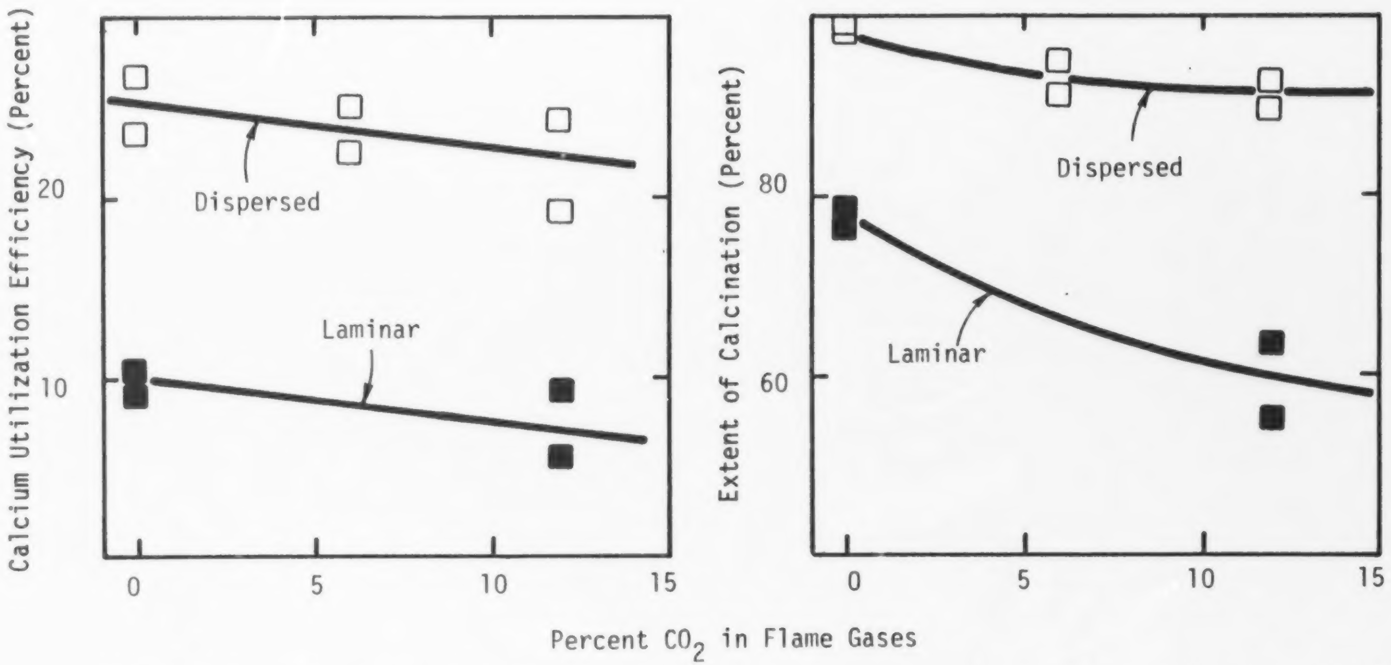

Figure D-2. The Effects of Injection Mode on SO_2 Capture and Calcination in the ITR. 1100°C, 1.4s, 3000 ppm SO_2, Quartz Probe Sampling. The Effects of CO_2 Concentration are Also Indicated as An Independent Variable.

As shown in Figure D-2, both the degree of calcium utilization and the extent of calcination are much higher with the dispersed-phase injection method, as expected. This result is probably due to the improved SO_2 contacting, the more rapid dispersion of the evolving CO_2 (reduced recarbonation), and the more rapid particle heating achieved with the dispersed-phase injection system. As a result of these data, the dispersed-phase injection system was used during all of the ITR testing described in this report.

It is to be noted from the Figure D-2 that variation of bulk CO_2 concentration has a definite, but not significant, impact upon utilization and calcination in the dispersed-phase mode.

The question remains whether SO_2 is sufficiently entrained, even with the dispersed-phase turbulent injection system, in order to eliminate bulk diffusion control over sulfation. To address this question, the ITR was operated with the dispersed-phase injection system with varying levels of SO_2 in the entraining air which transports the sorbent through the injector tube. The bulk flame gases also contained SO_2, at a level of 3600 ppm. The intent of the test was to determine whether efforts to reduce the need for SO_2 entrainment into the sorbent jet, by including SO_2 in the jet itself, would improve sorbent utilization. The results are shown in Figure D-3. In the case where there is zero SO_2 in the sorbent jet (all reaction takes place with entrained SO_2 from the bulk gas), the sorbent utilization is the same as in the cases where increasing levels of SO_2 are included directly in the sorbent transport gas. This result suggests that, at least under the conditions of 1100°C and 0.53 sec ITR residence time, entrainment of SO_2 into the turbulent sorbent jet is not rate limiting.

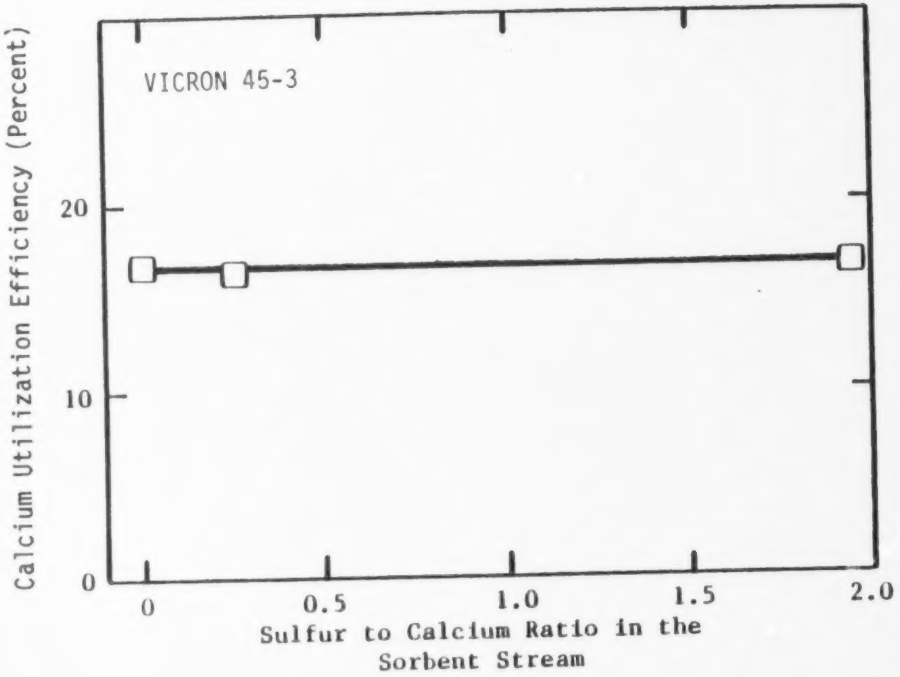

Figure D-3. The Effect of Initial SO_2 Concentration in the Sorbent Stream on Calcium Utilization in the ITR. 1100°C, 3600 ppm SO_2 0.53s, Water-cooled Sampling Probe with Filter at 140°C.

APPENDIX E

Sampling Technique Evaluation

APPENDIX E. SAMPLING TECHNIQUE EVALUATION

In the development of procedures for use of the water-cooled sampling probe (Figure 4-4), several effects were discovered concerning the sensitivity of the sorbents, especially precalcines, to the sampling conditions. Both temperature at the filter and the sampling period had profound influence on the results obtained for in-situ sulfation. The grain model was applied to the conditions prevalent in the sample filter holder, and the subsequent comparison with data provided insight concerning the amount of SO_2 uptake occurring there.

The temperature of the sample filter holder affected the measured calcium utilization of samples sulfated in-situ in the ITR. This is shown in Figure E-1 for three sorbents, Vicron 45-3, D3002 dolomite and D60 precalcine. The filter temperature was varied from about 130°C to 270°C for these tests. The samples were collected from a short residence time, 1100°C, H_2-air flame laden with 3600 ppm SO_2. The sample collection time was 30 minutes. The fact that total utilization increases with increasing filter temperature demonstrates that SO_2 uptake does continue after the samples leave the reaction environment.

Figure E-2 shows the results of tests to determine the potential for in-filter sulfation of precalcines. In this case, unsulfated sorbents were added directly to the filter holder with no prior exposure to flame gases. SO_2-laden gases from a hydrogen-air flame were then drawn through the filter which was maintained at the indicated temperature by controlling the cooling water flow rate. Samples were exposed to the flame gases for 30 minutes. The filter, containing the sorbent, was preheated in an electric oven to prevent condensation of water vapor. Grain model calculations for the experimental conditions are also shown.

Discrepancy between the model and data is not surprising because the model kinetics were developed from data collected at temperatures above 700°C. However, the difference in the trend as well as the magnitude could suggest a different mechanism for SO_2 uptake at low temperatures. Sulfur

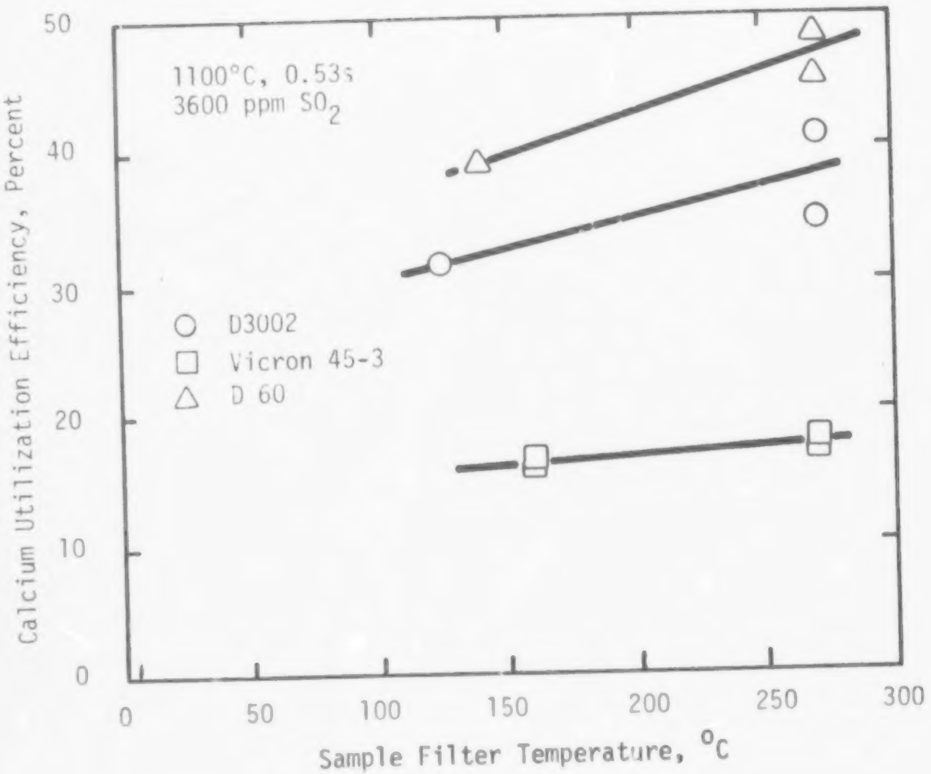

Figure E-1. Effects of Sample Filter Temperature on Measured Calcium Utilization by Three Sorbents in the ITR, 1100°C H_2-Air Flame, 3600 ppm SO_2 0.53 s Residence Time.

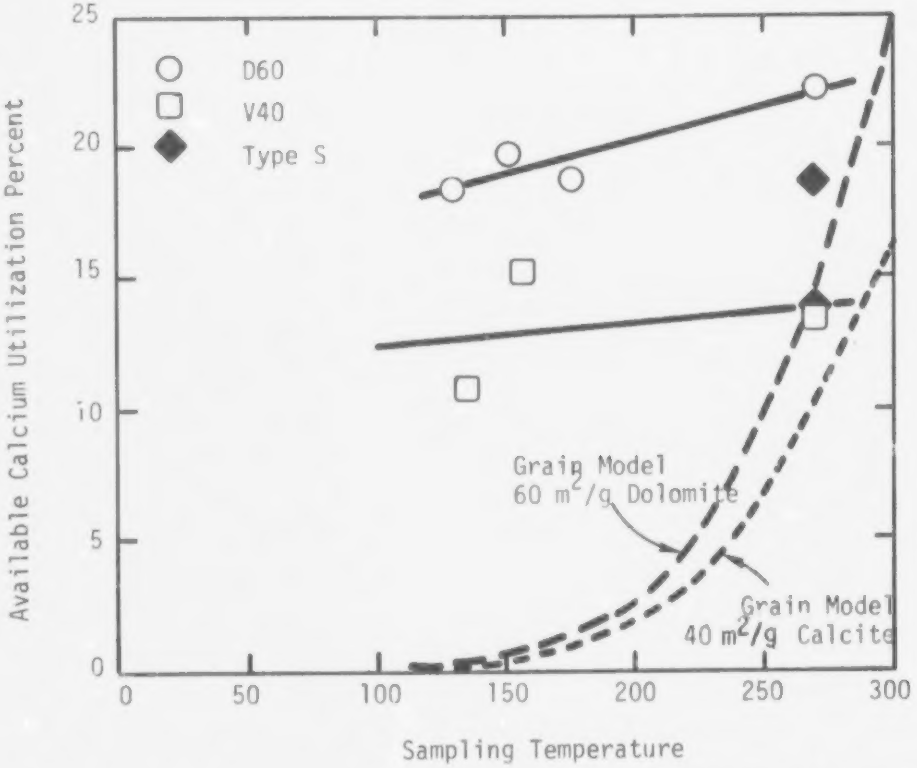

Figure E-2. Effects of Temperature on SO$_2$ Uptake by Pre-calcines In-Filter. The Grain Model Prediction is Shown for 60 m^2/g Dolomite and 40 m^2/g Calcite Calcines. 3600 ppm SO$_2$ in H$_2$-Flame Gases Was Used to Sulfate the Samples. 30-Minute Exposure.

capture by the type S material shows that hydroxides can react directly with SO_2 without the need of prior calcination. In fact, the similarity in calcium utilizations between the type S material and the precalcines could reflect the need for H_2O to be present for rapid, low-temperature sulfur capture.

Possible alternate mechanisms for low-temperature SO_2 capture were examined by repeating the tests involving placement of precalcines directly into the filter holder. Rather than flame gases, however, dry N_2 and dry air, each with 3600 ppm SO_2 added, were drawn through the sample. Figure E-2 demonstrates the results of 30 minute exposures of precalcines to 3600 ppm SO_2 in air or N_2 between 150 and 300°C. No great difference is apparent between using air or N_2. Since the formation of $CaSO_4$ requires oxygen, these results demonstrate that SO_2 capture is occurring by formation of calcium sulfite, i.e.:

$$CaO + SO_2 \longrightarrow CaSO_3 \qquad \text{E-1}$$

at these temperatures. Finally, the data trend in Figure E-3 shows that the filter capture is leveling off at a temperature near 150°C. This indicates that further reduction in sampling temperature may be unnecessary. Too low a sampling temperature must be avoided because of the increasing potential for formation of hydroxides. Eventually, of course, condensation also occurs.

Having established that the sampling temperature must be around 150°C., the effects of sampling time were investigated. D60 precalcine was exposed to SO_2 in-filter at 180°C for times ranging from 5 to 60 minutes. Figure E-4 shows these data. There are two important aspects of the results of this test. First of all, the in-filter capture can be reduced dramatically if the sample residence time in-filter is limited to about 5 minutes or less. Secondly, after a certain level of utilization is reached, about 20 percent in this case, the rate of SO_2 uptake is reduced dramatically. This latter observation is especially significant because it demonstrates that samples which are well sulfated in the reaction zone of the ITR will experience less

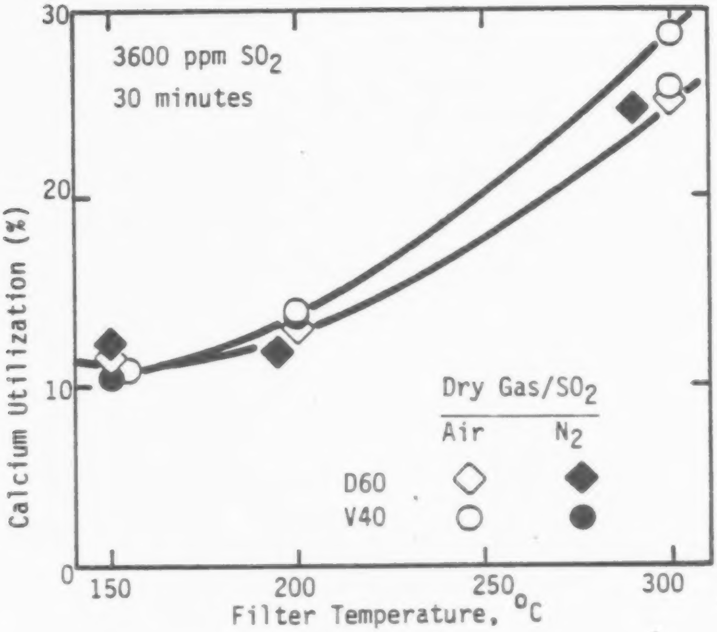

Figure E-3. SO_2 Uptake by D60 and V40 Precalcines in Dry Air and Dry N_2 Between 150 and 300°C, 3600 ppm SO_2, 30 Minutes Exposure Time.

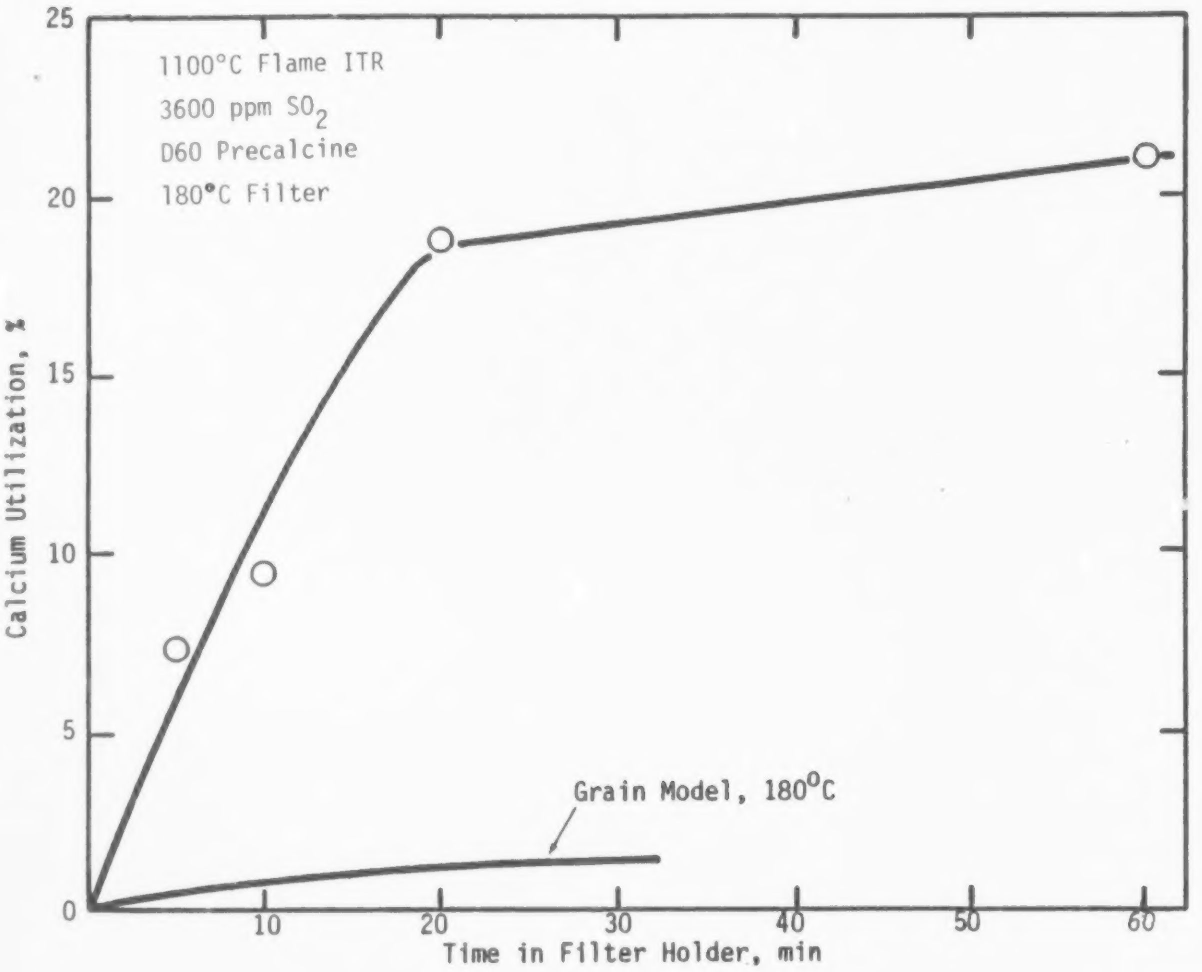

Figure E-4. In-Filter SO_2 Uptake by D60 Precalcines. 3600 ppm SO_2 in H_2 Flame Gases. Filter Temperature is 180°C.

additional uptake than demonstrated for raw precalines placed directly in-filter.

The effect on sampling time of samples sulfated in the reaction zone of the ITR is shown in Figure E-5 for Vicron 45-3 and D60 precalcine. Both materials were collected from three different flames and with sampling times between 2 and 15 minutes, with the sample filter held at 150°C. Vicron 45-3 shows very little effect of sampling time at any condition. D60 precalcine, on the other hand, displays a substantial effect of sampling time, especially at the 1000°C condition where it is most reactive.

The effect of the sampling system on measured specific surface areas also was examined. The D60 and V40 precalcines were used to determine whether highly reactive materials could be sampled for surface area measurements. All of these tests involved placing the precalcines directly into the filter holder and exposing them to flame gases. Subsequently their surface areas were measured and compared with their starting values.

The effect of sampling temperature on surface area loss is illustrated in Figure E-6. The sorbents were exposed to flame gases for 30 minutes at the indicated temperature. Subsequently, they were analyzed for surface area and H_2O and CO_2 content. The samples were not dried before analysis. Loss of surface area increased approximately linearly with temperature over the range studied. The loss was especially severe for V40 precalcine at 270°C. The precalcines also reacted chemically with the flame gases. Between 50 and 90 percent of the CaO in every sample was converted to $Ca(OH)_2$ and 8-40 percent conversion to $CaCO_3$ was also experienced. This latter result was surprising for sorbents exposed to hydrogen flame gases, however, the amount of CO_2 in the burner air can easily account for this much conversion. The samples exposed to methane flame gases exhibit higher conversions to carbonate with correspondingly lower H_2O uptake.

Figure E-7 shows the effect of time in the filter on surface area loss by precalcines placed directly into the filter holder at 150°C. Even at times as short as five minutes, no reduction in desurfacing was noticed.

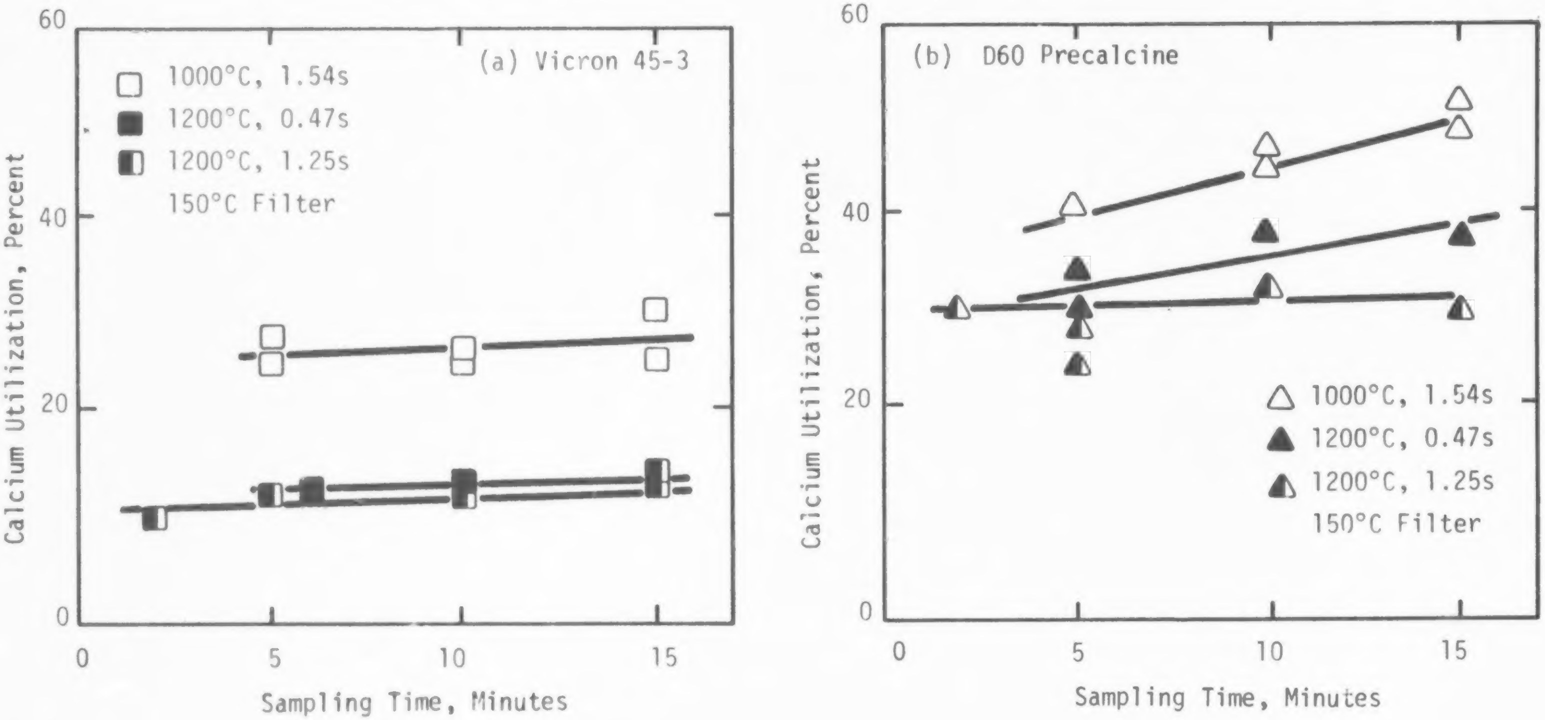

Figure E-5. Impact of Sampling Time on Measured Calcium Utilization by (a) Vicron 45-3, (b) D60 Pre-Calcine, 3600 ppm SO_2, H_2-Air Flames in the ITR.

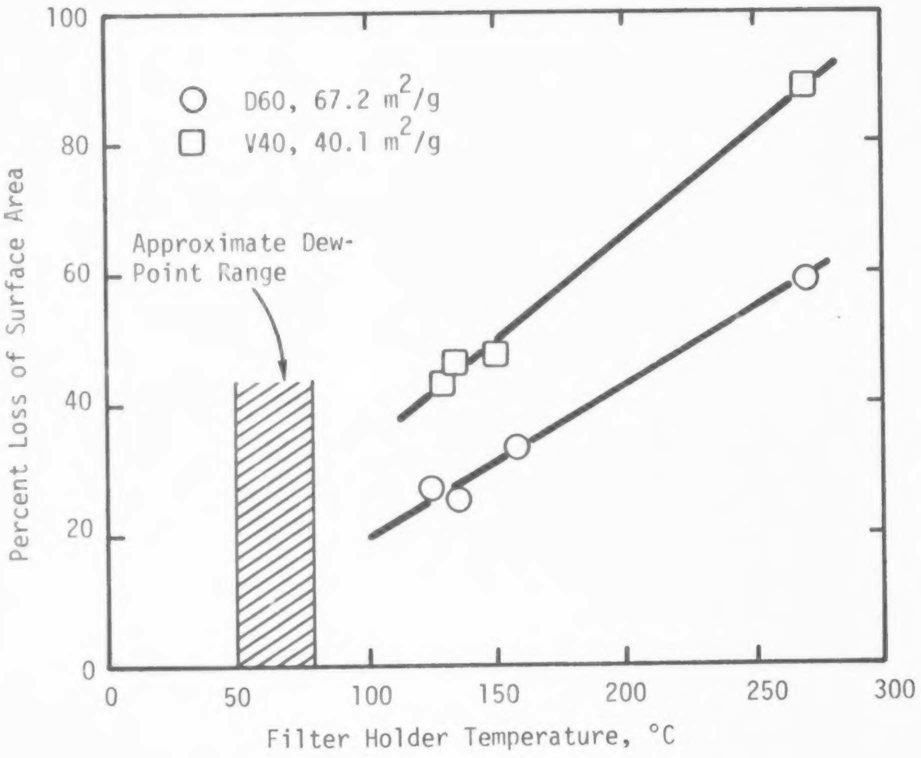

Figure E-6. Loss of Surface Area with Sampling Temperature for Precalcines Exposed to Flame Gases in the Sample Filter Holder. Samples were Exposed for 30 Minutes.

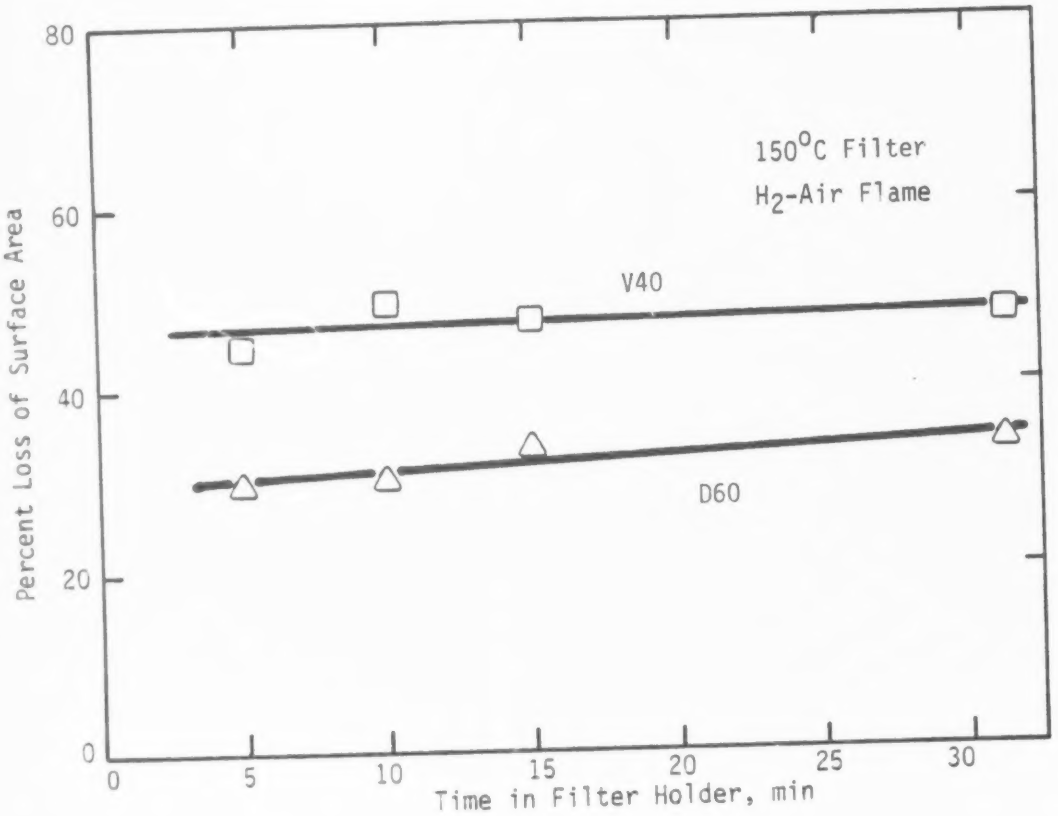

Figure E-7. Loss of Surface Area by Precalcines Placed Directly into the Sampling System Filter.

This suggests either that desurfacing is very fast, or occurs as a result of a slow reaction between water and lime between the time of sample collection and sample analysis. The latter hypothesis is probably not likely because all of the samples were removed and immediately placed under vacuum (<130 Pa) after exposure to flame gases. The data for desurfacing of precalcines are tabulated in Table E-1.

Conclusions and Recommendations

Based upon the results presented in this appendix the following guidelines were adopted for the sampling of sulfated sorbents from the ITR:

1. Sample collection times of five minutes or less are to be used.

2. Filter temperatures during sampling should not lie outside of the range of 130-180°C.

In addition, it was concluded that samples collected for surface area analysis would not exhibit the surface area actually existing in the reactor. Therefore, this approach to determining surface areas should be abandoned. The possibility still exists however, that measured surface areas are at least qualitatively reflective of those existing in the ITR.

The requirement of reduced sampling time was one of the considerations leading to the development of the water-cooled stainless steel probe, described in Section 4.2.2. The one-inch sampling orifice in this probe permits the collection of adequate quantities of solid sample for analysis within a five-minute sampling period, at sampling rates no more than two times isokinetic.

TABLE E-1. SURFACE AREA LOSS BY PRE-CALCINES IN THE FILTER HOLDER.

Sample	Sorbent	Filter Temp, °C	Time in Filter, Min.	Wt % $Ca(OH)_2$[a]	Wt % $CaCO_3$[a]	BET Surface Area, m^2/g
114277	V40	-	-	24.8	2.2	40.1
114278	V40	150	5	89.5	5.4	22.3
114279	V40	150	10	88.8	6.3	20.1
114280	V40	150	15	90.7	7.2	21.2
114281	D60	-	-	21.5	3.2	67.2
114282	D60	150	5	58.8	7.9	47.1
114283	D60	150	10	64.4	7.4	46.9
114284	D60	150	15	63.2	9.2	44.7
114141[b]	V40	130	30	53.3	17.3	23.8
114142[b]	D60	125	30	43.7	15.2	47.4
114144	D60	157	30	60.6	10.4	43.3
114146	V40	150	30	87.7	9.7	21.9
114147	V40	133	30	87.3	8.3	22.5
114148	D60	135	30	62.5	9.4	48.3
100698[b]	V40	270	30	32.6	8.7	4.9
114103[b]	D60	270	30	31.1	37.8	26.8

[a] Data are shown as percent $Ca(OH)_2$ and $CaCO_3$ only for comparison, in dolomite the hydroxide and carbonate may be combined with MgO also.

[b] Exposed to CH_4 - air flame gases

APPENDIX F

Quartz Probe Sampling in the ITR

APPENDIX F. QUARTZ PROBE SAMPLING IN THE ITR

Prior to the construction of the water-cooled stainless steel probe that was used for most of the ITR testing reported here, a quartz probe was employed. This probe was utilized in two ways:

a) Most commonly, the probe was used in a configuration referred to as the "dispersed-phase SO_2 reactivity probe," described in Reference 22. In this configuration, the furnace being sampled (the TDR or the ITR) would be operated without SO_2, and the samples being extracted would thus be calcined but not sulfated. The extracted sample would be cooled in the quartz probe down to 650^oC, then sulfated under controlled conditions (1100^oC, 0.6 sec, 6 percent SO_2) in a separate zone. This probe served its original purpose of providing comparable reactivity (sulfation) data decoupled from the calcination environment.

b) On occasion, the quartz probe was used solely to extract a solids sample for external analysis, in cases where the ITR was operated with SO_2 present in the furnace. The quartz probe was abandoned for this purpose in favor of the water-cooled probe. One problem was that the low thermal conductivity of the quartz provided a very slow quench, effectively extending the reaction zone well beyond the sampling location in the furnace. A second problem was that the quartz probe typically required on the order of 30 minutes to collect adequate solids sample for analysis; as discussed in Appendix E, this length of sampling time can result in significant additional sulfation occurring in the sample filter, especially since the filter operated at a relatively high temperature (270^oC) in this mode.

The purpose of this appendix is to present the results from ITR tests with the quartz probe, which are not reported elsewhere. In addition to the tests discussed here, the major ITR test series conducted with this probe is the Cr_2O_3 testing described in Section 5.5.1. Also, all TDR sampling was done with the quartz probe.

Figure F-1 shows the results of ITR tests to determine the effects of CO_2 concentration on sorbent utilization in the SO_2 reactivity probe. Also shown is the effect of CO_2 on specific surface area measured after sample collection from the ITR. And 1100°C H_2-air flame was used for these tests. The CO_2 concentration was varied at constant temperature by replacing some air with a CO_2-O_2 mixture having the approximate heat capacity of air. The samples represented in Figure F-1 (a) were collected from the ITR at 1.4 s residence time. They then passed into the probe reaction zone with a residence time of 0.6 s, peak temperature of 1100°C and 6 percent SO_2. The results show a small impact of CO_2 concentration up to 12 percent. The effect on measured surface area under the same conditions, without SO_2, was somewhat more dramatic. However, surface area was probably lost as a result of sample carbonation in the filter holder, as discussed in Appendix E. Also, it is quite possible that some recarbonation occurred in the 650°C region of the reactivity probe.

The quartz probe was then used (without the reactivity/sulfation section) to collect samples sulfated in-situ in the ITR. For this test the probe was not heated; however, the sampling volume was increased and so the filter temperature was approximately 270°C. Figure F-2 (a) shows the effect of CO_2 on in-situ sulfation. (These data were shown previously in Figure D-2.) Again the effect is small, less than 20 percent loss in utilization at 12 percent CO_2. The effect on calcination (of the same samples), shown in Figure F-2 (b) is less clear. The measured extent of calcination dropped from about 99 percent to near 90 percent, yet this too could be a result of sample recarbonation on the filter.

The utilizations and extents of calcination observed with in-situ sulfation are somewhat higher than those observed with the reactivity probe. Among the possible explanations for this results are: 1) the sorbent might be more reactive when sulfation is occurring simultaneously with calcination (i.e., the SO_2 is present during the transient peak areas suggested in Figure

- ITR, 1100°C, 1.45
- Reactivity Probe Sampling

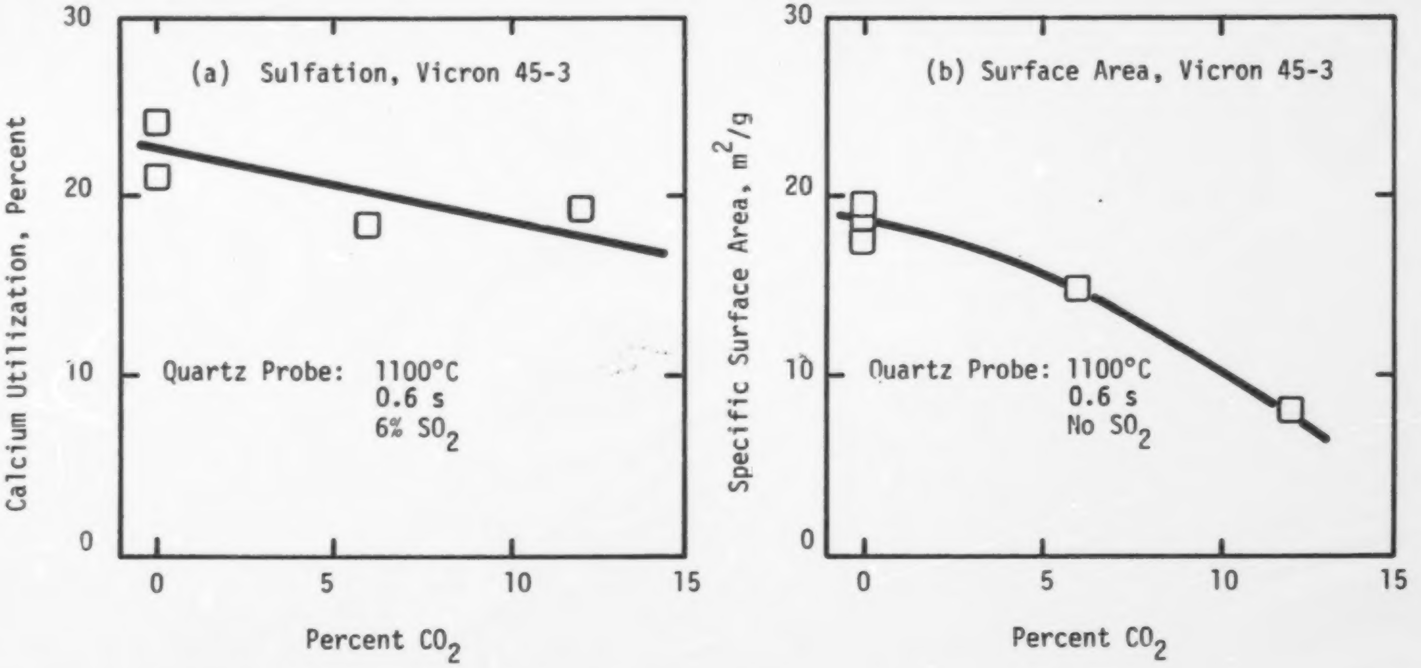

Figure F-1. The Effect of CO_2 Concentration on (a) SO_2 Capture and (b) Surface Area Development for Samples Collected with the Dispersed-Phase Quartz SO_2 Reactivity Probe.

- ITR, 1100°C
- In-flame Sulfation, Vicron 45-3
- 3000 ppm SO_2, Ca/S 1
- 1.4s

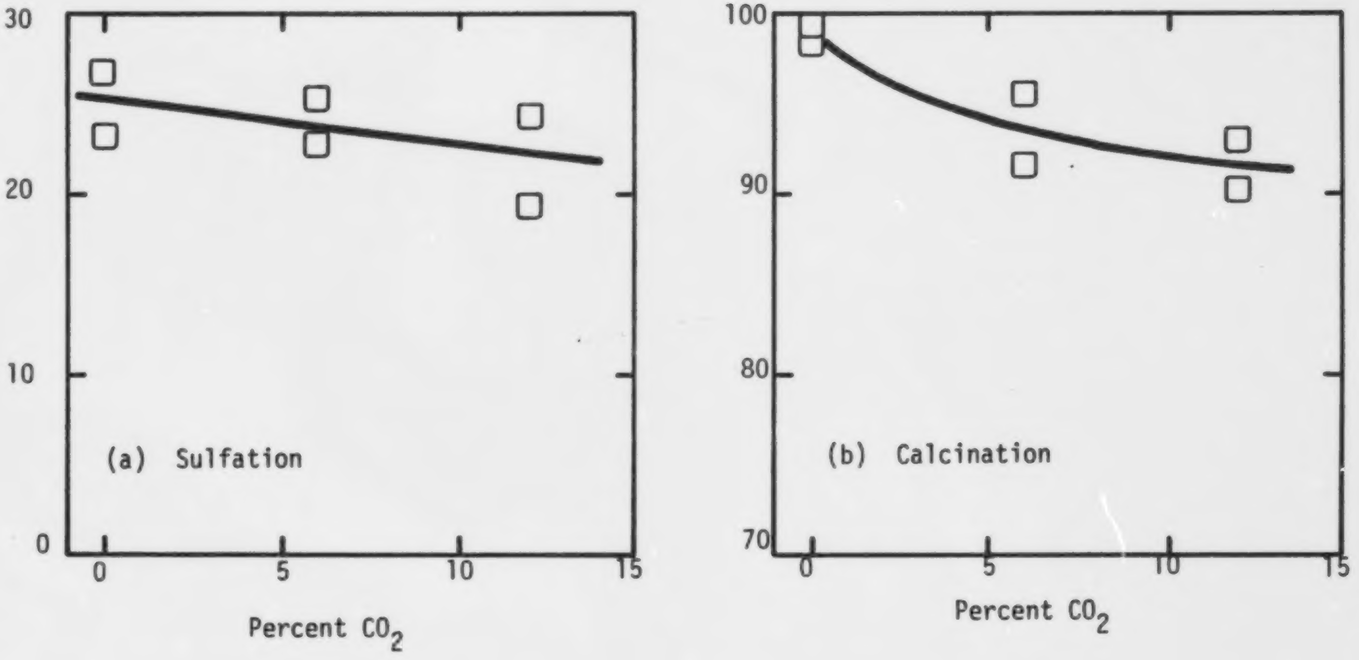

Figure F-2. Effect of CO_2 Concentration on (a) Sulfation and (b) Calcination of Vicron 45-3 in the ITR. 1100°C, H_2-air Flame with CO_2 and 3000 ppm SO_2 Added to the Flame Premixture. Samples were collected with the Quartz Probe and a Sampling Temperature of 270°C

5-37); b) additional sulfation might have occurred in the sample filter in the in-situ case due to the higher filter temperature (270°C versus 130°C in the reactivity probe case); and c) additional recarbonation might have occurred in the reactivity probe case due to the residence time at 650°C prior to sulfation.

Finally, the effect of time at temperature prior to sulfation was examined. Samples of Vicron 45-3 were exposed to different residence times in the ITR at 1100°C prior to sulfation in the quartz reactivity probe. Figure F-3 shows that residence time at 1100°C has no effect on the utilization of Vicron 45-3 over the range of temperatures examined. This likely reflects that the surface area or reactivity developed by the sorbent upon calcination has reached a steady state within 0.5 s. (As shown by the ITR data in Table A-3, Vicron is about 85 percent calcined within 0.5 sec at 1100°C.

Samples collected from the ITR using the quartz probe, including those presented with the Cr_2O_3 addition data in Section 5.5, show significantly higher levels of utilization than comparable samples obtained with the water-cooled rapid-quench probe. Reviewing results from the quartz and water-cooled probes, it was possible to determine some of the sampling system conditions which could result in additional sulfation within the sampling system. It was also shown how to reduce sulfation in the sampling system. Results with the quartz probe should be regarded as qualitatively indicative of the trends resulting from the variation of furnace parameters (e.g., peak temperature or CO_2 level). However, the quartz probe results do not represent the actual sorbent utilizations existing in the TDR or ITR.

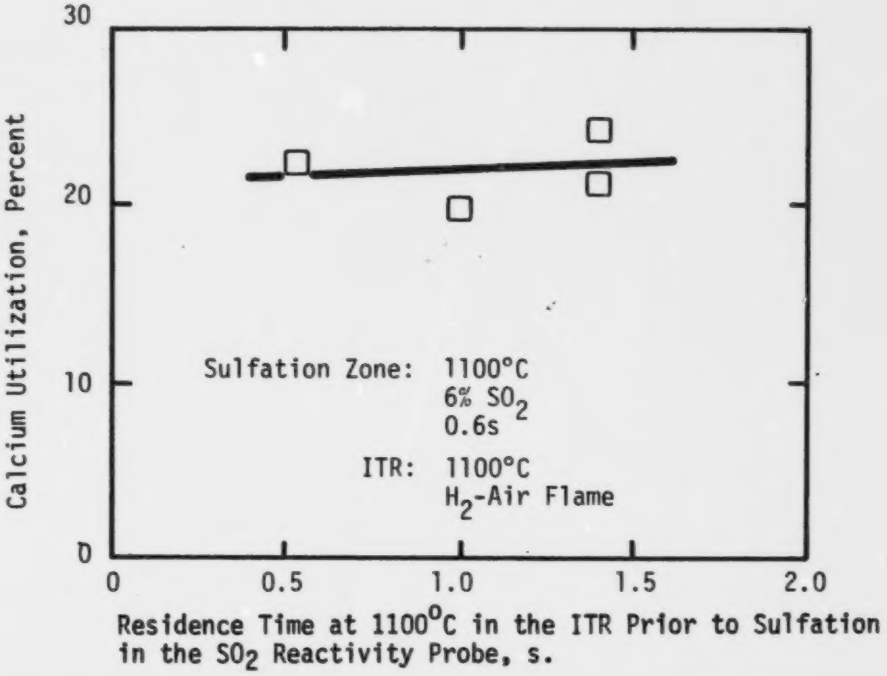

Figure F-3. The Effect of Time at Temperature Prior to Sulfation of Vicron 45-3. ITR Conditions: 1100°C, H_2-Air Flame. Probe Conditions: 1.6s, 6 Percent O_2, 1100°C.

APPENDIX G

Quality Control Evaluation Report

APPENDIX G. QUALITY CONTROL EVALUATION REPORT

The objectives for data quality established at the outset of this program were attained by the results presented in the preceding report and its appendices. These objectives were to provide data of sufficient quality to be useful to the ongoing LIMB development program and to the development of mathematical models describing the limestone sulfation process. The data quality was monitored constantly throughout the program through checks and rechecks of the analytical and experimental techniques and apparatus. These quality control procedures and their effects on establishing limits of reliability of the data are discussed in the following section.

Data quality control procedures were divided into two areas: experimental control, and analytical procedures. Discussion of quality assurance procedures is presented under these two subjects. Experimental quality control and evaluation in this program consisted of assuring accurate and reproducible experimental conditions. The major experimental parameters were temperature, and residence time. Measurements of gas composition (especially SO_2 concentration) and sorbent feed rates (Ca/S molar ratio) were of secondary importance. Model estimations, based on fundamental sulfation rate data, indicated that calcium utilization (the primary parameter measured here) would be a weak function of both calcium-to-sulfur ratio and SO_2 concentration in the range of this study. Figures G-1 and G-2 provide both model predictions (34, 41) and data (31, 38) which support these assumptions. Analytical quality control procedures consisted of confirming the accuracy of measurements against known standards, as well as precision determinations based on repeatability of individual samples' measurements.

G-1. Experimental

G-1.1 Temperature Measurements

Temperature measurements within the ITR were made with a 0.025 mm diameter butt-welded, supported, type-S thermocouple. Temperature readings in degrees Celsius were obtained with an electronic readout containing an

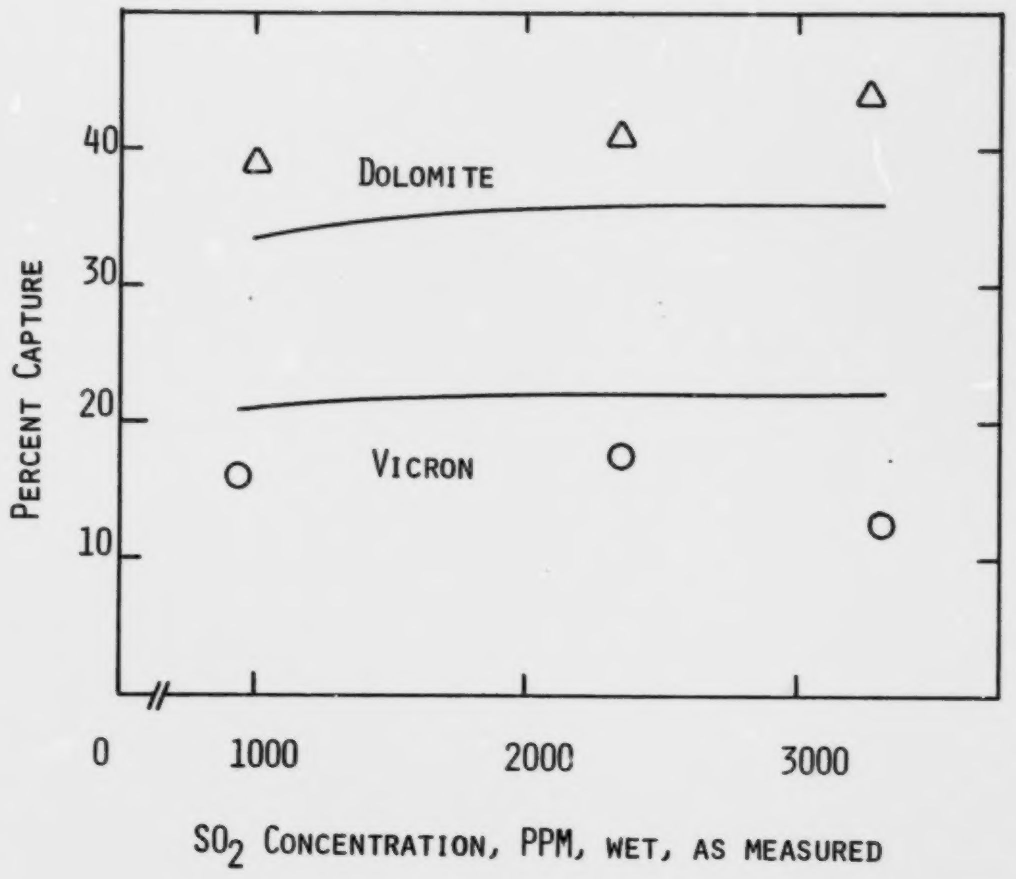

Figure G-1. Percent Capture as a Function of SO_2 Concentration for Vicron 45-3 and Dolomite. The Solid Lines are Grain Model Predictions. Experimental Conditions were Ca/S = 2 τ = 0.46s, T = 1110°C. The Data are from Ref. 31 and were Obtained Under Isothermal Conditions.

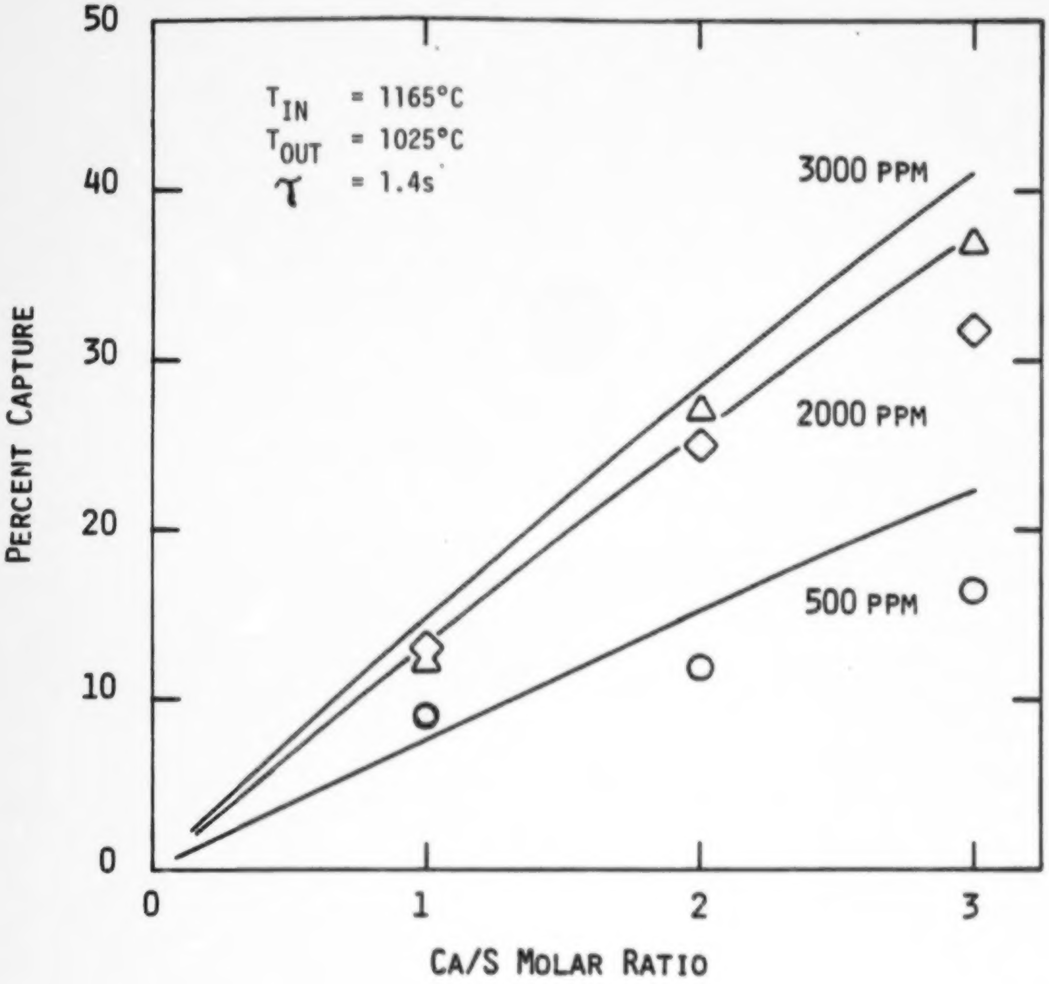

Figure G-2. Percent SO_2 Capture as a Function of Ca at Three SO_2 Concentrations. Data are from Ref. 38 and were Obtained in a Non-Isothermal Flow Reactor.

icepoint reference and with an accuracy specified at ± 2.3°C. The fine wire thermocouple was utilized in order to minimize the uncertainties of radiation corrections.

Radiation corrections to the thermocouple readings were determined by balancing the equations for heat transfer away from the thermocouple wire

$$q_{conv} = h_o A (T_{tc} - T_{gas}) \qquad \text{G-1}$$

$$q_{rad} = \epsilon\sigma A (T_{tc}^4 - T_{env}^4) \qquad \text{G-2}$$

where:

q_{conv} = convective heat loss
q_{rad} = radiative heat loss
h_o = convective heat transfer coefficient
A = surface area per unit length of t.c. wire
T_{wire} = t.c. wire temperature, K
t_{gas} = gas temperature, K
T_{env} = temperature of surroundings, K
ϵ = emissivity of platinum, $\epsilon = 0.18$
σ = Stefan-Boltzman constant

The heat transfer coefficient was determined by the equation (42):

$$\frac{h_o D_o}{k_f} = \left(\frac{C_p \mu}{k_f}\right)^{0.3} \left[0.35 + 0.56 \left(\frac{\rho V D_o}{\mu}\right)^{0.52}\right] \qquad \text{G-3}$$

where:

D_o = t.c. wire diameter

k_f = gas thermal conductivity

$\frac{C_p \mu}{k_f}$ = prandtl number, 0.7

$\frac{\rho V D_o}{\mu}$ = Reynolds number, 0.1

Solving these equations yielded $h_o = 4.4 \times 10^{-2}$ $\mathrm{cal \cdot cm^{-2} \cdot s^{-1} \cdot K^{-1}}$. Setting equations G-1 and G-2 equal to each other

$$T_{gas} = T_{wire} + \frac{(T_{wire}^4 - T_{env}^4)}{1.79 \times 10^{11}} \qquad \text{G-4}$$

where T_{env} is taken as the wall temperature of the ITR. The correction is significant (>5 K) only when the thermocouple temperature differs from the ITR temperature by more than about 75 K. This condition occurred when the ITR was operated under "non-isothermal" conditions, i.e. during the chromium effects testing (Section 5.5.1). The temperature profiles in Appendix B reflect these corrections.

Radial temperature gradients in the ITR were small while operating under isothermal conditions. No attempt was made to measure or estimate radial temperature gradients for the non-isothermal operating conditions because those conditions were not utilized for fundamental rate data for which such information would be critical. Table G-1 shows how the temperature varied from the center of the ITR at 900°C. The reactor was divided into four quadrants which were labeled by their closest compass points: N, S, E, and W. The temperature was measured "near the wall" in each direction away from the ITR axis. In all but one case, duplicate measurements were made.

The temperature of the ITR itself was monitored by a programmable control unit using four type R (Pt/Pt-13 percent Rh) thermocouples. These

TABLE G-1. RADIAL TEMPERATURE CHANGE IN THE ITR AT A NOMINAL 900°C ISOTHERMAL CONDITION.

Distance from Burner, cm	Temperature, °C Axis	N	S	E	W
107	897	895	895	899	895
94	909	910	911	910	910
	905	906	904	904	900
81	904	907	909	906	910
	903	905	906	902	905
69	903	902	908	904	906
	904	906	911	910	913
56	903	902	912	901	907
	909	908	916	913	912
43	903	902	910	909	906
	902	904	906	903	909
30	900	898	896	902	898

thermocouples are normally stable and were at no time subjected to the reactive flame gases. Therefore, they were not checked for deterioration during the course of the experimental work.

G-1.2 Gas Flow Rates

All gas flow rates were measured by suitably sized rotometers which, with one exception, were all manufactured by Dwyer Instruments Inc. The exception was a Matheson Tube Cube flowmeter calibrated for low flow rates of sulfur dioxide.

In general, flowmeters were not calibrated because temperature, not stoichiometry, was the significant control variable. Calibration for H_2 and SO_2 are shown in Figures G-3 and G-4.

Flow rates were corrected for pressure and specific gravity (relative to air) using the formula

$$Q = Q^{o}\left[\frac{P}{101.3\text{kPa}} \times \frac{1}{\text{S.G.}}\right]^{1/2} \qquad \text{G-5}$$

where:

Q = true flow rate
Q^{o} = measured flow rate
P = outlet rotometer pressure, kPa
S.G. = gas specific gravity

Corrections for ambient temperature were not made. All of the flowmeters were factory calibrated and specified accurate to ± 5 percent, or better, of the full-scale reading. Experimental conditions were repeatable within the ability to read the flowmeter.

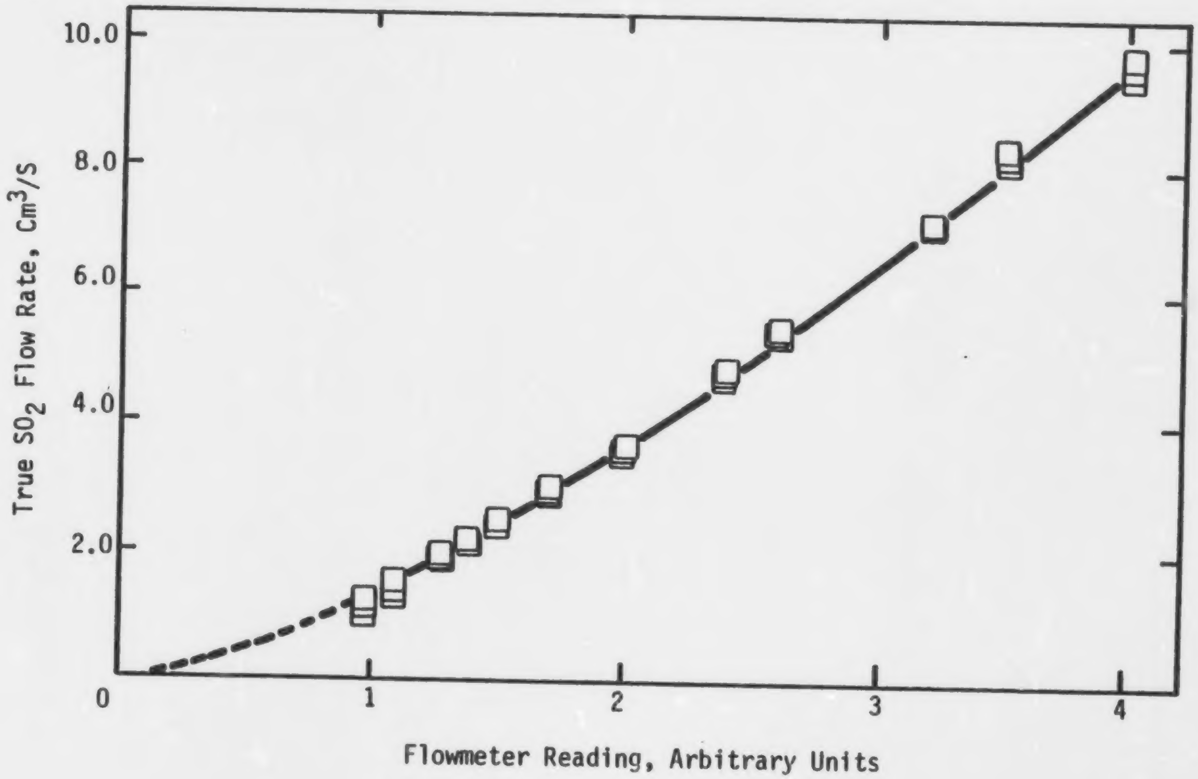

Figure G-3. Calibration of the SO_2 Flowmeter at Room Temperature with Negligible Outlet Pressure.

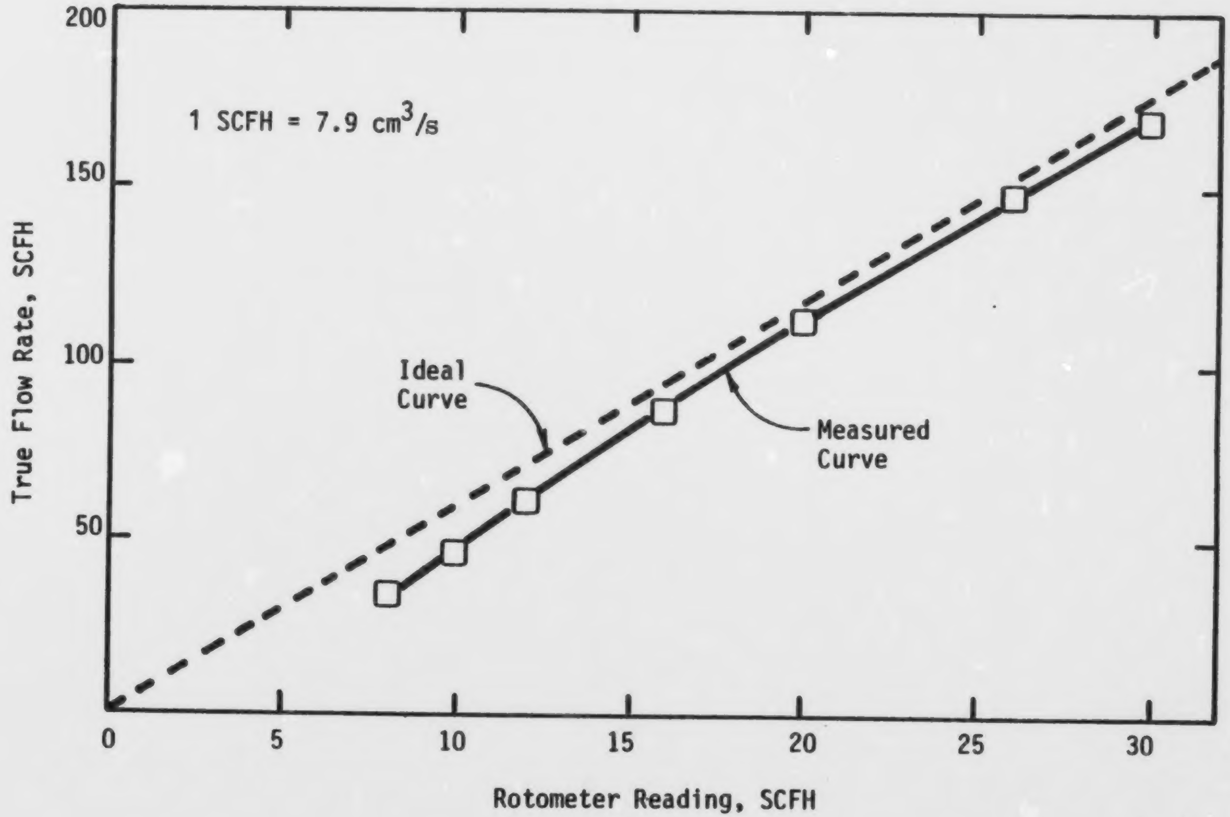

Figure G-4. H_2-rotometer calibration curve. Data were obtained using a dry-test volume displacement meter corrected for pressure and ambient temperature.

Reproducibility of gas flow rates was indicated most significantly by the reproducibility of the temperature profiles within the ITR. The temperature profiles shown in Appendix B indicate the level of precision obtained in reproducing thermal conditions. In most instances at least two temperature measurements were made. The only instance where difficulty was encountered was the case of the 1950°C flame being fired into the ITR at 1100°C. In that instance a stoichiometric flame was used and in that region of the temperature-stoichiometry curve the flame temperature is very sensitive to the fuel-to-air ratio. Table G-2 provides a set of temperature profiles obtained for the 1360°C isothermal condition. Mean, $\bar{x}$, and standard deviation, s, are provided for each position. Data were obtained by measuring a temperature profile and then checking and/or adjusting the gas flow rates prior to collecting the next set of measurements. All of the data collected are shown in Table G-2. The data at 94 cm which were clearly out of line were not presented in Figure B-8 of Appendix B.

Residence times also were directly affected by the gas flow rates. The accuracy and precision of the residence time calculations are subject to the levels of uncertainty in the gas flow rates discussed above and the temperature measurements such as those shown in Table G-2. Calculation of residence times and heating rates is discussed in Section 4.1.2.

G-1.3 Measurement of Sorbent Flow Rates

Sorbent flow rates were regulated and monitored for two reasons which could impact the repeatability of the experiments: 1) to avoid thermally overloading the reactor volume occupied by the sorbent stream, and, 2) to maintain a favorably low calcium-to-sulfur ratio in the reaction zone. Sorbent feed rates were not infinitely adjustable and were dependent on the operating conditions of the fluidized bed as well as those of the offtake tube assembly. However, suitable flow rates could be attained and were

TABLE G-2. REPRODUCIBILITY OF FLAME CONDITIONS IN THE ITR. DATA ARE FOR THE 1360°C ISOTHERMAL CONDITION

Distance from Burner, cm	Temperature, °C		$\bar{x}$	s
30	1360	1365		
	1345	1363		
	1357		1358	7.9
43	1360	1350		
	1354	1357		
	1350	1366	1356	6.2
56	1355	1357		
	1360	1361		
	1359		1358	2.4
69	1359	1361		
	1357			
	1363		1360	2.6
81	1360	1375		
	1362			
	1376		1368	8.4
94	1313	1361		
	1323	1362		
	1373		1346	26.6
107	1350	1353		
	1365			
	1364		1358	7.6
			Average S.D.[a]	5.9

[a] Data obtained at 94 cm were rejected by Chauvenet's Criterion.

generally reproducible even if the sorbent flow was halted for a few minutes and then restarted.

The objective of monitoring the sorbent feed rates was to ensure that no change in feed rate had occurred which might impact the validity or representativeness of a sample. Feed rates were measured immediately before and after each sample was collected and the results recorded.

Procedure

After the desired fluidized bed operating conditions were set and a visibly steady sorbent flow rate was obtained, the sorbent feed tube was placed into a tared 50 ml Erlenmeyer flask. The sorbent was ejected into the flask for either 30 or 60 seconds depending on the flow rate. The flask was then reweighed. An electronic balance with automatic tare and zero was used so that the sorbent mass was obtained directly. This procedure was performed immediately before and immediately following flame injection and sampling.

During the filling of the flask, fine material was carried out of the flask by the transport gas. Several means were used to trap the fine material. These included:

- Filling the flask with shredded paper to provide a high surface area and tortuosity to trap the fines.
- Placing water in the flask to act as a dust trap.
- Fitting paper and glass fiber filters to the mouth of the flask.
- Plugging the mouth and neck of the flask with a fiber such as glass wool.

The latter technique was the most effective at reducing the visible efflux of fines from the flask. However, it was found that the fines constituted a negligible fraction (could not be measured) of the total mass of material collected so this precaution was generally disregarded.

Data which demonstrate the reproducibility of sorbent feed rates are shown in Table G-3.

G-2. Analytical

G-2.1 BET Analysis

Specific surface area measurements were carried out at 77 K using N_2-adsorption isotherm analysis by the Brunauer-Emmett-Teller (BET) technique. This method provides a representative measure of specific surface area for a given material. The repeatability of the measurements was checked by multiple analyses of randomly chosen samples throughout the period of the program. Results of the repeatability tests are listed in Table G-4.

In addition, two certified surface area standards were analyzed to determine the overall accuracy of both the instrument and operation. These standards were No. 8008, SiO_2, 5.15 m^2/g and No. 7008, Al_2O_3, 1.97 m^2/g. Analyses are given in Table G-5.

G-2.2 Perkin-Elmer 240B Elemental Analyzer

The Perkin-Elmer 240B elemental analyzer was used to determine the CO_2 and H_2O content of solid samples. For unsulfated samples this information was used to directly determine the extent to which the sample was calcined (mol percent basis). Recalibration of the instrument was carried out each time a series of samples was analyzed. In addition, both accuracy and precision studies were performed. Standards for the accuracy study were benzethonium chloride monohydrate, 2,5-bis-(4-biphenylyl)oxazole, and acetanilide. The precision study utilized the five replicate samples of benzethonium chloride monohydrate. Results of these tests are shown in Table G-6. Accuracy was $+1.0 \pm 2.5$ percent for carbon and -0.6 ± 3.0 percent for

TABLE G-3. REPRODUCIBILITY OF SORBENT FLOW RATES BEFORE AND AFTER SAMPLE COLLECTION

Sorbent	Flow Rate, g/min Before Sampling	Flow Rate, g/min After Sampling	Change
25K75V	0.60	0.58	-0.02 g/min
5B95V	0.80	0.80	0
10B90V	0.85	0.88	0.03
Bentonite	0.40	0.34	-0.06
Kaolin	0.30	0.25	-0.05
Kaolin	0.43	0.22	-0.21
Vicron 45-3	0.51	0.42	-0.09
Vicron 45-3	0.48	0.63	+0.15
Vicron 45-3	0.64	0.70	+0.06

TABLE G-4. REPRODUCIBILITY OF BET SPECIFIC SURFACE AREA MEASUREMENTS

Sample Description	Surface Area	Standard Deviation
Vicron 45-3, partly calcined	5.06 4.79	3.9%
Bentonite	137.25 141.06	1.9%
Al_2O_3	0.58 0.54	5.1%

TABLE G-5. BET SPECIFIC SURFACE AREA STANDARDS TESTING

BET Standard	Actual Surface Area m^2/g	Measured Surface Area, m^2/g	Difference m^2/g
No. 8008 SiO_2	5.15	4.25	-0.90
No. 7008 Al_2O_3	1.97	1.40	-0.57
		mean difference	-0.74 m^2/g
		standard deviation	0.23 m^2/g

TABLE G-6. ACCURACY AND PRECISION TESTS FOR THE PERKIN-ELMER 240B ELEMENTAL ANALYZER

Accuracy Tests

Standard	Actual Composition -Percent-		Measured Difference -Percent-	
	Carbon	Hydrogen	Carbon	Hydrogen
Benzethonium chloride monohydrate	69.58	9.51	+3.4	-2.5
			3.4	1.3
			2.8	4.8
			3.3	3.6
			3.3	2.5
2,5-bis (4-biphenylyl) oxazole	86.84	5.13	0.1	+0.4
			0.1	2.3
			-3.2	3.7
			3.0	4.3
Acetanilide	71.09	6.71	+1.0	-2.2
			0.4	0.6
	$\overline{x}$		+1.0	-0.6
	s		2.5	3.0

Precision Tests

Standard	Measured Composition -Percent-	
	Carbon	Hydrogen
Benzethonium chloride monohydrate	71.92	9.29
	71.95	9.39
	71.53	9.05
	71.88	9.17
	71.88	9.27
$\overline{x}$	71.83	9.23
s	0.17	0.13

hydrogen. The relative precision was ± 0.2 percent for carbon and ± 1.4 percent for hydrogen.

G-2.3 Leco SC-32 Sulfur Analyzer

The Leco SC-32 sulfur analyzer was used to determine the sulfur content of sulfated and sulfidated sorbents as well as possible trace levels of sulfur in the sorbents and mineral additives. The sulfur contents were then used, along with the 240B data, to determine directly the extent of calcination of sulfated sorbents as well as the calcium utilization efficiency. The SC-32 sulfur analyzer was calibrated prior to running each sample. In addition, a series of tests was run to determine the accuracy and relative standard deviation of the instrument. The standard materials were four coals (0.96 percent S, 2.05 percent S, 1.68 percent S and 3.02 percent S) provided by Leco as calibration standards. Results of these tests are shown in Table G-7.

The Leco instrument measures sulfur content by igniting the sample in an oxygen-rich atmosphere at high temperature. The resultant volume of SO_2 is measured and the percent-by-weight of sulfur is calculated internally by the instrument. Tests involving inorganic sulfur as sulfate showed poor recovery and reproducibility. To solve this probe several combustion accelerators were tested. Vanadium pentoxide was found to work satisfactorily with sulfated limestones. The V_2O_5 is ground to a powder and added to the sample after taring and weighing.

G-2.4 Overall Check of Chemical Analyses by Mass Balance

In order to provide an overall check on the accuracy of the chemical analyses, a mass balance was performed for each sample. The data returned from the 240B instrument were percent C, percent H and percent ash. The ash value was obtained from the net weight of the sample after ignition in the instrument.

TABLE G-7. ACCURACY AND RELATIVE STANDARD DEVIATION DETERMINATIONS FOR THE LECO SC-32 SULFUR ANALYZER

Coal Sulfur Content	0.96%S	2.05%S	1.68%S	3.02%S
Measured Percent Sulfur	0.93	2.10	1.73	3.02
	0.93	2.05	1.68	2.98
	0.96	2.13	1.65	3.13
	0.96	2.07	1.62	
	0.92	1.98	1.67	
	0.94	2.03	1.72	
	0.94	2.08	1.63	
	0.95	2.05	1.64	
	0.99	2.03	1.65	
	0.93	2.05	1.63	
	0.94	2.00	1.66	
	0.94	2.04	1.68	
	1.00	2.12	1.69	
	0.97	2.08	1.64	
		2.02	1.75	
		2.07	1.74	
		2.06	1.68	
		2.00		
		2.06		
$\bar{x}$	0.95	2.06	1.67	3.04
RSD	2.5%	2.0%	2.4%	2.6%
$\frac{\bar{x}-x}{x} \times 100\%$	-1.04%	+0.49%	-0.60%	0.66%

For unsulfated limestones (e.g. Vicron 45-3) the sample was assumed to contain CaO, CaO_3 and $Ca(OH)_2$ only. Trace impurities and Mg compounds were not considered. The carbon content was then stoichiometrically equivalent to $CaCO_3$ with a factor of 8.33; hydrogen, in turn, equivalent to $Ca(OH)_2$ with a factor of 37. Calcium oxide, the remaining compound, was determined by difference. The mass balance involved simply calculating the total calcium in the sample from the CaO, $CaCO_3$ and $Ca(OH)_2$ measurements. The percent calcium was then compared with the percent calcium in the ash, which was assumed to be all CaO.

With unsulfated dolomite samples, the same procedure was employed, except that the separately determined Mg/Ca ratio was used to correct the percent Ca (from H and C measurements) to percent CaO plus MgO. The total CaO plus MgO was then compared with the percent ash, which was assumed to be MgO plus CaO.

With sulfated samples the Leco SC-32 sulfur analyzer results also were employed. The sulfur was assumed to be $CaSO_4$ which was retained in the ash. The CaO was determined as $100 - (CaSO_4 + CaCO_3 + Ca(OH)_2)$ and the ash value was compared with:

$$CaSO_4 + CaO + \frac{56}{100} CaCO_3 + \frac{56}{100} Ca(OH)_2$$

Example calculations are shown below:

Unsulfated Vicron 45-3 Sample 1-23-0683

$\% C = 1.42 = 11.83\% CaCO_3 = 4.73\% Ca$

$\% H = 0.29 = 10.73\% Ca(OH)_2 = 5.80\% Ca$

$\% CaO = 100-11.83-10.73 = 77.44\% = 55.31\% Ca$

$\% Ash = 92.60 = 55.14\% Ca$

$4.73 + 5.80 + 55.31 = 65.84\% Ca$

$$\text{mass balance} = \frac{65.84}{66.14} \times 100\% = 99.55\%$$

Unsulfated Dolomite Sample 3-27-0983

% C = 4.32 = 36.0% $CaCO_3$ = 20.16% CaO

% H = 0.25 = 9.25% $Ca(OH)_2$ = 7.00% CaO

100 - (36.0 + 9.25) = 54.75% CaO + MgO

% Ash = 81.27

total CaO = MgO = 20.16 + 7.0 + 54.75 = 81.91

$$\text{mass balance} = \frac{81.91}{81.27} \times 100\% = 100.79\%$$

Sulfated Vicron 45-3 Sample 3-32-0383

% C = 2.30 = 19.17% $CaCO_3$ = 7.67% Ca

% H = 0.10 = 3.7% $Ca(OH)_2$ = 2.0% Ca

% S = 3.64 = 15.47% $CaSO_4$ $CaSO_4$ = 4.55% Ca

% CaO = 100 - (19.17 + 3.7 + 15.47) = 61.66 + 44.04% Ca

% Ash = 91.65 = CaO + $CaSO_4$

91.65 - 15.47 = 76.18% CaO = 54.41% Ca

7.67 + 2.0 + 44.04 = 53.71% Ca

$$\text{mass balance} = \frac{53.71}{54.41} \times 100\% = 98.71\%$$